



SHEAR BEHAVIOUR OF FIBREGLASS ROCK BOLTS FOR GROUND REINFORCEMENT

A thesis submitted by

Peter Gregor, B Eng.

For the Award of

Doctor of Philosophy

2022

ABSTRACT

Glass-Reinforced Polymer (GRP) bolts are increasingly used in Australian coal mines as a means of rib support in heading development and for coal-face equipment recovery. Unlike metallic rock bolts, GRP bolts are made through pultrusion resulting in anchor bolts with differing performance characteristics to that of steel. Therefore, previous studies of steel rock bolts could not be utilised to describe the load transfer characteristics of their fibreglass counterparts. This thesis expanded on the shear load transfer mechanisms of fully grouted fibreglass rock bolts utilising a double shear system. Analytical and numerical models were also developed to simulate the shear performance of the fibreglass rock bolts. Two experimental test schemes were carried out. The first with clean shear interfaces and the second with infilled shear interfaces comprised of sandy clay, applied to a thickness of 5mm. Two types of fully grouted rock bolts; 20-tonne and 30-tonne were tested with pretension loads of 0kN, 10kN, 15kN and 20kN. It was found that increasing the pretension also increased the confining pressures at the shear interfaces for both clean and infilled joints. This in turn reduced the damage propagating from the bolt at the shear interface as well as reducing the hinge point bending. Infilled shear interface samples experienced a decrease in the failure displacement while also resulting in an increase to the peak shear force. The analytical model was developed utilising the Fourier transform, energy balance theory and linear elastic theory. The result was an empirical relationship that could determine the double shear performance of fibreglass rock bolts with close agreement to the experimental data. Coefficients were incorporated to facilitate model calibration and tuning. Finally, three-dimensional (3D) modelling was utilised to conduct numerical simulations of fibreglass rock bolts subjected to single shear and double shear scenarios. The numerical model was calibrated against experimental data and then extended to conduct a sensitivity analysis on fibreglass rock bolts subjected to variations of the double shear test parameters. Scenarios included rock bolt installation angles, shearing rates and various host rock strengths. The combined experimental, analytical and numerical studies provide a comprehensive understanding of the shear behaviour of fibreglass rock bolts. By studying the impact of pretension and shear interfaces, this research has successfully modelled the shear failure mechanisms of 20-tonne and 30-tonne fibreglass rock bolts.

CERTIFICATION OF THESIS

I, Peter Gregor, declare that the PhD Thesis entitled Shear behaviour of fibreglass rock bolts for ground reinforcement is not more than 100,000 words in length including quotes and exclusive of tables, figures, appendices, bibliography, references, and footnotes. This thesis contains no material that has been submitted previously, in whole or in part, for the award of any other academic degree or diploma. Except where otherwise indicated, this thesis is my own work.

Date: 23 September 2022

Endorsed by:

Professor Kevin McDougall

Principal Supervisor

Associate Professor Ali Mirzaghobanali

Associate Supervisor

Professor Naj Aziz

External Supervisor

Student and supervisors' signatures of endorsement are held at the University.

LIST OF PUBLICATIONS

Journal papers submitted for publication:

- **Gregor, Peter**, Mirzaghobanali, Ali, McDougall, Kevin, Aziz, Naj, Jodeiri Shokri, Behshad (2022) Shear behaviour of fibreglass rock bolts for various pretension loads
- **Gregor, Peter**, Mirzaghobanali, Ali, McDougall, Kevin, Aziz, Naj, Jodeiri Shokri, Behshad (2022) Investigating shear behaviour of fibreglass rock bolts reinforcing infilled discontinuities for various pretension loads
- **Gregor, Peter**, Mirzaghobanali, Ali, McDougall, Kevin, Aziz, Naj, Jodeiri Shokri, Behshad (2022) Developing an analytical model for investigating shear behaviour of fibreglass rock bolts with considering various pretension loads for reinforcing clean and infilled discontinuities
- **Gregor, Peter**, Mirzaghobanali, Ali, McDougall, Kevin, Aziz, Naj, Jodeiri Shokri, Behshad (2022) Developing a 3D numerical model and experimental tests for investigating shear behaviour of fibreglass rock bolts for reinforcing clean and infilled discontinuities

Conference articles:

Conference Level: International (A)

- Zohaib, Muhammad, Mirzaghobanali, Ali, Helwig, Andreas, Aziz, Naj, **Gregor, Peter**, Rastegarmanesh, Ashkan, and McDougall, Kevin (2020) Shear strength properties of artificial rock joints, Coal Operators' Conference, Wollongong, Australia
- Mirzaghobanali, Ali, **Gregor, Peter**, Alfahed, Abdullah, Aziz, Naj and McDougall, Kevin (2019) Strength Properties of Grout for Strata Reinforcement, Coal Operators' Conference, Wollongong, Australia
- Mirzaghobanali, Ali, Alenzi, Faisel, **Gregor, Peter**, Aziz, Naj and McDougall, Kevin (2019) Shear strength of Rock Joints under Constant Normal Loading Conditions, Coal Operators' Conference, Wollongong, Australia
- Mirzaghobanali, Ali, **Gregor, Peter**, Alkandari, Hamed, Aziz, Naj and McDougall, Kevin (2018) Mechanical Behaviours of Grout for Strata Reinforcement, Coal Operators' Conference, Wollongong, Australia

ACKNOWLEDGEMENTS

I would like to acknowledge the University of Southern Queensland for providing funding for this study as part of the Domestic PhD Stipend Scholarship. I am also thankful to the School of Engineering, who provided laboratory space, equipment, and expertise.

Words cannot express my gratitude to my supervisors Prof. Kevin McDougall and A/Prof. Ali Mirzaghobanali of the University of Southern Queensland and Prof. Naj Aziz of the University of Wollongong, for their continued patience, support, and feedback throughout the completion of this research project. I would also like to extend my thanks to the technical staff of the Centre for Future Materials Laboratories, Mr Brian Lenske, Mr Wayne Crowell, Mrs Piumika Ariyadasa and Mr Martin Geach, for their generous collaboration and availability during the completion of my experiments. I would like to recognise the postgraduate and post-doctoral team at the Centre for Future Materials for welcoming me to the team and ensuring I enjoyed my research, even during the stressful periods.

Special thanks to the School of Engineering and Centre for Future Materials academic team for providing me with the opportunity to expand into pedagogy, allowing me to gain invaluable experiences.

Lastly, I am extremely grateful to my partner and family, especially my parents and siblings. Their unconditional love and belief in me maintained my spirits and high motivation over this period. To them I dedicate this thesis.

This research has been supported by the Australian Government Research Training Program Scholarship.

Table of Contents

ABSTRACT.....	i
CERTIFICATION OF THESIS.....	ii
LIST OF PUBLICATIONS	iii
ACKNOWLEDGEMENTS	iv
LIST OF FIGURES.....	xi
LIST OF TABLES	xxiii
ABBREVIATIONS.....	xxiv
LIST OF SYMBOLS	xxv
CHAPTER 1: INTRODUCTION	1
1.1 Background	1
1.1.1 Rock bolts.....	1
1.2 Research problem, aim and objectives.....	2
1.2.1 Research problem.....	2
1.2.2 Research aim and objectives	3
1.2.3 Research questions	3
1.3 Research justification	4
1.4 Research approach	4
1.5 Structure of the thesis.....	5
1.6 Scope and limitations	8
1.7 Summary	8
CHAPTER 2: LITERATURE REVIEW	9
2.1 Introduction.....	9
2.2 Background to tendons.....	9
2.2.1 Types of tendons	11
2.3 Axial load transfer mechanisms	17
2.3.1 Experimental studies	20

2.3.2 Modelling and numerical simulation	34
2.4 Shear load transfer mechanisms	38
2.4.2 Mathematical and numerical modelling.....	47
2.5 Infilled discontinuities.....	56
2.5.1 Two-dimensional infill studies.....	56
2.5.2 Three-dimensional infill studies.....	63
2.6 Summary	67
CHAPTER 3: RESEARCH DESIGN AND METHODS.....	68
3.1 Introduction.....	68
3.2 Experimental design.....	68
3.3 Experimental plan for clean discontinuities	69
3.4 Experimental plan for infilled discontinuities.....	70
3.5 Equipment design.....	71
3.5.1 Shear box.....	72
3.5.2 Mould design.....	74
3.6 Sample preparation.....	76
3.6.1 Concrete preparation	76
3.6.2 Pre-tensioning	79
3.6.3 Grouting	80
3.6.4 Composite grout.....	83
3.6.5 Infilled discontinuities.....	84
3.7 Initial testing.....	86
3.7.1 Unconfined shear samples.....	86
3.7.2 Confined shear samples.....	88
3.7.3 Grout material properties	89
3.8 Fibreglass rock bolt properties	98
3.8.1 Tensile	100

3.8.2 Bending	102
3.8.3 Punch test	104
3.8.4 Single shear	105
3.9 Summary	108
CHAPTER 4: RESULTS OF THE DOUBLE SHEAR TESTING OF FIBREGLASS ROCK BOLTS IN CLEAN JOINTS	109
4.1 Introduction	109
4.2 Overview of the testing process	109
4.2.1 Double shear calculations	111
4.3 Results for 20-tonne rock bolts, double shear testing	111
4.3.1 Shear behaviour profile	111
4.3.2 Pretension profile	114
4.3.3 Impact of pretension on shear strength	117
4.3.4 Failure characteristics.....	121
4.4 Results for 30-tonne rock bolts, double shear testing	123
4.4.1 Shear behaviour profile	123
4.4.2 Pretension profile	126
4.4.3 Impact of pretension on shear strength	129
4.4.4 Failure characteristics.....	133
4.5 Comparison between 20-tonne and 30-tonne rock bolts.....	136
4.5.1 Shear behaviour profile	136
4.5.2 Pretension profile	139
4.5.3 Impact of pretension on shear strength	141
4.5.4 Failure characteristics.....	144
4.6 Understanding the behaviour of fibreglass rock bolts.....	148
4.6.1 Shear behaviour profile	148
4.7 Summary	152

CHAPTER 5: RESULTS OF THE DOUBLE SHEAR TESTING OF FIBREGLASS ROCK BOLTS IN INFILLED JOINTS	155
5.1 Introduction	155
5.2 Overview of the testing process	156
5.2.1 Double shear calculations	157
5.3 Results for 20-tonne rock bolts, infilled double shear testing.....	157
5.3.1 Shear behaviour profile	157
5.3.2 Pretension profile	160
5.3.3 Impact of pretension on shear strength	163
5.3.4 Failure characteristics.....	166
5.4 Results for 30-tonne rock bolts, infilled double shear testing.....	172
5.4.1 Shear behaviour profile	172
5.4.2 Pretension profile	174
5.4.3 Impact of pretension on shear strength	177
5.4.4 Failure characteristics.....	181
5.5 Comparison between 20-tonne and 30-tonne rock bolts.....	183
5.5.1 Shear behaviour profile	183
5.5.2 Pretension profile	187
5.5.3 Impact of pretension on shear strength	188
5.5.4 Failure characteristics.....	191
5.6 Summary	196
CHAPTER 6: ANALYTICAL AND NUMERICAL MODELLING OF ROCK BOLTS IN DOUBLE SHEAR.....	198
6.1 Introduction	198
6.2 Analytical modelling of shear behaviour of fibreglass rock bolts	199
6.2.1 Requirement for a new analytical model	199
6.2.2 Development of analytical model	200
6.2.3 Model calibration for reinforcing clean joints	206

6.2.4 Model calibration for reinforcing infilled joints	212
6.3 3D numerical simulation	216
6.3.1 Development of the rock bolt model.....	217
6.3.2 Developing the rock and joint model.	220
6.3.3 Single shear conceptual model.....	222
6.3.4 Numerical simulation of single shear.....	223
6.3.5 Double shear conceptual model	225
6.3.6 Numerical simulation calibration of double shear clean joints.....	226
6.4 Sensitivity analysis.....	230
6.4.1 Host rock strength variation	231
6.4.2 Rock bolt angle	234
6.4.3 Shear speed.....	236
6.5 Summary	238
CHAPTER 7: CONCLUSIONS AND RECOMMENDATIONS	240
7.1 Introduction	240
7.2 Key research outcomes	240
7.2.1 Objective One: Critical review of research.....	240
7.2.2 Objective Two: Test scheme and experimental design.....	241
7.2.3 Objective Three: Clean interface shear study	241
7.2.4 Objective Four: Infilled shear interface study.....	242
7.2.5 Objective Five: Analytical model	243
7.2.6 Objective Six: Numerical model.....	243
7.3 Recommendations for future research	244
REFERENCES.....	246
Appendix A	258
Appendix B	265
Appendix C	271

Appendix D	275
Appendix E.....	285
Appendix F.....	291

LIST OF FIGURES

Figure 1.1: Research flow diagram	5
Figure 1.2: Thesis structure.....	7
Figure 2.1: Cable bolt tool box (Hutchinson et al., 1996, DSI-UNDERGROUND, 2022, Jennmar, 2022, Minova, 2021a).....	12
Figure 2.2: Bolt reinforcement failure modes (Hutchinson et al., 1996)	19
Figure 2.3: Reinforcing systems key components (Windsor, 1997).....	19
Figure 2.4: Ground reinforcement load transfer diagram (Thompson et al., 2014)...	20
Figure 2.5: Rock bolt shear and axial failure modes (MINOVA et al., 2006).....	21
Figure 2.6: Rock bolt instrumented with strain gauges (Waclawik et al., 2019).....	22
Figure 2.7: Axial test setup as conducted by Benmokrane et al. (1995).....	23
Figure 2.8: Axial load performance of threaded and stranded anchors with varying embedment lengths (Benmokrane et al., 1995).....	24
Figure 2.9: Cross-section of rotation controlled axial testing apparatus (Martin et al., 2011)	25
Figure 2.10: Pull-out test comparing rock bolts, resin and grout (Martin et al., 2011)	26
Figure 2.11: In-situ hydraulic pull test apparatus (Forbes et al., 2020)	27
Figure 2.12: Grout contact surface for a bolt with a diameter of 7/8th inch (Pile et al., 2003).	27
Figure 2.13: (a) Rock bolt installed with reamed and standard length (b) Rock bolt installed reamed and over-drilled (Craig et al., 2013)	28
Figure 2.14: Diagram of rock bolt modified with fibre-optic cable (Forbes et al., 2020).	29
Figure 2.15: Rock bolt anchorage lengths tested by the pull test scheme (Forbes et al., 2020)	29
Figure 2.16: Strain distribution for rock bolts installed with various anchored lengths (Forbes et al., 2020).	30
Figure 2.17: LSEPT apparatus schematic for rock bolts with resin anchoring (Clifford et al., 2000).....	31
Figure 2.18: LSEPT apparatus schematic for grouted cable bolts (Clifford et al., 2001)	32

Figure 2.19: Cross-sectional diagram of axial double embedment test (Clifford et al., 2000)	32
Figure 2.20: Sectional view of new LSEPT pull test apparatus designed by (Chen et al., 2016).....	33
Figure 2.21: Lumped parameter model for tendon/bolt, ground, and rock (Ivanovic, 2001)	34
Figure 2.22: (a) Bond behaviour model (b, c, d) sub models used for lumped parameter model (Ivanović et al., 2009)	35
Figure 2.23: Cutaway section of the modified Hoek Cell (Hyett et al., 1995)	35
Figure 2.24: Cable bolt simulations for varying confining pressures using the modified Hoek Cell (Hyett et al., 1995)	36
Figure 2.25: Rock bolt pull test simulation(Aziz et al., 2016a)	37
Figure 2.26: Comparison of the FLAC models against experimental analysis(Aziz et al., 2016a).....	37
Figure 2.27: FEM schematic of fully grouted bolt (Jahangir et al., 2021).....	38
Figure 2.28: FEM constitutive pull test model modified from (Jahangir et al., 2021)	38
Figure 2.29: Stress variations within stratification Nemcik et al. (2006)	39
Figure 2.30: [left] A view of the sheared sample in single shear, note the interaction between the strand and the steel tube (Aziz et al., 2016c). [right] Stress concentrations during BS7861-2 Single shear test (Aziz et al., 2015c)	40
Figure 2.31: Shear test apparatus (Goris et al., 1996).....	40
Figure 2.32: Single shear sectional diagram (Standard, 1996)	41
Figure 2.33: Single shear apparatus cross-section [left] Megabolt, [right] British single shear standard (Li et al., 2017b).....	42
Figure 2.34: Megabolt testing system (Mckenzie et al., 2015).....	42
Figure 2.35: Comparison of BSST and MSST shear force and shear displacement (Li et al., 2017b).....	43
Figure 2.36: Comparison of MSST and DST testing methods for shear force and displacement (Li et al., 2017b).....	43
Figure 2.37: Mark 1 testing apparatus developed by Aziz et al. (2003)	44

Figure 2.38: Schematic of the mark 1 double shear testing apparatus (Aziz et al., 2003)	44
Figure 2.39: Comparison of the cross-section of the MSST, BSST and DST testing methods (Li et al., 2017b)	45
Figure 2.40: Demonstration of concrete crushing during double shear testing with 40MPa concrete (Li et al., 2016)	46
Figure 2.41: Impact of pretension on the shear performance of dowels anchored in 60MPa concrete (Gilbert et al., 2015)	47
Figure 2.42: Geometry of rock bolt subjected to shear displacement (Haas, 1976)	48
Figure 2.43: FEM model of rock bolts installed at 0° and 30° inclinations (Spang et al., 1990)	48
Figure 2.44: Comparison of FEM models for shear inclinations of 0° and 30° and initial tensions of 25kN and 35kN (Spang et al., 1990)	49
Figure 2.45: Force component model of a rock bolt subjected to shearing (a) Elastic zone, and (b) plastic zone (Pellet et al., 1996)	49
Figure 2.46: Comparison of shear force analytical model and experimental results (Rasekh, 2017)	50
Figure 2.47: Comparison of analytical models and experimentally derived double shear results for 100MPa sample (Singh et al., 2021)	51
Figure 2.48: Comparison of analytical models and experimentally derived double shear results for 20MPa sample (Singh et al., 2021)	51
Figure 2.49: Three-dimensional finite element model subjected to shear loads. Modified from (Ghadimi et al., 2015)	52
Figure 2.50: Shear stress distribution during FEM shearing simulation. Modified from (Ghadimi et al., 2015)	53
Figure 2.51: Schematic used to develop the FLAC2D cable bolt double shearing model (Rasekh, 2017)	53
Figure 2.52: Shear stress distribution along the confining rock (Rasekh, 2017)	54
Figure 2.53: FLAC2D simulation of grouted cable bolt subject to the British standard of testing (Mirzaghorbanali et al., 2017b)	55
Figure 2.54: Comparison of FLAC2D simulated British standard of testing cable bolt shear test and experimental testing scheme	55

Figure 2.55: Roughness profile for JRC range (Barton et al., 1977)	56
Figure 2.56: Four categories of filled joints (Barton, 1973)	58
Figure 2.57: Effect of infill thickness on the shear strength of the idealised saw tooth discontinuity (Coon et al., 1970).....	59
Figure 2.58: Schematic of CNS apparatus (Haque et al., 2000)	60
Figure 2.59: Comparison of UDEC simulated shearing and CNS samples (Haque et al., 2000).....	60
Figure 2.60: Relationship between infill thickness and peak shear strength. Modified from (Oliveira, 2009)	61
Figure 2.61: Lined tunnel with infilled joints (Oliveira, 2009).....	61
Figure 2.62: Illustrated infilled rock joints with varying friction (Mirzaghorbanali et al., 2014).....	62
Figure 2.63: Cyclical shear test apparatus schematic (Mirzaghorbanali et al., 2014).....	62
Figure 2.64: Comparison between numerical dynamic model (lines) and laboratory results (symbols) of NCSR against number of shear cycles. Modified from (Mirzaghorbanali et al., 2014).....	63
Figure 2.65: Illustration of smooth-joint contact (Itasca, 2005)	64
Figure 2.66: (a) Discontinuity profile, and (b) shear test model (Karakus et al., 2016)	64
Figure 2.67: Comparison between simulation and Barton's model for clean joints (Karakus et al., 2016)	65
Figure 2.68: Constitutive models for CNL and CNS simulations (Shang et al., 2018)	66
Figure 2.69: Model of the crack propagation with an initial normal stress of 40MPa (Shang et al., 2018)	66
Figure 3.1: Outline of SANS Machine used for double shear testing.....	72
Figure 3.2: MK1.5 Double shear box design	73
Figure 3.3: Assemble double shear apparatus highlighting key features such 10mm spacing at each interface	73
Figure 3.4: Centre block rotation because of testing.....	74
Figure 3.5: Double Shear mould design.....	75
Figure 3.6: Double shear mould key features	76

Figure 3.7: Preparation for rifling simulation	76
Figure 3.8: Severe damage resulting from a weak concrete matrix.	77
Figure 3.9: Cast of double shear sample.	77
Figure 3.10: Cylindrical concrete samples for UCS testing.....	77
Figure 3.11: Concrete sample prepared for UCS testing	78
Figure 3.12: UCS concrete sample post test	78
Figure 3.13: Assembled double shear samples.	80
Figure 3.14: Hole positions on top of concrete blocks.....	81
Figure 3.15: Grouting quality examination after testing.....	81
Figure 3.16: UCS for fly ash content at varying curing times.	83
Figure 3.17: Layer of infill material on shearing plane of concrete section.	85
Figure 3.18: Close up of the mating of the shearing planes with infill material.	85
Figure 3.19: Minimising infilled drying during preparation.....	86
Figure 3.20: Initial unconfined test 30-tonne.....	87
Figure 3.21: (left) high quality encapsulation around fibre glass bolt (right) around the concrete medium	87
Figure 3.22: Fibre glass bolt double shear testing assembly.....	88
Figure 3.23: Assemble double shear system.....	89
Figure 3.24: Grout preparation.....	90
Figure 3.25: Large-scale and small-scale grout moulds.....	90
Figure 3.26: Prepared Sample 100 mm diameter (large scale) cylinder UCS	90
Figure 3.27: 70 mm side (small scale) cube UCS.....	90
Figure 3.28: UCS strength of small-scale and large-scale grout at various curing times	91
Figure 3.29: Dog-bone tensile testing setup.....	92
Figure 3.30: Sample secured in testing rig.....	93
Figure 3.31: Sample after failure	93
Figure 3.32: Grout comparative tensile test results.....	94
Figure 3.33: Average tensile results per curing period	95
Figure 3.34: Consolidation test of the sandy clay infilled material.	96
Figure 3.35: Undrained direct shear test of infilled material	97
Figure 3.36: Drained direct shear test of infilled material	98

Figure 3.37: Illustration of fibreglass bolt geometry	99
Figure 3.38: Double shear testing apparatus with double ended threads.....	100
Figure 3.39: Tensile test post failure.....	101
Figure 3.40: Tensile test comparison of 15-tonne, 20-tonne, and 30-tonne rock bolts	102
Figure 3.41: Four-point bending test setup of fibreglass rock bolts.	103
Figure 3.42: Rock bolt four-point bending test results	103
Figure 3.43: Punch test parallel fibreglass sample.....	104
Figure 3.44: Punch test perpendicular fibreglass samples	104
Figure 3.45: Single shear fibreglass samples	106
Figure 3.46: Single shear average peak load for 15-tonne, 20-tonne, and 30-tonne samples.....	107
Figure 3.47: Single shear average peak displacements for 15-tonne, 20-tonne, and 30- tonne rock bolts	107
Figure 4.1: Example of the three failure regions for 20-tonne rock bolts.....	112
Figure 4.2: Change in angle for each stage of the 20-tonne double shear profile....	113
Figure 4.3: Illustration of recurring reduction in shear force for 20-tonne sample..	114
Figure 4.4: Example of pretension zones in axial force for 20-tonne rock bolt with 0kN pretension	116
Figure 4.5: Comparison of pretension axial forces for the 20-tonne rock bolts with clean joints.	117
Figure 4.6: Change in shear profile due to pretension for 20-tonne rock bolts	118
Figure 4.7: Change in failure displacement due to increase from 10kN to 20kN pretension for 20-tonne rock bolts	119
Figure 4.8: Change in recorded shear dip due pretension increase from 10kN to 20kN for 20-tonne rock bolts	120
Figure 4.9: Changes to the strain-softening stage for 20-tonne rock bolts as a result of pretension	121
Figure 4.10: Angle of failure and rock bolt damage for 20-tonne 10kN pretension clean shear rock bolt	122
Figure 4.11: Angle of failure and rock bolt damage for 20-tonne 20kN pretension clean shear rock bolt	122

Figure 4.12: Damage caused to host material by the 20-tonne rock bolts of 10kN and 20kN pretensions.....	123
Figure 4.13: Example of the failure regions for 30-tonne rock bolt with a pretension of 0kN.....	124
Figure 4.14: Example of the recurring reduction in shear force for the 30-tonne sample with 10kN pretension	125
Figure 4.15: Comparison of 30-tonne rock bolt profile with and without shear force dip.....	126
Figure 4.16: Illustration of the pretension profile zones under axial loads for 30-tonne rock bolt with 0kN pretension and clean shear interfaces.....	127
Figure 4.17: 30-tonne rock bolt clean pretension profile comparison	129
Figure 4.18: Impact of pretension on the overall shear performance of 30-tonne rock bolts with clean shear interface	130
Figure 4.19: Impact of pretension on shear force dip for 30-tonne rock bolts tested in clean shear system.....	131
Figure 4.20: The effect of pretension on dip in shear force for 30-tonne rock bolts with pretensions of 0kN, 10kN and 15kN.....	132
Figure 4.21: Angle of failure for 30-tonne rock bolt with 20kN pretension with clean shear conditions.....	133
Figure 4.22: Angle of failure for 30-tonne rock bolt with 0kN pretension with clean shear conditions.....	134
Figure 4.23: Damage caused by 30-tonne rock bolt to host material with 20kN pretension	135
Figure 4.24: Shear interface comparison 0kN pretension and 20kN pretension.....	135
Figure 4.25: Shear profile comparison of 20-tonne and 30-tonne rock bolts.	137
Figure 4.26: Comparison of the axial force profile for both 20-tonne and 30-tonne 10kN pretension samples	140
Figure 4.27: Influence of pretension increase from 0kN to 10kN on shear force for 20-tonne and 30-tonne rock bolts	143
Figure 4.28: Influence of pretension increase from 15kN to 20kN on shear force for 20-tonne and 30-tonne rock bolts.....	144

Figure 4.29: Comparing rock bolt structural damage for 20-tonne and 30-tonne rock bolts with 10kN pretension	145
Figure 4.30: Representation of shear plane damage for 20-tonne and 30-tonne rock bolts	146
Figure 4.31: Comparing rock bolt structural damage for 20-tonne and 30-tonne rock bolts with 20kN pretension	147
Figure 4.32: Comparing shear plane damage of 20-tonne and 30-tonne rock bolts	148
Figure 4.33: Stages of the single shear profile for 20-tonne and 30-tonne rock bolts	150
Figure 4.34: Shear behaviour of 30-tonne rock bolts outlining double shear and single shear stages.....	151
Figure 4.35: Single shear samples post failure highlighting pinch point.....	152
Figure 5.1: Example of the three failure regions for 20-tonne rock bolts with infilled shear interfaces.....	158
Figure 5.2: Indication of damage to sample during strain-softening stage for the 20-tonne double shear infilled sample.....	159
Figure 5.3: Example of pretension zones in axial force for 20-tonne infilled rock bolt with 0kN pretension	161
Figure 5.4: Comparison of 20-tonne infilled pretension axial force results	163
Figure 5.5: Shear force and displacement comparison of all 20-tonne infilled samples	164
Figure 5.6: Change in recorded shear dip due to pretension increase from 0kN to 20kN for 20-tonne infilled rock bolts	166
Figure 5.7: Angle of failure and damage to grout and host rock for 20-tonne 0kN pretension infilled rock bolt sample	167
Figure 5.8: Angle of failure and rock bolt damage for 20-tonne 0kN pretension infilled rock bolt sample	168
Figure 5.9: Limited evidence of bending at the hinge point for the infilled 20-tonne 20kN pretension sample	169
Figure 5.10: Infilled 20-tonne 20kN sample demonstrating limited fracture propagation along the rock bolt element.....	169

Figure 5.11: Infill material that remained after disassembly of the 15kN pretension infilled 20-tonne sample.....	171
Figure 5.12: No evidence of scoring caused by dragging of the fractured rock bolt end on the 20-tonne 20kN infilled sample.....	171
Figure 5.13: Example of the failure regions for the 30-tonne infilled rock bolt with a pretension of 0kN.....	173
Figure 5.14: Example of the inflection and fluctuations in shear force for the 30-tonne sample with 10kN pretension.....	173
Figure 5.15: Illustration of the pretension profile zones for the 30-tonne 0kN pretension infilled sample	175
Figure 5.16: 30-tonne rock bolt infilled pretension profile comparison	176
Figure 5.17: Impact of pretension on the overall shear performance of 30-tonne rock bolts with infilled shear interfaces	178
Figure 5.18: Impact of pretension on the elastic to strain-softening region for 30-tonne rock bolts tested with infilled shear joints.....	179
Figure 5.19: The effect of pretension on the elastic region transitions for the 30-tonne rock bolts with infilled joints.	180
Figure 5.20: Angle of failure for 30-tonne rock bolt with 0kN pretension with infilled shear conditions.....	182
Figure 5.21: Angle of failure and damage propagation for 30-tonne rock bolt with 20kN pretension with infilled shear conditions	182
Figure 5.22: Damage propagating through element for 30-tonne rock bolt with 0kN pretension with infilled shear conditions	183
Figure 5.23: Shear profile comparison of 10kN pretension 20-tonne and 30-tonne rock bolts with infilled interfaces.....	185
Figure 5.24: Comparison of the elastic region transition and the failure region of the 20kN pretension 20-tonne and 30-tonne rock bolts with infilled shear planes.....	185
Figure 5.25: Comparison of the axial force profile for both 20-tonne and 30-tonne 0kN pretension samples with infilled shear planes.....	188
Figure 5.26: Influence of pretension increase from 0kN to 10kN on shear force for 20-tonne and 30-tonne rock bolts with infilled joints	190

Figure 5.27: Influence of pretension increase from 15kN to 20kN on shear force for 20-tonne and 30-tonne rock bolts with infilled joints	191
Figure 5.28: Comparing rock bolt structural damage for 20-tonne and 30-tonne rock bolts with 0kN pretension and infilled shear interfaces	193
Figure 5.29: Representation of rock bolt damage for 30-tonne rock bolt with infilled shear interfaces and 0kN pretension	193
Figure 5.30: Comparing shear plane damage of 20-tonne and 30-tonne rock bolts with infilled shear interfaces and 0kN pretension	194
Figure 5.31: Comparing rock bolt hinge point and rock bolt damage for 20-tonne and 30-tonne rock bolts with 20kN pretension and infilled shear interfaces.....	195
Figure 5.32: Comparing shear plane damage of 20-tonne and 30-tonne rock bolts with 20kN pretension and infilled shear interfaces	196
Figure 6.1: Illustration of shear regions	201
Figure 6.2: Demonstration of complex raw pretension profile for infilled 30-tonne 20kN pretension samples	204
Figure 6.3: Comparison of the Fourier transform approximation to the raw data of the clean shear 20kN rock bolt with 10kN pretension	205
Figure 6.4: Determining the transition to the strain-softening region for clean samples.	207
Figure 6.5: Calibration of the strain-softening region using the α constant to ensure model agreement.	208
Figure 6.6: Challenges in simulating the transition zones between the regions for 20-tonne rock bolts with clean joints.....	209
Figure 6.7: 30-tonne rock bolts with clean joints presenting with seamless transitions between regions.....	210
Figure 6.8: Analytical simulation results for clean joint testing scheme	211
Figure 6.9: Determining the transition to the strain-softening region for infilled samples.....	213
Figure 6.10: Calibration of the strain-softening region for samples with infilled shear interfaces using the α constant to ensure model agreement	214
Figure 6.11: Analytical simulation results for infilled joint testing scheme	215

Figure 6.12: Challenges in simulating the transition zones between the regions for 30-tonne rock bolts with infilled joints	216
Figure 6.13: FLAC3D Coupling spring concept (Itasca, 2005).....	218
Figure 6.14: Shear behaviour of rock bolt elements (Itasca, 2005)	219
Figure 6.15: Single shear conceptual model (left) and model dimensions (right) ...	223
Figure 6.16: Results of the numerical simulation and experimental test for the 20-tonne rock bolt subjected to single shear.	224
Figure 6.17: Comparison of the numerical simulation and experimental test for the 20-tonne rock bolt subjected to single shear.	224
Figure 6.18: Double shear conceptual model (top) and model dimensions (bottom)	226
Figure 6.19: Experimental data, analytical model, and numerical simulation for 20-tonne infilled 0kN pretension sample.	227
Figure 6.20: Experimental data, analytical model, and numerical simulation for 30-tonne clean joint 0kN pretension sample.	227
Figure 6.21: Comparison of experimental data, analytical model, and numerical simulation for 20-tonne infilled 0kN pretension sample.....	228
Figure 6.22: Comparison of experimental data, analytical, and numerical models for 30-tonne clean joint 0kN pretension sample.....	230
Figure 6.23: Results of changing the host rock UCS and its impact on the shear force of the 30-tonne rock bolt.	232
Figure 6.24: Zoomed in comparison of the effects of host rock strength on the shear force profile of the 30-tonne rock bolt.	232
Figure 6.25: Results of changing the host rock UCS and its impact on the shear force of the 20-tonne infilled rock bolt	233
Figure 6.26: Zoomed in comparison of the effects of host rock strength on the shear force profile of the 20-tonne infilled rock bolt.....	233
Figure 6.27: Conceptual model of the rock bolt installed at an angle.....	234
Figure 6.28: Impact of the shear force profile of a 30-tonne clean joint rock bolt installed at an angle compared to the original test parameter.	235
Figure 6.29: Impact of the shear force profile of a 20-tonne infilled rock bolt installed at an angle compared to the original test parameter.....	235

Figure 6.30: Impact of the shearing speed on the 30-tonne clean joint rock bolt compared to the original test parameter. 237

Figure 6.31: Zoomed in comparison of the impact of shearing speed on the 30-tonne clean joint rock bolt compared to the original test parameter. 237

Figure 6.32: Impact of the shearing speed on the 20-tonne infilled rock bolt compared to the original test parameter. 238

LIST OF TABLES

Table 2-1: Types of cable bolts used in Australia (Rasekh, 2017)	13
Table 2-2 Different types of rock bolts used in Australia (MINOVA, 2021b, Jennmar, 2021, DSI-UNDERGROUND, 2021, MEGA-BOLT, 2021)	14
Table 2-3: Types of corrosion in steel (Aziz et al., 2013).....	16
Table 2-4: Susceptibility of glass types to acid attack (Myers et al., 2007)	17
Table 3-1: Experimental matrix for effect of pretension	70
Table 3-2: Experimental plan for reinforced concrete blocks with infilled joints	71
Table 3-3: UCS test results of the concrete used for double shear casting	79
Table 3-4: Brazilian testing of concrete used for double shear casting	79
Table 3-5: Grout UCS comparison between small-scale and large-scale samples. ...	82
Table 3-6: Comparison of fibreglass rock bolts of different design strengths (DSI-UNDERGROUND, 2021).....	99
Table 4-1: Rock bolt properties for clean shear system.....	110
Table 4-2: Summary of gradients at each stage of the shear profile curve and angle at the hinge point post failure.....	137
Table 4-3: Summary of peak forces and shear stresses of all samples	138
Table 4-4: Gradient profiles for zones one, two and 3 and peak axial force for all samples.....	141
Table 5-1: Rock bolt properties for infilled shear system.....	157
Table 5-2: 20-tonne Infilled rock bolts failure properties.....	165
Table 5-3: Summary of peak forces and shear stresses of all infilled samples.....	186
Table 6-1: Analytical estimates of shear and displacement parameters for clean shear testing scheme	212
Table 6-2: Analytical estimates of shear and displacement parameters for infilled shear interface testing scheme	213
Table 6-3: 20-tonne and 30-tonne rock bolt simulation properties.....	220
Table 6-4: System properties for the strata, shear joints, infill material and washers	221

ABBREVIATIONS

2D	Two-dimension
3D	Three-dimension
AROA	Applied Research of Australia
BSST	British Single Shear Test
DHD	Drill Hole Diameter
DST	Double Shear Testing
CNL	Constant normal load
CNS	Constant normal stress
ESCC	Environmental Stress Corrosion Cracking
FEM	Finite Element Method
FLAC	Fast LaGrangian Analysis of Continua
FSEPT	Field Short Encapsulation Pull Test
GRP	Glass-Reinforced Polymer
kN	Kilonewton
LSEPT	Laboratory Short Encapsulation Pull Test
MKI	Mark One
MKII	Mark Two
MKIII	Mark Three
MSST	Megabolt Single Shear Test
RBA	Reserve Bank of Australia
SSS	Single Shear Strength
SWA	Safe Work Australia
UCS	Uniaxial Compressive Strength
UDEC	Universal Distinct Element Code
UTS	Ultimate Tensile Strength

LIST OF SYMBOLS

u	Displacement
u_e	Fourier series elastic region displacement matrix
u_n	Fourier series displacement matrix
$u_{ss,p}$	Displacement at strain-softening region peak force
u_{yield}	Displacement at elastic yield force
u_{peak}	Displacement at peak force
$u_{failure}$	Displacement at failure
K	Rock bolt axial stiffness for FLAC3D
K_e	Elastic stiffness of the rock bolt
K_p	Rock bolt plastic stiffness
K_f	Rock bolt failure gradient
ΔU	Change in energy of the system
Q	Original energy of the system
W	Work done by the system
τ	Shear stress (Barton model)
τ_{Stress}	Shear stress
τ_e	Elastic deformation
τ_{RB}	Rock bolt work contribution to the strain-softening region
τ_i	Shear interface shear force contribution
τ_{ss}	Strain-softening region shear force equilibrium value
$\tau_{ss,p}$	Peak strain-softening shear force
α	Initial applied pretension
σ_c	Unconfined compressive strength
σ_e	Matrix of the elastic region shear Fourier approximation
σ_n	Normal stress (Barton model)
σ_n	Matrix of the shear Fourier approximation
σ_m	Confining stress
\emptyset	Shear interface fiction angle
\emptyset_b	Angles of sliding friction

c	Shear interface cohesion
A	Rock bolt cross-sectional area for FLAC3D
A_s	Shear face surface area
E	Young's modulus
L	Length
p	Rock bolt perimeter
d	Rock bolt diameter
d_n	Peak dilation angle
r	Nominal rock bolt radius
ε_{pl}	Rock bolt plastic strain
ε_{pl}^{ax}	Rock bolt axial plastic strain
θ_{pl}	Rock bolt average angular rotation
$F_{Shear\ plane}$	Shear force exerted at each shear interface
$F_{Double\ shear}$	Total recorded shear force

CHAPTER 1: INTRODUCTION

1.1 Background

The mining industry is one of the largest industries in Australia. According to the Reserve Bank of Australia, the mining industry has seen a dramatic increase in its industry share from fifth position at 6.3% in 2016 to 11.1% in 2020, placing it as the second largest industry in Australia (Reserve Bank of Australia, 2020). Unfortunately, the mining industry also has the third highest fatality rate of 3.7 fatalities per 100,000 workers as indicated by Safe Work Australia (2021), surpassing the construction industry by 1.7 and trailing behind the transport industry and the agriculture industry which reached 5.9 and 11.2 respectively in 2018. With the current growth of the mining sector there is a need to prevent the increase of fatalities and it is the responsibility of the employer to provide a safe work environment. A safer work environment can be achieved through better design and understanding of environmental factors such as failure mechanisms and conditions that contribute to instability. One such way failure conditions and instability can be minimised is the correct installation of tendons. The implementation of tendons is highly efficient and cost effective technology that can be implemented as primary or secondary support systems. Primary support systems, usually rock bolts, are installed during excavation and aim to maintain or increase the strength properties of the rock mass. Secondary support systems are used to supplement the primary supports and can be implemented by either a passive or active method. Cable bolts are a commonly used as secondary supports and are widely implemented throughout Australian mines. Most mines throughout Australia have invested in tendon installation systems to provide stability to the work environment and as such rock bolts and cable bolts are synonymous with ground supports. It is therefore essential to develop an extensive understanding of the support properties of tendons. This facilitates optimised ground support design systems which can increase the inherent stability of the excavation environment. Increased excavation stability can enable a safer workplace for members of the mining operation and ultimately reduce the fatality rate of the mining industry.

1.1.1 Rock bolts

Rock bolt systems were first introduced for use as mining ground supports during the late 1940s (Mark, 2017). Within a year of inception, rock bolts tested in soft rock

systems proved to be highly successful by improving safety for heading works and allowing for better utilisation of excavated areas (Conway, 1948). However, the extent of their capabilities was not abundantly clear and as a result, rock bolts were classified as secondary support systems to propping. During the following decades it was identified that rock bolt performance was influenced by *in-situ* axial and shear stresses (Haas et al., 1974), and subsequently propelled research on axial and shear load transfer mechanisms (Farmer, 1975, Tang et al., 1985). As a result of these studies the vast capabilities of rock bolts were recognised and they became accepted as primary support systems in both active and passive applications (Peng et al., 1984, Brady et al., 1985, Gay, 1980). Further investigations have resulted in the classification of specific bolt support mechanisms including wedge/flake stabilisation, arching, tieback, suspension and forepoling (Li, 2017b, Tadolini et al., 2017). In light of the widespread implementation of rock bolt systems, numerous design variations were conceived to meet explicit criteria. The development of mechanical, resin and grout anchorage allowed for greater variation in rock bolt selection to meet specific operational requirements (Rajapakse, 2008). In addition to the axial and shear forces applied to rock bolts, the mineralogy of localised *in-situ* rock masses had a significant impact on the performance of metallic based rock bolts as a result of corrosion (Aziz et al., 2013). Corrosion has the potential to cause strength reductions of up to 39%, and can induce failures by three key modes; uniform corrosion attack, pitting corrosion and stress corrosion cracking (Hassell et al., 2004) and as a result can make metallic rock bolts a non-viable support option.

1.2 Research problem, aim and objectives

1.2.1 Research problem

Projects implementing rock bolt strata support systems need to evaluate each property of rock bolts to determine suitability and optimum performance. Due to environmental and operational constraints of metal rock bolts, alternatives such as fibreglass rock bolts can provide unique benefits to the system, but their capabilities need to be further explored. Currently there is limited understanding of the behaviour of fibreglass rock bolts, primarily when subjected to shear conditions and further research is required. Therefore, this research was conducted to improve our current understanding of the performance of fibreglass rock bolt systems under shear.

1.2.2 Research aim and objectives

The aim of this research is to model the shear failure mechanisms of fibreglass rock bolts for the use in advancing mining and civil applications. This research will involve extensive experimental work to determine the shear properties of fibreglass bolts combined with analytical models and numerical simulations utilising the finite difference software FLAC3D. Furthermore, conducting a numerical and analytical study will provide a simulation of the shear failure performance of fibreglass rock bolts.

The research objectives of this study are:

1. Critically investigating previous research studies on shear and axial load transfer mechanisms of anchor bolts,
2. To determine an appropriate experimental design and testing scheme to suitably test the shear performance of fibreglass rock bolts,
3. Undertake an experimental study to determine the shear strength of two fibreglass bolts under varying pretension values for clean joint interfaces:
4. Undertake an experimental study to determine the shear strength of two fibreglass bolts under varying pretension values for sandy clay infilled joint interfaces,
5. Develop an analytical model to predict the shear performance of fibreglass rock bolts subjected to pretension and clean and infilled joints,
6. Numerically simulate the shear behaviour of fibreglass bolts for clean and infilled joints and conduct a sensitivity analysis for various shearing conditions.

1.2.3 Research questions

In order to achieve the above objectives, the following key research questions will guide this research, developing a deeper understanding of the shear strength properties of fibreglass rock bolts used for strata reinforcement in both mining and civil applications:

1. How does the application of pretension affect the shear load transfer mechanism and final shear performance of fibreglass rock bolts?
2. What impact does various tensile strengths of fibreglass rock bolts have on the shear performance of fibreglass rock bolts with clean shear interfaces?

3. What are the impacts of infilled shear interfaces on the shear load transfer mechanisms and ultimate shear performance of fibreglass rock bolts?
4. Can analytical and three-dimensional numerical simulations accurately map the shear performance of fibreglass rock bolts incorporating the effects of the strata strength and infilled joints? Validating outputs against data gathered through experimental testing, and
5. How does varying the host UCS, rock bolt installation angle and shear speed impact the shear load transfer and ultimate shear failure of the fibreglass rock bolt?

1.3 Research justification

Procedures used for evaluating the shear strength of fibreglass bolts are based on various international standards such as American Standards of Testing Materials (1991) and the British Standard (2009). In general, these standards are invariably interrelated; however, the suitability of any particular standard, for testing the shear strength of the fibreglass bolt, will depend on the purpose, host medium properties and rock bolt pretension. The outlined standards, while commonly utilised, potentially have significant shortcomings and design flaws. The British standard testing apparatus for example simulates non-realistic testing environment where the rock bolt sample is bonded to a steel housing. Additionally, the testing equipment contaminates the results due to the unrealistic contact forces between each half of the testing frame (Aziz et al., 2015c). Currently, testing conducted under a standards scheme aims to examine the bolt's ideal properties. They do not account for load transfers between the strata, grout, rock bolt and tensioning nut, in addition to, defects within the strata, such as, clean, infilled, and angled discontinuities.

1.4 Research approach

This study will be conducted using experimental and theoretical pathways shown in Figure 1.1 with iterative verification whereby the numerical simulation will be validated against experimental data. Thus, the experimental data will be the foundation of the numerical simulation. Furthermore, the developed numerical model will be incorporated to evaluate the performance of rock bolts subjected to various parameters through sensitivity analysis using FLAC3D finite difference software.

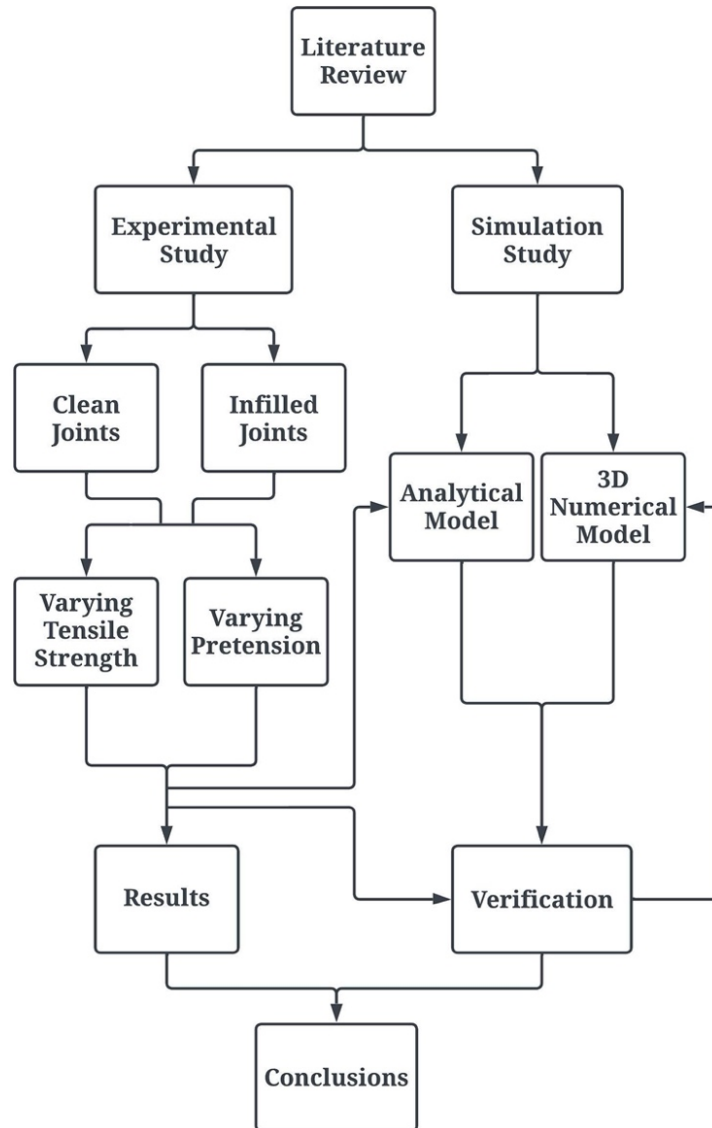


Figure 1.1: Research flow diagram

1.5 Structure of the thesis

This thesis consists of seven chapters followed by a list of references and an appendix. Outlined below is the structure and key components of each chapter. Figure 1.2 illustrates the contents of each chapter.

Chapter 1 introduces the background research for this study highlighting the thesis' key objectives and structure. This chapter also outlines the research questions that were used to achieve the research objectives.

Chapter 2 presents a comprehensive literature review on the history and general information about tendons and addresses objective one of the research. Included is a

detailed explanation of experimental, field, numerical and mathematical studies highlighting the performance of rock bolts subjected to tensile, pull, single shear and double shear tests. This chapter highlights the fundamental principles of the load transfer mechanisms of rock bolts and their ultimate strength. Finally, chapter two introduces fibreglass rock bolts outlining the key differences to conventional metal rock bolts. The studies selected for review focus on attempting to replicate shearing conditions in the laboratory and providing numerical and analytical simulations of shear testing.

Chapter 3 discusses equipment and design of the experimental plan used to complete testing. Additionally, chapter three will outline the modified testing apparatus that will be used to determine the shear strength properties of fibreglass rock bolt and the key material properties of the test system. This chapter discusses the material properties of the clean discontinuity sample set including the fibreglass rock bolts, the grout used for anchoring, and the concrete used to simulate strata. Finally, chapter three outlines the system properties of the novel infilled discontinuity system including the shear interface between the infill material and strata for varying normal loads as well as the internal shearing properties of the infill material.

Chapter 4 presents the results of the shear strength of fibreglass rock bolts subject to host strata containing clean discontinuities. This chapter reports on the results of rock bolts subject to constant loading with pretensions of 0kN, 10kN, 15kN and 20kN as indicated by objective two. The chapter also highlights the effect of different strength rock bolts outlined in objective three.

Chapter 5 introduces the novel experimentation of shearing strata containing multiple infilled discontinuities while reinforced by fibreglass rock bolt and addresses objective four. Finally, chapter five also addresses objective three by testing rock bolts of different strengths subjected to constant loading and rock bolt pretensions of 0kN, 10kN, 15kN and 20kN.

Chapter 6 proposes an incremental elasto-plastic constitutive model as part of objective five and is used to simulate the shear behaviour properties of fully grout encapsulated fibreglass rock bolts. This model simulates the rock bolts' behaviour throughout the elastic region, strain-softening region and ultimate failure zone using Fourier series. Chapter six also addresses objective six by demonstrating the numerical model of rock bolts subjected to double and single shear and sensitivity analysis

through the use of Fast Lagrangian Analysis of Continua (FLAC) with the results presented in FLAC three dimensional simulations.

Chapter 7 draws together chapters three, four, five and six by highlighting the key findings from the literature review in chapter two and the current study on fibreglass rock bolts subjected shear and infilled discontinuities. This chapter presents a summary of the findings and conclusions of this research study and provides recommendations for future studies.

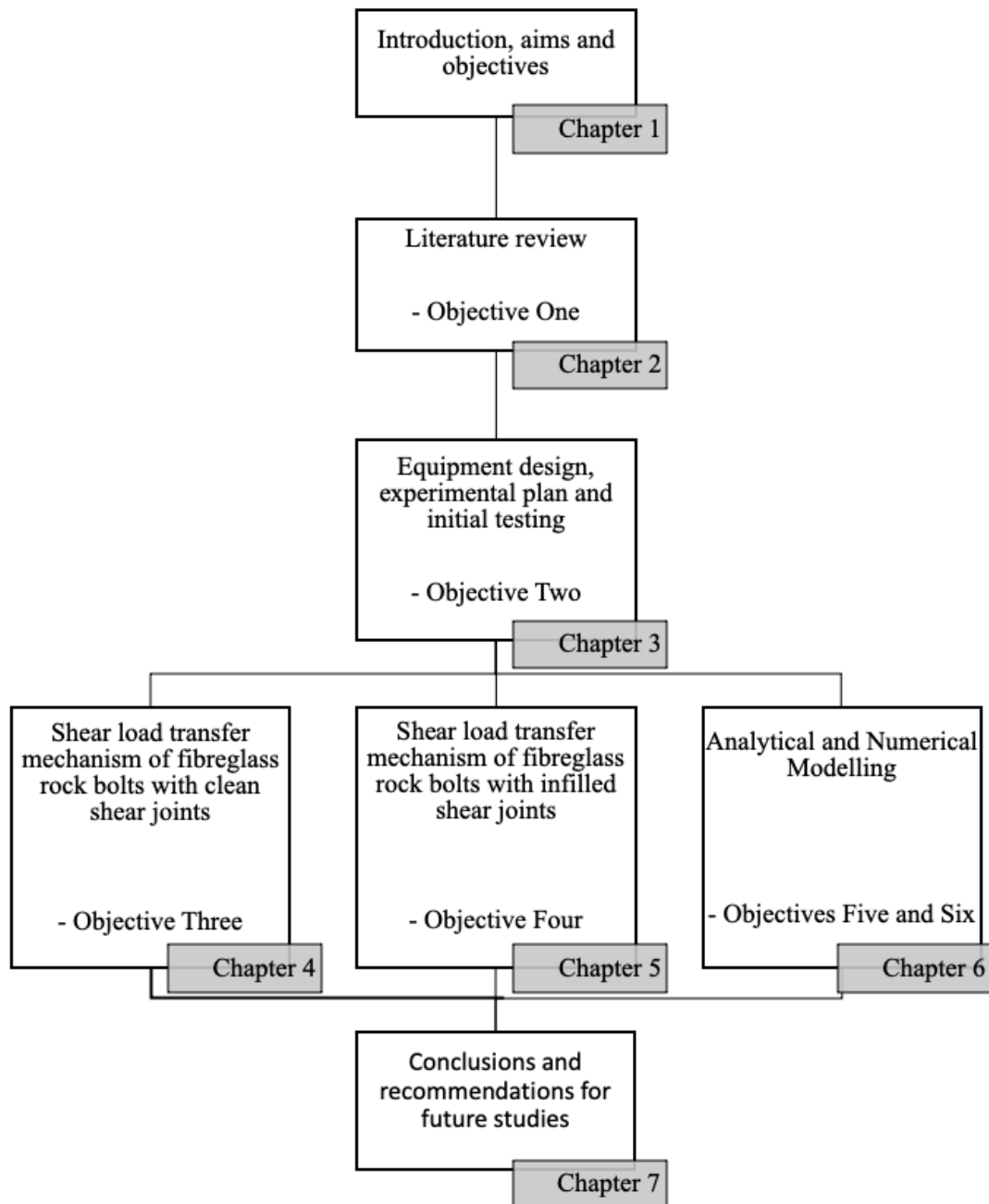


Figure 1.2: Thesis structure

1.6 Scope and limitations

The scope of this research is to establish the shear behaviour of fibreglass rock bolts encapsulated in jointed rock masses. In order to ensure the relevance of this research, the fibreglass rock bolts and anchoring grout used were chosen due to their wide use by industry. The two rock bolts selected were 20-tonne and 30-tonne dowels and in order to maintain standardisation through testing conditions, the selected rock bolts were of identical external dimensions and rib profiles. The grout selected was MINOVA's generic HS Stratabinder cementitious grout. Three series of tests were carried out in order to determine the effects of pretension, rock bolt strength and impacts of joint discontinuity properties. Due to the nature of the study, there were several notable limitations.

- Samples could not be tested *in-situ* due to the unpredictability of naturally applied loads and limitations to sensor technologies,
- Due to safety and equipment limitations only downsized samples with single rock bolts were utilised. The combined sample weight was in excess of 200kg and therefore required specialist lifting equipment,
- Numerical models were unable to simulate systems incorporating pretension due to software limitations. As a result, all numerical simulations were based on systems with 0kN pretension.

1.7 Summary

This research is comprised of comprehensive experimental, analytical and numerical analysis in order to explore the complex interaction of fibreglass reinforcing elements and strata. Fundamental aspects of the rock bolt system such as bolt strength, pretension, load rate, and infilled properties were controlled and altered. A modified double shearing equipment was developed and commissioned allowing the observation of the key aspects of the loading process. The outcome of this thesis gives insight into the shear load transfer behaviour of fibreglass rock bolts subject to clean and infilled discontinuities.

CHAPTER 2: LITERATURE REVIEW

2.1 Introduction

This chapter introduces and discusses tendons used for strata control outlining: the various types of tendons, their designed purpose and the load transfer mechanisms present in their respective design environment through an extensive review of experimental studies.

Tendons are used as part of support systems to stabilise strata and are divided into two main categories: cable bolts and rock bolts. All forms of tendons interact with the rock mass by altering intrinsic properties of the strata to ensure a self-supporting mass. The method of tendon reinforcement has been adopted by industry for several decades. In 1948, Conway (1948) discussed field studies of the impact that anchoring design had on the performance tendons. Tendons have become popular and cost-effective products for ground control by ensuring system safety and design longevity in both mining and civil applications. Currently, tendons are used throughout the mining industry due to their cost effectiveness, versatility and ability to be implemented with all mining excavation methods. Tendons are typically installed in underground mining excavations when there is a need to maintain tunnel integrity such as access shafts, roadways and ventilation tunnels, however, the application of tendons are not limited to underground strata control. When comparing open cut with underground operations there can be vast differences in excavation methods and stability requirements. However, due to the versatility of tendons, the technology is also utilised for slope stability, such as maintaining or increasing pit highwall stability. Tendons are similarly used in civil engineering projects, providing necessary reinforcements for slope stability, tunnel reinforcement and dam stabilisation.

2.2 Background to tendons

The name tendon is a generic assignment to a group of ground support systems that require the insertion of a bolt into the strata, they are implemented as either passive or active systems (Elrawy et al., 2020). Active tendon systems directly alter the supportive properties of the rock mass from the time of installation increasing the installed area's ability to resist movement and failure. Passively installed tendons on the other hand have little initial impact on the surrounding rock mass. They require the strata to fail prior to engaging with the rock mass, enabling the reinforcement.

Depending on the geotechnical properties of the rock mass and the project design requirements, it can be sufficient to implement one of these support systems. Areas of weaker strata systems, high personnel or equipment activity, and or structurally significant zones may require the installation of both passive and active tendons (Hutchinson et al., 1996).

The implementation of tendons has a number of significant benefits over conventional pillar support systems. Hutchinson et al. (1996) outline the advantages as:

- Increased rock mass stability,
- Providing safer work environments,
- Ability to be installed in sections of complex shapes,
- Control rock dilation in certain conditions,
- Installation simplicity due to compact packaging and in the case of certain products also flexibility, and
- Integration with other technologies such as plates, straps, mesh and shotcrete.

There are several different anchorage and installation methods used for tendons. Early iterations of tendons utilised mechanical anchoring relying on the friction between the anchorage point and the rock mass as outlined by the proceedings of Conway (1948). While in most cases this was an improvement over traditional support systems this method had several disadvantages:

- The tendon could only experience one failure event before being rendered ineffective,
- The securing nut and the anchorage mechanism experienced the entirety of the stresses, and
- Improper preparation could result in failure to deploy the anchorage point.

Increase in the popularity of tendons resulted in continuing design improvements and innovations. One such innovation that addressed the shortcomings of mechanical tendons was the encapsulated grout or resin tendons as discussed by Farmer (1975). The method of encapsulating the length of the tendon successfully addressed the key disadvantages of mechanically anchored tendons.

Depending on the intended use of the tendons there are several different installation methods. The correct method depends on the intended use of the tendon and if they are installed as a post or pre-failure reinforcement system. Pre-failure reinforcement allows the tendon to maintain or increase the strength of the rock mass. Subsequently

post-failure installation takes place when the rock mass has succumbed to unconstrained displacement and as a result no longer maintains its initial shear strength (Windsor et al., 1992).

2.2.1 Types of tendons

Tendons are divided into two main categories: cable bolts and rock bolts. While both bolts provide strata reinforcement, their design implementations are different. Rock bolts are mostly installed as part of the active reinforcement system while cable bolts are installed for either pre or post reinforcement (Windsor, 1997). Cable bolts have become widely implemented throughout the Australian mining and civil industry as secondary support systems (O'Grady et al., 1994). Cable bolts were first implemented in the 1960s as grouted steel elements from recycled steel ropes and subsequent years saw design adaptations and innovations to address key support requirements. The initial cable bolt design was grossly ineffective due to the quality of the chosen material and their design. Recycled steel ropes were too smooth and limited the bond between the rock mass and the cable bolts, while the use of recycled materials resulted in highly inconsistent and unpredictable failure behaviours. Modifications such as double strands and button strands (Schmuck, 1979, Thompson et al., 1987) to unique nutcase strand cable bolts (Hyett et al., 1993) aimed to improve the interaction between the rock mass and the cable bolt. The incremental improvements were highly successful, and the cable bolts were deemed suitable for use as permanent support systems. With the growing number of designs Hutchinson et al. (1996) defined the cable bolt toolbox that illustrated the differences between the various cable bolt designs as demonstrated in Figure 2.1. While cable bolt designs improved, they still experienced failures highlighting the need to explore the failure modes of the cable support systems.




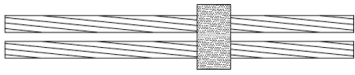









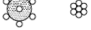










	Longitudinal Section	Cross Section	Product Image
Single plain strand			
Double plain strand with spacers			
Birdcaged strand			
Bulbed strand			
Ferruled strand			
Nutcaged strand			
Epoxy-coated or encapsulated strand			
Buttoned or swaged strand			

Figure 2.1: Cable bolt tool box (Hutchinson et al., 1996, DSI-UNDERGROUND, 2022, Jennmar, 2022, Minova, 2021a)

The design characteristics of cable bolts vary greatly depending on their required application. Rasekh (2017) discusses the variation between each property of commonly used Australian cable bolts and the impact on their performance. A summary of the findings is shown below in Table 2-1. Outlined are the variations of key factors such as: strand diameter, ultimate strand tensile strength, required drill hole diameter, lay length and elongation at strand failure.

Table 2-1: Types of cable bolts used in Australia (Rasekh, 2017)

Cable	Strand Diameter (mm)	UTS Strand (T)	Hole Diameter (mm)	Lay Length (mm)	Failure Elongation (%)
Indented	28	60	42	400	5-7
Plain	28	63	42	400	5-7
Plain SUMO	28	65	42	400	5-7
Indented SUMO	28	65	42	400	5-7
Plain Superstrand	21.8	60	42	300	6-7
Indented Superstran	21.8	60	42	300	6-7
Garford 15.2 mm Bulbed	2 x 15.2	53	35 - 51	180	6.5
Secura HGC	30	63	42	500	4.45
MB7	22	48	27	600	5-6
MW8.5S	24	58	28	600	5-6
Bowen Cable	21.8	60	42	-	-
MW9S Megastrand (Spiral, Bulbed)	31	62	42	600	5-6
MW9P Megastrand (Plain, Bulbed)	31	62	42	600	5-6
MB9S	31	62	42	600	5-6
MW10P	31	70	42	600	5-6
MB12	35	82	52	600	5-6

Similarly to cable bolts, there are a wide variety of rock bolt designs including mechanically anchored, fully encapsulated, cuttable and friction lock to name a few (Li, 2017a). Optimal bolt selection will depend on its intended purpose. Reinforcements installed to support longwall ribs must be cuttable in order to prevent damage to the shearer's head. Table 2-2 collates some of the various types of rock bolts commonly available for the Australian market and their key properties. The highlighted cable bolt properties can vary and are outlined as: bolt diameter, drill hole diameter (DHD), available length, anchorage type, ultimate tensile strength (UTS) and single shear strength (SSS). Additionally, Table 2-2 highlights the lack of knowledge regarding rock bolt parameters such as the single shear strength for several fibreglass rock bolt products.

Table 2-2 Different types of rock bolts used in Australia (MINOVA, 2021b, Jennmar, 2021, DSI-UNDERGROUND, 2021, MEGA-BOLT, 2021)

Rock bolt/Material	Bolt Diameter (mm)	DHD (mm)	Available Length (m)	Anchorage Type	UTS (kN)	SSS (kN)
Torque Tension Bolt Fibreglass	32	38 - 42	1.2 - 1.8	Resin	>500	>110
Injection Bolts GFRP	25	-	-	Expansion Sleeve	-	-
S20/200 GFRP	20	-	-	Grout/Resin	200	-
S22/250 GFRP	22	-	-	Grout/Resin	250	-
S25/350 GFRP	25	-	-	Grout/Resin	350	-
AH Solid Bar Steel	23.2	27 - 28	0.6 - 3	Resin	250	170
AROA GFRP	20	25	1.2 – 1.8	Resin	150 - 300	45 - 60
MB1F32G Fibreglass	32	42 - 55	2 – 5.7	Grout	420	140
MB1F32GRT Fibreglass	32	42 - 45	1.8	Resin	420	140
FBM Steel	47	43 – 45.5	-	Friction	340	-

2.2.1.1 Fibreglass rock bolts

Unlike steel, fibreglass rock bolts are a combination of two primary elements; linearly aligned glass fibres and thermo-set resin (Frketic et al., 2017). As such, the resultant rock bolt is comprised of a uniaxial structure that results in anisotropic performance (Maranan et al., 2015) in stark contrast to the isotropic matrix of metallic rock bolts.

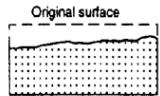
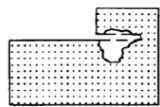
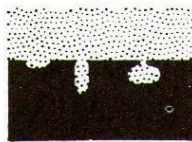
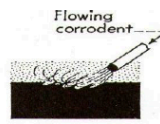
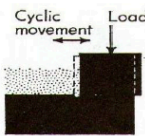

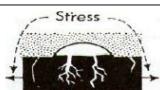
The effects of the differing structures are observed in the following key areas:

- Load transfer mechanisms,
- Lightweight,
- Application limitations (i.e. corrosive environments), and
- Cutability.

The study conducted by Aziz et al. (2015b) investigated the difference of isotropic and anisotropic rock bolts and concluded that axially loaded fibreglass rock bolts could achieve up to 85% of the ultimate tensile strength of steel. However, when loading the

sample perpendicular to the fibre direction (i.e. shear loading) the rock bolt's shear failure load averaged only 25% of the metallic rock bolt. The low shear performance of fibreglass rock bolts has limited their use to rib reinforcements (Li et al., 2016). Despite reduced performance limits to that of metallic rock bolts, fibreglass rock bolts possess significant benefits to their metal counterparts: including cutability and corrosion resistance. During coal extraction, rib supports are often removed with the advancement of shearers. Fibreglass rock bolts are often chosen over metallic rock bolts as the shearer heads can safely cut the fibreglass rock bolts without inflicting damage during the extraction (Gilbert et al., 2015). Additionally, studies conducted by Hassell et al. (2004), Spearing et al. (2010) and Aziz et al. (2013) outlined the detrimental effects of corrosion on metallic rock bolts and their susceptibility to such environments. Aziz et al. (2013) outlined the key forms of corrosion impacting steel as uniform, localised, mechanically and environmentally assisted degradation. The researcher further categorised and described the forms of corrosion as shown in Table 2-3. Due to the non-metallic nature of fibreglass rock bolts, they demonstrate an improved level of resistance to corrosive environments. As a result, fibreglass rock bolts are commonly implemented as supports in highly corrosive environments such as coal mines.

Table 2-3: Types of corrosion in steel (Aziz et al., 2013)

Forms	Categories	Description	
Uniform	Atmospheric	Corrosion of material exposed to air and its pollutants.	
	Galvanic	Corrosion due to electrolysis	
Localised	Crevice	Localised corrosion occurring on confined, closely spaced metal to metal or non metal to metal component surfaces. It is localised corrosion occurring in small areas of stagnant solution in crevices on joints. Crevice corrosion can also occur as a result of differential aeration mechanisms.	
	Pitting	Highly localized corrosion occurring on a metal surface. Pitting is marked by the development of sharply defined holes "pits". Occurs as a process where the metal loss is accelerated by the presence of a small anode and a large cathode. A dangerous form of corrosion as it can cause failure where only small weight loss of metal is observed	
Mechanically Assisted Degradation	Erosion	The removal of a metal surface material by the action of numerous individual impacts of solid or liquid particles.	
	Fretting	Occurs as the combined wear and corrosion between contacting surfaces, when the motion between the surfaces is restricted to very small amplitude oscillations. Oxidation is the most common element in the fretting process.	
Environmentally Assisted Degradation	Corrosion Fatigue	The process in which a metal fractures prematurely under conditions of simultaneous and repeated cyclic stress loading. This is likely to occur at lower stress levels with fewer cycles than would be required in the absence of the corrosive environment.	
	Stress Corrosion Cracking	This is a progressive development and growth of brittle cracks in a metal due to the combined effects from localised corrosion and tensile stress.	
	Hydrogen Embrittlement	This results from the combined action of hydrogen and residual or tensile stress. This type of failure occurs in quenched and tempered high-strength steels. The presence of hydrogen in steel reduces the tensile ductility of the material	
	Bacterial Corrosion	Sulphate reducing bacteria (SRB) metabolising sulphate in anaerobic conditions produce the most common form of attack. The sulphate ions, as the waste product of such metabolism, react with the metal to give metal sulphides. A deposit of black iron sulphides results when iron is corroded in sulphate bearing water-saturated ground.	

However, fibreglass rock bolts are not immune to corrosive degradation and just like steel, fibreglass is impacted by environmental stress corrosion cracking (ESCC) (Hogg et al., 1983, Bergman, 2001). ESCC occurs when the fibreglass is subjected to both an applied load and a corrosive environment such as acid, resulting in premature failure (Myers et al., 2007). Table 2-4 demonstrates the performance in the form of weight loss of a variety of fibreglass products when subjected to acid for one day.

Table 2-4: Susceptibility of glass types to acid attack (Myers et al., 2007)

Glass type	Application	One day weight loss in 10% H ₂ SO ₄ (%)
E-glass	General purpose fibers	39
ECR-glass®	Used where acid corrosion resistance is desired	6.2
S-2 glass®	Used for reinforcement in composite structural applications which require stability under extreme corrosive environments	4.1
C-glass	Used for chemical stability in corrosive acid environments	2.2
A-glass	General purpose fibers	0.4

While there may be significant ESCC degradation to some fibreglass products, the impacts can be avoided by selecting the correct glass for the applications resulting in a potential 38.6% reduction in weight loss. Despite fibreglass sharing one of ten corrosion failure modes with steel, selecting the optimum fibreglass product significantly reduced the impact of ESCC. This resulted in fibreglass rock bolts being the optimum choice for corrosive environments. As outlined previously, several studies have addressed the corrosion response of various fibreglass types to acid exposure; however, there appears to be little research studying the effect of ESCC on the mechanical properties of rock bolts used in corrosive strata environments. Despite the lack of studies addressing ESCC, fibreglass rock bolts have been subjected to numerous other tests in an attempt to understand their strata reinforcement properties and the mechanism behind their failure. A majority of the studies focus on metallic rock bolts and cable bolts such as (Aziz et al., 2013, Aziz et al., 2016b, Chang et al., 2017). The increased mechanisation of coal mining and advanced geotechnical projects such as tunnelling have prompted new investigations and comparisons of fibreglass rock bolt systems.

2.3 Axial load transfer mechanisms

Tendons are subject to two main loading behaviours along their length: axial loading, and shear loading. Axial loads are the stresses acting along the longitudinal length of the tendon. As such, the primary component of axial forces are determined by vertical stresses and therefore, can be said that the principle component of axial stress is gravity (Nemcik et al., 2006). While the load transfer mechanisms are the tendon's response to axial loading, it is complicated and dependent on several factors. Despite similar

installation locations rock bolts and cable bolts present differing results to axial loading as a result of the differences in design. Cable bolts are comprised of numerous smaller strands that have an individual response to an applied axial stress. Additionally, the method of anchorage such as mechanically anchored or grouted cable bolts experience different applications of stresses. Mechanically anchored bolts receive the entirety of the load at the points of contact to the rock mass via the washer plate and nut and the anchorage point. Unlike mechanically anchored cable bolts, resin and grouted cable bolts are uniformly encapsulated and therefore can experience multiple failure zones. Predicting such interactions are more complex as there are multiple stress interaction zones; the rock mass and grout/resin interface and the grout/resin to cable bolt interface.

Unlike cable bolts, rock bolts are either a singular rod or tube and comprise of several different design characteristics that alter the behaviour of axial stresses along the tendon. Some unique design elements include uniform ridges along the tendon, alternating ridges, threaded surfaces, smooth surfaces and split set radial strength (Rajapakse, 2016). Despite the design differences between rock bolts and cable bolts, axial loading mechanisms are conceptually similar. Thus, the fundamental failure modes are interrelated. Hutchinson et al. (1996) provided an update to the failure modes outlined by Jeremic et al. (1983) to include five unique failures. Figure 2.2 below illustrates the five fundamental failure modes that impact the performance of bolt reinforcement systems. Rupture of the tendon as highlighted by tendon A where the applied load exceeds the tensile failure limit of the cable. Tendon B demonstrates 'bond failure' between the grout/tendon interface and occurs due to low bond strength within the interface. Grout column failure occurs when the shear strength of the grout is lower than the failure yield limits of interfaces and the bolt shown by tendon C. Lastly, tendon D and E demonstrate failure of the rock and rock/grout interface whereby the tendon is anchored in a soft and weak rock mass. This failure resulted in either the rock mass experiencing internal failure or the rock mass sliding along the grout/cable column.

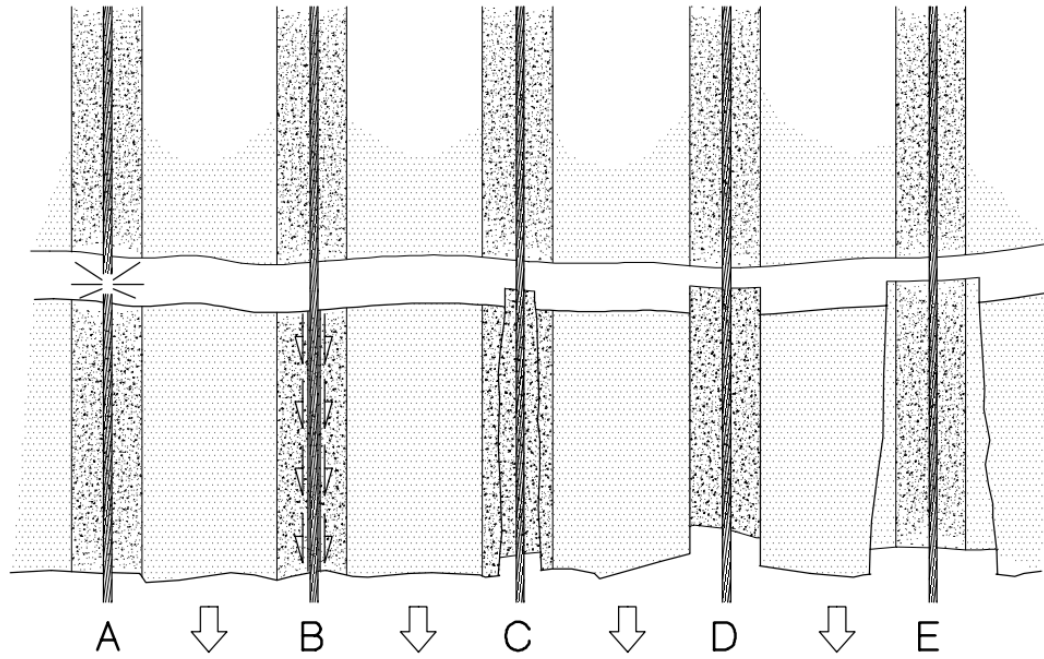


Figure 2.2: Bolt reinforcement failure modes (Hutchinson et al., 1996)

As such, the principal components for bolt reinforcements systems were defined as the rock, the element, internal fixture such as grout or resin and finally the external fixture (Windsor, 1997) as illustrated in Figure 2.3.

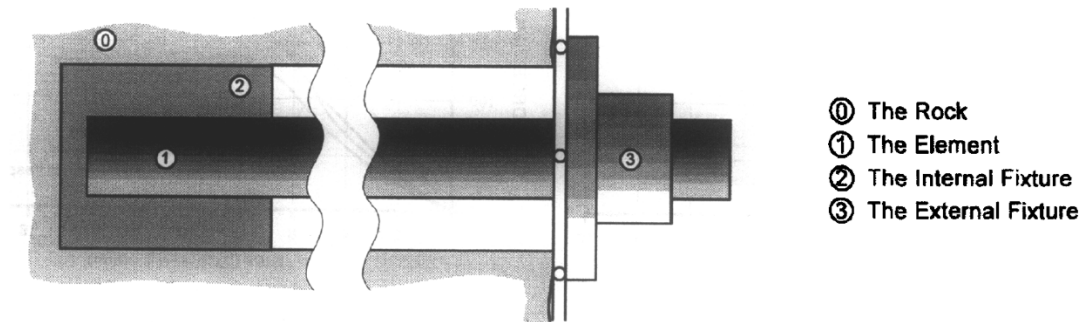


Figure 2.3: Reinforcing systems key components (Windsor, 1997)

Understanding of the key failure modes and principle components has resulted in researchers such as Hartman et al. (2003) outlining the tendon, rock mass and loading conditions as the three key factors influencing the load transfer along reinforcing elements and their overall performance. A more recent study conducted by Thompson et al. (2014) confirmed the validity of the Windsor et al. (1992) three load transfer mechanism categories. The three categories included: continuously mechanically

coupled for full resin/grout encapsulated bolt, continuously frictionally coupled for friction stabilisers such as split sets and discrete mechanically or frictionally coupled for mechanical anchors and short resin/grout encapsulation. Additionally, Thompson et al. (2014) illustrated the load transfer of an anchor subject to geological discontinuities and highlights the impact discontinuities have on the force distribution along a bolt, demonstrated in Figure 2.4.

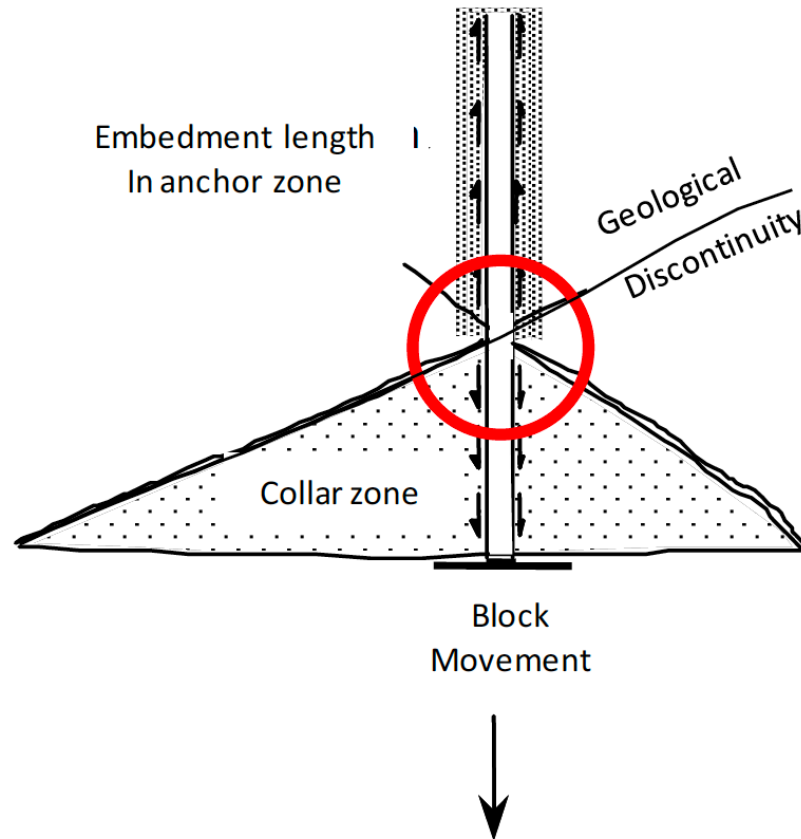


Figure 2.4: Ground reinforcement load transfer diagram (Thompson et al., 2014)

2.3.1 Experimental studies

The determination of axial load limits of rock bolt types has been a principal focus in identifying their optimum operational conditions, evident by the completion of extensive studies from the 1980 onwards (Peng et al., 1984, Feng et al., 2017, Aziz et al., 2016b, Ghadimi et al., 2016, Chang et al., 2017). As a result, a comprehensive understanding of the axial nature of rock bolts can be illustrated from studies including, the variations of grout and resin (Aziz et al., 2014), temperature effects (Li et al., 2017a), to the influence of corrosion on steel rock bolts (Aziz et al., 2013). Due to the

corrosive environments experienced by rock bolts (Spearing et al., 2010) fibreglass alternatives are actively used in high risk areas.

The methods in which axial failure occurs is universal across all types of rock bolts and cable bolts and is tested by multiple systems; tensile load application (VandeKraats et al., 1996), push testing (Aziz et al., 2016a) and pull-out testing (Mirzaghorbanali et al., 2017a). The axial load transfer mechanism occurs when a tensile force is applied to the rock bolt member causing shear displacement, as illustrated in Figure 2.5.

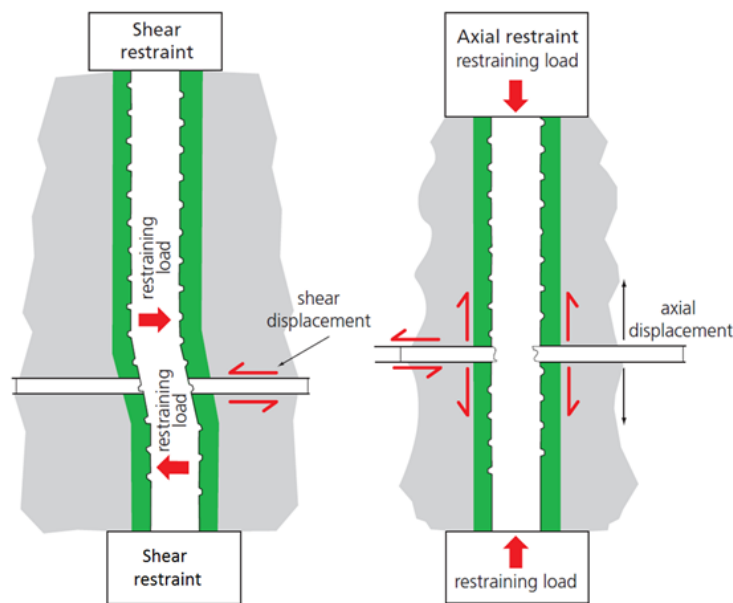


Figure 2.5: Rock bolt shear and axial failure modes (MINOVA et al., 2006)

The main system of measurement is the tensile load test as this determines the peak tensile load of a particular rock bolt where tests can be conducted onsite or in laboratories (Serbousek et al., 1987). Laboratory tensile testing has been achieved by securing both ends of the rock bolt in a universal testing machine with the centre portion unconfined and exposed (Gilbert et al., 2015). A tensile load was then applied until failure. As discovered by Gilbert et al. (2015), fibreglass rock bolts could achieve up to 85% tensile resistance to that of steel rock bolts. However, in addition to the peak tensile loads it was deemed beneficial to determine the load transfer capabilities of the tendons and was initially accomplished by the Short Encapsulation Pull Test (LSEPT) (Clifford et al., 2001). As a result, pull out testing was introduced to the British

Standards of testing (2009). The standard however has encountered errors, as it does not compensate for the rotation induced by spiral bound cable bolts. In order to alleviate this issue; the axially split double embedment pull test, developed by MINOVA (Mirzaghorbanali et al., 2017a), could successfully capture the increased extension resistance of spiral cable bolts.

The axial load transfer properties of rock bolts can be determined by both field-based analysis and experimental testing. Despite the widespread use of rock bolts, there are no standardised laboratory testing methods to determine their axial properties (Hagan et al., 2014). Therefore, researchers have developed several testing procedures to study the axial load transfer mechanisms. One method of study is in-field testing that can be further categorised by destructive and non-destructive testing procedures. The study conducted by Waclawik et al. (2019) adopted non-destructive testing methods to determine the amount of dilation that occurs in high stress conditions where the primary reinforcement were rock bolts spaced one meter apart. This was achieved by installing eighteen strain gauges along the length of the bolt as demonstrated in Figure 2.6.

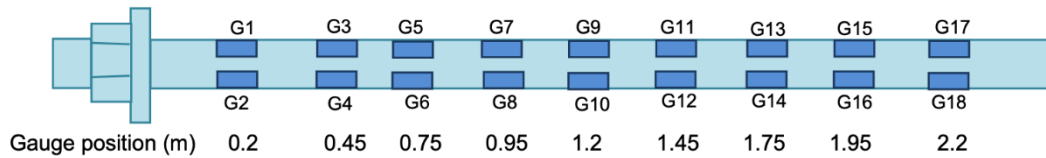


Figure 2.6: Rock bolt instrumented with strain gauges (Waclawik et al., 2019)

The efficient installation of the rock bolts resulted in rib deformations of 200-300mm with axial loads of 1–6.8 tonnes. Overall, the tested rock bolts were subjected to approximately 30% of the bearing capacity of the installed rock bolts. The study also concluded that in the specific conditions of the selected site; the average roof rock load remained below 10 tonnes.

Laboratory tests on the other hand typically are not constrained by the same limitations of field testing, resulting in the development of several testing methods. Studies have determined that rock bolts are sensitive to variations of the parameters of their securing interface, such as the grout bolt interface (Moosavi et al., 2005, Blanco Martín et al., 2013). Considering this new understanding and the ability to selectively manipulate properties in a laboratory environment, tests were developed to explore the influence

of key interface properties. Studies were subsequently conducted to test various parameters: rotation constraints, split segment, push testing, double embedment and short encapsulation scenarios as outlined by Rasekh (2017). The testing apparatus for each of the axial testing schemes have been utilised to test the axial performance of both rock bolts and cable bolts as performed by Hadj Hassen et al. (2015) and Thenevin et al. (2017).

2.3.1.1 Axial performance of bolts subjected to rotation constraints

The core design of reinforcing bolts when subjected to axial test schemes can have profound impacts on their axial performance. Properties such as the amount of spin of the fibres and strands of both fibreglass and metal rock bolts could interfere with their respective failure limits. Previous testing methods like the one conducted by Benmokrane et al. (1995) explored the fundamental axial performance of anchor bolts. As this study was conducted prior to the work of Moosavi et al. (2005), the impacts of interface properties would not have been known. Therefore, the testing apparatus used was designed to conduct a simple axial analysis of the bolts by incorporating the bolt, a load cell and an encapsulated length as depicted in Figure 2.7 and would be classified as a rotationally unconstrained pull-out test.

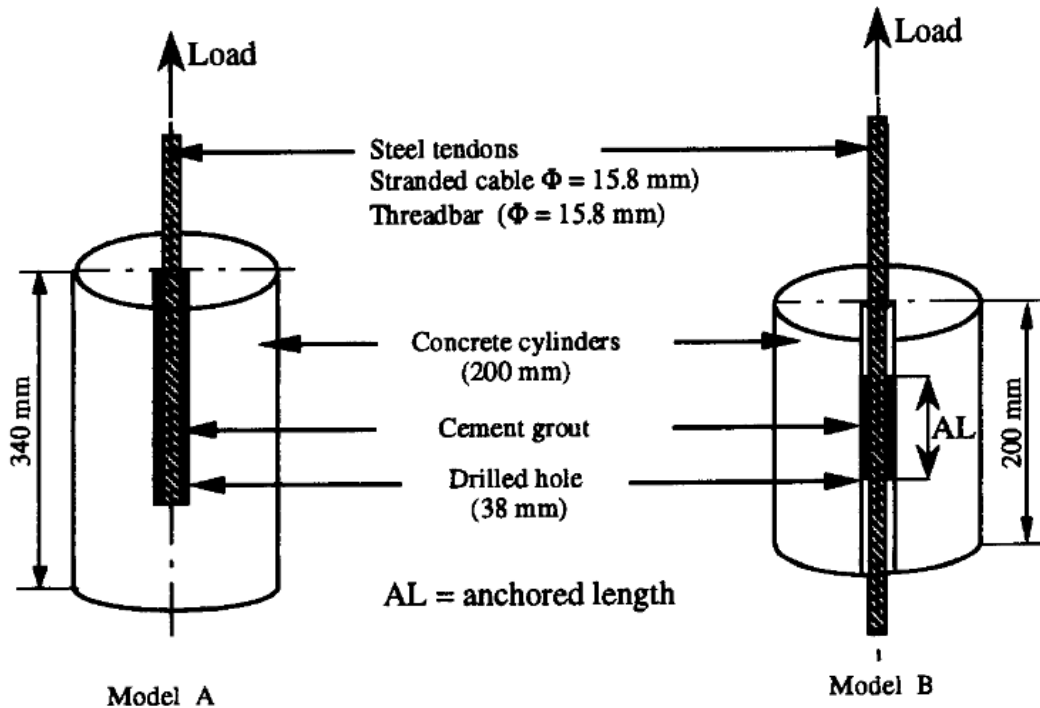


Figure 2.7: Axial test setup as conducted by Benmokrane et al. (1995)

The study was conducted on both threaded and stranded anchors. As the surface profile of these two products were different, their axial performance varied greatly as highlighted in Figure 2.8. It was later concluded that the product geometry that interacted with the grout had an increased influence on the performance of anchors at larger displacements.

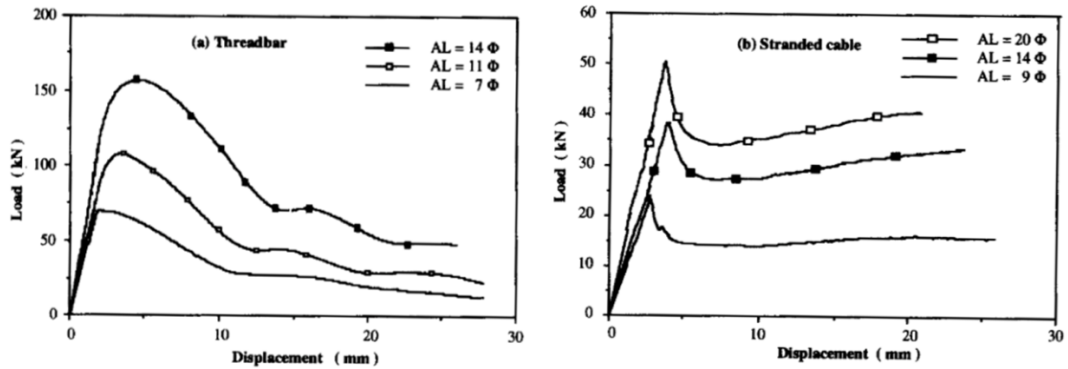


Figure 2.8: Axial load performance of threaded and stranded anchors with varying embedment lengths (Benmokrane et al., 1995).

Anchor bolts constructed with a spiralled design such that the fibres of a composite rock bolt or strands of a cable bolt were axially wound imparted unique behaviours during pull out testing to that of linearly aligned fibres and strands. Such design choices could result in either the bolt element rotating/unscrewing from the grout annulus or the fibres separating from the resin resulting in the behaviour like that of an outstretched spring (Thenevin et al., 2017). In a field environment this unravelling and spring phenomenon cannot occur and as a result is a shortcoming of laboratory based axial tests.

To mitigate the rotation during axial loading, new testing methods were developed. Martin et al. (2011) designed their axial test apparatus with a focus on addressing shortcomings of the previous testing apparatus. The resulting testing apparatus was therefore designed to perform studies on fully grouted rock bolts and cable bolts of varying parameters. These parameters included various installation parameters such as grout or resins properties, system properties including confinement pressures and embedment length and finally rock bolt design properties. The testing apparatus comprised of four key components: the sample chamber, bladder, piston assembly and load cell as highlighted in Figure 2.9. The main chamber housing of the rock samples

was encompassed by a bladder. This allowed the researcher to maintain a confining pressure during testing as well as providing the avenue to study the effects of confining pressures on the performance of rock bolts. Martin et al. (2011) also emphasised that this bladder system could also be utilised to measure the dilation of the samples during testing. However, the key feature distinguishing the Martin et al. (2011) testing apparatus from other test systems, such as the one utilised by Moosavi et al. (2005), was the cylindrical anti-rotation pins depicted by element 5 in Figure 2.9. These anti-rotation pins were used to minimise the influence of rock bolt unwinding during axial loading, providing a closer approximation to the axial response of rock bolts *in-situ*.

Due to the incorporation of the anti-rotation pins, the use of different rock bolt products and anchoring methods, direct comparison with previous studies was not possible. The results in Figure 2.10 highlight the performance of rock bolts subjected to the Martin et al. (2011) testing scheme. The average peak failure force occurred in excess of 170kN at approximate 3.5mm of average displacement, strikingly different to the performance of the rock bolts studied by Moosavi et al. (2005). During the Moosavi et al. (2005), rock bolts did not exceed an approximate average force of 120kN at an approximate average displacement of 3.5mm. However, as previously outlined it is not possible to conclude that the difference in peak failure load was a result of the anti-rotation modification.

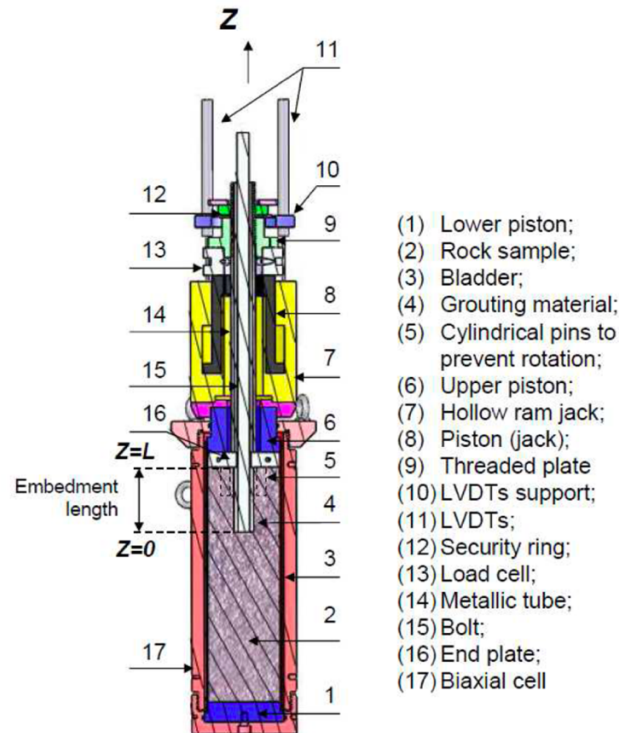


Figure 2.9: Cross-section of rotation controlled axial testing apparatus (Martin et al., 2011)

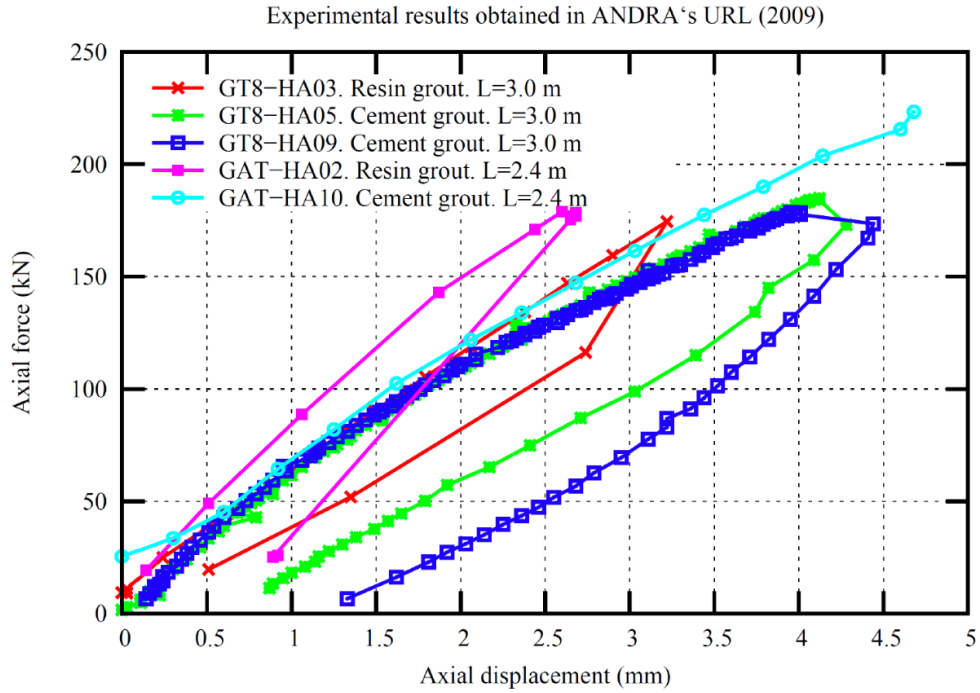


Figure 2.10: Pull-out test comparing rock bolts, resin and grout (Martin et al., 2011)

2.3.1.2 Short encapsulation performance of rock bolts.

Short encapsulated pull testing of anchor bolts fall into two test categories, the first focused on determining the optimum encapsulation length of *in-situ* bolts and the second was laboratory based testing to simulate the performance of bolts. Field short encapsulation pull tests (FSEPT) studies typically assess a different set of criteria when compared to laboratory short encapsulated pull tests (LSEPT) with early studies setting their primary goal of determining the optimum installation parameters for a given geology. Studies like the one conducted by BHP at their San Juan Coal Mine (Pile et al., 2003, Chugh et al., 2016) set out to evaluate the anchorage capacity of their fully grouted bolting systems. Unlike LSEPT, completing a FSEPT study only required simple hydraulic pull testing apparatus consisting of a load frame, hydraulic cylinder, pump and displacement sensor as illustrated in Figure 2.11. The study conducted by Pile et al. (2003) utilised this testing method to evaluate the impact the grout annulus and anchorage length have on the performance of their bolting system. The testing scheme evaluated a range of installation configurations as depicted in Figure 2.12. It was concluded that the length should be sufficient to reach high anchorage layers but not extend further, however due to environment and installation variabilities it wasn't possible to determine an optimum grout annulus utilising *in-situ* methods.

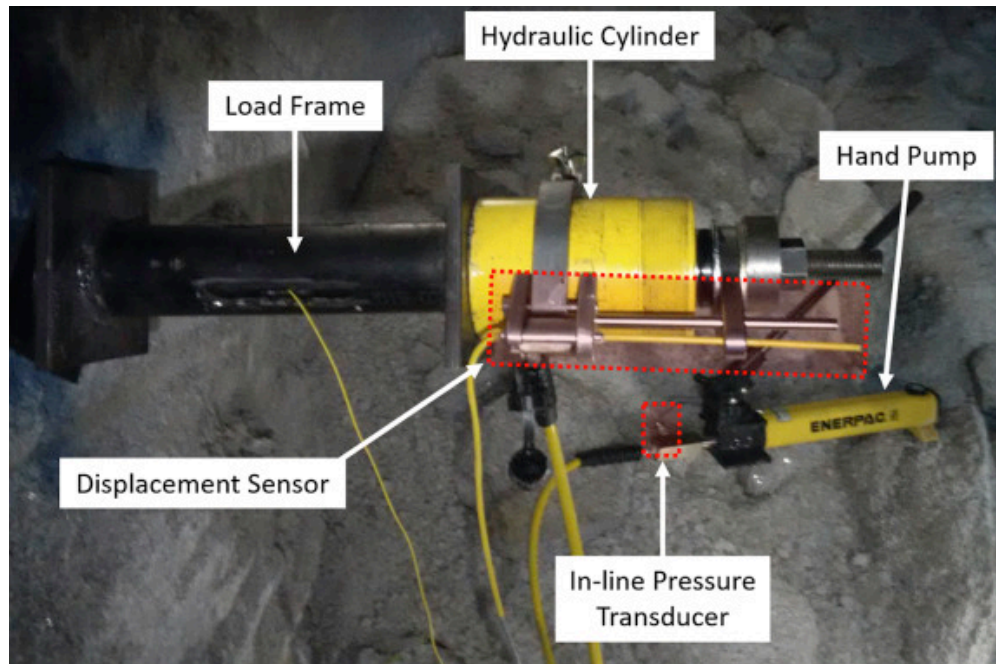


Figure 2.11: In-situ hydraulic pull test apparatus (Forbes et al., 2020)

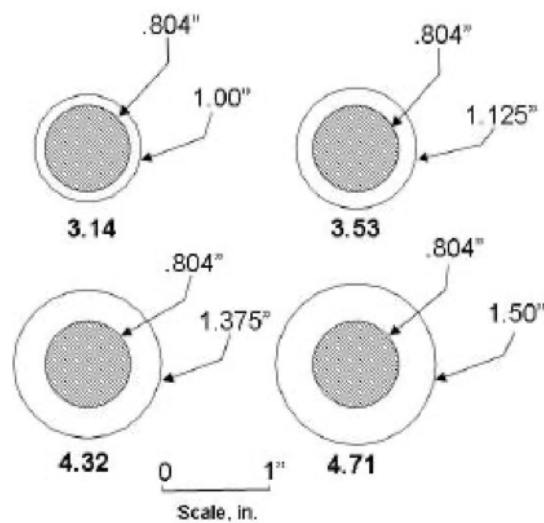


Figure 2.12: Grout contact surface for a bolt with a diameter of 7/8th inch (Pile et al., 2003).

Other studies conducted by Craig et al. (2013) evaluated the performance of anchorage methods focusing on the impact, reaming, over drilling and resin mixing has on the pull out performance of rock bolts. Rock bolts were all installed with a reduced length resin capsule of 200 – 300mm, approximately 20% of the typical installation length with a set of rock bolts prepared utilising under mixed resin, standard resin mixing and over mixed resin. Selected sample sets were installed using a 45mm reaming process; with or without 50mm over-drilling as highlighted in Figure 2.13.

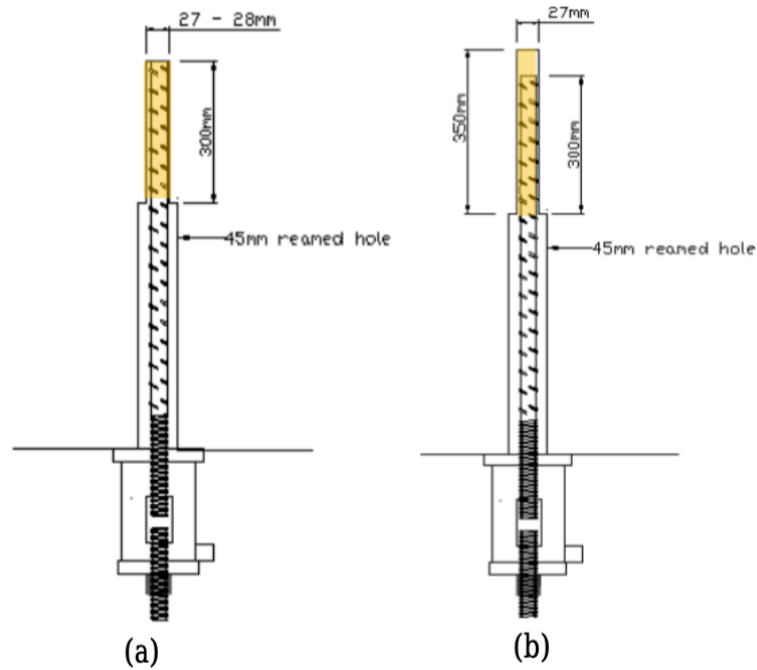


Figure 2.13: (a) Rock bolt installed with reamed and standard length (b) Rock bolt installed reamed and over-drilled (Craig et al., 2013)

It was discovered through the FSEPT study that over-drilling the rock bolts installation hole resulted in improved performance, attributed to the over-drill providing a catchment void for the resin film to settle. As there were no rock bolt or resin present in the over-drilled section, the film could no longer interrupt the load transfer process between the resin, rock bolt and strata.

A study conducted by Forbes et al. (2020) employed advanced fibre-optic sensors to map the bolts' behaviour during loading and further developing our understanding of the stress strain responses of rock bolts. To conduct the study two rock bolts with diameters of 19.05mm and 22.22mm were modified to carry an optical fibre with a sensing length of 1.4m as illustrated in Figure 2.14. The rock bolts were then installed using four different anchoring techniques. For the first technique rock bolts were installed with a full anchored length, the second was installed with an anchored length half that of the rock bolt's length, the third incorporated an anchored length one quarter the rock bolt length and finally the last was installed with a mechanical point anchor at the end of the rock bolt shown in Figure 2.15.

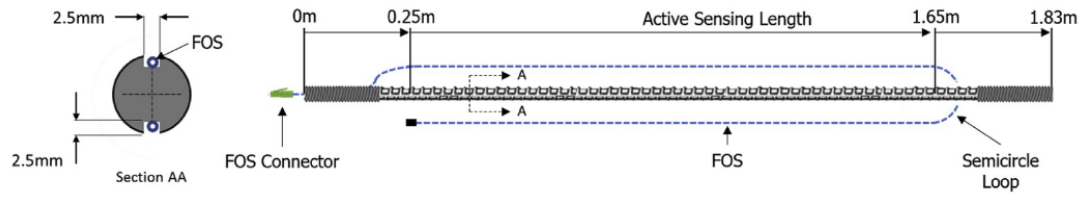


Figure 2.14: Diagram of rock bolt modified with fibre-optic cable (Forbes et al., 2020).

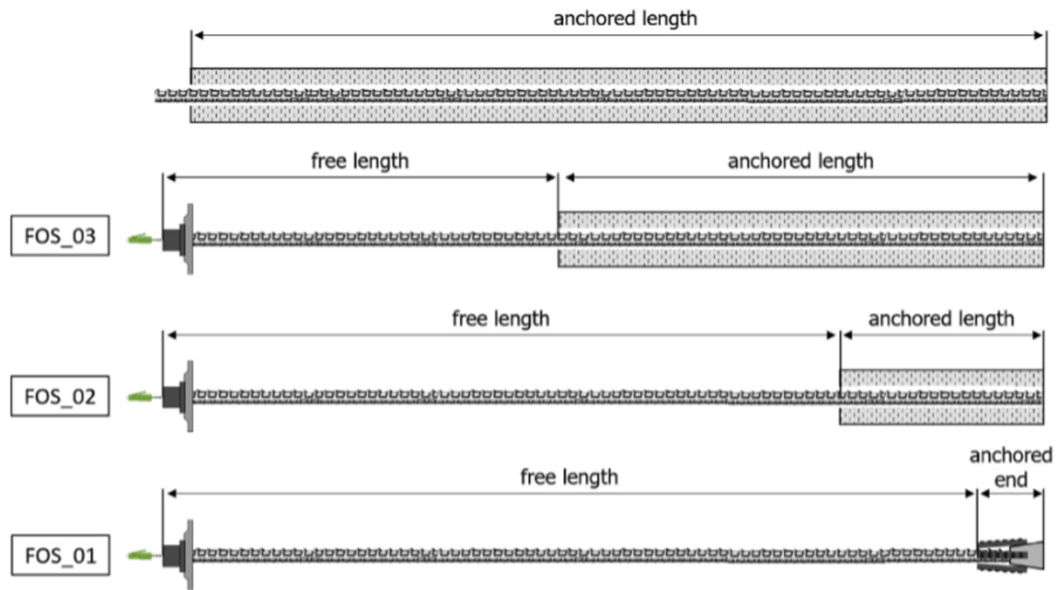


Figure 2.15: Rock bolt anchorage lengths tested by the pull test scheme (Forbes et al., 2020)

The optical fibre sensor was sensitive enough to record the strain response at 0.65mm intervals allowing Forbes et al. (2020) to map the impact rock bolt encapsulation had on its performance. Furthermore, it was determined that the rock bolts only experienced a notable variation in strain from the point where the anchored length began and culminating at the end of the rock bolt as shown in Figure 2.16, confirming that optical fibres could be used to determine borehole encapsulation.

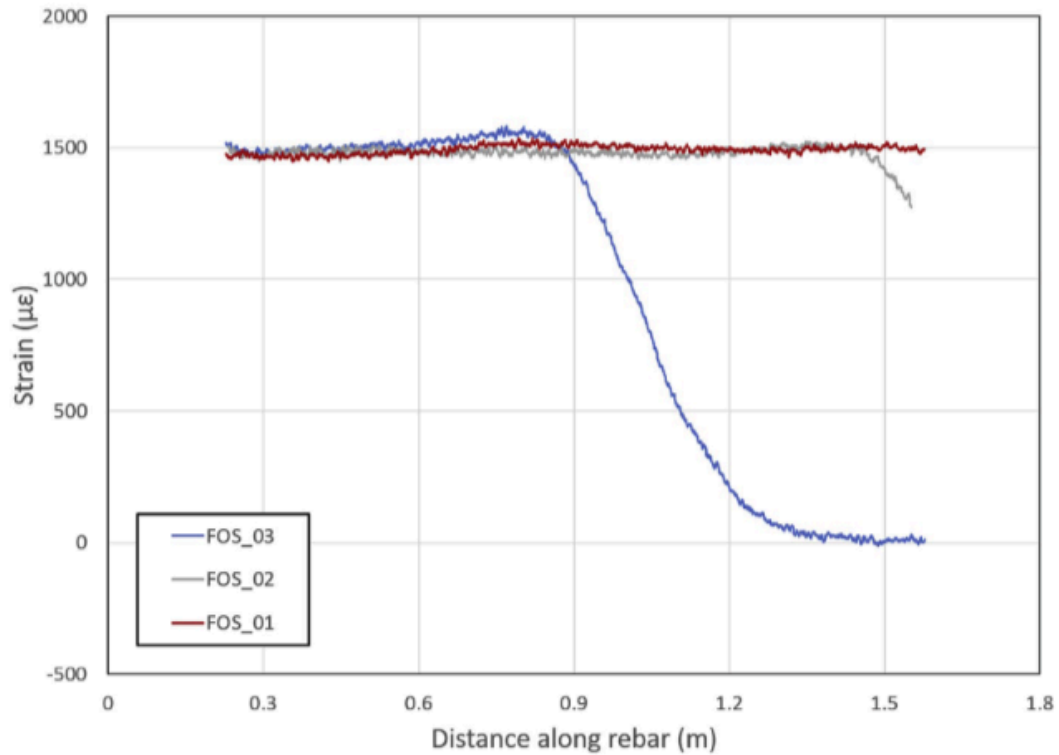


Figure 2.16: Strain distribution for rock bolts installed with various anchored lengths (Forbes et al., 2020).

Laboratory short encapsulated pull tests (LSEPT) have been developed to expand on the testing capabilities of the FSEPT by utilising system design flexibilities that are otherwise not possible in the field. Unfortunately, LSEPT present with a unique issue regarding variations in tortional stiffness between rotating and non-rotating ground support bolts, a phenomenon not present during field testing. The low tortional stiffness is a result of exposed lengths of bolts and impact the test capacities of the anchor bolts (Rasekh, 2017). As this impacted the bearing capacity of rock bolts Clifford et al. (2000) devised an apparatus to minimise the rotating phenomenon when testing resin secured rock bolts. The test system was comprised of a hydraulic jack, bearing plate, sandstone sample and a biaxial cell as shown in Figure 2.17. At the time the LSEPT provided the opportunity to test previous unknowns in rock bolt behaviours including impacts of pretension as well as confining pressures (Clifford et al., 2000).

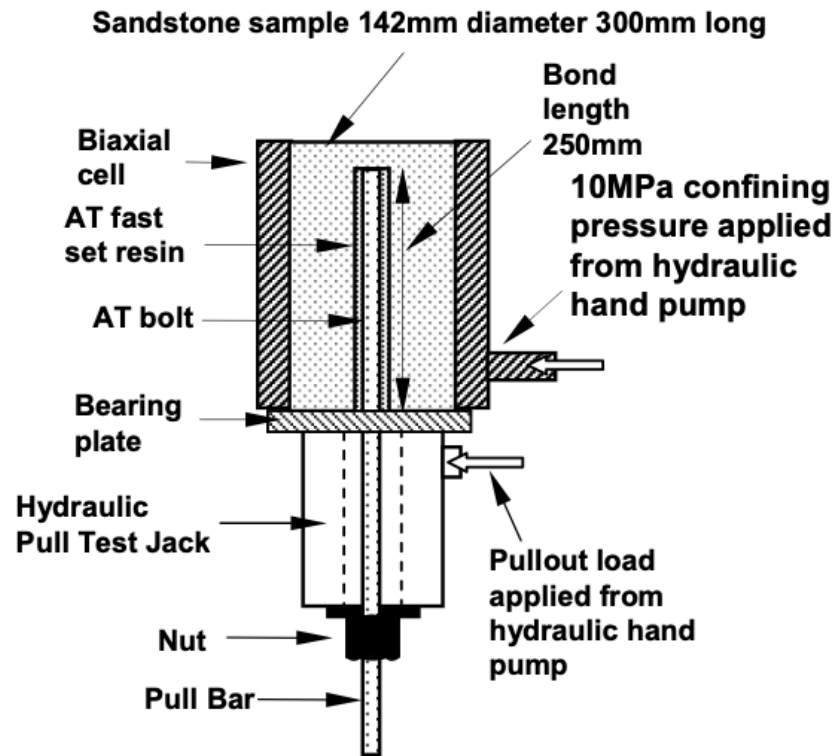


Figure 2.17: LSEPT apparatus schematic for rock bolts with resin anchoring (Clifford et al., 2000)

Despite the rock bolt LSEPT testing apparatus capabilities; notably its ability to conduct numerous field-like studies with varying parameters in the confines of a laboratory, its product range compatibility was limited to resin rock bolts and small diameter cable bolts. As a result Clifford et al. (2001) revised the design to allow for compatibility with varying cable bolt and grout designs. The overall design remained largely unchanged and utilised similar design concepts as evident in Figure 2.18. Unfortunately, the modifications meant the LSEPT lost some of its capabilities such as the application of confining pressure and measuring or constraining sample dilation (Holden et al., 2014). Notwithstanding, the modified LSEPT gained popularity and was widely utilised by many researchers such as Bigby (2005), who conducted comparisons with other pull test methods citing them as unsatisfactory and artificial. Similarly more recent studies conducted by Thomas (2012) evaluated the LSEPT's suitability when compared to test methods such as the double embedment test developed by (Hutchins et al., 1990), highlighted in Figure 2.19 and concluded that the latter was insufficient in studying the load transfer interface between the grout and the rock, while the cable LSEPT had the propensity for the free end of the cable to potentially unwind from the core.

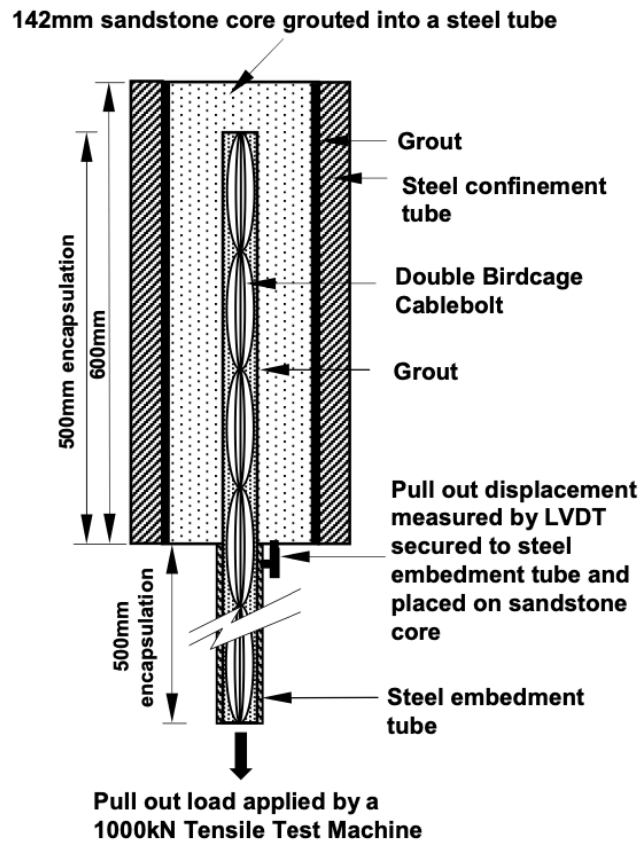


Figure 2.18: LSEPT apparatus schematic for grouted cable bolts (Clifford et al., 2001)

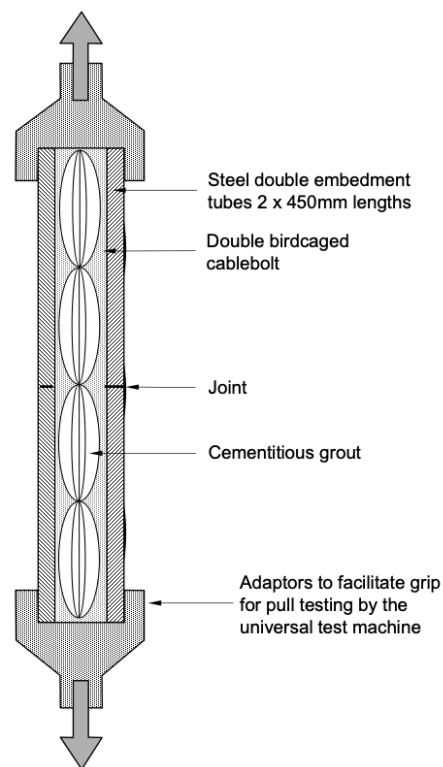


Figure 2.19: Cross-sectional diagram of axial double embedment test (Clifford et al., 2000)

The next iteration of the LSEPT was developed by Chen et al. (2016) to address the shortcomings of the Thomas (2012) variation. Some of the notable improvements included changes to the core housing, system diameter and locking mechanisms. The newer version of the LSEPT was now compatible with sample cores manufactured out of concrete as opposed to sandstone. This opened the possibility of testing the impact of host rock composition on the performance of the bolts as well as providing a more consistent testing environment across samples, eliminating natural rock variabilities between samples. The next notable improvement was the device's compatibility with varying borehole diameters. The modification enabled Chen et al. (2016) to study the impact of increasing the bore hole size from 42mm to 52mm. It was concluded that the increase in bore hole diameter improved the performance of the peak and residual strength of cable bolts embedded into a weak sample core. This compatibility with larger diameter holes resulted in the LSEPT being used almost exclusively for cable bolts. Finally, the housing design incorporated a number of locking nuts, locking keys and abutment plate with the goal of reducing the amount of rotation during loading. By reducing the amount of rotation during loading it was possible to lessen its impact on the torsional rigidity of the bolt and ensure minimal impact on the recorded bearing capacity of the tested product.

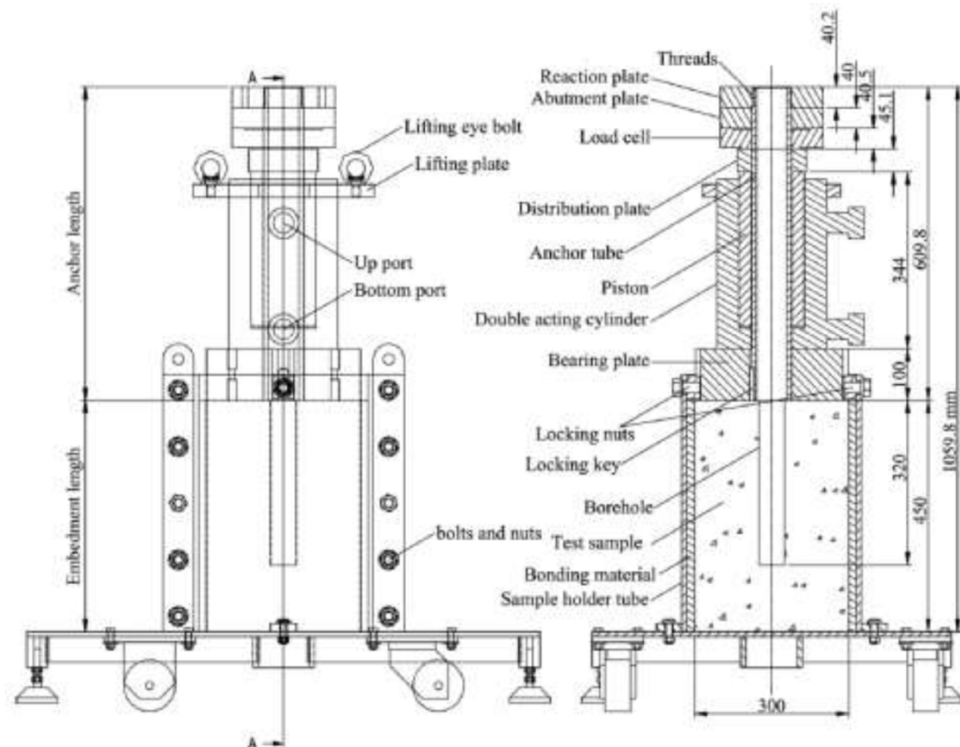


Figure 2.20: Sectional view of new LSEPT pull test apparatus designed by (Chen et al., 2016)

2.3.2 Modelling and numerical simulation

Extensive research has been conducted in the past two decades to model and numerically simulate the influences of axial forces on both cable bolts and rock bolts (Jalalifar, 2011). By developing an analytical understanding of the axial load transfer properties, strata support designs were streamlined and trial and error risks was minimised (Aziz et al., 2005). Later studies categorised the key stages of the pull out failures as; elastic, elastic softening, elastic softening-debonding, softening debonding and debonding with stage specific numerical simulations (Chen et al., 2015). In addition to numerical simulations (Ma et al., 2013), the use of the explicit finite difference software FLAC2D has been incorporated to model the complex behaviours of rock bolts and cable bolts.

Research conducted by Ivanovic et al. (2001) developed an early model to replicate the processes for the dynamic loading of rock bolts. This model accounted for the system's three key subsets: the rock mass, resin/grout annulus and the rock bolt as shown in Figure 2.21. The foundation for the model assumed a linear bond behaviour typical of a perfect system. This resulted in limited correlation with field data due to the presence of system flaws (Ivanović et al., 2009).

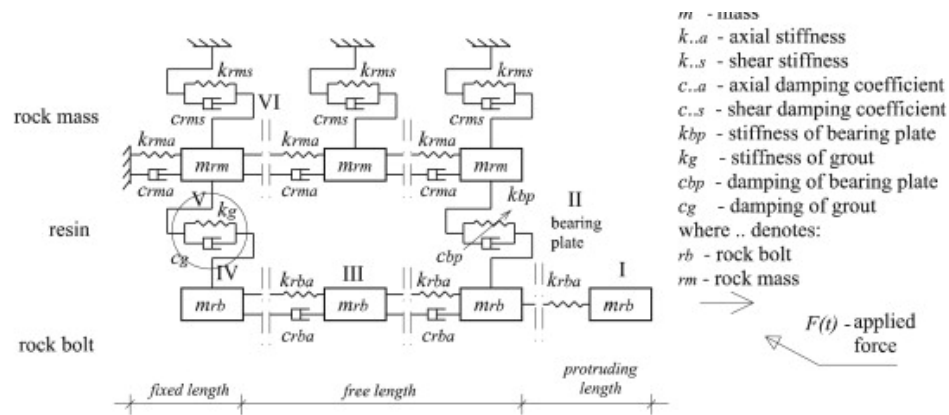


Figure 2.21: Lumped parameter model for tendon/bolt, ground, and rock (Ivanovic, 2001)

While the lumped parameter allowed for some analysis of rock bolt behaviour, its shortcomings needed to be rectified to provide a robust model capable of simulating scenarios of systems with imperfections. As a result Ivanović et al. (2009) modified the lumped parameter model by creating three new sub models representing bond behaviour as shown in Figure 2.22. These new models allowed for the incorporation of both debonding and residual load, based on the outcome of laboratory testing.

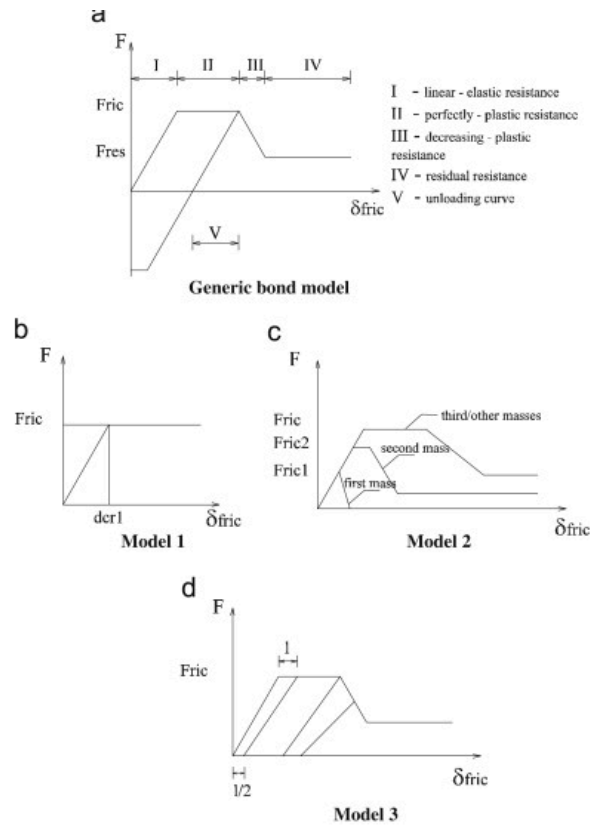


Figure 2.22: (a) Bond behaviour model (b, c, d) sub models used for lumped parameter model (Ivanović et al., 2009)

Other early models were also developed to simulate bond failure of cable bolts with respect to laboratory testing equipment such as the Hoek Cell and Modified Hoek Cell shown in (Hyett et al., 1995).

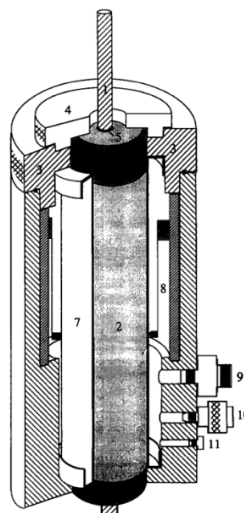


Figure 2.23: Cutaway section of the modified Hoek Cell (Hyett et al., 1995)

The above modified Hoek Cell was able to impose various environmental conditions on the cable bolts such as a range of confining pressures. As a result, the corresponding models were able to simulate the response of cable bolts for variable confining pressures as shown in Figure 2.24. Therefore, providing the ability to simulate the performance of cable bolts subjected to varying environmental conditions. Jahangir et al. (2021) have since developed newer analytical models to incorporate key system characteristics such as elastic phase prior to interface creation and multi-stage dilatancy. The incorporation of such aspects allowed for greater understanding of the processes occurring during loading while also providing a robust foundation for the transition to numerical modelling.

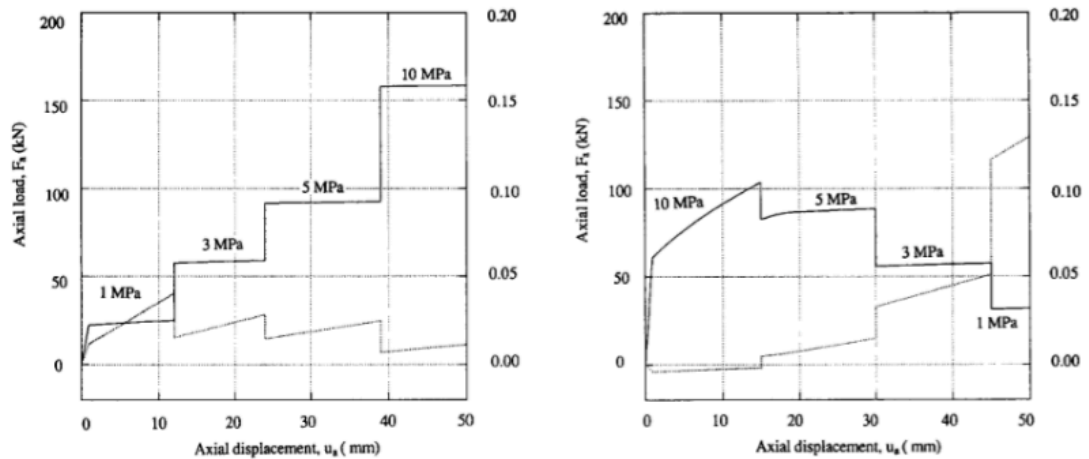


Figure 2.24: Cable bolt simulations for varying confining pressures using the modified Hoek Cell (Hyett et al., 1995)

With the advent of computer assisted simulations, software such as FLAC2D was developed to provide a quick and reliable method of simulating various bolt scenarios without the need of cumbersome calculations. FLAC2D was used to identify the axial load profile of grouted rock bolts both in roof and rib supports as shown in Figure 2.25. The FLAC2D model allowed for the analysis of axial forces on each fully grouted rock bolt in an underground excavation. As such, it allowed the identification of high-risk zones and the simulated design of the safest and most effective rock bolt application.

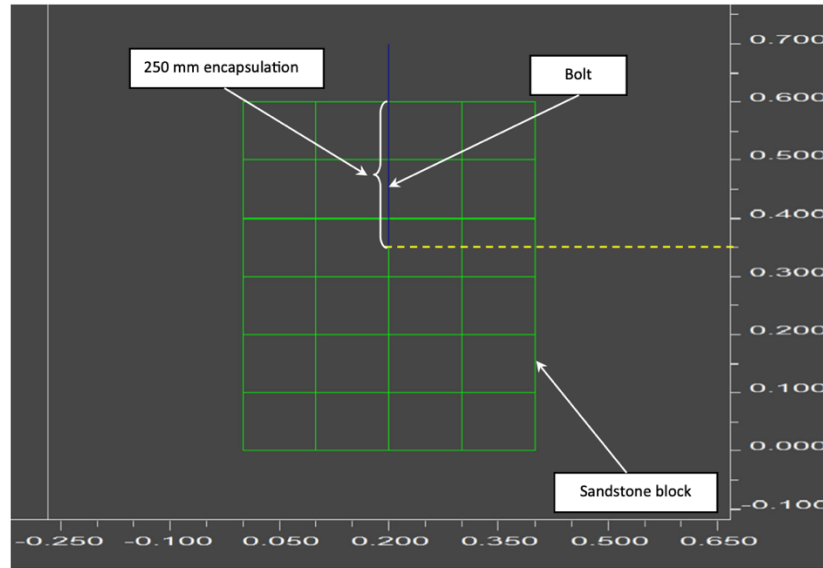


Figure 2.25: Rock bolt pull test simulation(Aziz et al., 2016a)

Aziz et al. (2016a) used FLAC2D to simulate axial load transfer mechanisms of steel rock bolts. The numerical simulation was carried out to model the pull testing experimental data collected from coal mines in the Sydney basin and Southern Coalfield. Two embedded constitutive models, namely constant shear bond strength (model 1) and displacement weakening shear bond strength (model 2) were applied in the simulation as shown in Figure 2.26. It was concluded that model 2 was able to satisfactorily replicate the softening behaviour of bond strength due to pulling displacement. On the other hand, it was shown that model 1 described accurately the elastic stage of pulling load.

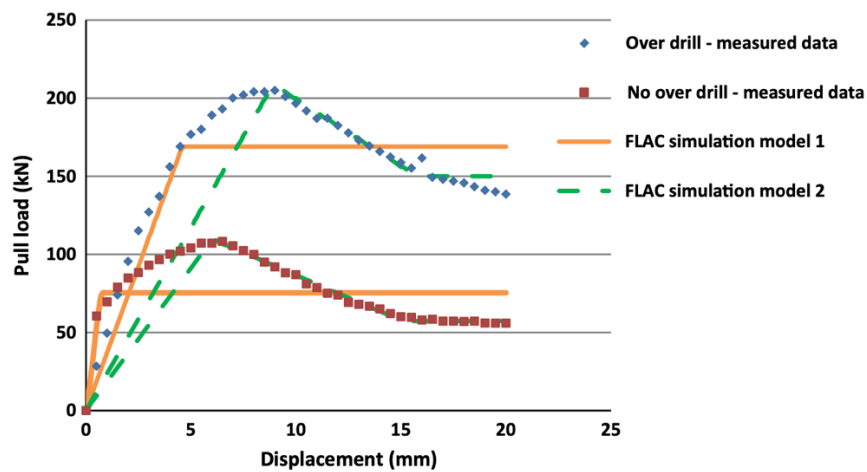


Figure 2.26: Comparison of the FLAC models against experimental analysis(Aziz et al., 2016a)

While FLAC has been a popular choice for modelling rock bolt and cable bolt performances, researchers have also adopted finite element method (FEM) to perform various numerical simulations. Jahangir et al. (2021) used FEM to transform their analytical rock bolt and cable bolt models to a platform that could better assist with system design and optimisation. By developing the FEM schematic and constitutive model shown in Figure 2.27 and Figure 2.28 respectively, Jahangir et al. (2021) was able to implement their proprietary FEM code to perform simulations based on their analytical model addressing radial displacement, dilatancy and pre-joint interface phase.

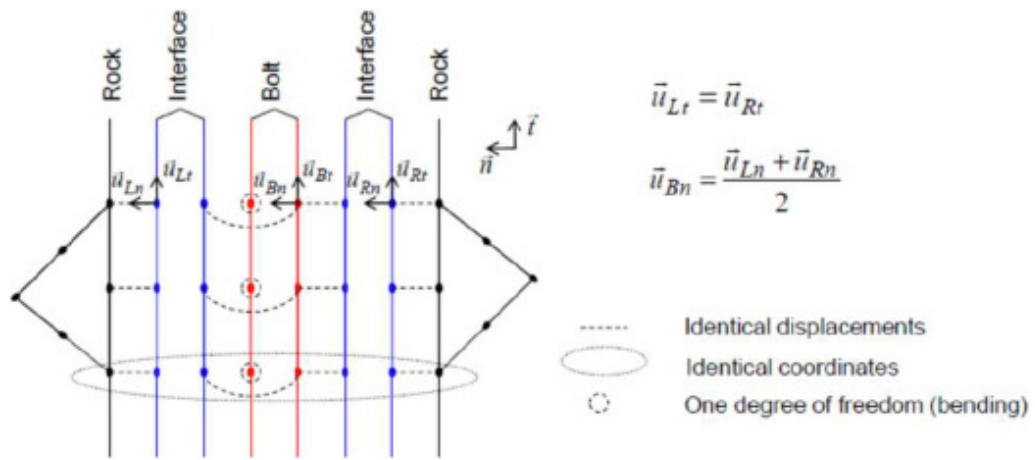


Figure 2.27: FEM schematic of fully grouted bolt (Jahangir et al., 2021)

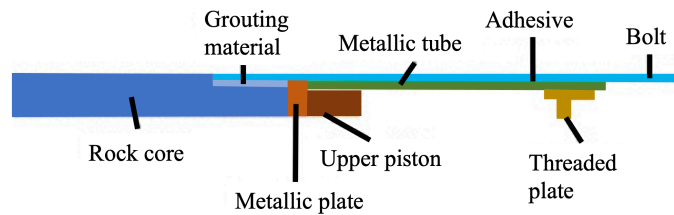


Figure 2.28: FEM constitutive pull test model modified from (Jahangir et al., 2021)

2.4 Shear load transfer mechanisms

Due to the differing tectonic forces translated across varying strata, significant shearing forces are exerted along the bedding planes and onto rock bolts (Nemcik et al., 2006). The intensity of the shearing forces is dependent on the stiffness of the bedding plane as illustrated by Figure 2.29. The observed shear loads induce resistive forces along the shear displacement plane and opposite to that of the applied load.

Unlike axial load transfer tests, shear load transfers are limited to laboratory testing. Due to the difficulties of determining the localised shearing forces located within *in-situ* strata, numerous studies have been conducted to determine the shearing properties of the rock bolts and cable bolts (Li et al., 2016, Song et al., 2008, Aziz et al., 2015c).



Figure 2.29: Stress variations within stratification Nemcik et al. (2006)

The shearing performances of rock bolts can be determined using a number of methods each with a varying representation of the bolts *in-situ* conditions. Shearing tests developed include; the single shear guillotine test in accordance with the British Standard for testing (2009), the double shear guillotine test and concrete embedded double shear testing (Gilbert et al., 2015). Testing requirements for rock bolts and cable bolts are identical and various adaptation to these tests methods have been developed (Li et al., 2017b).

2.4.1.1 Single shear testing

Single shear testing is accomplished by cutting the tendon along a single plane. According to Li et al. (2017b), single shear testing does not accurately determine shear strength properties as the:

- Rock bolt is not encapsulated inside concrete medium, thus not representing rock strata,
- Single shear testing overestimates the shear strength of the cable bolt due to the two opposing metal frame bodies contacting during shearing shown in Figure 2.30 (Aziz et al., 2015c), and
- Single shear testing is a passive shear test whereby the rock bolt is sheared without pre-tensioning.

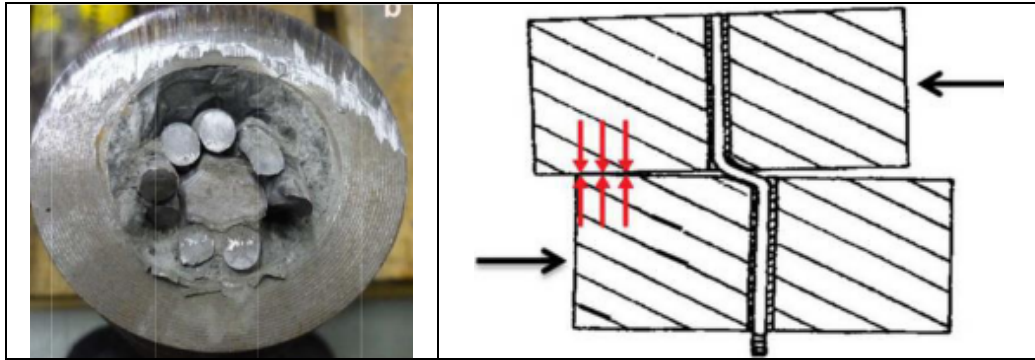


Figure 2.30: [left] A view of the sheared sample in single shear, note the interaction between the strand and the steel tube (Aziz et al., 2016c). [right] Stress concentrations during BS7861-2 Single shear test (Aziz et al., 2015c)

While not all single shear test methods resulted in metal on metal induced over estimations, earlier test methods had significant shortcomings. Goris et al. (1996) developed the single shear test method shown in Figure 2.31 which allowed for the embedment of a cable bolt into a host rock. While this method was important to determine the failure mechanisms of the entire system, it had some significant drawbacks. This method was unable to explore the influence of pretension and confining pressure on the shear properties of the bolt.

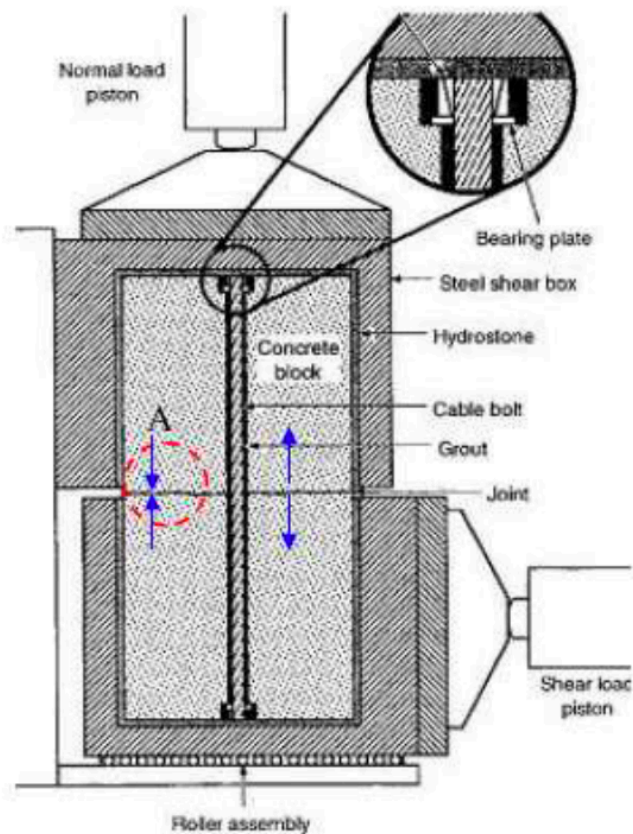


Figure 2.31: Shear test apparatus (Goris et al., 1996)

Three testing systems have since been developed and are still in use today, including the British Standard (2009) single shear test (BSST), direct single shear and the Megabolt single shear tests (Aziz et al., 2017). Each test evaluates different aspects of the tendon's performance. The direct single shear test applies the shear load directly to the bolt with no incorporated buffer and as such identifies the pure shear property for the bolt. The BSST method aims at testing the performance of bolts in strata, however, only requires the bolt to be grouted to the shearing tube seen in Figure 2.32 and Figure 2.33. This method does not provide an accurate representation of the bolts' system shear strength (Li et al., 2017b). Instead it provides an indication of the cable bolts' pure shear performance due to the direct load transfer to the bolt as shown in Figure 2.32.

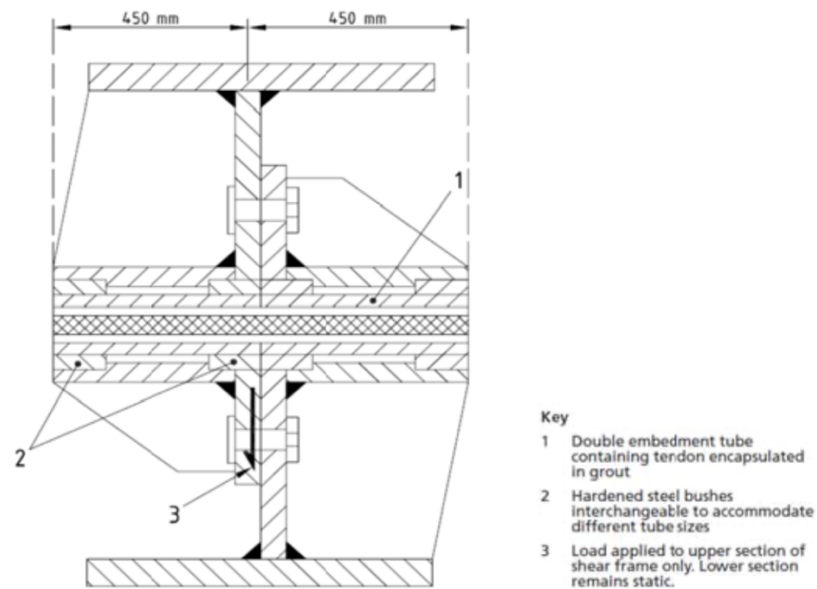


Figure 2.32: Single shear sectional diagram (Standard, 1996)

It has been determined that shear failure is a function of confinement strength and crack propagation (Li et al., 2015). As a result, the Megabolt shear test apparatus was developed by Mckenzie et al. (2015). The Megabolt required the bolt to be embedded into a strata simulator, accomplished by grouting the bolt into a specific strength concrete shown in Figure 2.33 and Figure 2.34. This allowed the Megabolt shear tester to demonstrate the shear force distributions across the bolt, grout and strata (Li et al., 2017b). The Megabolt testing machine was exclusively designed for high strength cable bolts where the length of encapsulation could go up to 4 meters (Li et al., 2017b).

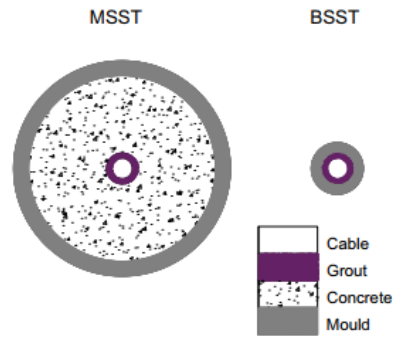


Figure 2.33: Single shear apparatus cross-section [left] Megabolt, [right] British single shear standard (Li et al., 2017b)



Figure 2.34: Megabolt testing system (Mckenzie et al., 2015)

Further studies were conducted by Li et al. (2017b) provided a comparison of the testing methods to determine suitability and consistency. It was found that there were significant differences between the MSST and BSST testing methods. Figure 2.35 demonstrated a significant underestimation of the shear properties of the cable bolts as well as early strand failure when using the BSST testing method. Conversely, when the MSST was compared against the double shear testing apparatus (DST) there was a strong correlation between their shear profiles when concrete joint friction was incorporated as shown in Figure 2.36.

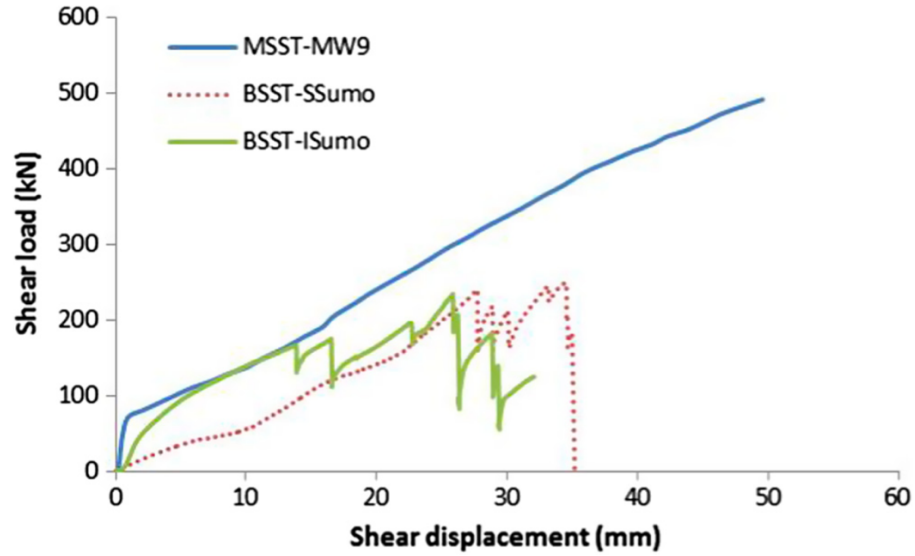


Figure 2.35: Comparison of BSST and MSST shear force and shear displacement (Li et al., 2017b)

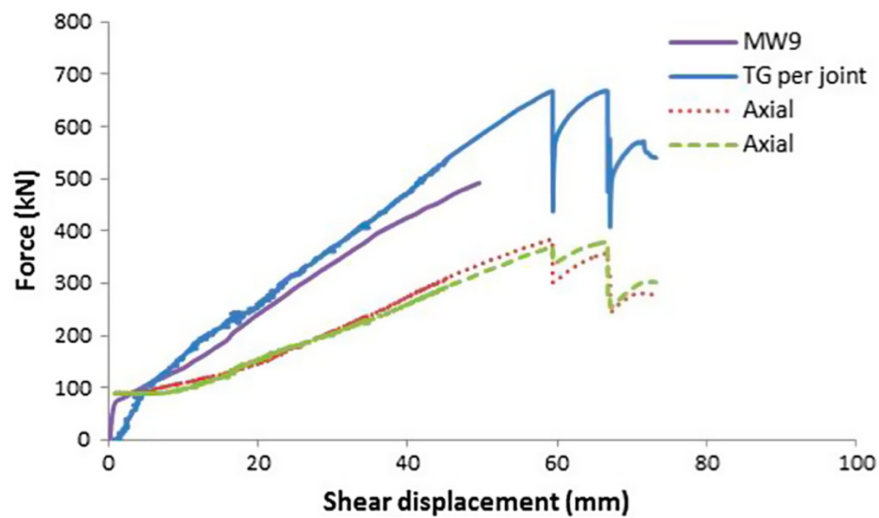


Figure 2.36: Comparison of MSST and DST testing methods for shear force and displacement (Li et al., 2017b)

2.4.1.2 Double shear Testing

Due to the presence of strata bedding, multiple shear planes could be induced on a single bolting system (Nemcik et al., 2006). As a result, the double shear testing method was developed to simulate the actual field conditions. The double shear testing apparatus highlighted in Figure 2.37 consisted of a single bolt grouted into three concrete blocks as first developed by Aziz et al. (2003). Tests conducted at the University of Wollongong consisted of three prismatic blocks with a load subjected to the centre block (Li et al., 2016) as shown in Figure 2.38.

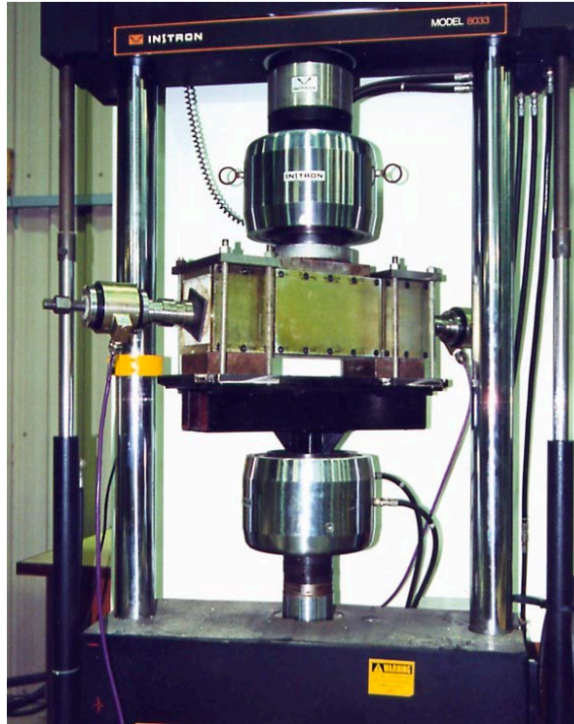


Figure 2.37: Mark 1 testing apparatus developed by Aziz et al. (2003)

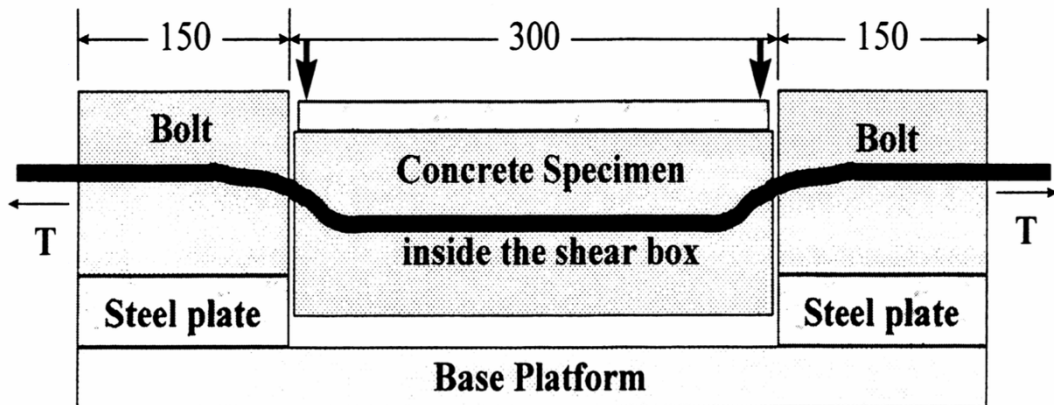


Figure 2.38: Schematic of the mark 1 double shear testing apparatus (Aziz et al., 2003)

Double shear testing methodology was designed with three types namely MKI, MKII and MKIII (Aziz et al., 2016c). MKIII is the modified version of MKII and both were used for the shear strength determination of high strength tendons such as cable bolts. The double shear box was comparable to Megabolt shear test as it incorporated simulated concrete strata to replicate the effects of localised crushing (Aziz et al., 2015a) as demonstrated in Figure 2.39.

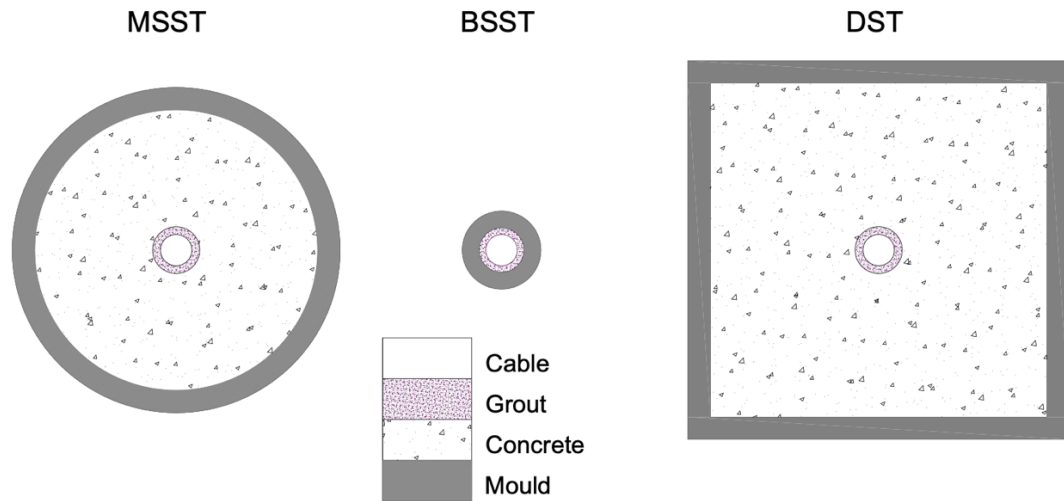


Figure 2.39: Comparison of the cross-section of the MSST, BSST and DST testing methods (Li et al., 2017b)

The double shear box was initially used for the investigation of varying host strata UCS. The study conducted by Gilbert et al. (2015) using the MK1 double shear apparatus provided an understanding of the relationship between shear strength and host UCS by subjecting rock bolts to host rock strengths of 40MPa and 60MPa. As a result, the study observed two unique and increasing ultimate shear failure loads and as such, concluded that the shear performance of rock bolts was a function of the host rock UCS. Gilbert et al. (2015) as well as using the MK1 double shear testing apparatus from the Aziz et al. (2003) study also compared the shear load transfer mechanisms of fibreglass rock bolts using the single shear testing method (i.e. Guillotine box). A limited number of tests were carried out on fibreglass rock bolts using double shear testing method (MKI). When compared to the single shear test method, it was concluded that:

- Single shear testing of guillotine box underestimates the shear strength of fibreglass rock bolts,
- Shear strength of fibreglass rock bolts is a function of pretension values, and
- Strata strength (i.e. concrete strength) affects the shear strength of fibreglass rock bolts.

Furthermore, Li et al. (2016) identified the mechanism whereby the weaker host rock crumbles at the shearing plane allowing the rock bolt to flex inducing additional stresses on the rock bolt element as highlighted in Figure 2.40

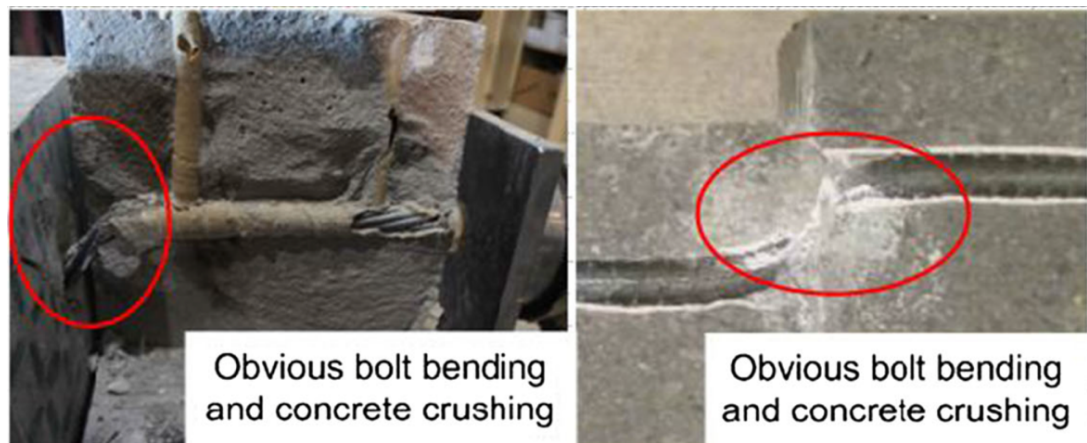


Figure 2.40: Demonstration of concrete crushing during double shear testing with 40MPa concrete (Li et al., 2016)

Samples tested at 60MPa were identified as less susceptible to this phenomenon and as such indicated that an increase in the host rock UCS resulted in an increase in the overall shear performance of the rock bolts. The MK1 double shear box was further modified to allow for the investigation of varying bolt pretensions. The study conducted by Aziz et al. (2015b) adopted the MK1 double shearing apparatus to investigate the effect of pretension on the shear performance of rock bolts. Pretension values of 2.5, 5, 10 and 15kN were chosen for the study and despite the non-uniform distribution of pretension values the study highlighted an increase in the ultimate shear failure in the presence of pretension, shown in Figure 2.41. MKI was the suggested testing method for non-metallic rock bolts such as fibreglass bolts as per Aziz et al. (2015b).

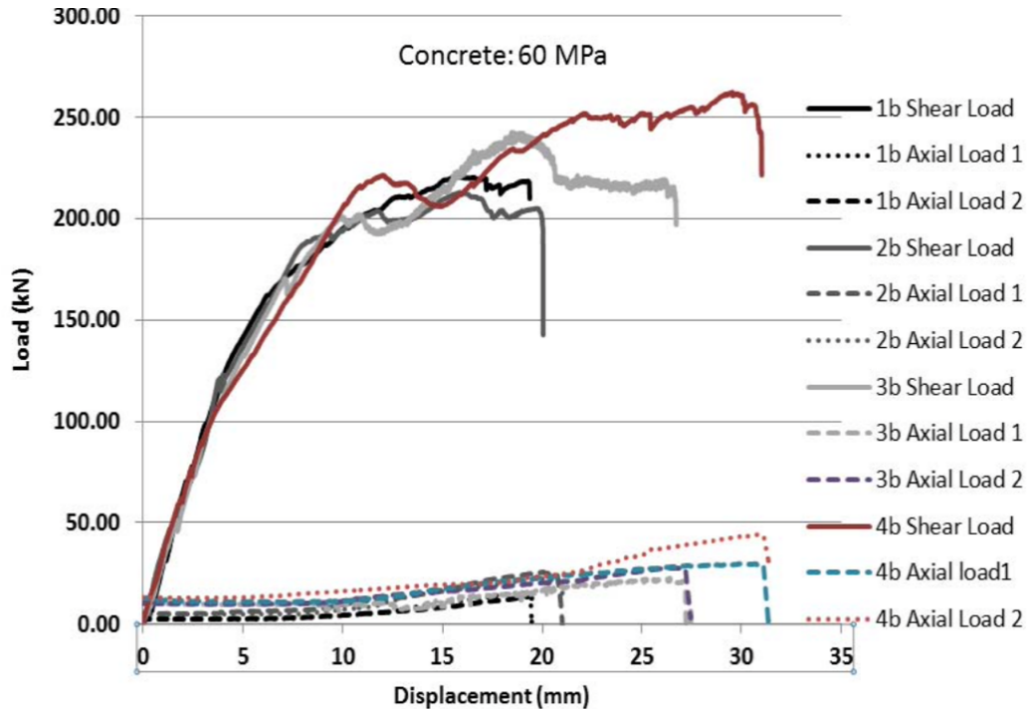


Figure 2.41: Impact of pretension on the shear performance of dowels anchored in 60MPa concrete (Gilbert et al., 2015)

2.4.2 Mathematical and numerical modelling

Mathematical and numerical modelling has been adopted to better understand the intrinsic stresses experienced by rock bolts (Song et al., 2008). Models from as early as the 1970s were developed to calculate the shear resistance of bolted rock systems (Haas, 1976). Based on the geometry illustrated in Figure 2.42, Haas (1976) developed the following expression for calculating the average shear stress by:

$$\tau_{ave} = \tau_0 + \frac{\mu T \cos \theta_1 + T \sin \theta_1}{A_s} \quad (2.1)$$

Whereby, T_0 is the bolt tension, θ_0 is the initial bolt orientation, A_s is the shear area, μ is the friction coefficient, τ_0 is the average stress without a rock bolt and τ_{avg} is the average initial stress with a rock bolt.

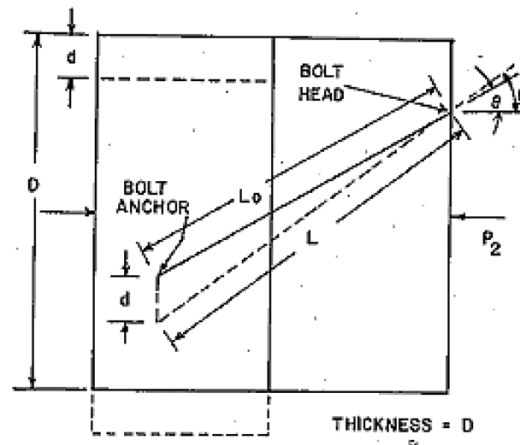


Figure 2.42: Geometry of rock bolt subjected to shear displacement (Haas, 1976)

The early 1990s saw the incorporation of computational analysis with the use of FEM model simulations (Spang et al., 1990). This facilitated the exploration of simulating varying bolt installation parameters such as bolt angle as shown in Figure 2.43. The FEM model highlighted the influence of installation angle whereby samples subjected to 0° resulted in a larger gap at the shear plane compared to that of the 35° samples, shown in Figure 2.44. Utilising a three-stage failure model including an elastic stage, yield stage and plastic stage, the appropriate analytical behaviour could be initiated. Such that, the elastic stage was represented by the Mohr-Coulomb relationship, while the von Mises failure criteria was used for the plastic stages. The model presented with numerous limitations by not accounting for both the friction at the joint as well as the grout interface.

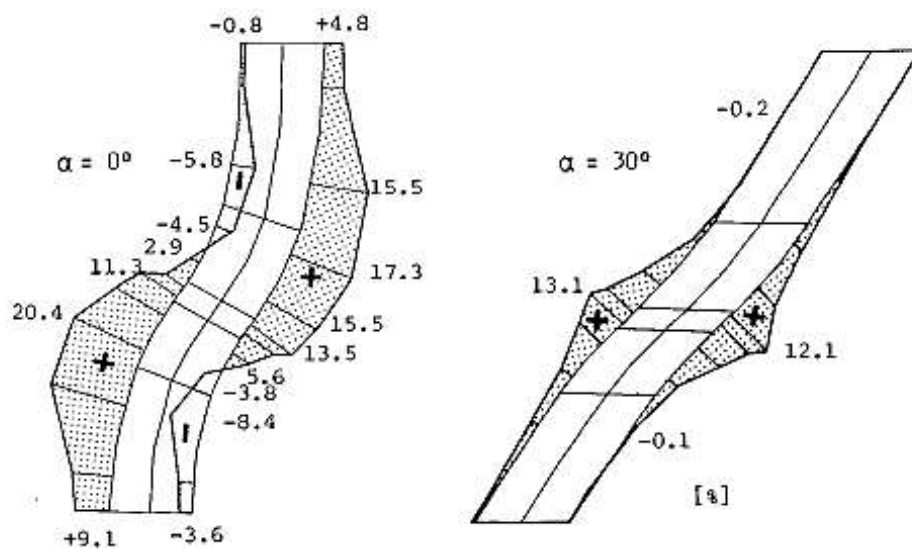


Figure 2.43: FEM model of rock bolts installed at 0° and 30° inclinations (Spang et al., 1990)

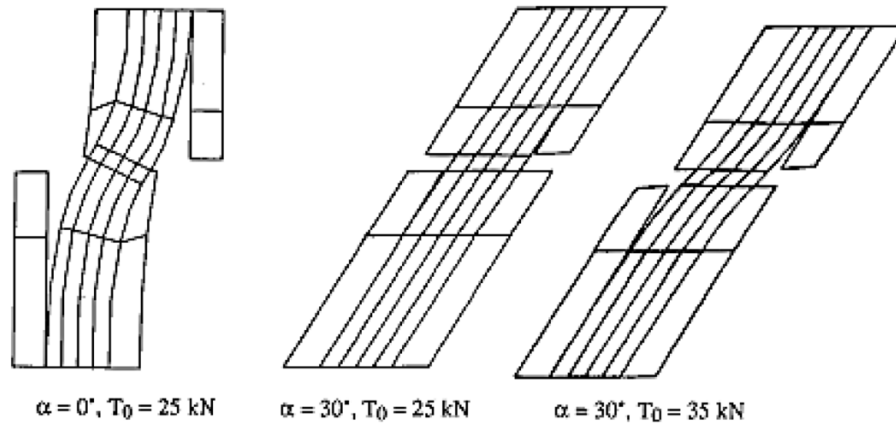


Figure 2.44: Comparison of FEM models for shear inclinations of 0° and 30° and initial tensions of 25kN and 35kN (Spang et al., 1990)

A model later developed by Pellet et al. (1996) determined the impacts of rock bolts on sheared rock joints utilising the Tresca criterion. Due to the Tresca criterion's ability to model a combination of axial shear forces at failure, it was selected as the primary failure model of this analytical model. The relationship between shear and axial force transitions using the force component model is shown in Figure 2.45.

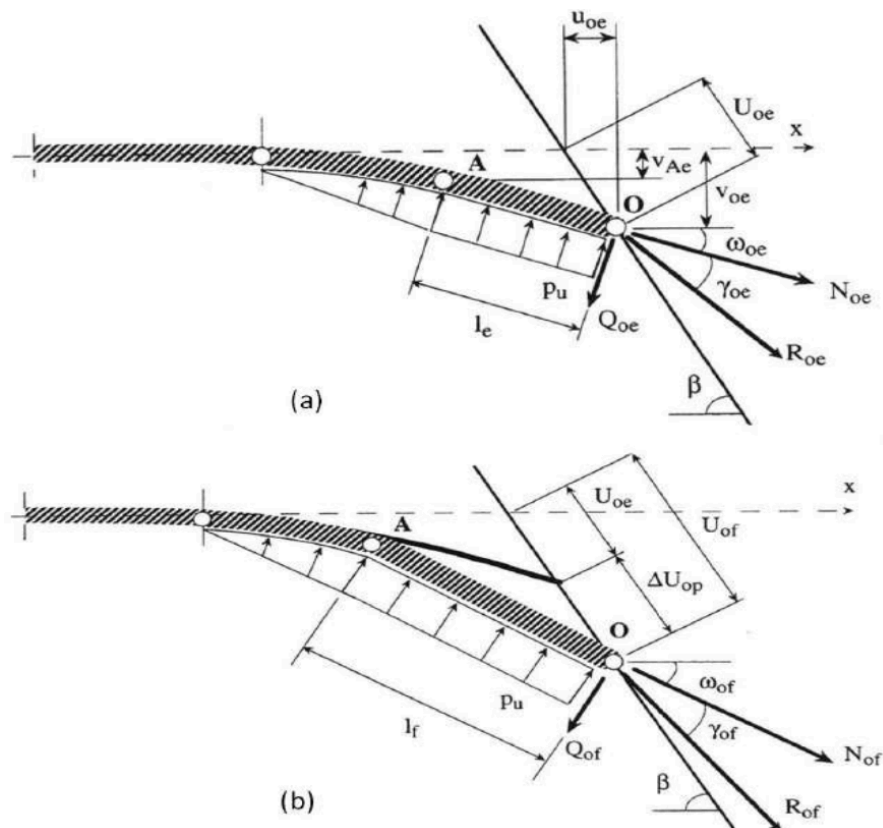


Figure 2.45: Force component model of a rock bolt subjected to shearing (a) Elastic zone, and (b) plastic zone (Pellet et al., 1996)

Further development of these models has seen the incorporation of Fourier series, producing highly accurate simulations (Aziz et al., 2015a, Rasekh, 2017). Rasekh (2017) developed an analytical model on the foundations of Aziz et al. (2015a) Fourier series model. This revised model calculated the shear response of cable bolts at the three defined stages of shearing, the elastic stage, strain-softening stage and finally the failure stage using the following equations:

$$S_{elastic} = Kv \quad (2.2)$$

$$S_{strain\ softening} = \beta Kv \quad (2.3)$$

$$S_{failure} = \left[\frac{a_0}{2} + a_1 \cos \frac{2\pi u}{T} + a_2 \cos \frac{4\pi u}{T} + a_3 \cos \frac{6\pi u}{T} \right] (\cos i \cot i - \sin i) + \sigma_y A_t \cot i + \sigma_s A_s \quad (2.4)$$

Where values for a_0 , a_1 , a_2 and a_3 were calibrated coefficients, S is the shear load, A_s the broken area of cable subject to shear, A_t is the broken area of cable subjected to tension, σ_y is the yield strength and σ_s is the shear strength. Overall, the model presented a suitable agreement with the experimental study as shown in Figure 2.46. However, some discrepancies presented at the failure stage where the model was unable to portray the various peaks and troughs during the failure process of the cable bolt.

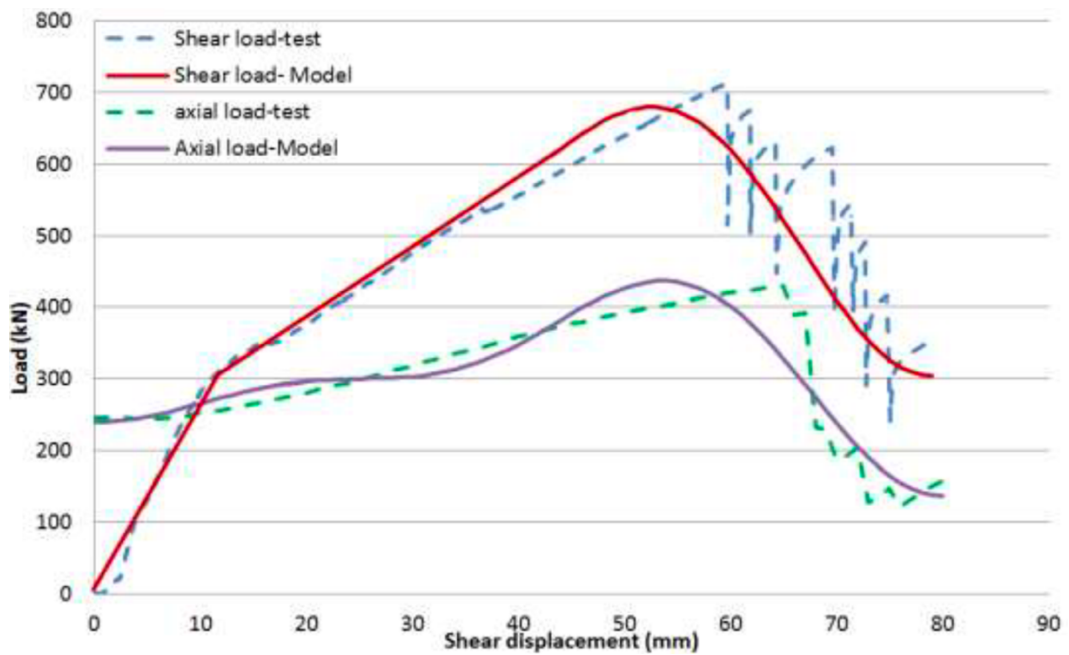


Figure 2.46: Comparison of shear force analytical model and experimental results (Rasekh, 2017)

A more recent study conducted by Singh et al. (2021) utilised static mechanics, kinematic relationships for the elastic and plastic conditions respectively while building on the works of Maekawa et al. (1996) and Dight (1982) to define the yield and failure limit. The model was then compared against experimentally derived double shear data and an earlier model developed by Pellet et al. (1996), shown in Figure 2.47. While the model showed a closer alignment to the experimental results compared to the Pellet et al. (1996) model for the 100MPa sample, it was less successful with the 20MPa test scenario as demonstrated in Figure 2.48. A further shortcoming of the model was that it incorporated the material properties of steel bolts. This prevented the model's adaption to fibreglass and other composite based reinforcement systems.

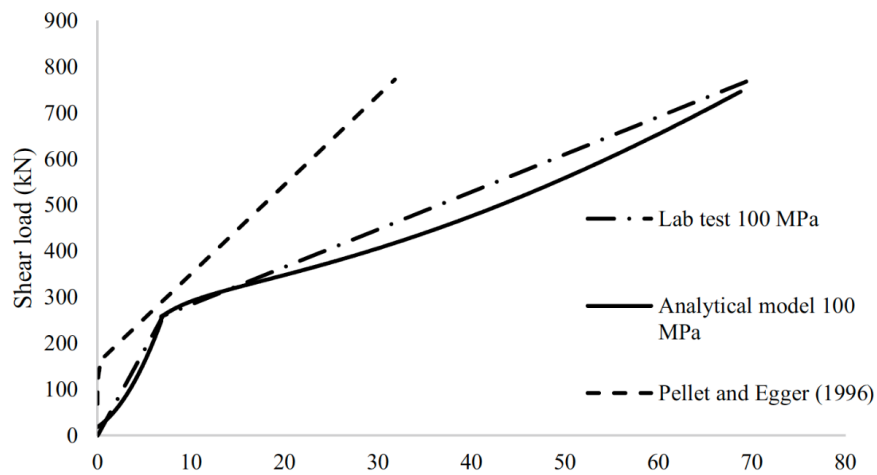


Figure 2.47: Comparison of analytical models and experimentally derived double shear results for 100MPa sample (Singh et al., 2021)

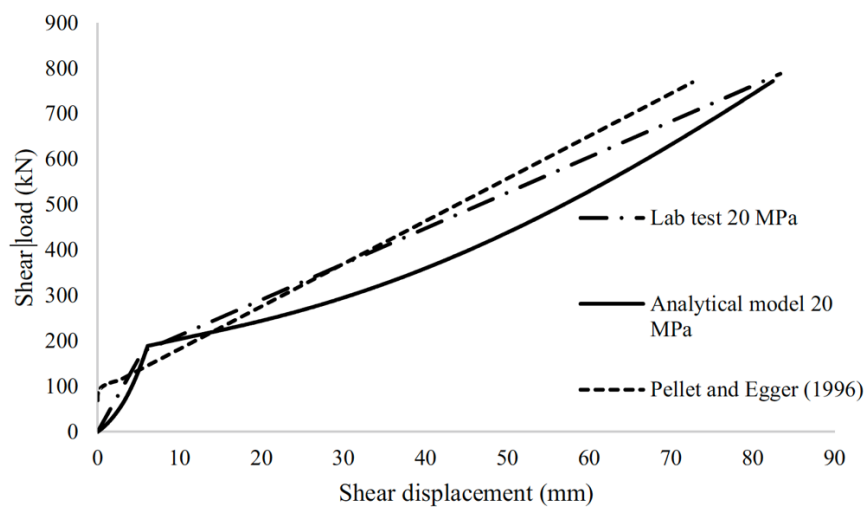


Figure 2.48: Comparison of analytical models and experimentally derived double shear results for 20MPa sample (Singh et al., 2021)

The development of analytical models representing the shear behaviours of rock bolts and cable bolts over previous decades have enabled the development of a strong foundation for numerical analysis utilising tools. Numerical models have been developed using finite element models, FEM, and explicit finite difference software. Ghadimi et al. (2015) utilised FEM through the ANSYS software to investigate the shear stress distribution along a metal rebar. A constitutive model was developed as shown in Figure 2.49 and upon running the shearing simulation the shear stresses were mapped along the rock bolt element.

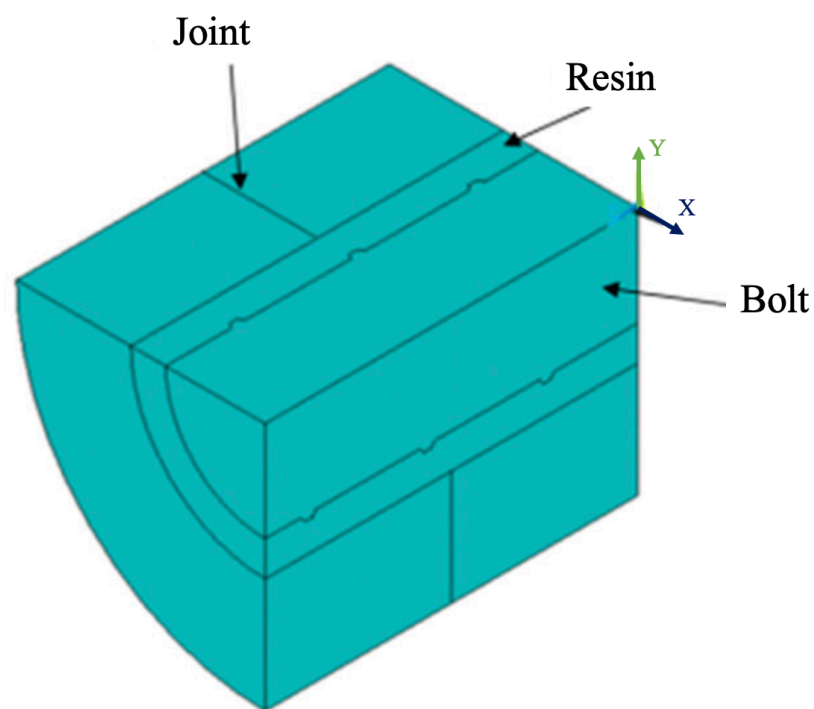


Figure 2.49: Three-dimensional finite element model subjected to shear loads. Modified from (Ghadimi et al., 2015)

The jointed simulation depicted in Figure 2.50 demonstrates visually how the shear stresses concentrated at the shear plane. Ghadimi et al. (2015) determined that there was an exponential relationship between the shear stress and its distance from the joint surface. Additionally, the intensity of this relationship was determined by the material properties of each of the system components.

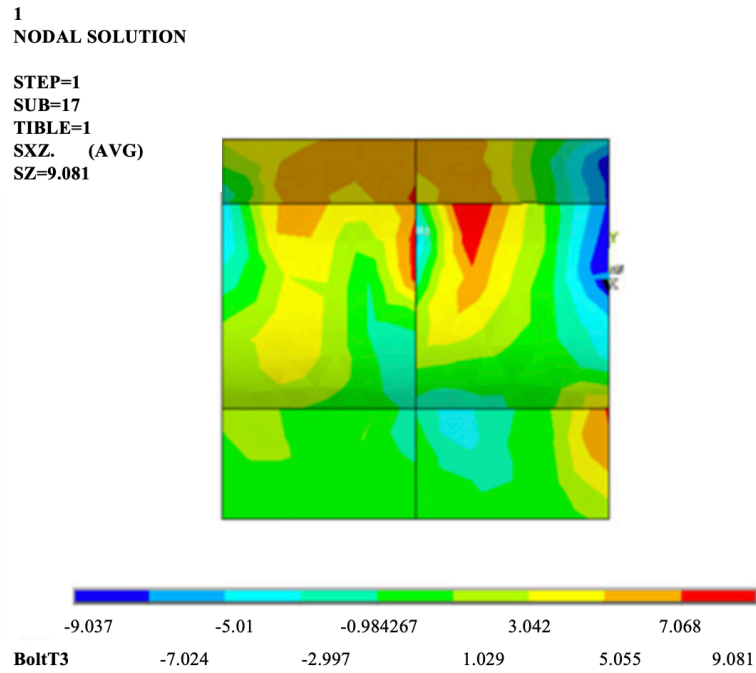


Figure 2.50: Shear stress distribution during FEM shearing simulation. Modified from (Ghadimi et al., 2015)

Studies conducted by Rasekh (2017) utilised FLAC2D to conduct explicit finite difference for the modelling of cable bolts subjected to double shearing. FLAC2D was selected as it combined analytical expressions with spatial modelling in order to explore the element by element influence of shear stress on a complete rock bolt system (Ma et al., 2014). The foundation of the FLAC2D model was defined by the double shear constitutive model depicted in Figure 2.51, indicating the boundary conditions and dimensions of the simulated system. The overall model was designed to match that of the double shear apparatus used in their experimental testing scheme.

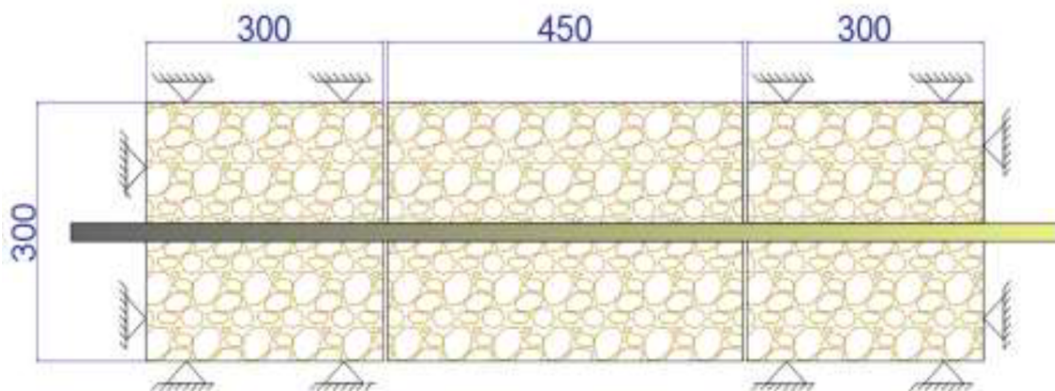


Figure 2.51: Schematic used to develop the FLAC2D cable bolt double shearing model (Rasekh, 2017)

The completed simulation successfully mapped the shear stresses along the cable bolt element as well as the confining rock body with the latter shown in Figure 2.52. Throughout the model it was evident that the shear stresses concentrated in proximity to the shear planes throughout the elements surrounding the cable bolt.

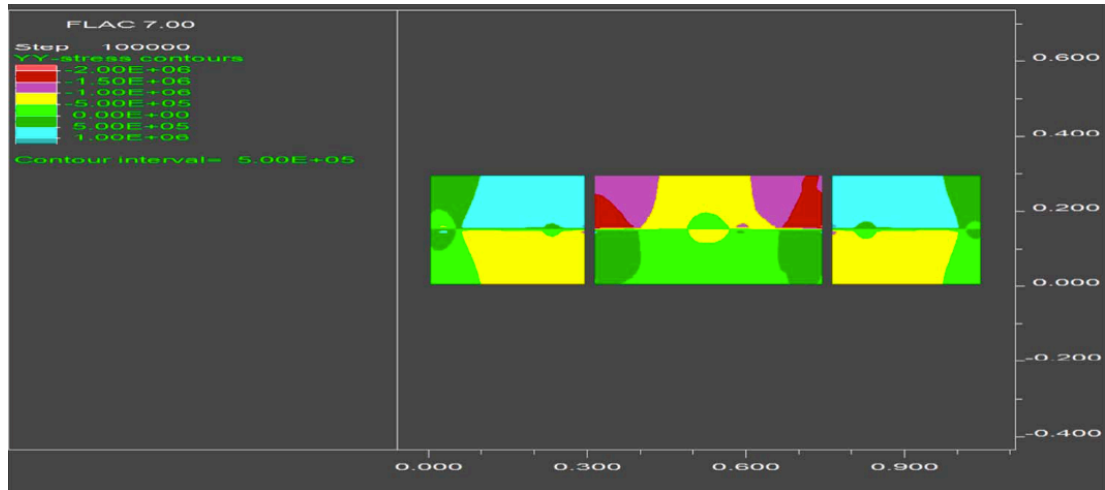


Figure 2.52: Shear stress distribution along the confining rock (Rasekh, 2017)

In addition to simulating novel shearing scenarios, Mirzaghobanali et al. (2017b) revisited the established British Standard shearing testing scheme of cable bolts in order to develop a model of the shear behaviour using FLAC2D shown in Figure 2.53. Ultimately, Figure 2.54 showed good agreement between the shear profiles generated through experimental testing and numerical modelling, leading Mirzaghobanali et al. (2017b) to conclude that numerical simulations were successfully able to model existing testing methods.

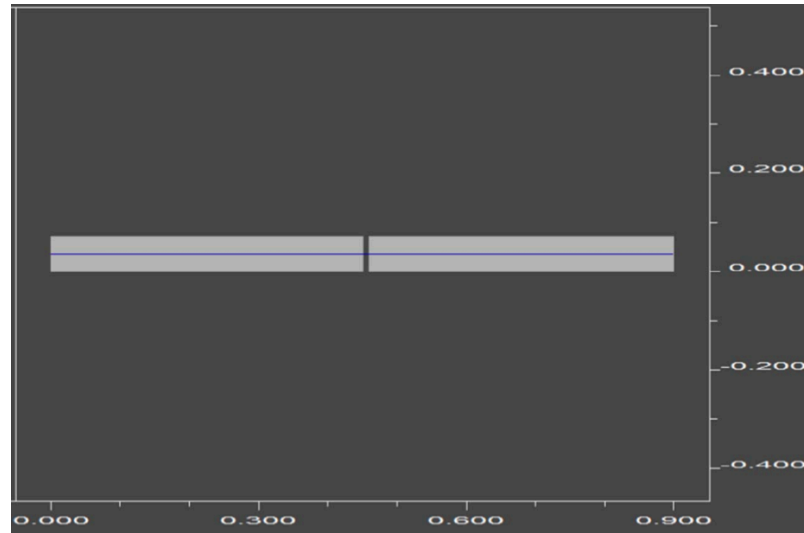


Figure 2.53: *FLAC2D simulation of grouted cable bolt subject to the British standard of testing (Mirzaghobanali et al., 2017b)*

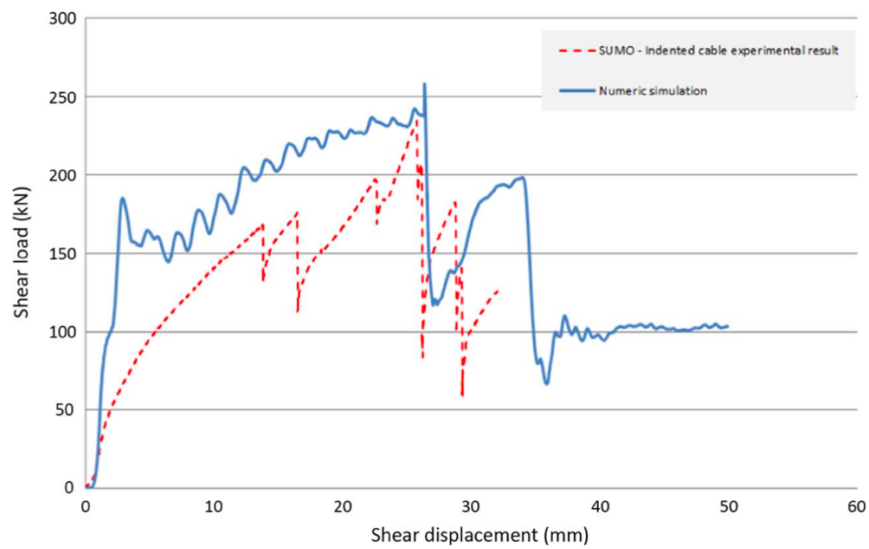


Figure 2.54: *Comparison of FLAC2D simulated British standard of testing cable bolt shear test and experimental testing scheme*

Analytical and numerical studies have predominantly focused on metallic rock bolts and cable bolts as indicated by Aziz et al. (2016a), Aziz et al. (2015a) and Mirzaghobanali et al. (2017b). To the best of the authors' knowledge, only a limited number of studies have been conducted in the shear performance of fibreglass rock bolts for various pretension and strata strength values which is the subject of this research study. Additionally, there is a significant lack in the numerical modelling of fibreglass rock bolts with limited numerical investigation on load transfer mechanisms of metallic cable bolts (Mirzaghobanali et al., 2017b, Ghadimi et al., 2015).

2.5 Infilled discontinuities

2.5.1 Two-dimensional infill studies

In the previously outlined shearing studies, test parameters were limited to bolt type, confining ultimate compressive strength and pretension where the effect of the contact plane was only considered for clean joints (Aziz et al., 2015a, Rasekh et al., 2017). Contrary to the tested samples, there is significant variation in real world scenarios between the surfaces of the shearing planes including: friction and infill material. Both clean and infilled joints are susceptible to a range of asperity properties that impact their overall shear performance. Barton (1971) statistically analysed the joint properties of varying roughness by mapping the asperities from re-created shear tests with high normal stresses. One of the outcomes of this study was to categorise the asperity profile which later developed into the roughness profile classification as shown in Figure 2.55. This classification is still in use with studies adopting the profiles to test shear behaviour of infilled joints (Mirzaghobanali et al., 2022, Zohaib et al., 2020), with 3D printed studies conducted by (Mirzaghobanali et al., 2019a).

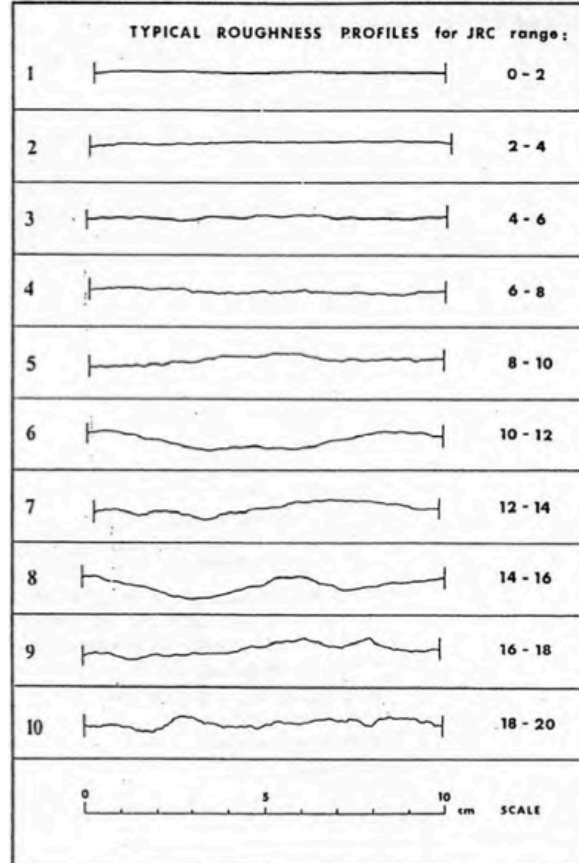


Figure 2.55: Roughness profile for JRC range (Barton et al., 1977)

Barton (1971) used the results of the shear samples to map the different relationships between the peak stress ratio and peak dilation angle as well as between the normal stress and peak dilation angle, resulting in the following representation of the criterion of peak strength for rough joints:

$$\frac{\tau}{\sigma_n} = \tan \left[20 \log_{10} \left(\frac{\sigma_c}{\sigma_n} \right) + 30^\circ \right] \quad (2.5)$$

This criterion was adopted for both weathered and unweathered samples, however, to determine the strength criterion of unknown roughness the following was used:

$$\frac{\tau}{\sigma_n} = \tan \left[\frac{(90-d_0)}{d_0} d_n + d_0 \right] \quad (2.6)$$

These criteria were paired with computer drawn asperity profiles for statistical analysis to provide a deeper understanding of the shearing properties of slopes with clean joints and ultimately aiding slope design. While this study focused on clean joints, it also developed the foundation for analysing the shear strength of filled joints as later explored by Barton (1973). Barton (1973) went on to define shear characteristics for four examples of filled joints. The theoretical examples were designed so that the thickness progressively increased to the point where the fill prohibited direct contact between the two sides of the asperity as shown in Figure 2.56.

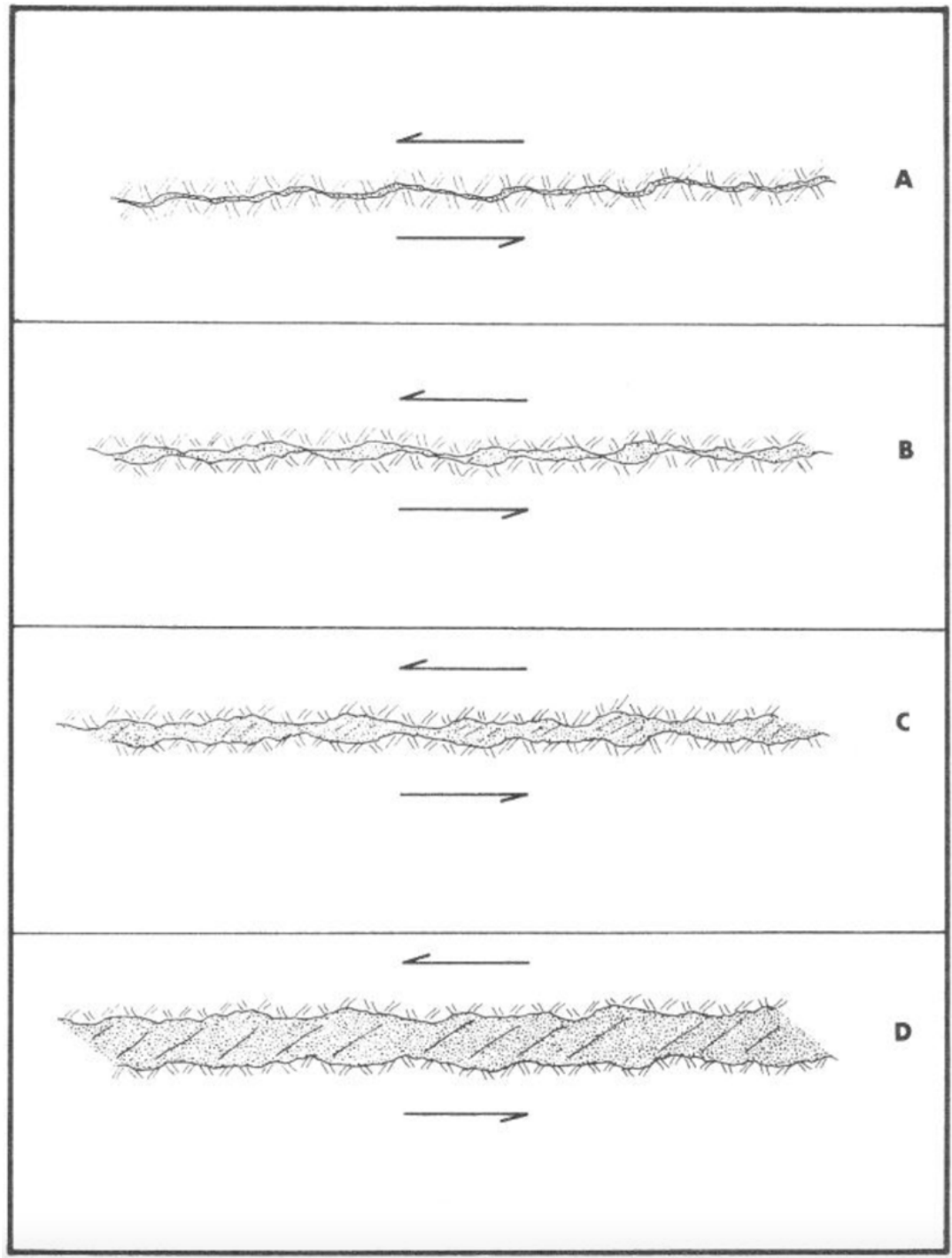


Figure 2.56: Four categories of filled joints (Barton, 1973)

Building on the works of Coon et al. (1970), Barton (1973) successfully compared and quantified the shear strengths properties of filled joints through comparison against the ideal saw toothed joint analysis shown in Figure 2.57.

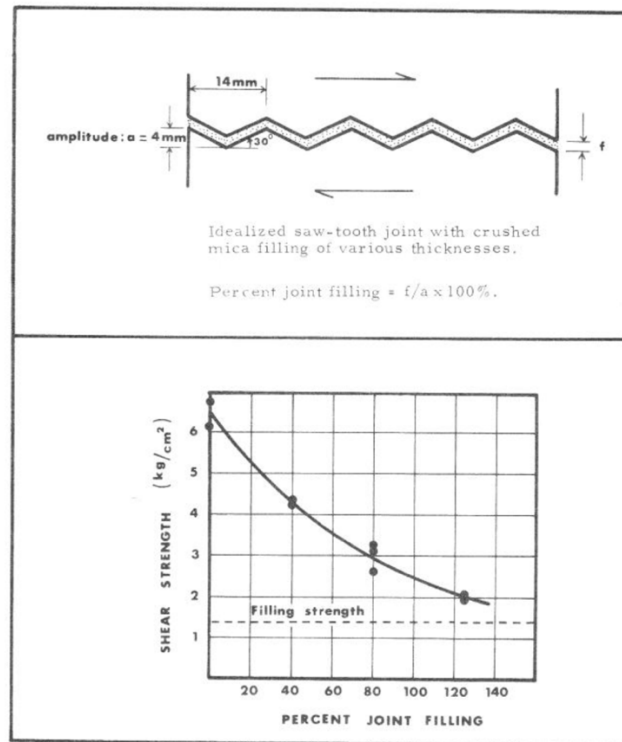


Figure 2.57: Effect of infill thickness on the shear strength of the idealised saw tooth discontinuity (Coon et al., 1970)

Previously adopted testing methods typically comprised of extremely complex *in-situ* direct shear testing apparatus that required the floor of mining tunnel to be excavated in a precise manner (Barton, 1971). Due to the complexity of the system, difficulty in locating ideal discontinuities and the inability to replicate, laboratory-based analysis gained favour as the preferred method of testing. However, this presented the challenge of replicating each element of the system. Due to the influence of material variability on its mechanical behaviour, Indraratna (1990) developed synthetic materials to simulate soft rock. This was later incorporated as part of the constant normal stress (CNS) shear apparatus, shown in Figure 2.58, a testing system designed to subject artificial discontinuities, such as the ideal saw tooth discontinuities, to normal and shear forces (Haque et al., 2000). As the system was synthetic, it allowed for simple and reliable replication. Haque et al. (2000) also developed a two-dimensional numerical simulation utilising Universal Distinct Element Code (UDEC) to digitally model the CNS test apparatus. UDEC simulations typically demonstrated good agreement with the CNS data set as shown in Figure 2.59 indicating that the numerical simulation could be used to accurately measure the shearing properties of infilled joints with the ideal saw tooth asperity.

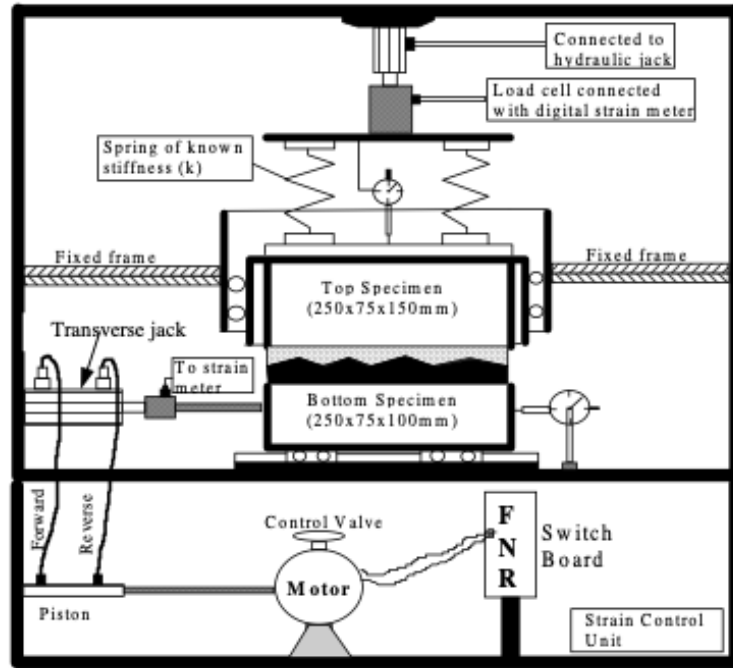


Figure 2.58: Schematic of CNS apparatus (Haque et al., 2000)

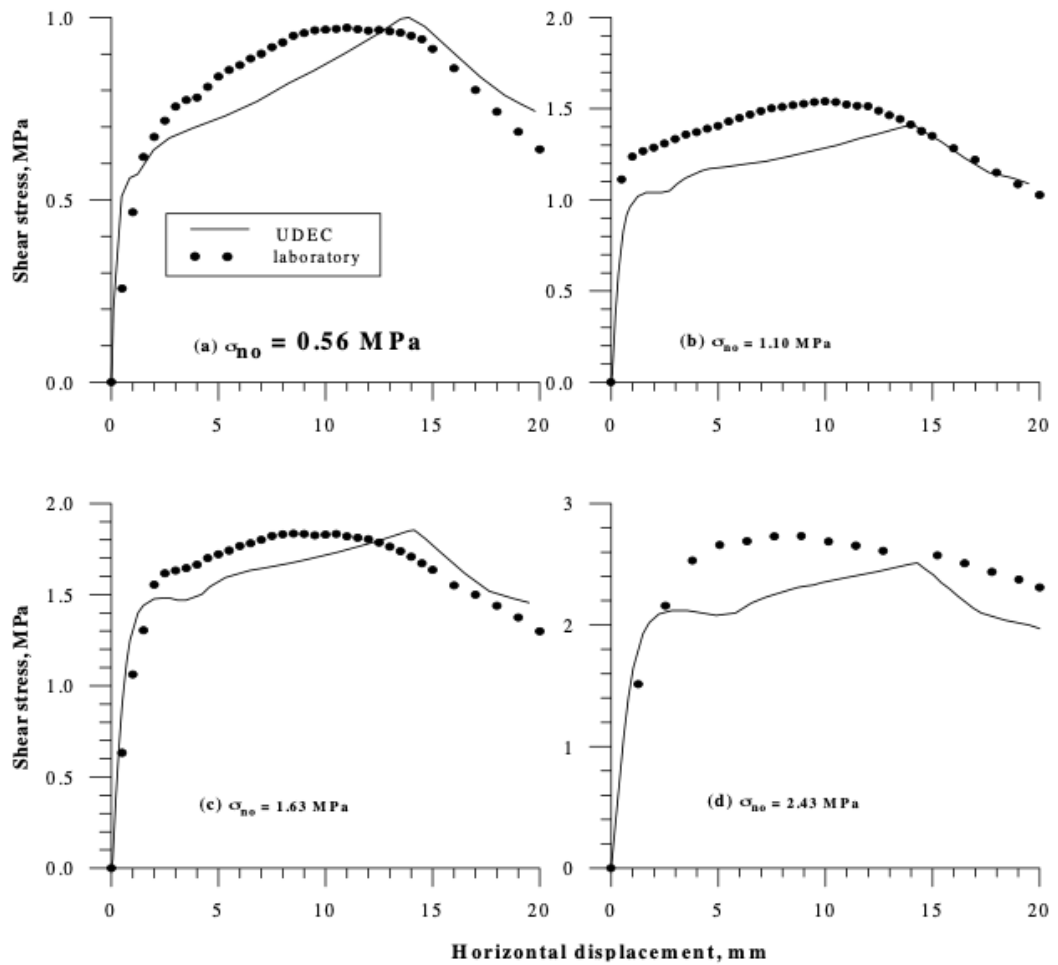


Figure 2.59: Comparison of UDEC simulated shearing and CNS samples (Haque et al., 2000)

Oliveira (2009) also utilised the CNS testing method and developed the normalised peak shear stress model highlighting the impact asperity thickness has on the joints' shear strength properties. This testing model demonstrated a decrease in shear strength for each increase in thickness ratio as shown in Figure 2.60.

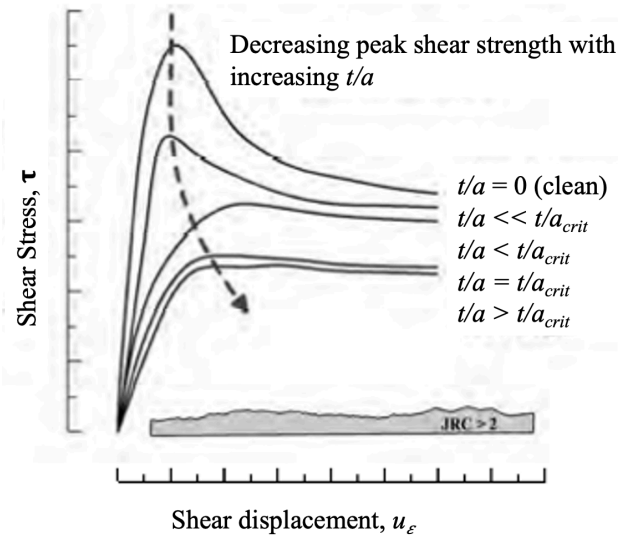


Figure 2.60: Relationship between infill thickness and peak shear strength. Modified from (Oliveira, 2009)

The analytical analysis was then expanded to a 2D numerical simulation. Constitutive equations were developed for the yield function, flow rule and hardening and softening components of the model. The resulting model was then adapted to a practical case study to aid in tunnel stability design as shown in Figure 2.61

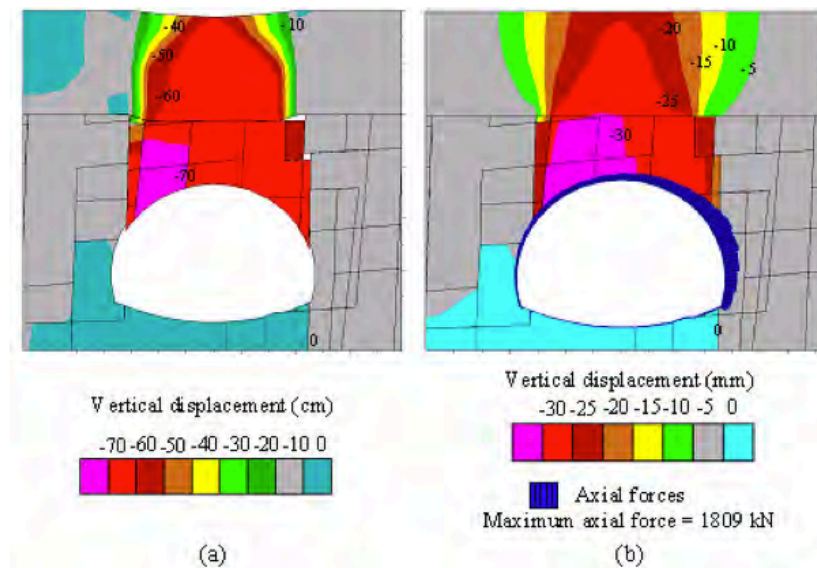


Figure 2.61: Lined tunnel with infilled joints (Oliveira, 2009)

Building on Oliveira (2009), Indraratna et al. (2012) and Mirzaghobanali et al. (2013) expanded the CNS shear capabilities to focus on dynamic loading. Two models were created, the CS model to determine the limiting shear strength and the Cy model accounting for progressive damage. The models were also developed to consider multiple variations of the ideal saw tooth discontinuity model as shown in Figure 2.62. Using these models and the laboratory experimental plan illustrated in Figure 2.63, Mirzaghobanali et al. (2014) achieved good agreement between the normalised index and the number of shear cycles between the developed model and laboratory testing as shown in Figure 2.64. However, the study was limited to a single infill material and therefore could not address the suitability of other specified infill materials.

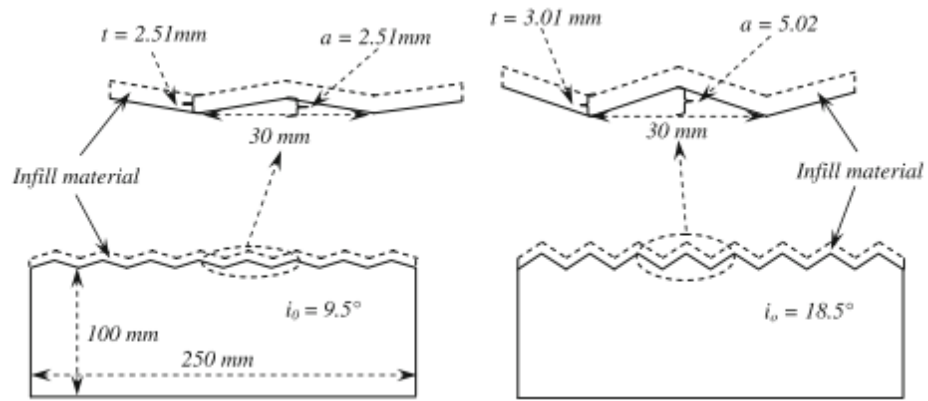


Figure 2.62: Illustrated infilled rock joints with varying friction (Mirzaghobanali et al., 2014)

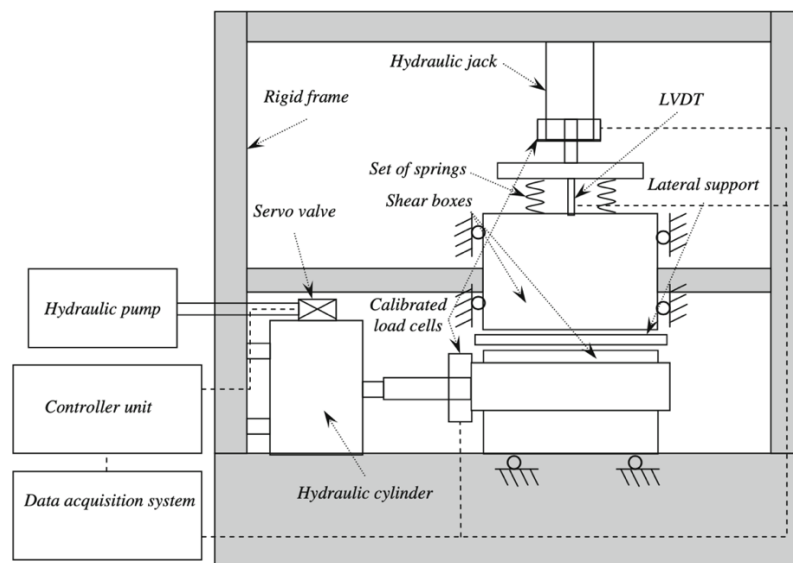


Figure 2.63: Cyclical shear test apparatus schematic (Mirzaghobanali et al., 2014)

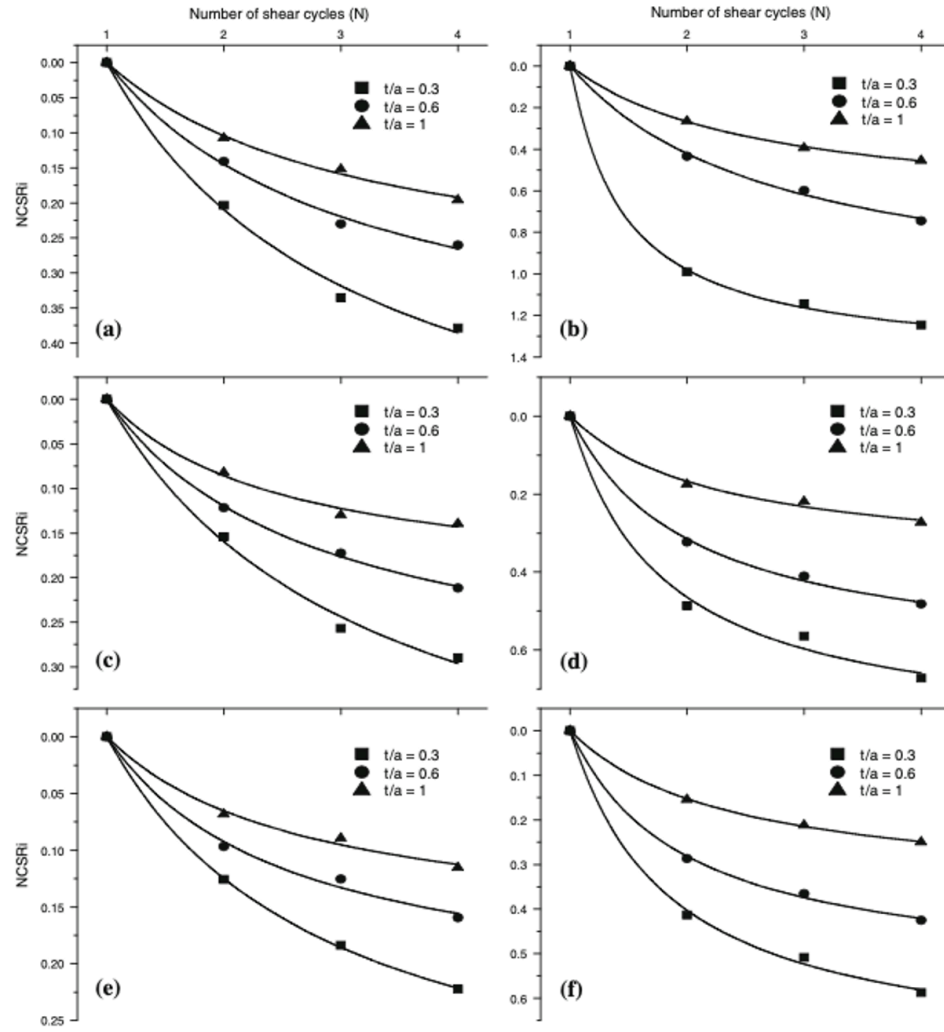


Figure 2.64: Comparison between numerical dynamic model (lines) and laboratory results (symbols) of NCSR against number of shear cycles. Modified from (Mirzaghobanali et al., 2014)

It has been determined that clay and sandy clay materials have a detrimental effect on the shear performance of rock joints due to their lubricating properties (Mirzaghobanali et al., 2014). Despite the numerous studies investigating the effects of infill joints, no identifiable study has been conducted on the effects of the infill material on the shear strength properties of rock bolts.

2.5.2 Three-dimensional infill studies

In addition to the two-dimensional investigations, limited studies have extended to include three-dimensional models. The simulations conducted by Karakus et al. (2016) extended the smooth joint contact model used by Lambert et al. (2014) as shown in Figure 2.65 to the flat joint-model. These models allowed for the discretisation of rock masses into spherical bodies.

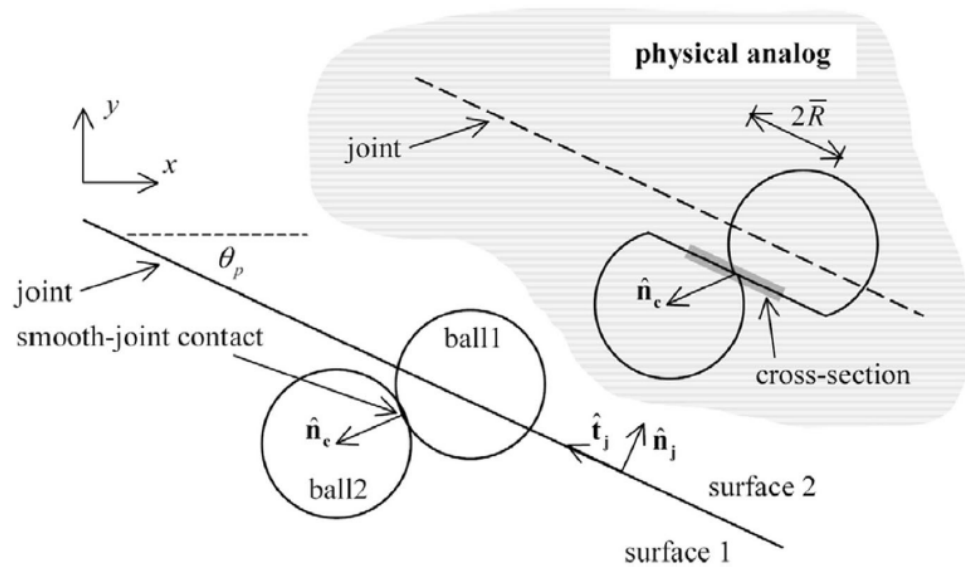


Figure 2.65: Illustration of smooth-joint contact (Itasca, 2005)

Karakus et al. (2016) modelled the shear joint profile by utilising the bond-particle model where each rock mass was discretised and represented by interactive spherical bodies outlined in Figure 2.66. Unfortunately, as the study was purely numerical it was unable to draw comparisons to laboratory based tests and instead drew comparison from the Barton model (Barton et al., 1977) for clean joints. However, the model presented close agreement with the clean joint model shown in Figure 2.67, but further verification against infilled tested samples was required to determine model suitability and reliability.

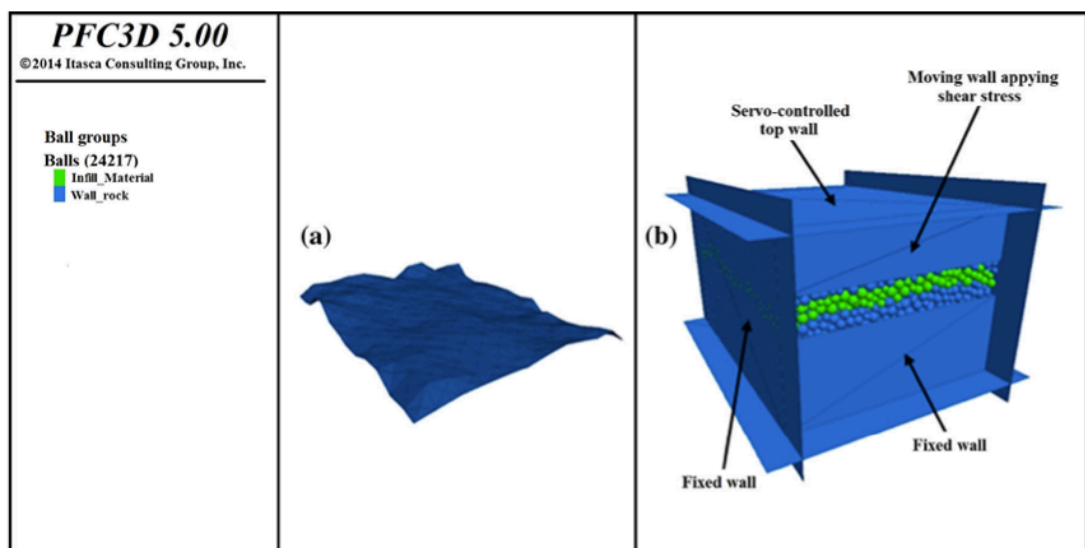


Figure 2.66: (a) Discontinuity profile, and (b) shear test model (Karakus et al., 2016)

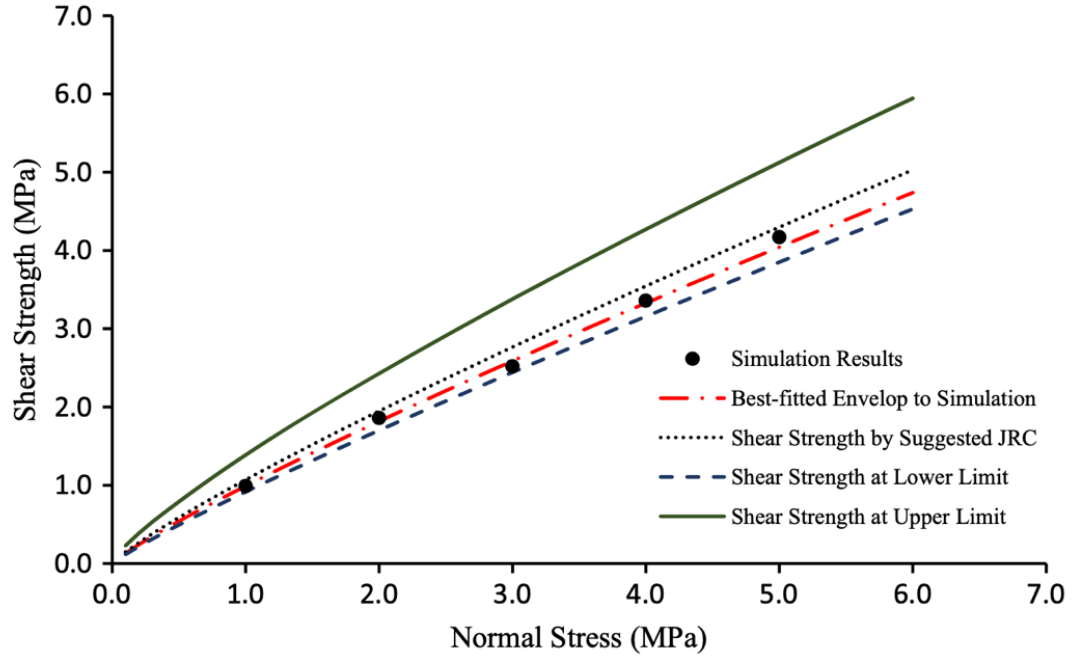


Figure 2.67: Comparison between simulation and Barton's model for clean joints (Karakus et al., 2016)

Extending on the bond-particle method, Shang et al. (2018) evaluated the effects of constant normal load and constant normal stiffness on the host rocks direct shear properties. By incorporating a discrete element method model using particle flow analysis as shown in Figure 2.68, it was possible to simulate the constant normal load (CNL) and constant normal stiffness (CNS) shearing methods in three-dimensional rock masses. While Shang et al. (2018) was able to provide a unique insight to the formation of shear and tensile micro-cracks, shown in Figure 2.69, the researchers faced numerous challenges with model calibration for samples with high normal stress. Additionally, due to the nature of this study, it was challenging to conduct physical experiments, rendering the study as theoretical.

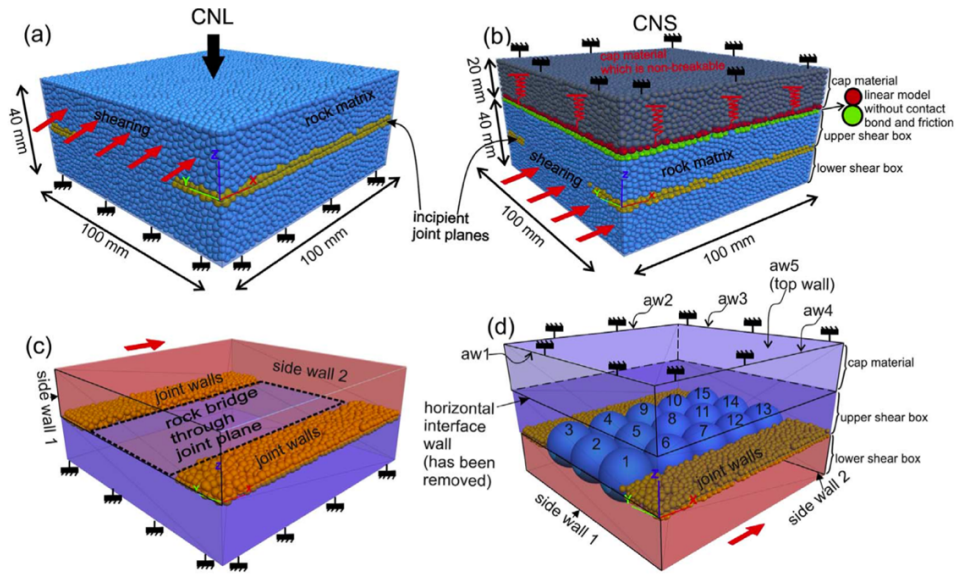


Figure 2.68: Constitutive models for CNL and CNS simulations (Shang et al., 2018)

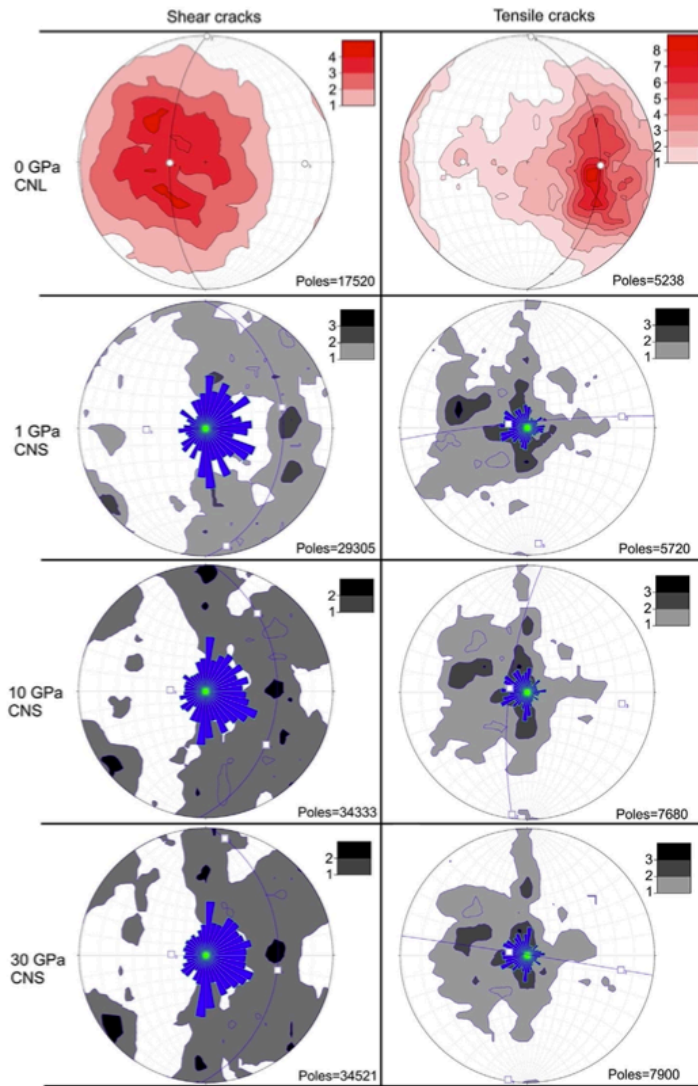


Figure 2.69: Model of the crack propagation with an initial normal stress of 40MPa (Shang et al., 2018)

2.6 Summary

As demonstrated by the above literature review, there are significant differences between steel and fibreglass rock bolts extending from mechanical performance including tensile load limits, corrosion resistance and usability limitations such as cutability. Extensive research has been conducted to quantify the load transfer mechanisms of rock bolts and cable bolts. However, it is noted that a majority of the studies discussed, only explored the load transfer mechanisms of metal rock bolts and cable bolts. As such, this literature review has identified three key gaps where the literature is lacking in the understanding of the shear behaviour of fibreglass rock bolts. Firstly, most of the reviewed testing schemes: tensile, single shear and double shear primarily evaluate the load transfer properties of metallic rock bolts and cable bolts. Few studies evaluate the performance of fibre-glass rock bolts. Secondly, there appears to be plentiful research addressing the impact infill has on the shearing properties of discontinuities. However, to the best of the author's knowledge, there is no systematic research study to investigate the effects of infill material on shear load transfer mechanisms of fibreglass rock bolts. Thirdly, analytical and three-dimensional numerical studies carried out in the literature are also limited to metallic rock bolts and cable bolts; primarily in a two-dimensional framework that does not accurately represent strata failure mechanisms.

Therefore, this study will focus on addressing the literatures' shortcomings by conducting a comprehensive investigation. Test schemes will include the shear behaviour of fibre-glass rock bolts with various tensile ratings under a range of pretension values, clean shear interfaces, and infilled shear interfaces. Furthermore, an analytical model verified by experimental tests will be developed to map the various shear responses of the fibreglass rock bolts. FLAC3D will be used to develop a numerical model to conduct a three-dimensional simulation of the shear behaviour of fibreglass rock bolts, as well as to conduct a sensitivity analysis. To successfully complete this research, the experimental design and testing schemes along with the initial testing have been outlined in Chapter 3.

CHAPTER 3: RESEARCH DESIGN AND METHODS

3.1 Introduction

This chapter outlines the research design and testing methods adopted to address the shear failure mechanisms of fibreglass rock bolts. Systematic tests were conducted to determine the mechanical properties of the system components including the grout, fibreglass, concrete, and infill material. Testing methods for the grout included dog-bone tensile, UCS and modified mixture UCS. The fibreglass mechanical properties were determined by: UCS, bending, tensile and single shear tests as well as parallel grain and perpendicular grain punch tests. Concrete properties were determined using UCS and Brazilian tests and finally, infilled parameters were found through direct shear testing and consolidation testing. The properties were then used as input values for the numerical models. Double shear testing methods were used to determine the shear load transfer mechanisms of fibreglass rock bolts. The double shear design, test setup and preparation are discussed in this chapter.

3.2 Experimental design

As outlined in chapter two the shearing performances of rock bolts can be determined using a number of methods each with varying representations of the bolts *in-situ* conditions. Shearing tests developed include; the single shear guillotine test in accordance with the British Standard for testing (2009), the double shear guillotine test and concrete imbedded double shear testing (Gilbert et al., 2015). Testing requirements for rock bolts and cable bolts are identical with various adaptations of these tests developed (Li et al., 2017b).

The shear behaviour of rock bolts can be determined using single and double shear testing. According to Li et al. (2017b), single shear testing does not accurately determine shear strength properties as the:

- Rock bolt is not encapsulated inside a concrete medium, thus, not representing rock strata,
- Single shear testing overestimates the shear strength of the rock bolt due to the two opposing metal frame bodies contacting during shearing shown in Figure 2.30 (Aziz et al., 2015c),
- Single shear testing is a passive shear test whereby the rock bolt is sheared without pre-tensioning, and

- Single shear tests are arduous to assemble and difficult to repeat.

The shear test apparatus developed by Aziz et al. (2003) and revised at the University of Wollongong (Li et al., 2016) provided a mode of testing that improved the accuracy of the shear failure mechanism of clean plane surfaces for rock bolts and cable bolts. However, there are still a number of shortcomings to the testing method including the lack of ability to determine the impacts of infilled discontinuities and the interference from the supporting frame as shown in Figure 2.30.

The interrelated properties of tendons, in addition to the modelling and numerical simulations conducted by Li et al. (2015) and Mirzaghobanali et al. (2017b), to develop and further refine the fibreglass rock bolt shearing numerical model in a three dimensional framework. Studies conducted by Indraratna et al. (2012), Oliveira (2009), Oliveira et al. (2010) and Karakus et al. (2016) on the shear properties of infill materials were also incorporated to transform the initial numerical simulation into a robust model for strata and infill conditions and bolt configurations.

Extending the research study carried out by Mirzaghobanali et al. (2017b), the testing apparatus (MKI) was modified to depict the clean plane shear/UCS relationship of fibreglass bolts in a medium scale setting.

The numerical model was then used to carry out sensitivity analysis to determine the significance of each parameter of the system. The study was also extended to include the effects of the shear plane surface (i.e. infill joints) on the fibreglass bolt's performance. This was accomplished by bonding the sandy/clay infill material to the shearing plane. The joint infill study was conducted primarily with a homogeneous shear interface relationship to allow for cross validation with the initial clean interface double shear testing apparatus. It was essential to maintain a uniform testing procedure for both clean and infill joints due to the limited understanding of the latter.

3.3 Experimental plan for clean discontinuities

Testing was conducted on several fibreglass rock bolts with commonly used load capacity ratings of 20 and 30-tonnes. Double shear testing was conducted through investigating the effect of bolt strength on the shear performance of fibreglass rock bolts at a range of pretension values.

Fibreglass rock bolts of various strengths were tested to determine the rock bolts performance on a passive rock bolt system (i.e. no pretension). The results formed the baseline performance data of rock bolts for a simplified uniform environment. The

strata UCS value was chosen following the study conducted by Li et al. (2016). This study identifies the host strata UCSs of 20MPa, 40MPa and 60MPa as an accurate representation of field conditions. The 40 MPa concrete strength was then chosen for casting simplicity. Additionally, wet concrete at a target strength of 40MPa was found to have ideal workability. The weaker 20MPa and stronger 60MPa mixtures were either too wet or too stiff to handle efficiently. The second experimental study explored the effects of varying pretension values on the shear strength of fibreglass rock bolts. To maximise sample uniformity, a single host media strength of 40MPa was used. The fibreglass bolts were fastened using their respective nuts and washers and torqued to pretension values of 0kN, 10kN, 15kN and 20kN in accordance with industry standards as indicated by Gilbert et al. (2015). The prepared samples were then sheared at the rate of 1 mm/min (Gilbert et al., 2015). Finally, data gathered from the investigations were used to validate the numerical and analytical models.

Table 3-1 outlines the experimental plan that was followed to successfully conduct the in-depth analysis of the mechanical properties of fibreglass rock bolts used to reinforce clean joints. A total of eight tests were conducted for the completion of clean discontinuities investigation.

Table 3-1: Experimental matrix for effect of pretension

Dowel (tonne)	Strata (MPa)	Pretension (kN)
20	40	0
		10
		15
		20
30	40	0
		10
		15
		20

3.4 Experimental plan for infilled discontinuities

The infill joint experimental study was divided into two investigations, namely:

- the effects of a sandy clay infill joint on the shear performance of fibreglass rock bolts.

- the impact of a range of pretension values on the shear performance of fibreglass rock bolts subjected to infilled conditions.

The double shear testing method was extended to infilled joints whereby joints were separated by 5 mm of the infill material at initial moisture content of 20%. The type, thickness and moisture content of infill material were selected based on studies by Oliveira et al. (2010) and Mirzaghobanali et al. (2014). As outlined in Table 3-2 eight tests were conducted to test two FRP rock bolts under varying pretensions. As the infilled material acts as a lubricant decreasing friction between rock strata, its lower shear strength was expected when testing infilled joints in comparison to those of clean joints.

Table 3-2: Experimental plan for reinforced concrete blocks with infilled joints

Dowel (Tonne)	Pretension (kN)
20	0
	10
	15
	20
30	0
	10
	15
	20

3.5 Equipment design

Double shear testing was carried out using the 150-tonne compression testing machine at the Engineering laboratory of the University of Southern Queensland. The prepared samples were positioned inside of the testing machine and then subjected to shearing at the shearing rate of 1 mm/min (Gilbert et al., 2015). The shear displacement was exerted on top of the middle block by a levelling load plate and the shear load measured using a calibrated load cell as highlighted in Figure 3.1. The load cell was attached directly to the shearing plate and the data collected using an inbuilt data acquisition system.



Figure 3.1: Outline of SANS Machine used for double shear testing

3.5.1 Shear box

In order to provide confinement around the concrete block during shear testing, a steel shear box shown in Figure 3.2 was designed and manufactured according to the samples dimensions and as per the shear testing procedure (Li et al., 2016). The confinement impeded premature failure of the concrete blocks during shear testing, allowing fibreglass to achieve its maximum shear strength capabilities. In civil and mining field conditions, confinement is provided naturally via surrounding strata.

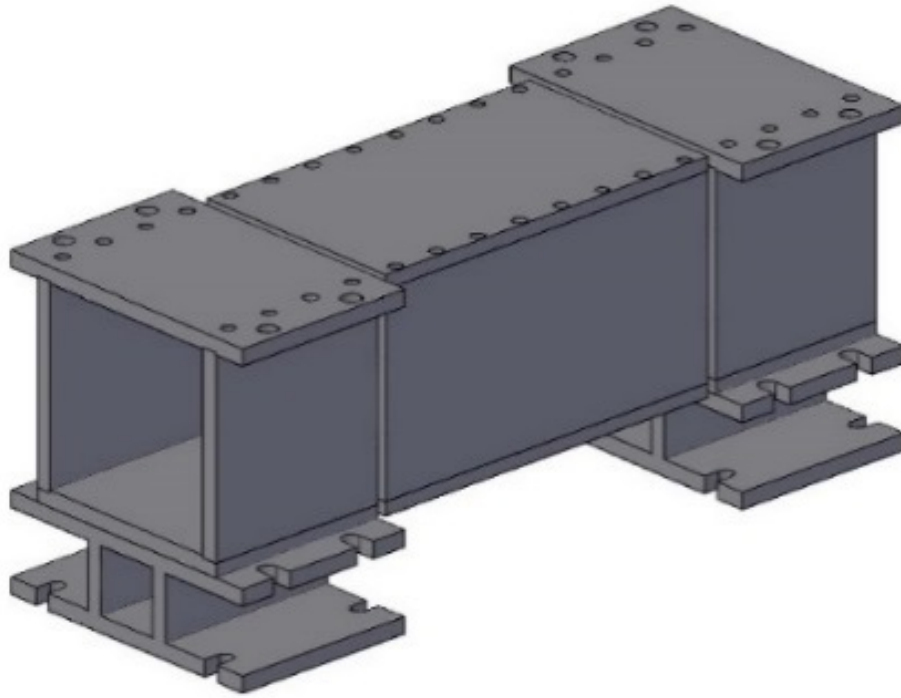


Figure 3.2: MK1.5 Double shear box design

The overall length of the confining box was 780mm with the total concrete length being 800mm. The 20mm difference in length created a 10mm allowance for the shearing planes. It was essential to minimise the unencapsulated surface area and maintain symmetry as the exposed area encounters different confinement pressures and has the potential to cause premature concrete failure around the jointed section. As such, the 20mm spacing was applied 5mm to each side of the shearing plane as illustrated in Figure 3.3.

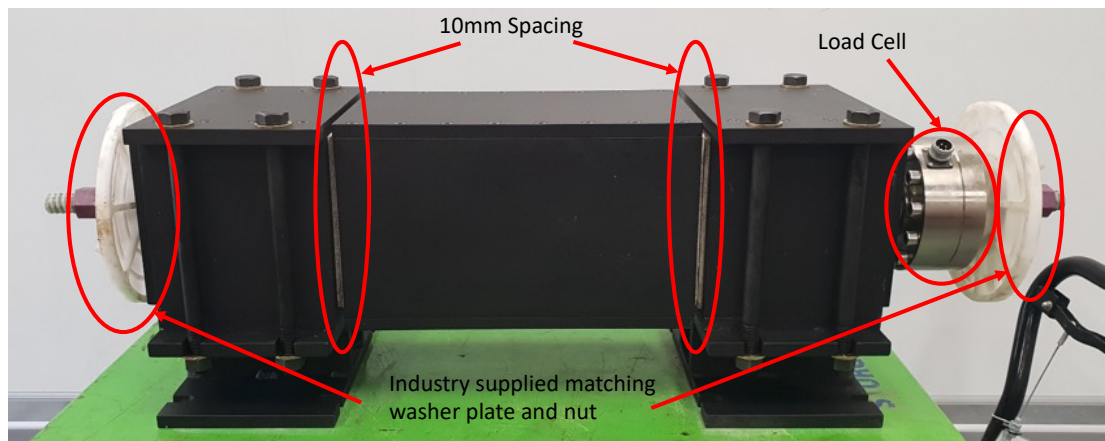


Figure 3.3: Assemble double shear apparatus highlighting key features such 10mm spacing at each interface

The 5mm spacing on each side of the shearing plane successfully addressed the issues relating to frame wedging encountered by the British standards testing method as depicted in Figure 3.1. Despite the British standard of testing measuring single shear performance, the rotation encountered during testing was also present during double shear testing as shown in Figure 3.4. It is noted that the addition of the 5mm spacer was successful with no evidence of frame wedging. While this method doesn't remove the presence of bending at the shear planes, it does successfully minimise the potential of mechanical interference of the test frame at the shear planes.

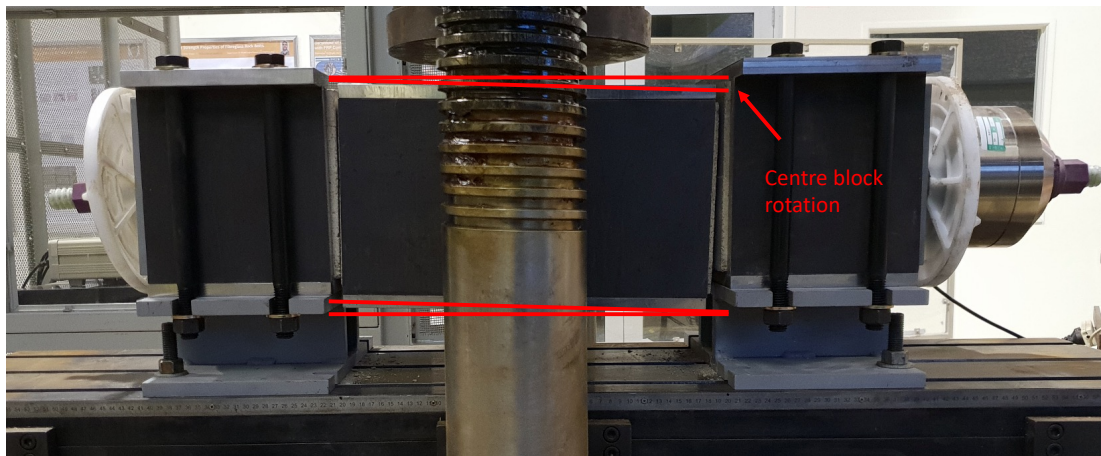


Figure 3.4: Centre block rotation because of testing

3.5.2 Mould design

Moulds were constructed utilising the UniSQ workshop CNC facilities to ensure uniform casting parameters as per the design illustrated in Figure 3.5. Each mould was designed to produce three individual concrete blocks that were later assembled to form a system with two shear planes. The blocks of the outer edge of the double shear system were cast to the dimensions of 200mm by 200mm by 200mm and the centre block to the dimensions of 200mm by 200mm by 400mm with a longitudinally intersecting hole with a radius of 16mm.

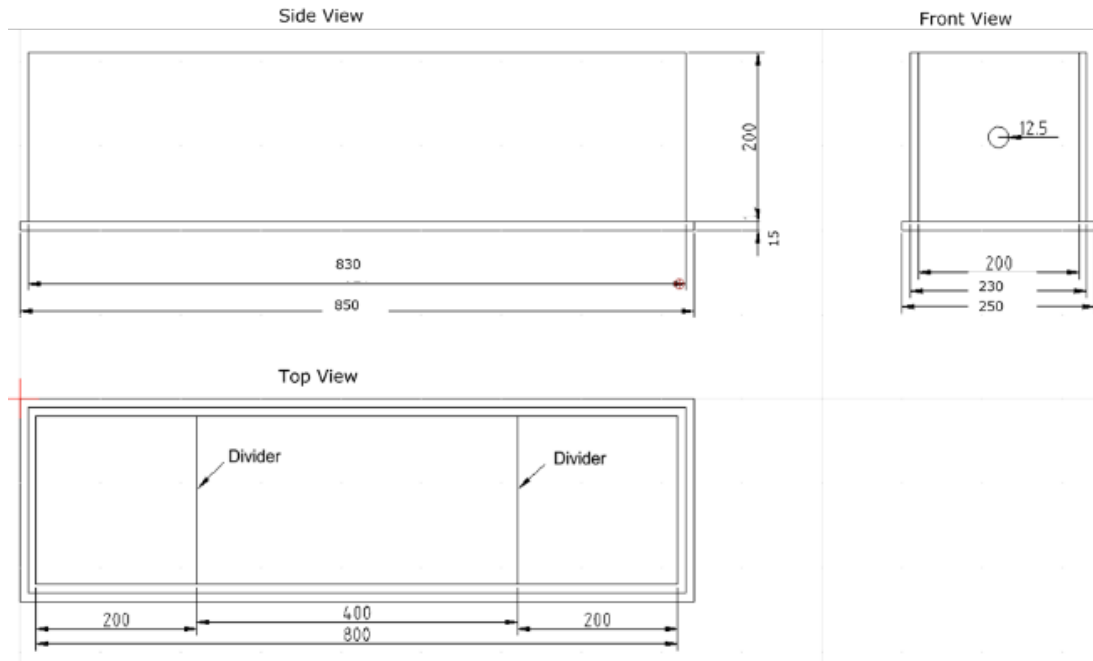


Figure 3.5: Double Shear mould design

The mould consisted of a series of timber panels, metal dividers, braces and an intersecting PVC pipe as shown in Figure 3.6. The braces were used to minimise mould deformation under the weight of the concrete during curing. To create a cavity for the rock bolt and to simulate the rifling that results from the drilling process, a rope was wrapped around the PVC pipe as illustrated in Figure 3.7. Care was taken to not wrap the rope too tightly as initial attempts resulted in the rope exerting inward axial forces on the pipe increasing the difficulty of disassembly. Once the concrete was poured and levelled, PVC conduits were then inserted into the centre of each block intersecting the PVC pipe. The conduits created a small channel directly to the rock bolt location allowing for a simpler grout charging process. Excess concrete was then poured into 100mm diameter by 200mm steel moulds for future UCS testing.

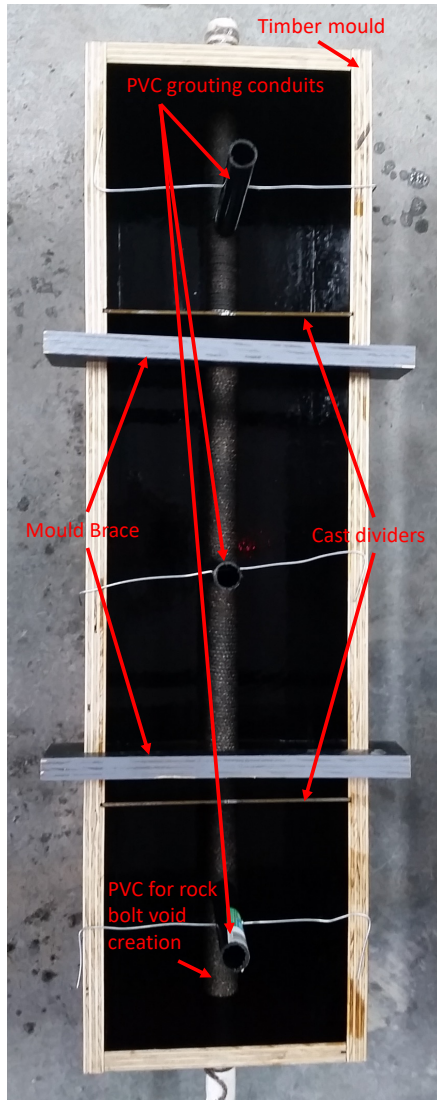


Figure 3.6: Double shear mould key features



Figure 3.7: Preparation for rifling simulation

3.6 Sample preparation

3.6.1 Concrete preparation

As per the experimental plan, the concrete blocks were cast to 40MPa specifications using a mortar recipe following the guidelines from Gilbert et al. (2015). Two specifications of concrete were cast with the first designed to achieve a UCS of 20 MPa and the second achieving 40 MPa. Initially the low strength 20MPa sample was cast using the cement, sand, and water ratio of 1:3:0.7, successfully resulting in a consistency similar to that of sandstone. Coarse sand was used instead of aggregate in an attempt to maintain cross-sectional uniformity. By adopting a low strength mortar-based recipe, the initial testing of samples proved the mixture did not have sufficient strength to shear the rock bolt. Figure 3.8 shows the severe damage sustained by the

concrete blocks prior to achieving failure within the rock bolt element. As such the mixture was adjusted to achieve a minimum strength of 40MPa using a cement, sand, and water ratio of 1:2.2:0.42.



Figure 3.8: Severe damage resulting from a weak concrete matrix.

The concrete production was completed using the climate-controlled facilities and curing room at the University of Southern Queensland to maintain the consistency and high-test quality. Each batch of concrete was mixed using the onsite concrete mixer and set into the moulds using a vibrator and scraper to remove bubbles and impurities resulting in clean uniform samples as shown in Figure 3.9 and Figure 3.10. The concrete was left to set for 24 hours, after which the moulds were disassembled, and the blocks placed into the curing room for a minimum of 28 days. The 28-day curing period was essential for ensuring the concrete was at peak design strength.



Figure 3.9: Cast of double shear sample.



Figure 3.10: Cylindrical concrete samples for UCS testing

As shown in Figure 3.10, excess concrete was cast into cylindrical samples and cured using the same process as the double shear blocks for testing the concrete properties. Samples were capped using plaster of Paris to minimise the impact of stress concentrations forming from surface imperfections as a result of casting. The fine composition of the plaster filled the surface irregularities and facilitated optimum transfer of forces. Prior to testing of the double shear blocks, the cylinders of the corresponding batch were tested under compression conditions. Only the peak value was recorded in order to determine the actual host UCS as shown in Figure 3.10 and Figure 3.11.



Figure 3.11: Concrete sample prepared for UCS testing



Figure 3.12: UCS concrete sample post test

The recorded properties were then used as inputs for the numerical simulation and to calibrate the simulated environment. The UCS results are presented in Table 3-3 and indicate an average of 57MPa. All samples tested met the minimum strength requirements and as a result all double shear tests were successfully performed to achieve rock bolt failure prior to host medium failure.

Table 3-3: UCS test results of the concrete used for double shear casting

Sample	UCS (MPa)	Load (kN)
1.3	52.65	413.3
2	50.50	396.6
3	55.90	438.8
4	50.90	400.0
6	59.40	466.8
7.2	61.50	482.9
9	67.50	529.7
Average	56.91	446.9

In addition, the cylinders were subjected to Brazilian testing methods to determine the equivalent tensile strength of the sample. Table 3-4 indicates an average tensile strength of 4.7MPa.

Table 3-4: Brazilian testing of concrete used for double shear casting

Sample	Tensile strength (MPa)	Load (kN)
1.2	5.20	163.0
1.4	4.30	133.8
2	3.53	110.9
3	5.15	161.7
4	5.00	157.6
5	4.76	149.5
7.1	3.52	110.6
7.2	5.40	169.7
7.3	5.10	159.0
Average	4.70	146.2

3.6.2 Pre-tensioning

Once the concrete samples were cured, the fibreglass bolts were positioned into the precast holes for final assembly. The rock bolt, concrete blocks, axial loadcell and the washer plates were assembled loosely and in the correct order for final tightening as illustrated in Figure 3.13. The pretension was then applied to the desired value as per the experimental plan in Table 3-1. The pretension (kN) was determined using the hollow load cell installed previously for the monitoring of axial loads. The pretension value varies between 0kN to 20kN similar to those currently applied in Civil and Coal Mining industries (Gilbert et al., 2015). The minimum pretension value of 0kN was achieved by installing wedges in the edge of the holes to overcome the weight forces of the washers, rock bolt and load cells and ensure the system was centred. The

remaining pretensioned samples had sufficient axial loads to ensure the system was centred. In order to minimise the effects of creep and settling, all samples had their respective pretensions applied 24 hours prior to grouting.



Figure 3.13: Assembled double shear samples.

3.6.3 Grouting

In the last stage of sample preparation, the reinforced concrete blocks were grouted through holes on top of the sample as shown in Figure 3.14. Additional cube samples were cast as suggested by (Aziz et al., 2014) for measuring of the grout mechanical properties. As determined during preliminary testing, grout mechanical properties such as UCS, shear strength and elastic modulus are a function of time (Mirzaghornanali et al., 2018). The grouted sample was left undisturbed for a period of seven days prior to the shear box assembly. This ensured that the grout UCS was greater than that of the concrete blocks and that the initial curing stage of the grout was complete, to achieve consistent performance during shear testing.



Figure 3.14: Hole positions on top of concrete blocks

Once the samples were cast and grouted, any excess grout was removed from the injection holes and then cleaned smooth to prevent stress concentrations. The sheared samples were then dismantled to investigate the grout encapsulation quality. As demonstrated in Figure 3.15, the rock bolt appropriately centred within the bore and the grout successfully encapsulated the entirety of the bolt with minimal voids. The highlighted section of Figure 3.15 illustrates the micro ridges formed by the rope technique adopted in section 3.5.2. The adopted techniques allowed for uniform encapsulation throughout the whole annulus area on all samples. Samples were left for an additional seven days to allow the grout/fibreglass interface to strengthen and ensure the grout strength exceeded that of the concrete.



Figure 3.15: Grouting quality examination after testing

3.6.3.1 Grout UCS test results

The grout UCS properties were evaluated to ensure an accurate understanding of all elements within the shear test schemes (Mirzaghornanali et al., 2018). As discussed, the grout preparation process was identical across all test schemes to ensure consistency and reduce variability of results. Results from the grout analysis were also utilised as a constant throughout all simulated states during the numerical analysis. The grout was subjected to an extensive comparative analysis to ensure confidence in its determined UCS property. This was accomplished by tracking the performance of the grout across increasing curing periods as well as testing the impact of sample volume on its UCS property. It was essential to know the impact of curing time on the UCS performance of grout as it was not viable to let each double shear sample cure for enough time for the grout to reach peak strength due to time constraints. The goal was to determine when the UCS of grout surpassed the UCS of the concrete as this would facilitate sufficient load transfer between each component. Samples were cast using a 75mm cubic mould for the small-scale samples while a standard cement cylindrical mould of 100mm diameter and 200mm height was utilised for the large-scale samples. It was determined that for small scales samples seven days curing was sufficient to exceed the strength of the host concrete while large samples required twice as long. Variations of the UCS performance between small-scale and large-scale samples could be an indication of underlying curing properties. Larger samples may have experienced a lagged curing period resulting in reduced yield strengths. Additionally, smaller rock and concrete samples in general show higher UCS values. This scale effect can be ascribed to the higher number of small joints in the larger samples when compared to small scale samples. Due to the minimal volume of grout utilised within the double shear samples, the small-scale strength properties were adopted and the samples were left to cure for a minimum of seven days.

Table 3-5: Grout UCS comparison between small-scale and large-scale samples.

Curing Time (Days)	Small Scale UCS (MPa)	Large Scale UCS (MPa)
1	44.1	25.9
7	68.0	28.0
14	72.0	49.0
21	84.1	71.7

3.6.4 Composite grout

During the sample preparation stage, a novel study was conducted to determine the effect of fly ash on the strength properties of the chosen grout. The tests were conducted to determine whether a composite grout should be adopted for the research study. As such, thirty-six samples were prepared using the outline method in section 3.6.3 and then tested at 1, 7, 14, 21 and 28 days of curing for fly ash content of 5%, 10%, 15%, 20%, 25% and 30% tests. Each set of tests contained six identical samples to ensure accuracy of the collected data.

The comparative UCS values for the samples at various curing times are presented in Figure 3.16. It is observed that while there was an overall increase in UCS for both sample sizes, the values of the 10% and 15% samples were consistently higher than all other samples for various fly ash content. The difference between in UCS was more pronounced from fourteen days curing where the UCS of the 10% sample was 89 MPa, whereas the 5% sample was 57 MPa. Figure 3.16 indicates a consistent strengthening process of the 10% samples where the observed UCS difference between 1 day and 28 days were 29 MPa and 89MPa respectively.

The observed failure mechanisms were typical to that of non-composite general grout samples and presented in three stages. At the initial stage of failure, micro-cracks were initiated. The second stage involved crack propagation. Finally, the third stage presented as complete failure.

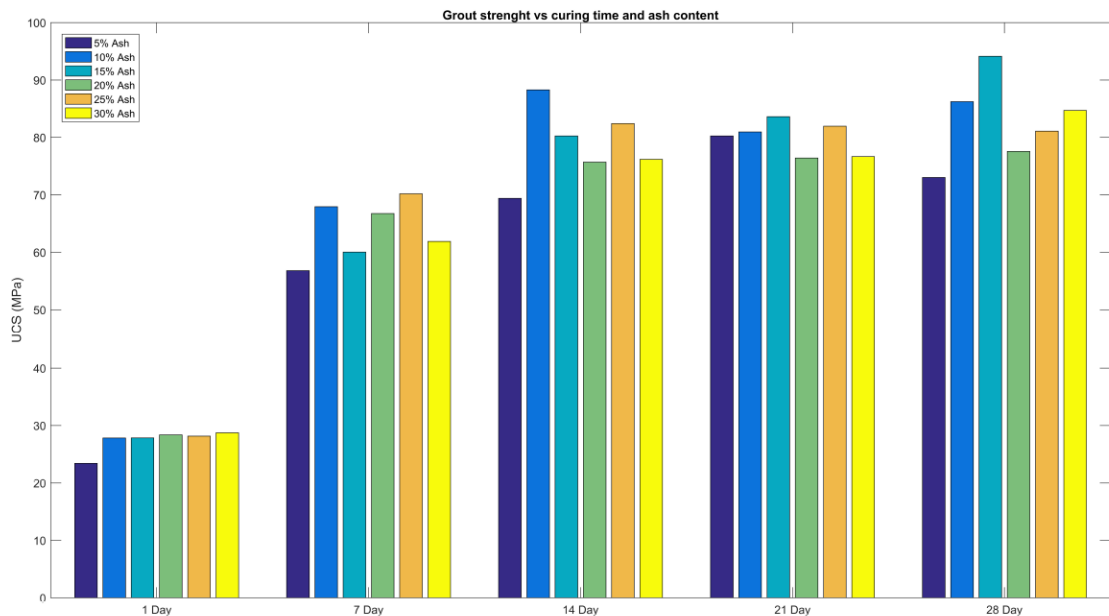


Figure 3.16: UCS for fly ash content at varying curing times.

The composite grout/ash study indicated significant strength improvements over the 10% to 15% ash content range reaching a maximum of 92MPa when mixed with the standard water ratio. Samples greater the 15% ash content, while indicating greater strength to that of the standard grouts, presented lower UCS values similar to that of the 5% samples.

3.6.5 Infilled discontinuities

Infilled material was applied to the double shear samples to assess the performance of rock bolts under more *in-situ* like shearing environments. To achieve this, the clean joint sample preparation was modified. An infill material comprised of sand and clay was created using a sand, clay and water ratio of 1:1:0.48 forming an easy-to-handle paste. This material was chosen as it replicates the composition of possible joint fill found in field environments (Mirzaghobanali et al., 2014).

The manufacturing of the infilled samples remained largely similar to that of the clean joint preparation. To adapt the sample preparation to include infill materials the following steps were included to the clean sample preparation method. Prior to aligning the blocks in preparation for inserting the rock bolt, the infill paste was applied to the surface of the shear face of two outer blocks to a depth of 5mm using a scraper ensuring a hole was left for the dowel as shown in Figure 3.17.



Figure 3.17: Layer of infill material on shearing plane of concrete section.

Once both outer blocks were completed, they were aligned and lightly pressed into shape against the centre block. Any gaps were then filled and smoothed off as shown in Figure 3.18.



Figure 3.18: Close up of the mating of the shearing planes with infill material.

Finally, the edges of the shear plane were surrounded in tape to minimise drying as shown in Figure 3.19. At this point the clean joint sample preparation technique was resumed.



Figure 3.19: Minimising infilled drying during preparation

3.7 Initial testing

3.7.1 Unconfined shear samples

Two preliminary double shear tests were carried out on reinforced concrete blocks without confinement. The results of the test were undertaken to trial the success and efficiency of the preparation method adopted. Tests were performed on 20MPa and 40 MPa concrete blocks reinforced with 30-tonne fibreglass rock bolts with no confining pressure as can be seen in Figure 3.20. Bolts were set to passive mode (i.e. no pretension) and sheared at 1 mm/min shearing rate.



Figure 3.20: Initial unconfined test 30-tonne

After one day of curing, the prepared sample was positioned in the compression-testing machine shown in Figure 3.22 and sheared to failure.

The peak shear load values were 5.7 and 8.5-tonne for 20 and 40 MPa concrete blocks, respectively. This highlighted the influence of the hosting medium UCS on the shear performance of fibreglass rock bolts that will be investigated in detail for both clean and infilled joints as part of this research study. Due to samples being tested in an unconfined environment, the rock bolts did not achieve failure and the test became an analysis of the systems bending performance.

Samples were carefully dismantled after testing to investigate the quality of grouting and encapsulation as shown in Figure 3.21. High quality encapsulations were observed for both the fibreglass bolt and concrete medium.

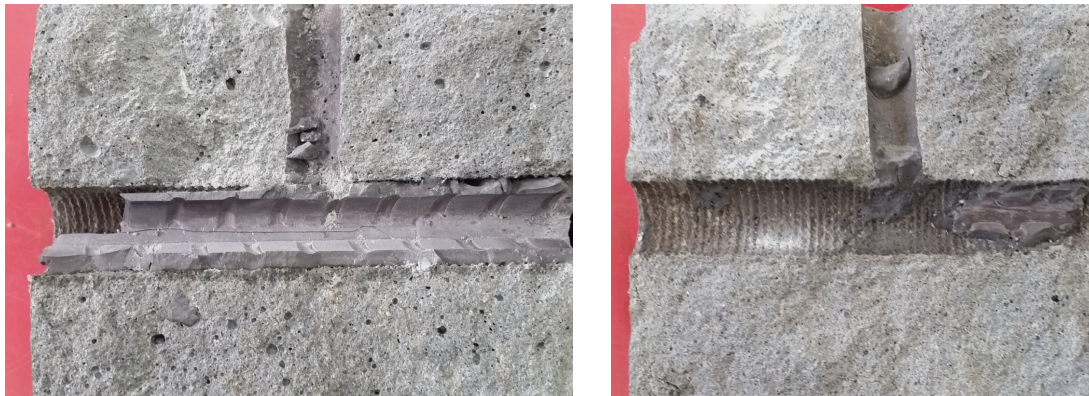


Figure 3.21: (left) high quality encapsulation around fibre glass bolt (right) around the concrete medium



Figure 3.22: Fibre glass bolt double shear testing assembly

3.7.2 Confined shear samples

The main double shear tests were carried out on reinforced concrete blocks using the MK1.5 designed confinement shear box as shown in Figure 3.23.

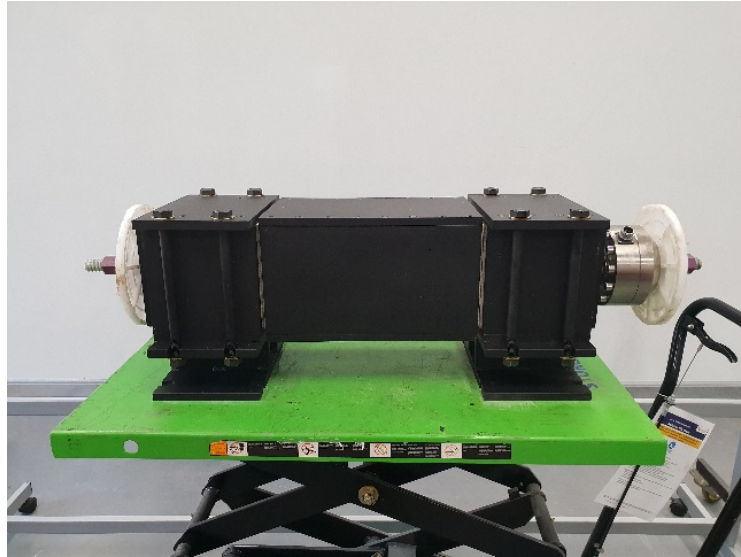


Figure 3.23: Assemble double shear system

Tests were performed on 20MPa concrete blocks reinforced with 30-tonne fibreglass bolts. The bolt was set with a pretension of 10kN and sheared at 1 mm/min shearing rate. The sample preparation procedure including concrete casting was previously defined in section 3.6.

The first test was conducted using the pretension of 10kN. It was evident that there was a significant axial transfer of load resulting in the pretension doubling to 22kN. Additionally, confined samples have also achieved a greater shear load to that of the preliminary study.

3.7.3 Grout material properties

To conduct the UCS tests eight samples were prepared at 1, 7, 14 and 21 days curing time for both small and large-scale tests as shown in Figure 3.24, Figure 3.25, Figure 3.26 and Figure 3.27. Some tests were repeated to ensure accuracy of the collected data.

The comparative UCS values for initial large scale and small-scale samples at the various curing times are presented in Figure 3.28. It was observed that while there was an overall increase in UCS for both sample sizes, the values of the small-scale samples were consistently higher than those of the large-scale samples for various curing times. The difference between the UCS of the large scale and small-scale samples was more pronounced for seven days curing times where the UCS of the small scale was 68 MPa, whereas the large-scale was 28 MPa. The two sample sizes were then compared to

determine a scale ratio. The scale ratio is defined as the UCS value of small-scale samples to large-scale samples. Figure 3.28 also indicated a delay in the strengthening process of the large-scale samples where the observed UCS difference between 1 day and 7 days for the large-scale test was just 2.1 MPa as opposed to 23.9 MPa for the small-scale test.

The observed failure mechanisms were typical of general grout samples and presented in three stages. At the initial stage of failure, micro-cracks formed. The second stage involved crack propagation. Finally, the third stage presented as complete failure.



Figure 3.24: Grout preparation

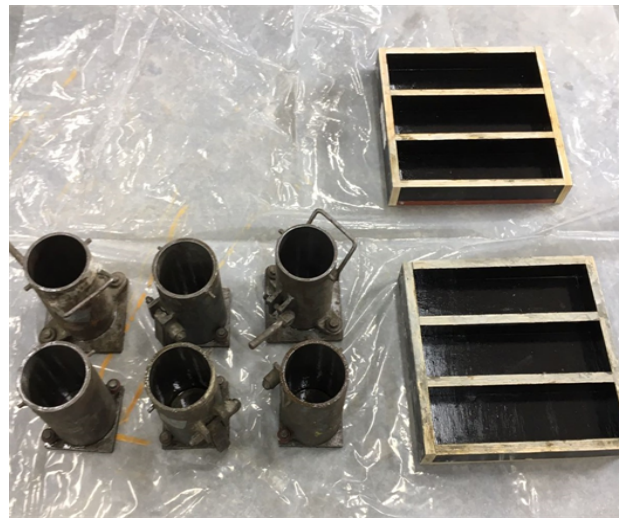


Figure 3.25: Large-scale and small-scale grout moulds

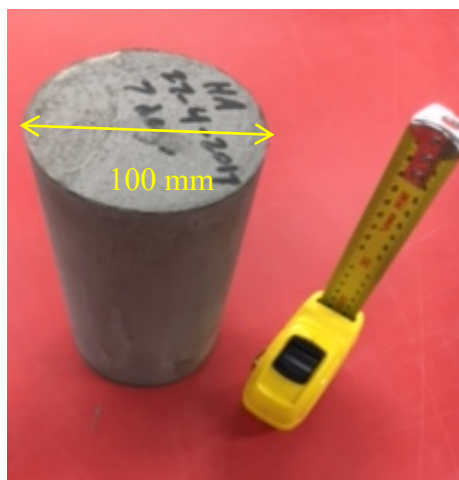


Figure 3.26: Prepared Sample 100 mm diameter (large scale) cylinder UCS

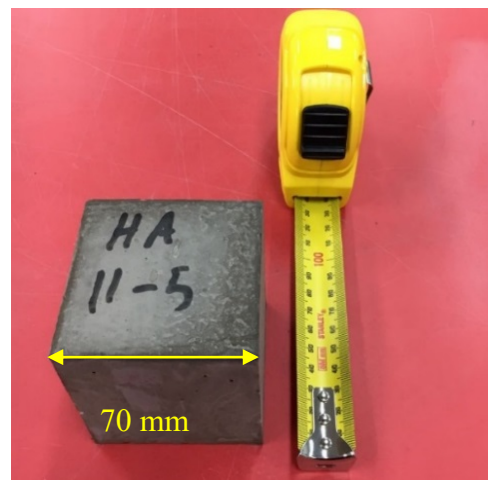


Figure 3.27: 70 mm side (small scale) cube UCS

The UCS values of each curing time for both the small-scale and large-scale samples are shown in Figure 3.28. The obtained UCS values show an increase in strength over the 21-day curing period for both small and large-scale samples, 44.1 MPa to 84.1 MPa and 25.9 MPa to 71.7 MPa respectively.

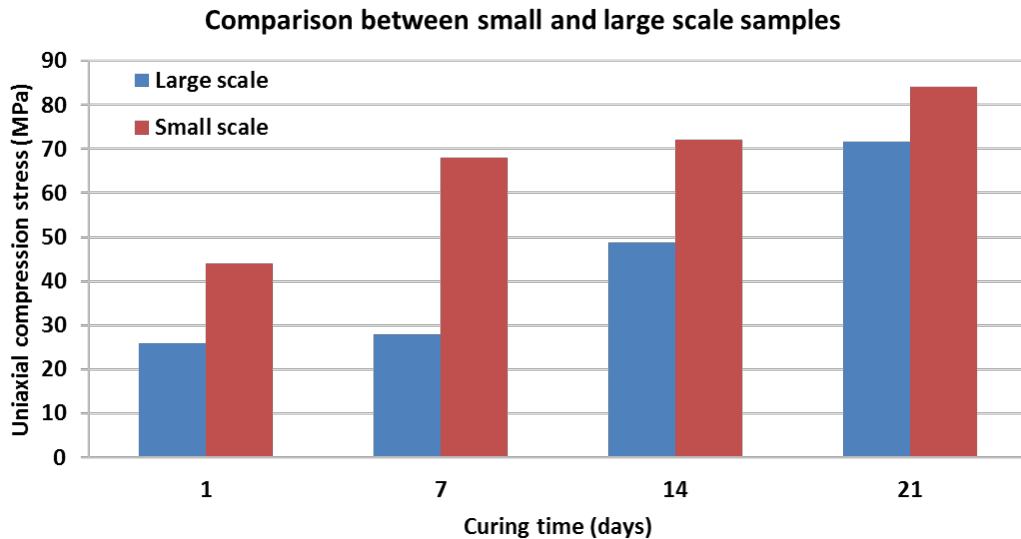


Figure 3.28: UCS strength of small-scale and large-scale grout at various curing times

Tensile grout mechanical properties were also determined by conducting a series of dog bone tests (Mirzaghobanali et al., 2019b). The dog bone tests were conducted for the determination of tensile strength properties according to the ASTM D638-02a standard using the Hounsfield tensile testing machine. The testing machine consists of two loading arms where the bottom arm is fixed, and the top arm subjects the load as determined by the software's input parameters and can be seen in Figure 3.29. The test equipment includes an internal automatic data logger with data recorded at a displacement of 0.001 mm.



Figure 3.29: Dog-bone tensile testing setup

During testing, the dog bone samples were placed into the top and bottom of the loading arms with each sample locking into place by seating into a bed of the same geometry as shown in Figure 3.30. A constant displacement of the upper arm at a rate of 0.2 mm/min was applied until failure of the sample. Upon reaching the yield point the sample ruptured as shown in Figure 3.31. After each test, the samples were removed, and the equipment thoroughly cleaned to ensure no broken fragments were present in the arms. The subsequent samples were then installed and tested using the same procedure.



Figure 3.30: Sample secured in testing rig



Figure 3.31: Sample after failure

A set of six samples were cast and tested for each of the curing periods: 1, 7, 14, 21 and 28 days. Figure 3.32 presents a comparison of all tensile samples. The determined yield point for each curing period was calculated as an average of the six samples and is presented in Figure 3.33. Figure 3.33 also shows that the yield strength of Stratabinder HS grout increases gradually with the curing period. The samples cured for 24 hours achieved a yield point of 550 Pa which then gradually increased at a rate of approximately 25 Pa for each subsequent curing period. The final 28-day samples saw an increase of 100 Pa compared to that of the 21-day samples and an increase of 180 Pa when compared to the one day cured samples.

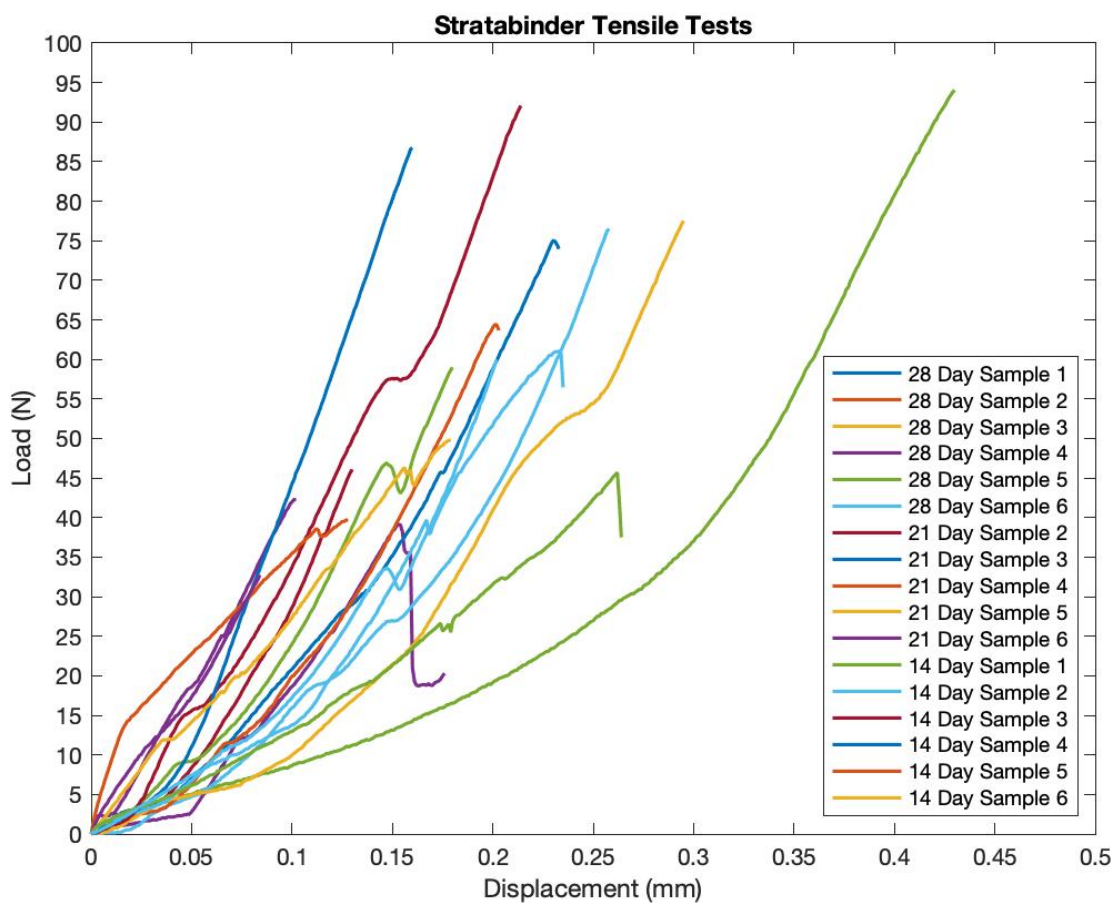


Figure 3.32: Grout comparative tensile test results

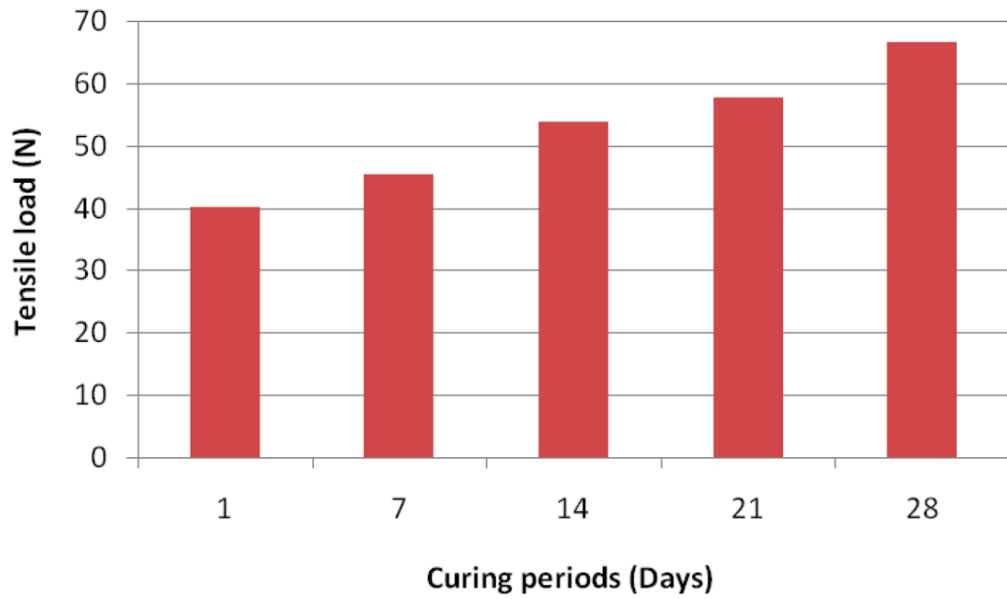


Figure 3.33: Average tensile results per curing period

This indicated that the tensile strength of Stratabinder HS grout was closely related to the curing time. Grout samples that cured for 28 days recorded the highest strength values.

3.7.3.1 Infill material properties

Analysis on the infill soil properties were conducted to ensure a comprehensive understanding of their behaviour under shearing and compression. Consolidation and direct shear tests were conducted under various conditions to determine how the chosen material would behave within the double shear system. The outcome of this study was then incorporated into both the analytical and numerical simulations of Chapter 6.

3.7.3.1.1 Consolidation testing

The understanding of the consolidation properties of the infill materials was relevant to the analytical and numerical component of this study, as it was vital for the development of accurate models. The inclusion of pretension subjected the shear interfaces to compressive forces. This resulted in the eventual reduction in void space. The infilled sample with an initial moisture content of 17.6% was subjected to the consolidation test with normal stresses of 0kPa, 6kPa, 12.5kPa, 25kPa, 50kPa, 100kPa and 200kPa. Each setting of the normal stress was maintained for a 24-hour period. Figure 3.34 highlights the infilled materials void ratio response to compressive loading

over time. As a result, a compressive index of 0.32 was determined and then adopted within the later simulations.

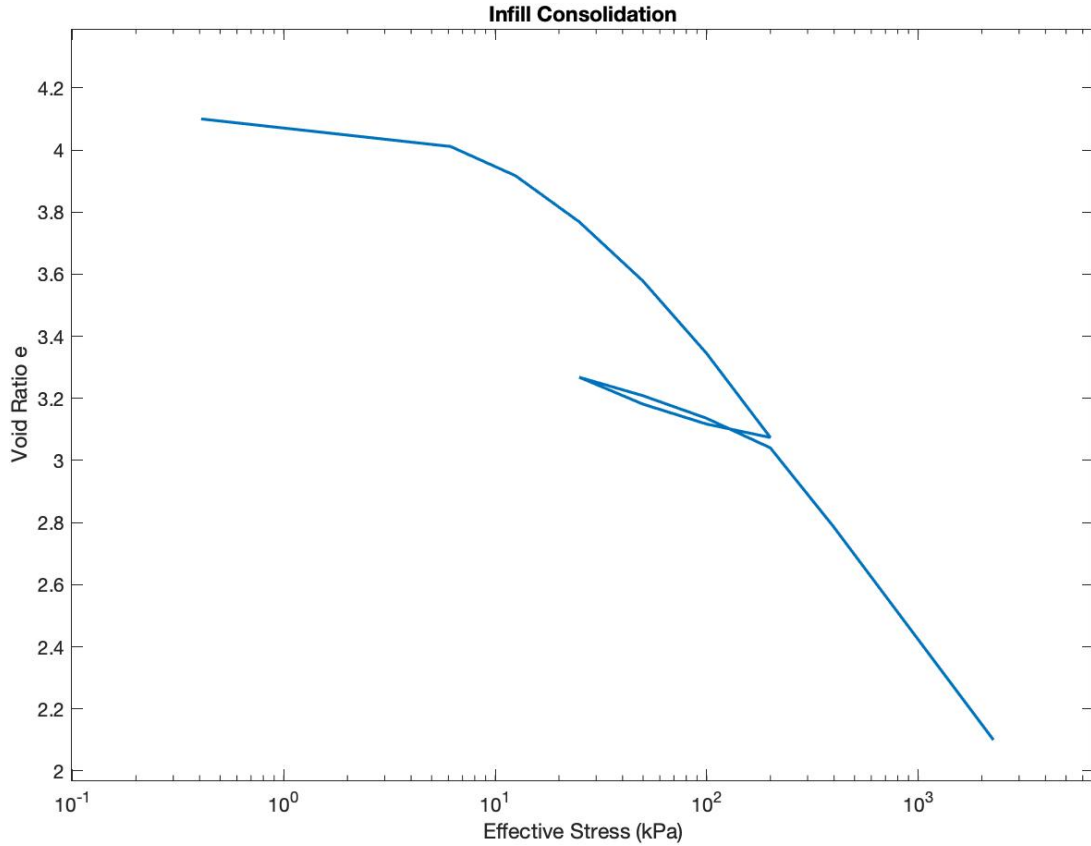


Figure 3.34: Consolidation test of the sandy clay infilled material.

3.7.3.1.2 Shear strength properties of the infill

The direct shear tests were conducted in two states, undrained and drained consolidation. Depending on the localised environment of the infilled material, infill in the field can present in both forms. However due to the double shear sample preparation process, all tested samples were in a state of drained consolidation. Despite this, the undrained properties were determined for comparison. During the grout curing process, moisture was drawn from the infilled material by the concrete and surrounding atmosphere. The drained consolidation results were chosen as the primary data set for the future modelling as this closely aligned with the experimental testing scheme. Normal constant stresses of 0kPa, 125kPa, 250kPa, 375kPa and 500kPa were applied to the infilled samples during shearing. Samples were sheared at a rate of 1mm/min to provide consistent test parameters with the double shear test systems. Drained consolidation samples registered increased moisture content losses with each increase to the normal constant stress. Samples subjected to a normal constant stress

of 250kPa experienced the greatest reduction in moisture content with a drop of 4.45 during testing. From plots in Figure 3.35 and Figure 3.36 the drainage condition and increasing normal pressures did show over consolidation characteristics and the two test types presented slight differences to the materials shearing properties. As the normal stress was increased, the undrained samples did not plateau with the increasing displacement but continually increased throughout the entire displacement range. Conversely, the drained samples settled to a constant shear force prior to the end of the tests. The direct shear test results were then used to determine the friction angle of the infilled material in each state. It was clear that changing the drainage property of the samples resulted in sufficient changes to the friction angle of the material where the undrained samples recorded an angle of 32.2° while the drained samples presented an increase of more than 7° resulting in a friction angle of 39.5° .

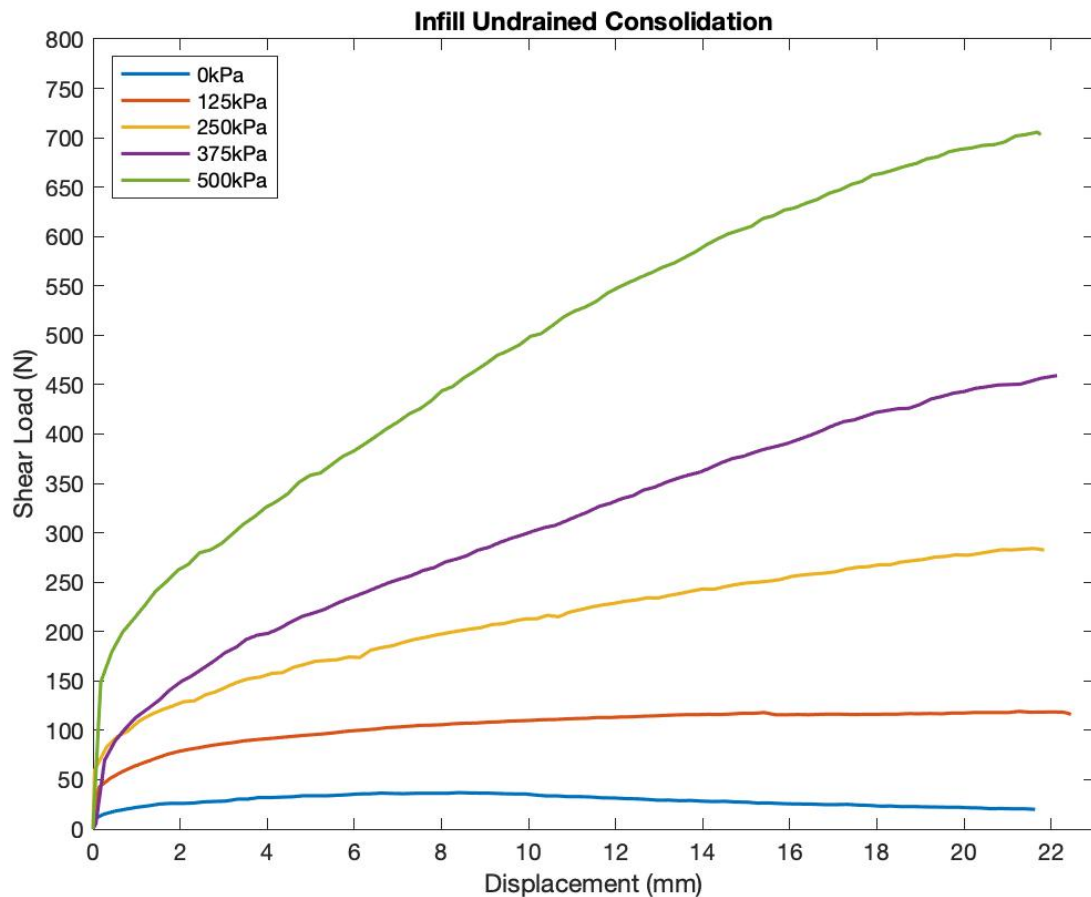


Figure 3.35: Undrained direct shear test of infilled material

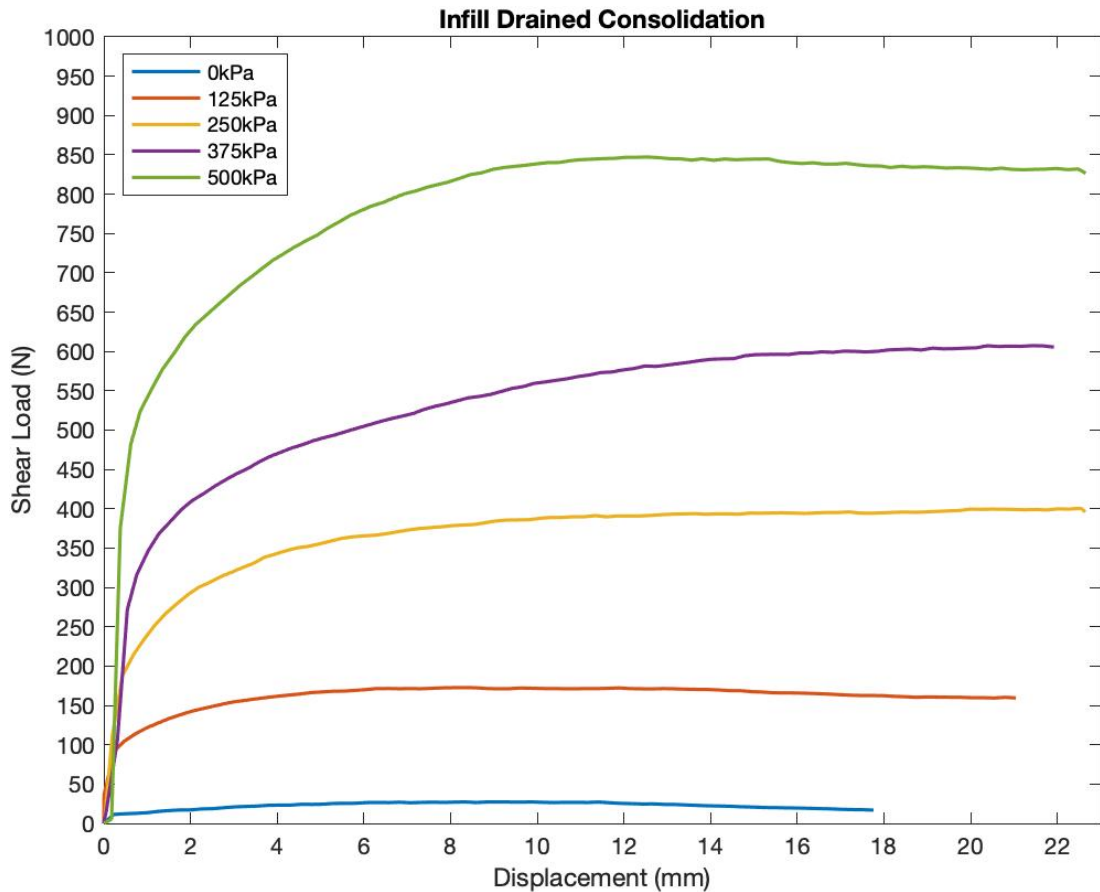


Figure 3.36: Drained direct shear test of infilled material

3.8 Fibreglass rock bolt properties

The GRP bolts selected for this study were supplied solely by Applied Research of Australia (AROA) and were manufactured using the pultrusion method. This is a production technique where glass strands are mechanically pulled through a saturated thermoset resin and heated. Afterwards the strands are guided through a heated forming and curing die. The combined glass-resin then leaves the die in a solidified state and is tensioned through a pulling system creating a matrix with large resistance to tension (Frketic et al., 2017). The pultrusion method results in continuing strands that are then cut to the design lengths, typically 1200mm, 1500mm, and 1800mm, however, custom lengths are available.

Table 3-6 below outlines the design specifications of the range of AROA bolts available on the market. The bolts selected for testing include the 20-tonne dowel and the 30-tonne dowel.

Table 3-6: Comparison of fibreglass rock bolts of different design strengths (DSI-UNDERGROUND, 2021)

	15 Tonne Dowel	20 Tonne Dowel	30 Tonne Dowel
Tensile Strength	150kN	200kN	300kN
Nut/Thread Tensile Strength	50kN	55kN	55kN
Single Shear Strength	45kN	50kN	60kN
Nut Breakout Torque	38-41Nm	38-41Nm	38-41Nm
Mass Per Metre	645g	645g	645g
Nominal Bolt Diameter	20mm	20mm	20mm
Nominal Cross Section Area of Bolt	310mm ²	310mm ²	310mm ²
Major Bar Dimension	25mm	25mm	25mm
Specific Gravity in grams/cm³	1.7-1.8	1.8-1.9	2.1-2.2

Due to the unconventional testing method adopted throughout the double shear stage of this study, custom samples were required: both in length and thread design. As indicated in Figure 3.37 below, the typical bolt design includes threads at only one end of the dowel as the other end remains embedded in the strata. The modified double shear testing equipment, however, required both ends of the dowel to remain exposed to allow for symmetry of the system and the application of pretension, this can be seen in Figure 3.38.

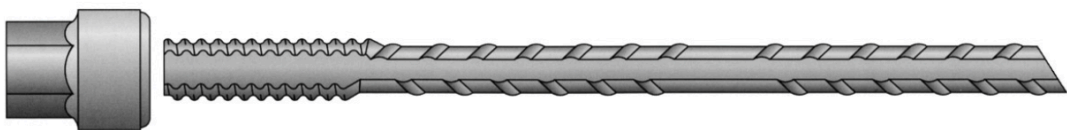


Figure 3.37: Illustration of fibreglass bolt geometry

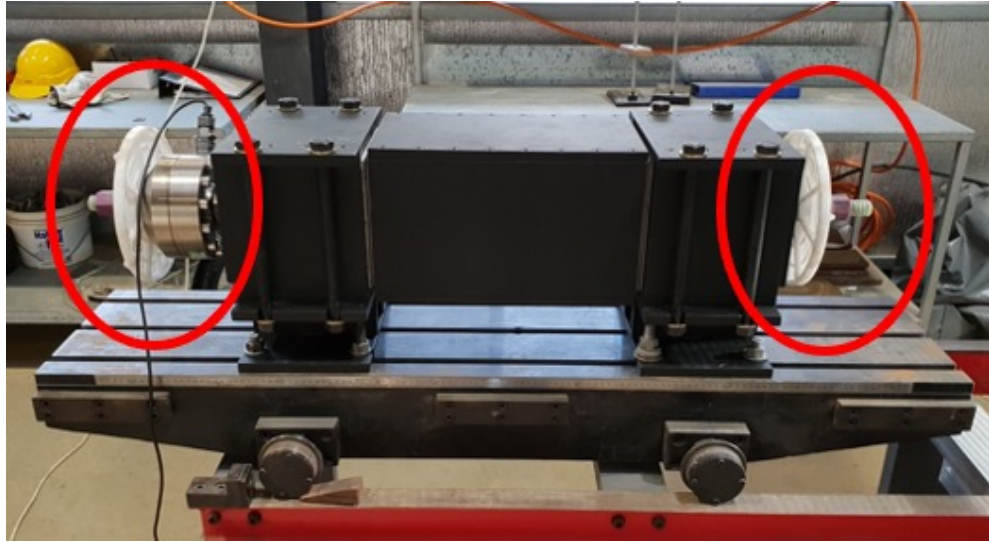


Figure 3.38: Double shear testing apparatus with double ended threads

3.8.1 Tensile

Tensile tests were conducted on the rock bolts to determine key failure characteristics including elastic yield, plastic yield and peak yield failure. The dowels used were the standard one-sided thread bolts. The supplied bolts did not match the required length specifications and as such were cut using a bandsaw to a length of 1.3m resulting in an exposed length of 400mm. The dowel was anchored on each end using 42mm diameter threaded metal sleeves. The base of each sleeve was sealed using a 45mm diameter metal bolt with 100mm thread. To ensure sufficient sleeve bondage, 150g of Bristar 100 expansive grout was poured into the sleeve. Due to the fast curing of the grout, the dowels were immediately but slowly inserted into the sleeve. To minimise bubble formation, slight rotation was applied during insertion and plastic wedges were then used to ensure the dowel was centred and level. The sample was then left to cure for a minimum of six hours at which point the dowel was inverted and the same process applied to the other end. Once both sides were grouted the sample was left for a minimum of three days prior to testing.

When the minimum cured period had lapsed and the sample was scheduled for testing, the exposed dowel section was wrapped in plastic to prevent debris. The samples were then secured into the testing equipment. However, due to the spiral bound design of the fibres, unravelling had the potential to negatively affect the strength properties of the dowel and as such the bolts were axially secured using a Stillson wrench. Figure 3.39 highlights the aggressive unravelling of the fibres during testing.



Figure 3.39: Tensile test post failure

Figure 3.40 compared all three rock bolt tensile results. Sample A was a 15-tonne rock bolt and was the weakest with peak values averaging 15.5kN. Sample B was a 20-tonne rock bolt and averaged 17.8 tonnes and as such achieved 89% of its designed rating. The performance of sample C or the 30-tonne rock bolt was 25.6 tonnes at 85% of its design load. The overall test variation was calculated at 6% to 18% and was considered a sufficient test quality, however, all samples failed to meet their design load. This was most likely due to variation in testing methods, testing equipment and sample preparation. The industry determined tensile properties do not indicate the exposed length of the rock bolt and as such will achieve different results.

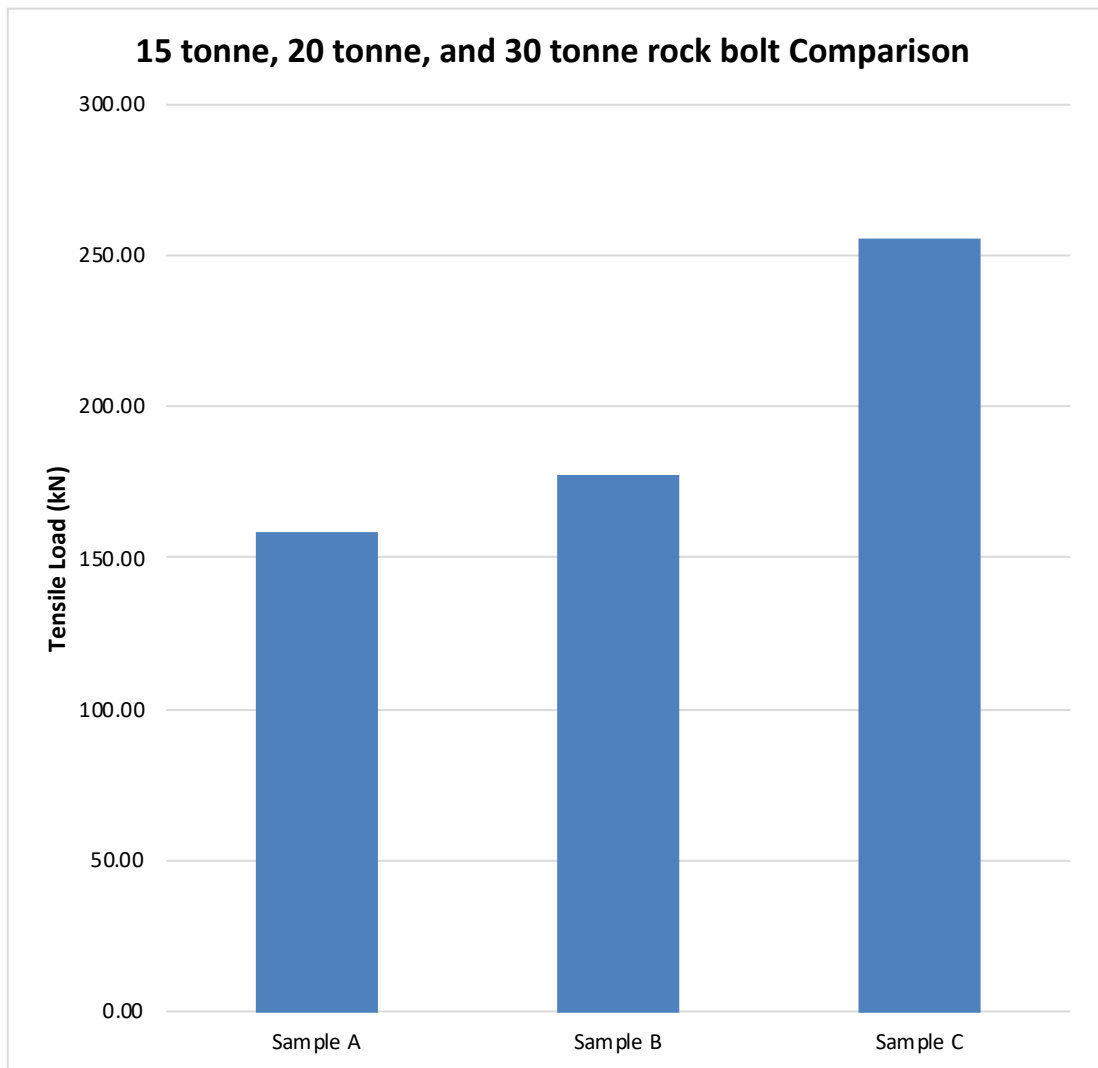


Figure 3.40: Tensile test comparison of 15-tonne, 20-tonne, and 30-tonne rock bolts

3.8.2 Bending

Bending tests were conducted using a four-point bending frame connected to the compression testing machine as illustrated in Figure 3.41. Tests results were inconclusive as shown in Figure 3.42. There was no discernible pattern of failure with each sample recording significant differences in the elastic region, plastic deformation zones, peak failure and residual loads. The only similarity evident was the gradient of the elastic region, however, this could not be confirmed as each sample recorded unique displacement ranges for this region.



Figure 3.41: Four-point bending test setup of fibreglass rock bolts.

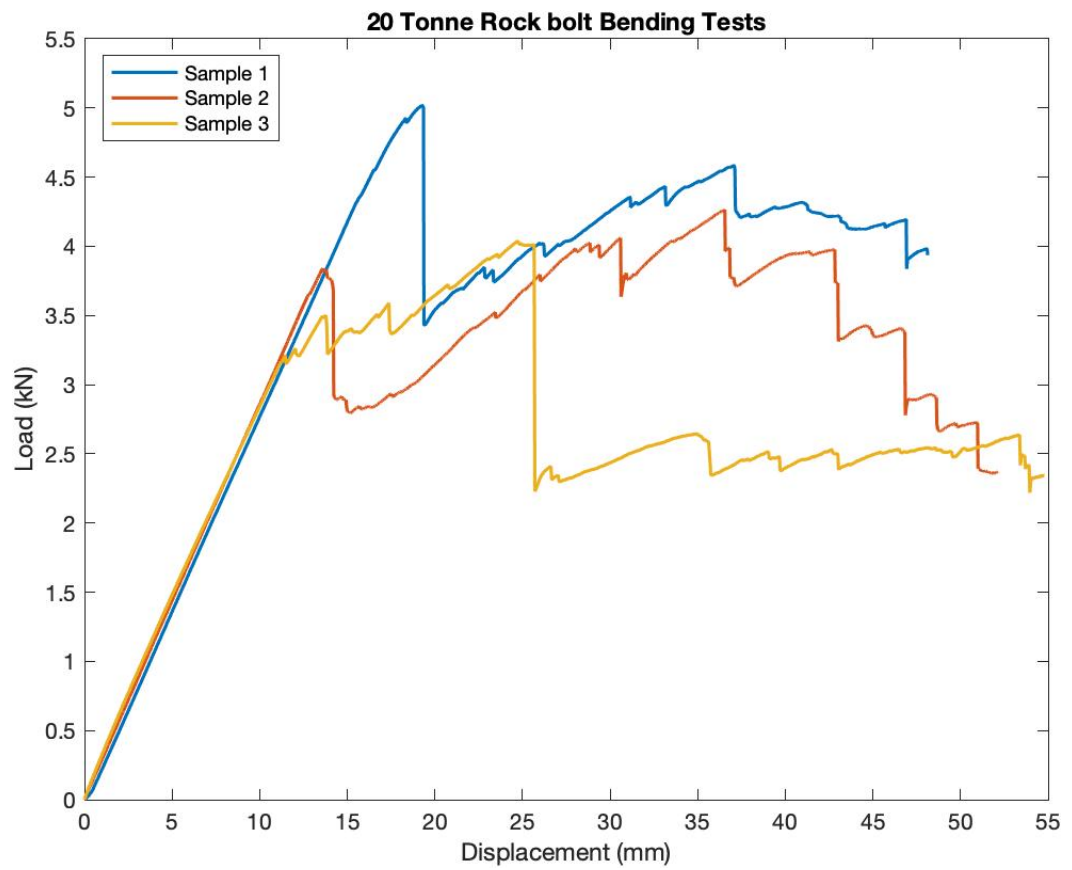


Figure 3.42: Rock bolt four-point bending test results

3.8.3 Punch test

The punch test was used to determine the strength properties across a small section of the dowel. The testing was conducted both parallel and perpendicular to the fibres within the dowel. To prepare the samples for the parallel punch test, the dowels were cut to a 3mm thickness perpendicular to the axis, resulting in circular samples as shown in Figure 3.43. The perpendicular test samples were cut to a 3mm thickness parallel to the axis along the centreline which resulted in the rectangular test samples shown in Figure 3.44.



Figure 3.43: Punch test parallel fibreglass sample



Figure 3.44: Punch test perpendicular fibreglass samples

Once the dowels were prepared, the samples were then placed in to frame with a centre ram. The centre ram was then inserted so the sample could be aligned to ensure the ram exerted on the centre of the sample. A locking screw was then used to secure the sample in place. Once the sample had been prepared and the apparatus assembled it was aligned in the centre of the compression testing machine to ensure accurate and uniform load application.

The calculations for the perpendicular tests were split into peak stress and elastic stiffness; however, the parallel tests only used the peak stress calculation. A load ratio between the perpendicular and parallel test was calculated to determine the strength variation to fibre orientation.

The perpendicular failure test results indicated a failure load of approximately 13 to 14kN and so there appears to be limited correlation between the rated dowel strength and small area punch failure and no variation in failure displacement across samples. However, the elastic stiffness varied across samples. The 20-tonne rated dowels averaged a stiffness between 14.2kN/mm and 16.3kN/mm while the 30-tonne rated samples resulted in an elastic stiffness of 18.4kN/mm. These stiffness variations indicate that the 30-tonne dowel can withstand slightly greater forces prior to deformation compared to the 20-tonne samples.

Similar to the perpendicular failure, the parallel punch test peak loads trend independently to dowel strength ratings with average peak loads ranging between 3.5kN and 4.1kN. By comparing the failure loads of both the perpendicular and parallel tests a ratio could be determined. Sample B and C resulted in similar load ratios with an average of 3.81, while sample A only scored 3.26. As such it was assessed that sample A was a weaker sample. Overall, the punch test was successful with only one discarded test. Sample C Test 1 was discarded due to reaching the limit of the compression tester resulting in an invalid result.

3.8.4 Single shear

The single shear test was conducted to identify the ultimate shear strength of the fibreglass rock bolts. The metal shear apparatus utilised does not reflect the failure mechanism encountered in real world applications, however the results of this test inform the calibration of the numerical simulation.

All samples had a diameter of 20mm with partial threads and were cut to a length of 150mm as shown in Figure 3.45.



Figure 3.45: Single shear fibreglass samples

A comparison of the peak forces for each sample indicated negligible correlation between shear strength and the samples' tensile rating. Figure 3.46 demonstrates similar average shear performance across rock bolts of all strengths. There does however appear to be a relationship between load rating and displacement. As the load rating increased, the failure displacement decreased as indicated by Figure 3.47. The cracks found throughout the dowels appeared to form parallel to the plane and could have been a results of design issues with the resin. The cracked samples were tested, and it was identified there was no significant variation in results.

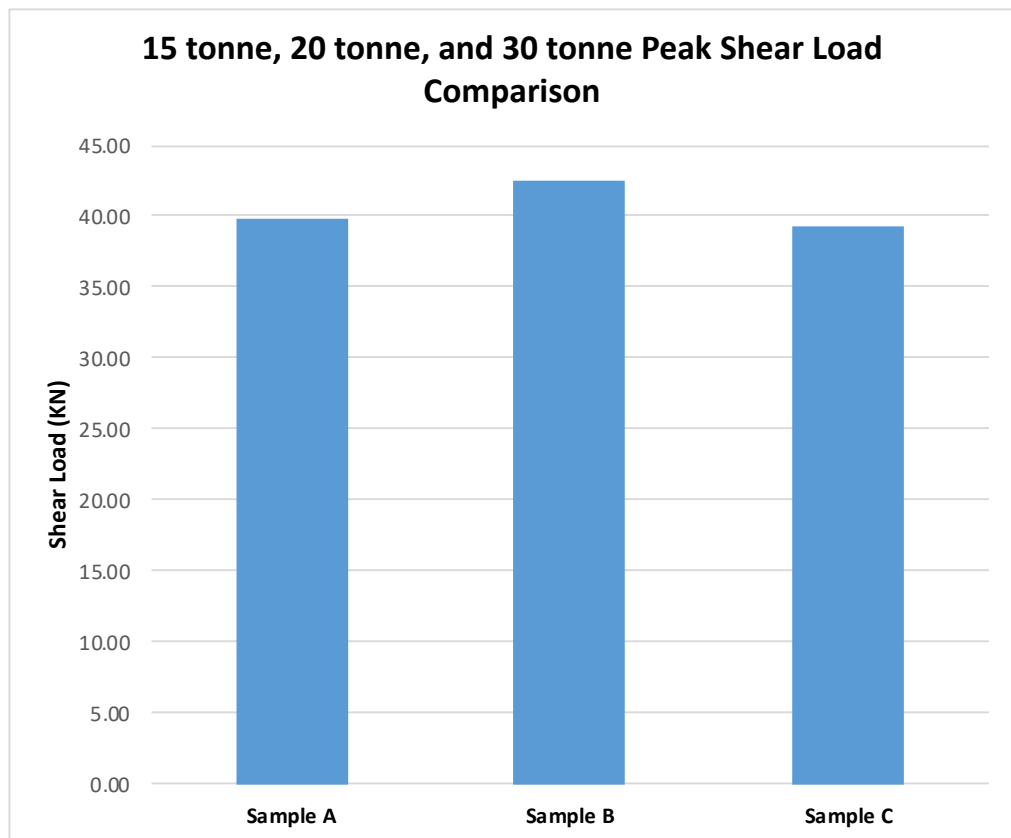


Figure 3.46: Single shear average peak load for 15-tonne, 20-tonne, and 30-tonne samples.

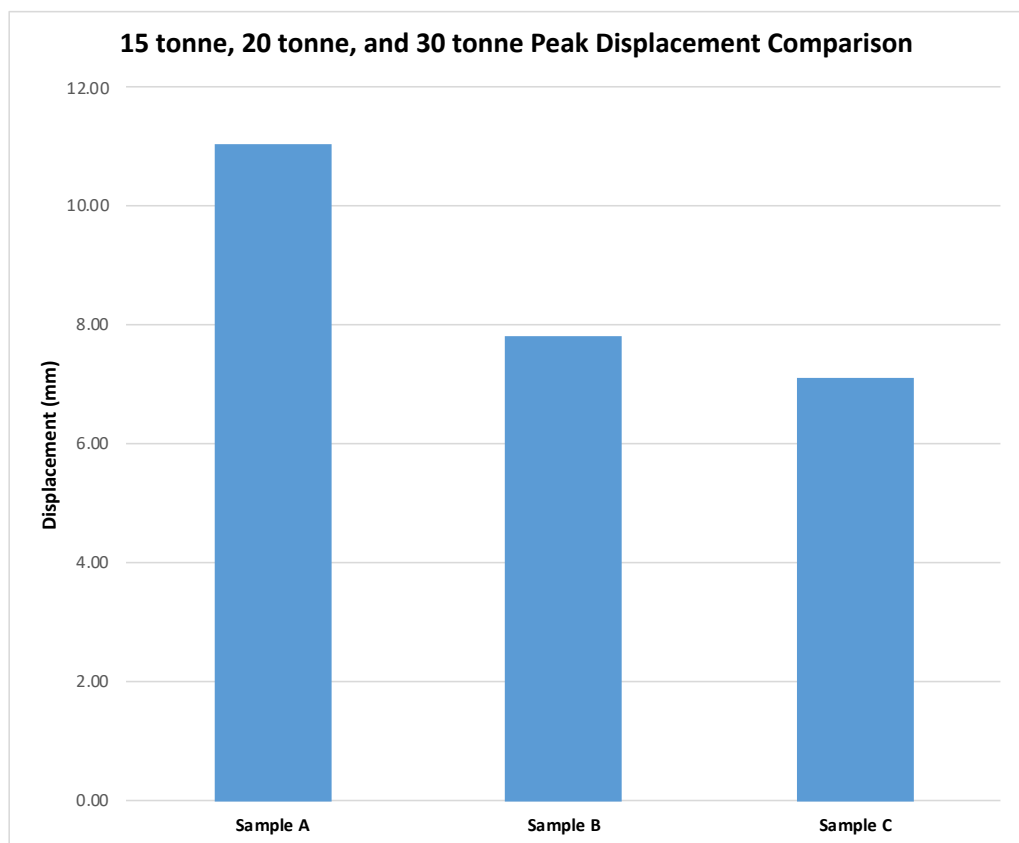


Figure 3.47: Single shear average peak displacements for 15-tonne, 20-tonne, and 30-tonne rock bolts

3.9 Summary

The double shear testing apparatus was modified to address the issues and shortcomings of the established testing methodology. The modified testing apparatus provided new insights to the shear behaviour properties of fibreglass rock bolts while also minimising the limitations encountered by previous studies. The test scheme and equipment were designed to allow for the testing of additional system parameters simultaneously while subjecting shear forces. This allowed the testing apparatus to monitor the rock bolts' axial response to shearing but also to examine the influence changes to the system's conditions can have on the overall performance of the rock bolts. These conditions were incorporated as infilled shear interfaces utilising a sandy clay mixture. To ensure all aspects of the shear system were captured, the testing scheme was designed to test the performance of the rock bolt under various shear interface conditions as well as pretension settings. Each aspect of the rock bolts' performance was determined by recording both shear and axial loads using an inline load cell along the rock bolt element and a compression load cell.

The following chapters explore the influence of pretension and shear interface properties in detail. Additionally, each component of the shear system was tested and catalogued to provide sufficient insight into their individual material properties. These included the compressive and tensile strengths of the rock bolt, simulated host rock and grout, and determining the consolidation and direction shear properties of the infilled sandy clay. These properties were then utilised as the key elements of the numerical model explored in detail in Chapter 6.

CHAPTER 4: RESULTS OF THE DOUBLE SHEAR TESTING OF FIBREGLASS ROCK BOLTS IN CLEAN JOINTS

4.1 Introduction

Rock bolts are commonly installed in compromised host rocks in both mining and civil projects. The complex geometry of such rock is often challenging to replicate in a laboratory environment and to perform comprehensive field studies is very time consuming, costly and often impractical. The development of a modified double shear testing apparatus in this study provides the ability to utilise small scale testing methods to simulate individual reinforcing elements subject to shear and axial forces. This chapter analyses the shear load transfer mechanism of fibreglass rock bolts subjected to clean shear interfaces using double shear testing. The double shear testing scheme also investigated the effect of bolt strength and pretension on the shear performance of fibreglass rock bolts with clean joint interfaces.

Furthermore, the double shear results were analysed in conjunction with the fibreglass rock bolts tested using the single shear testing apparatus to determine the shear behaviours of fibreglass rock bolts subjected to a pure shear system. The double shear tests were used to identify and compare the peak strength of 20-tonne, and 30-tonne dowels in a simulated multi-shear plane environment with clean shear interfaces. The host material was set at a strength of 40MPa to simulate moderate strength rock conditions and the applied pretensions ranged from 0kN to 20kN to simulate industry installation practices. A comparative analysis of the results was then undertaken to develop a comprehensive understanding of the shear behaviours of fibreglass rock bolts.

4.2 Overview of the testing process

As detailed in Chapter 3, the testing was conducted on fibreglass rock bolts commonly used by the industry with design load capacity ratings of 20 and 30-tonnes. Samples were prepared utilising a host media strength of 40MPa and then the fibreglass bolts were fastened using their respective nuts and washers. Smooth shear interfaces were achieved during the casting process by utilising metal plates. Samples were then torqued to pretension values of 0kN, 10kN, 15kN and 20kN. Table 4-1 outlines the

rock bolts' properties and their designed pretension forces when subject to the clean shear interface test programme. Also highlighted in Table 4-1 are the physical design characteristics of the selected bolts along with their designed pretension, achieved pretension and rate of loading. It is noted that there were variations to the achieved pretension values due to the rock bolts' settling during curing. Unfortunately, this element could not be controlled and some rock bolts experienced greater amounts of settling than others. To minimise the variation of settled pretensions several steps were implemented. Corrections were made during the initial hour of the grout's curing process, until the grout was sufficiently set. After the initial setting stage any additional adjustments would have limited impact on the internal pretension of the system. In an attempt to minimise pretension variation, the initial applied pretension was set to 3kN greater than the designed limit. Unfortunately, each sample varied and some experienced greater reductions in pretension, resulting in values less than the target pretension. In contrast, other samples exhibited reduced rates of settling and achieved values slightly greater than the target pretension.

Table 4-1: Rock bolt properties for clean shear system

Bolt Type	Rock bolt Diameter (mm)	Rock bolt Length (mm)	Design Shear Capacity (t)	Designed Pretension (kN)	Tested Pretension (kN)	Rate of Loading (mm/min)
20T0kN C	20	1200	20	0	1	1
20T10kN C	20	1200	20	10	12.8	1
20T15kN C	20	1200	20	15	13.5	1
20T20kN C	20	1200	20	20	20.5	1
30T0kN C	20	1200	30	0	0.8	1
30T10kN C	20	1200	30	10	11	1
30T15kN C	20	1200	30	15	12	1
30T20kN C	20	1200	30	20	17.5	1

4.2.1 Double shear calculations

The results of the double shear tests were analysed and reduced to both material properties and overall system performance. Each test output was reported as force and displacement represented by kilonewtons and millimetres. The optimal method of calculating shear strength accounts for the progressively reducing rock bolt diameter during shearing. However, it was not experimentally possible to measure this property with the chosen system design and therefore nominal rock bolt diameters were utilised for calculations. Furthermore, the shear force data represented the overall double shear force and therefore, equation 4.1 reduced the data to represent the forces exerted on each plane. Additionally, the recorded results did not outline the stresses experienced by the rock bolts at the peak shear loads. Therefore, equation 4.2 was used to calculate the peak shear stress and results in a value with the units of gigapascals.

$$F_{Shear\ plane} = \frac{F_{Double\ shear}}{2} \quad (4.1)$$

$F_{Double\ Shear}$ = The raw test data in Newtons (N)

$F_{Shear\ plane}$ = The forces isolated to the failed shear plane in Newtons (N)

$$\tau_{Stress} = \frac{F_{Shear\ Plane}}{\pi r^2} \quad (4.2)$$

$F_{Shear\ plane}$ = The forces isolated to the failed shear plane in Newtons (N)

τ_{Stress} = The ratio between shear force and cross-sectional area in (N/m²)

r = The nominal rock bolt radius in meters (m)

4.3 Results for 20-tonne rock bolts, double shear testing

4.3.1 Shear behaviour profile

The 20-tonne rock bolts were installed in the simulation system with applied pretensions of 0kN, 10kN, 15kN and 20kN and then tested as part of a clean shear environment. Shear loads were applied to the centre of the sample using a compression testing machine and the shear force and displacement data was simultaneously measured by internal load cells and subsequently recorded in the data logger. Each 20-

tonne sample exhibited similar shear load profiles consisting of three stages: elastic, strain-softening and failure as highlighted in Figure 4.1.

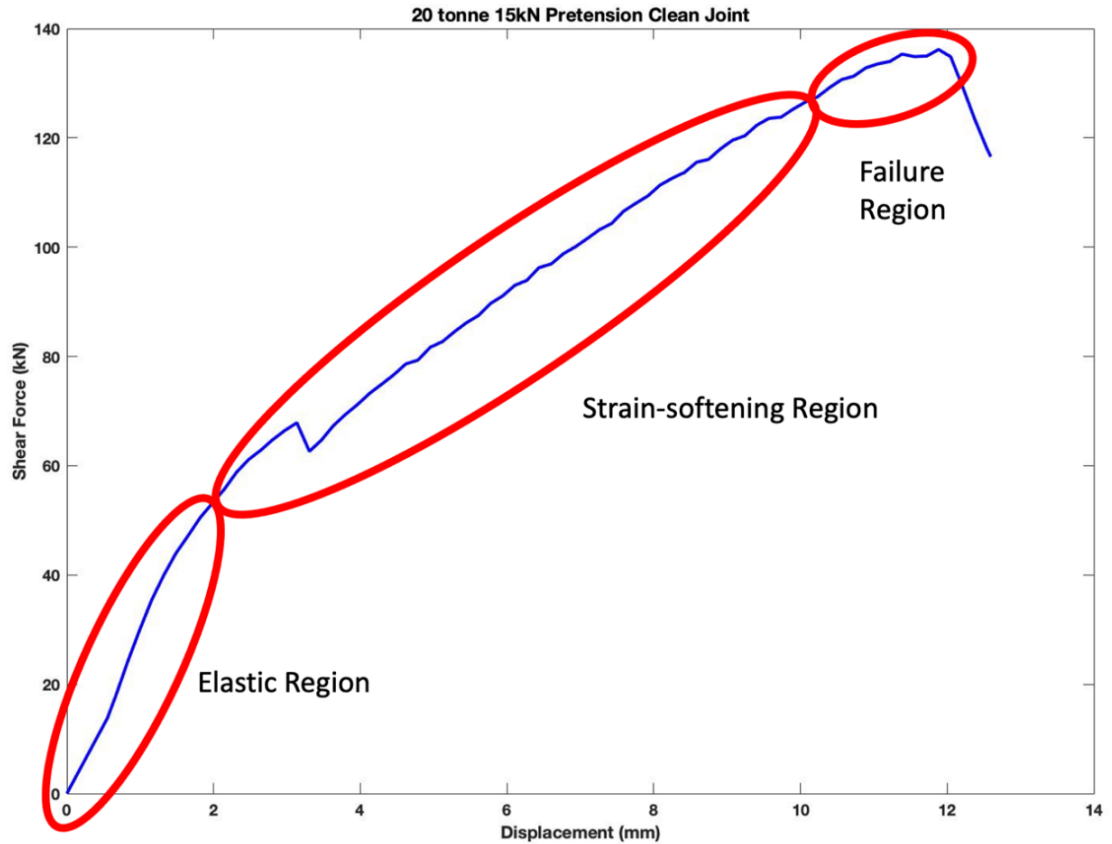


Figure 4.1: Example of the three failure regions for 20-tonne rock bolts

The elastic stage commenced after the initial resting stage of the sample and continued to the elastic yield point, at which the system no longer was able to recover elastically. Any further displacement resulted in plastic deformation characterised by the following strain-softening stage. The deformation experienced during the elastic stage was temporary and reversible. The transition to the strain-softening stage was characterised by a distinct change in slope gradient continuing until the sample reached the failure stage. This strain-softening profile could be considered atypical as it didn't represent progressive deterioration. The gradient of the strain-softening region was linear and considerably shallower than the slope characteristics of the elastic stage. This atypical strain-softening profile was attributed to a combination of fibres failing and remaining intact fibres compensating and absorbing some of the shear force. Figure 4.2 illustrates how the sample subjected to 20kN pretension displayed an approximate 2° decrease in gradient when transitioning from the elastic region to the strain-softening region. When the sample transitioned into the strain-softening stage,

any further deformation could not be reversed resulting in permanent damage to the rock bolt. This process continued until the sample reached the failure stage. The failure stage was identified by cascading internal strand failures culminating in the ultimate failure of the rock bolt. Due to the fibreglass rock bolts being comprised of many fine strands, the failure stage does not exclusively encompass the ultimate failure of the rock bolt and in fact begins when enough strands begin to fail resulting in the sample being unable to withstand increasing shear forces. This was characterised by the rapid decrease in curve gradient, demonstrated in Figure 4.2, with the peak shear force occurring at 0°. The peak shear force represented the ultimate shear capacity of the system including rock bolt strength, shear plane friction and induced confinement from the applied pretension. When the samples passed their peak shear force, the fibres within the bolt instantaneously broke resulting in the shear load dropping to the residual value of the system.

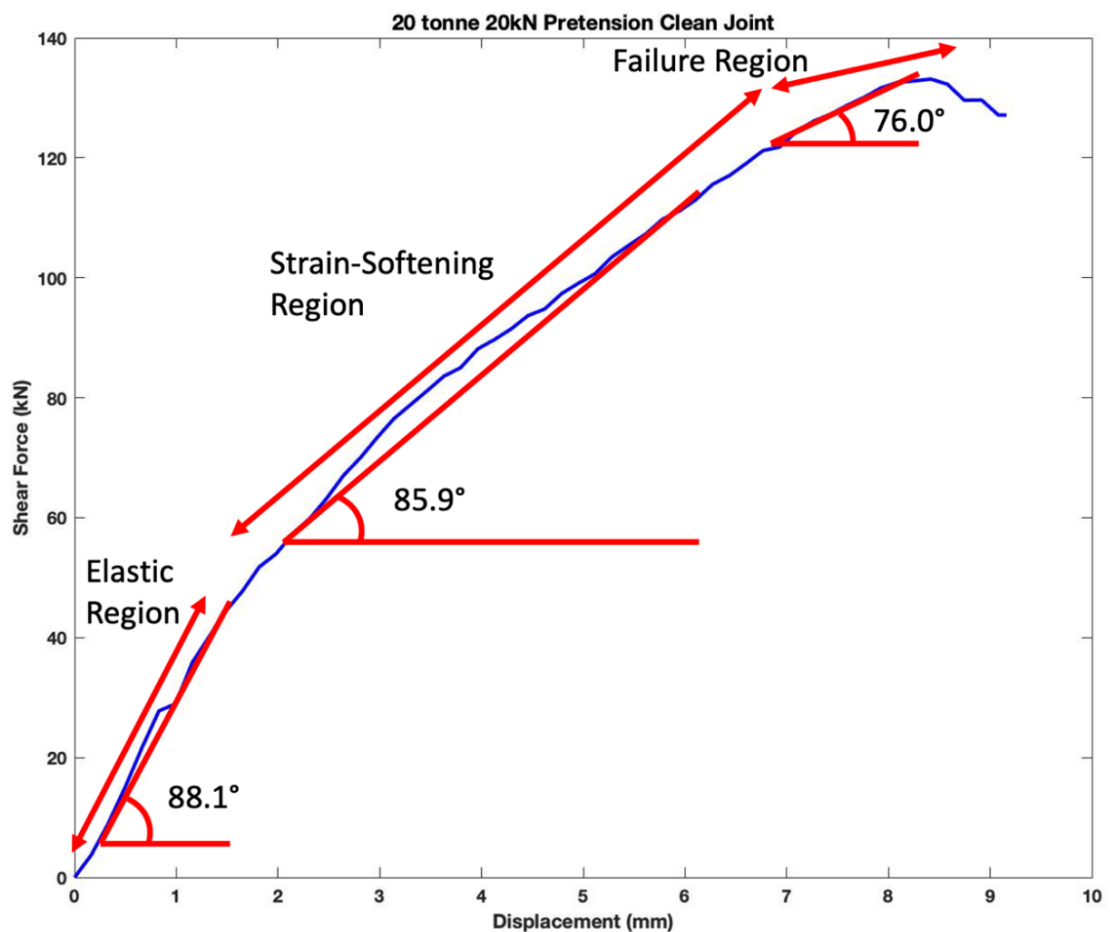


Figure 4.2: Change in angle for each stage of the 20-tonne double shear profile

Analysis of the data identified a phenomenon impacting the shear force response of most samples during the transition from the elastic region to the strain-softening region. This behaviour was characterised by a distinct drop in the recorded shear force of approximately 2kN to 5kN and was accompanied by an audible marker from within the sample. Upon completion of the sudden shear force drop, the samples recovered and successfully progressed through the subsequent stages of failure as highlighted by Figure 4.3. This shear force drop behaviour was identified as a recurring and repeatable event and therefore was inferred to have resulted from internal processes caused by forces dissipating throughout each component of the system. The data set representing the 0kN pretension sample was discarded from analysis due to premature host material failure during testing.

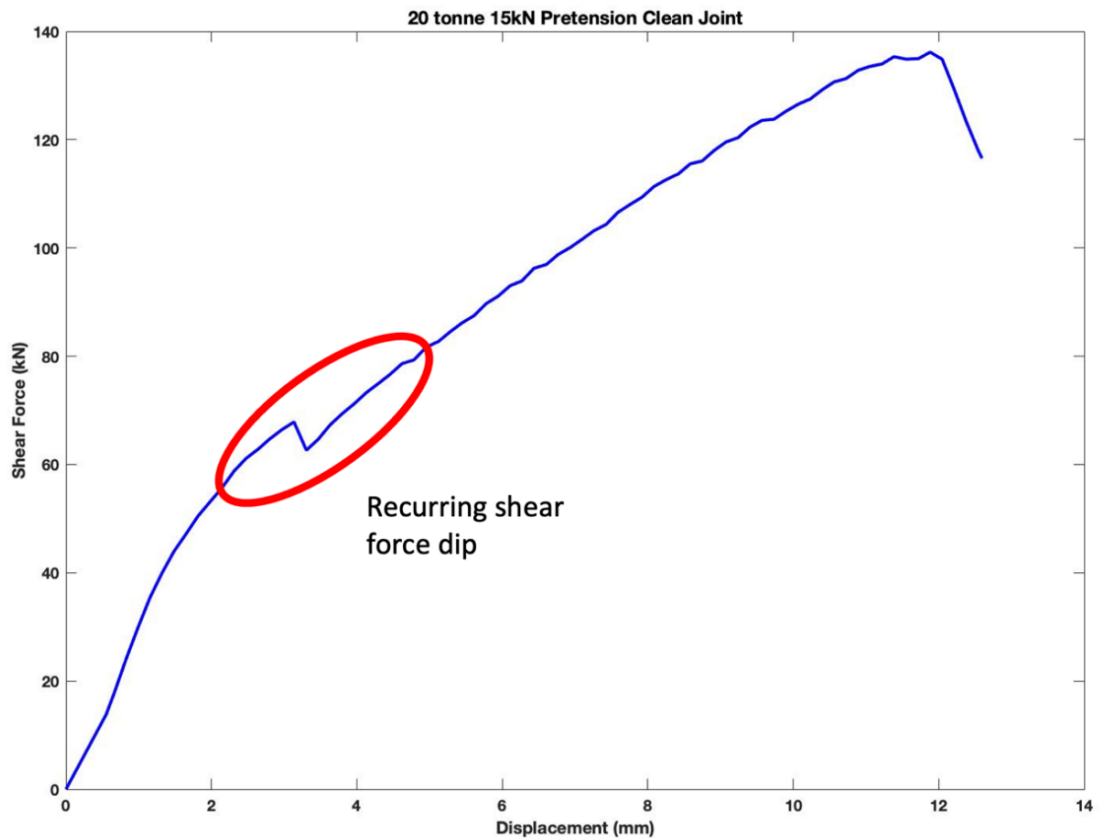


Figure 4.3: Illustration of recurring reduction in shear force for 20-tonne sample

4.3.2 Pretension profile

Pretension is the application of axial load on the rock bolt and was achieved using a combination of industry supplied nuts and washers. The change in axial load during

the shearing process was monitored using a load cell aligned to record axial forces along the rock bolt element and by a complementary data acquisition system. The resulting data sets illustrated how the applied shearing forces are transmitted from the loading ram to each material of the system impacted by the axial performance of the rock bolt setup. The design parameters of the 20-tonne clean double shear tests simulated small-scale real-world scenarios and not to form a system of perfect shear. This chosen system design ensured a complex force transfer relationship between each material of the system and therefore, when components such as the grout and host material failed, shear forces were subsequently transformed to axial forces. These transformed axial forces, combined with the applied pretensions, were the basis for defining the pretension profile. Figure 4.4 outlines that each pretension profile consisted of three stages: zone one, zone two and zone three. The first zone was represented by a minor linear increase in axial force, suggesting that almost none of the applied shear force was transformed to axial force because of internal material failure. This indicated little to no change of state between each interacting element throughout the path of shear load transformation. The graphical properties of this zone did not identify whether the rock bolt was performing in an elastic or strain failure manner. However, the defined behaviour of zone one did indicate that the elements of the double shear system such as, the grout encapsulation and host material were in a state prior to failure. The transition into zone two was defined by a significant change in gradient when compared to zone one where the average gradient change was approximately 3.4° . Additionally, the displacement duration of both zones one and two closely matched, indicating the applied shear forces did not transform to axial forces until approximately 50% through the shearing process. The increase of axial forces observed in zone two could be attributed to deteriorating interfaces between the materials within the system, resulting in the inability to withstand increasing loads. These failures could have occurred between the host material and grout as well as the grout to rock bolt interface. This could enable the shear forces to transform axial forces and transfer through the rock bolt. Zone three was the final observed component of the pretension profile, indicating the transition to total system failure. Total system failure was identified by the rapid drop in slope angle where increases in displacement no longer yielded increases to the recorded axial forces. This behaviour was a result of the fibreglass strands within the rock bolt systematically failing until the system achieved catastrophic failure of all strands within the rock bolt.

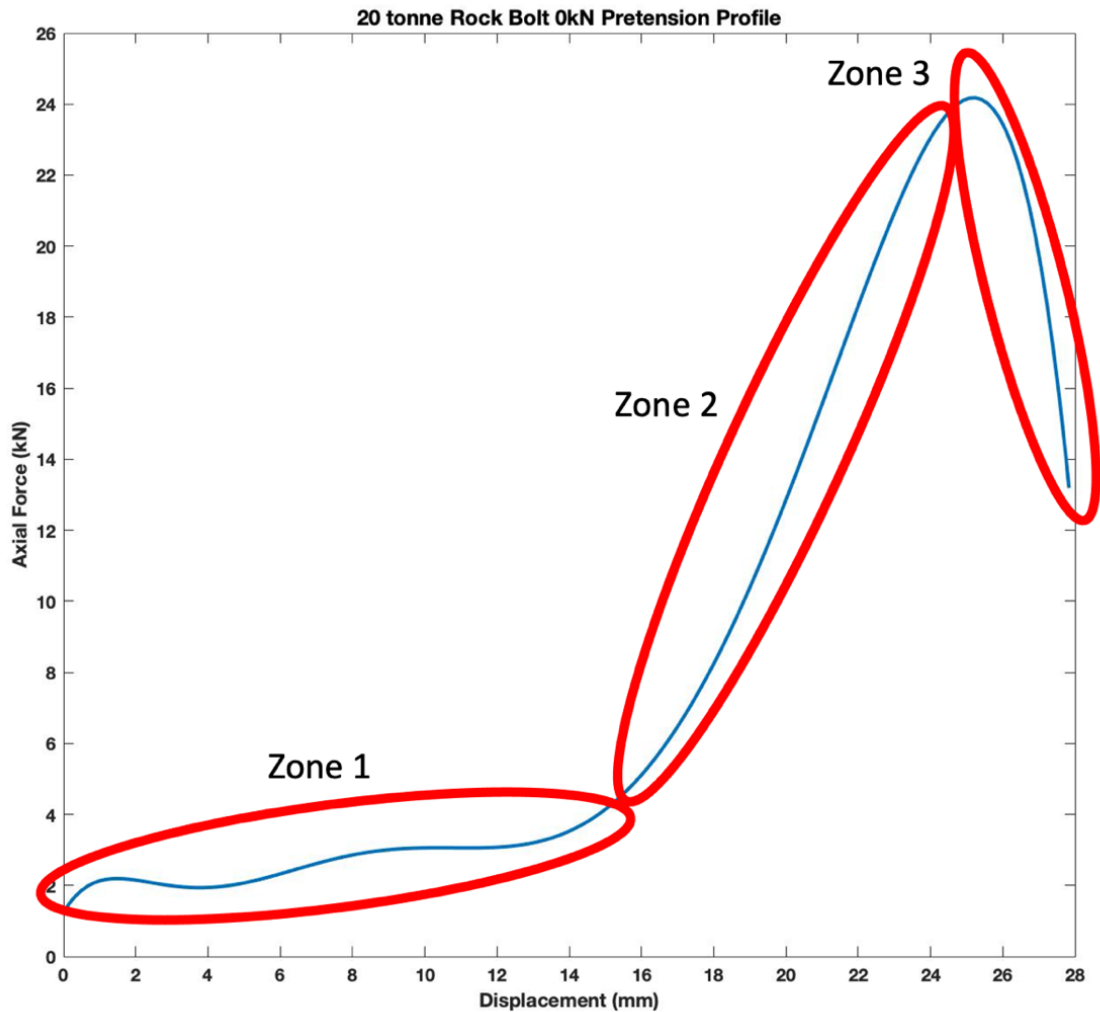


Figure 4.4: Example of pretension zones in axial force for 20-tonne rock bolt with 0kN pretension

When evaluating the pretension performance of the 20-tonne rock bolts, several characteristics were identified. The increase to pretension values had no impact on the peak axial force for samples subjected to pretension values of 10kN and less. As a result, both the 0kN and 10kN pretension samples achieved peak axial forces of approximately 24kN as shown in Figure 4.5. Samples subjected to pretension values of 15kN and higher also achieved matching peak axial forces of approximately 20kN to 22kN, however, these were lower compared to the samples of 0kN and 10kN pretension as also indicated in Figure 4.5. In addition to the changes in peak axial forces, there was an observed decrease in displacement at failure. Unlike with the peak axial force's stepped response to increased pretension, the displacement at the peak force drastically reduced when the samples were subjected to pretensions greater than 0kN, suggesting a correlation between the designed pretension and failure displacement. The observed decrease in displacement remained constant for each

subsequent increase in pretension with an observed displacement range of 8mm-12mm as opposed to the 0kN pretension sample's displacement of 25mm as shown in Figure 4.5. It is noted that the samples experienced force variations during curing and force settling prior to testing, resulting in variability from the designed pretension settings.

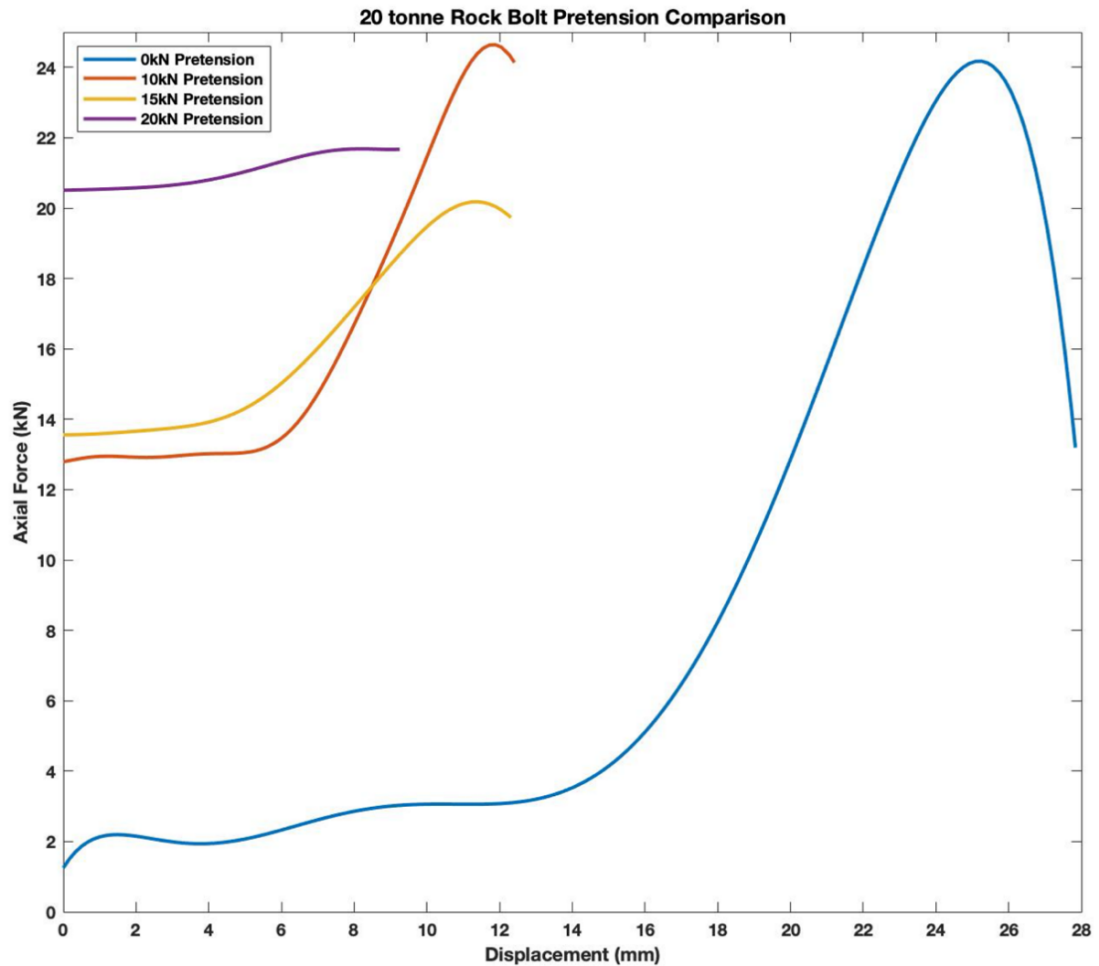


Figure 4.5: Comparison of pretension axial forces for the 20-tonne rock bolts with clean joints.

4.3.3 Impact of pretension on shear strength

Applying pretension to the 20-tonne samples had notable impacts on the shear performance properties of the rock bolts such as, failure displacement and shear profile. Unfortunately, data representing the performance of the 20-tonne 0kN pretension sample was excluded from analyses due to inconsistencies in the recorded data. While the application of pretension was identified to have impacts on the performance of the 20-tonne rock bolts, it was also discovered to not having an impact on the peak shear force of the rock bolts. Due to several logistical limitations, repeated

tests could not be conducted. Figure 4.6 demonstrates how the application of pretension had no discernible impact on the achieved peak shear force of each sample. As such, each sample achieved an approximate shear failure force of 135kN. Additionally, samples with lower pretension setting did not present any significant changes to either peak shear and peak displacement as shown in Figure 4.6.

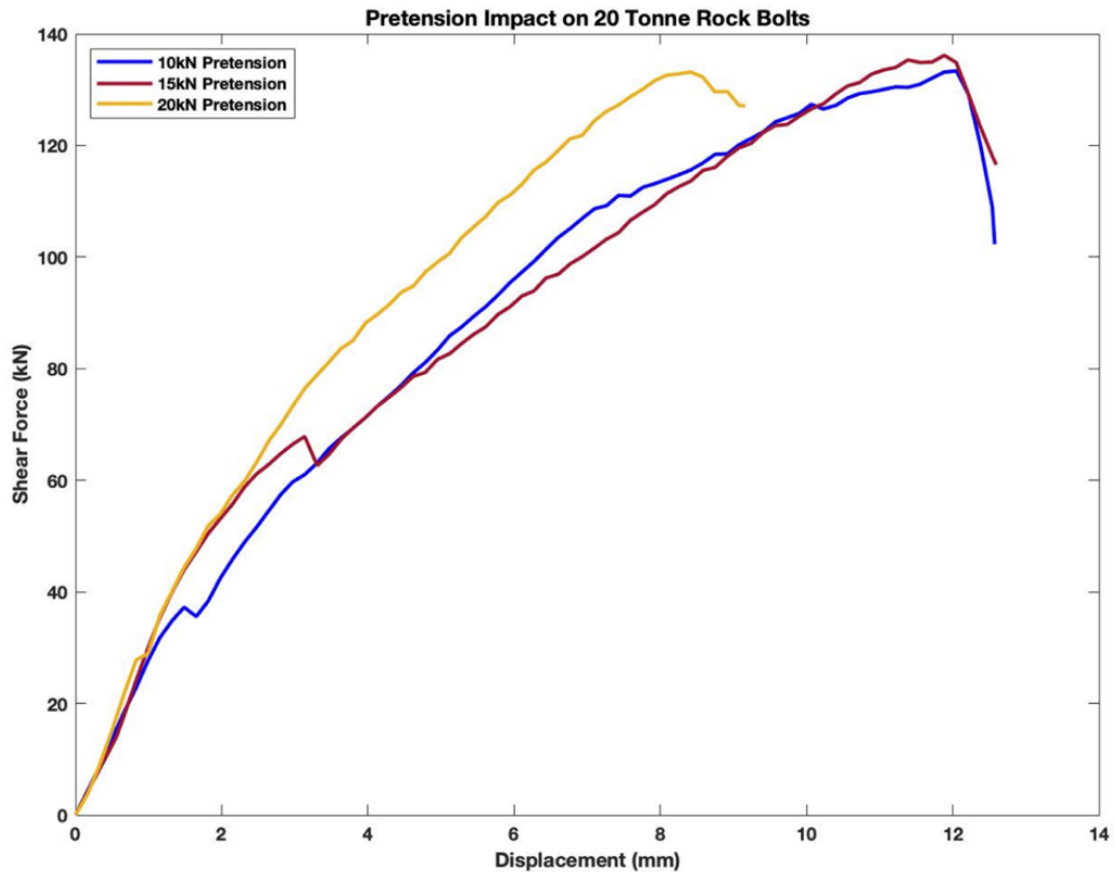


Figure 4.6: Change in shear profile due to pretension for 20-tonne rock bolts

Comparing the results from the 10kN and 20kN pretension samples, it was evident that increasing the pretension setting had a direct impact on the failure displacement of the rock bolt. Figure 4.7 demonstrates that the failure displacement between the two samples reduced from approximately 12mm to 8.5mm. The change in displacement may be attributed to increased compressive forces across each shear plane as a result of the applied axial load imparted on the rock bolts. This force then transferred through the washer plates forcing the outer blocks together. The artificial pressures applied to the shear planes appear to have altered the confinement pressures within the grout, host rock and their interface zones allowing them to withstand higher forces prior to

failing. Increasing the confining pressures of the system facilitated a more efficient force transfer path between the loading ram and the shear planes due to less dissipation losses. As a result, a greater percentage of the applied forces were transferred to the bolt earlier in the shearing process, causing the bolt to achieve its failure limit quicker. The reduction in the dip in shear force experienced at the beginning of the strain-softening region further highlights the significance of the altered internal pressures and is explained in section 4.3.1. The sample subjected to a pretension of 20kN exhibited a greatly reduced loss in shear force compared to the 10kN pretension sample. During shearing, the shear force halted for only approximately 0.2mm. Figure 4.8 demonstrates how the 10kN sample utilising a lower pretension experienced a shear drop of approximately 2kN over the same region.

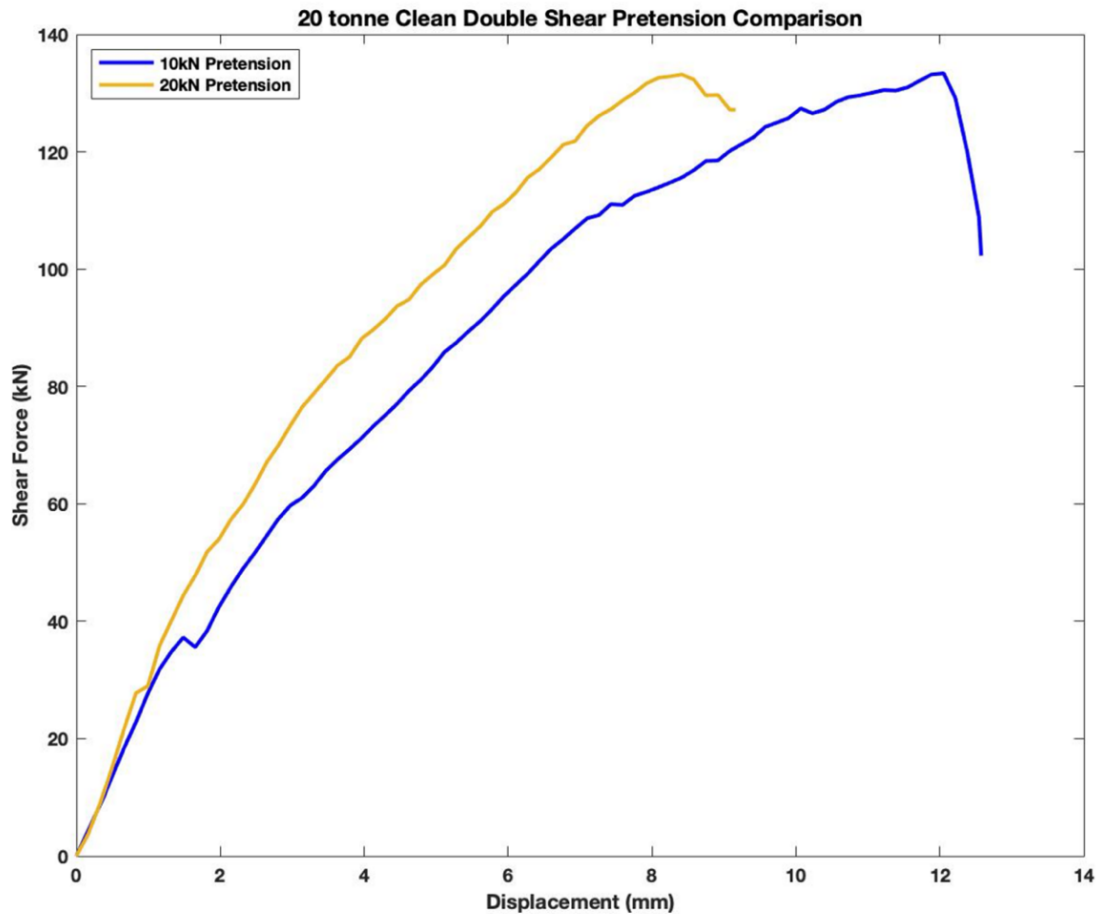


Figure 4.7: Change in failure displacement due to increase from 10kN to 20kN pretension for 20-tonne rock bolts

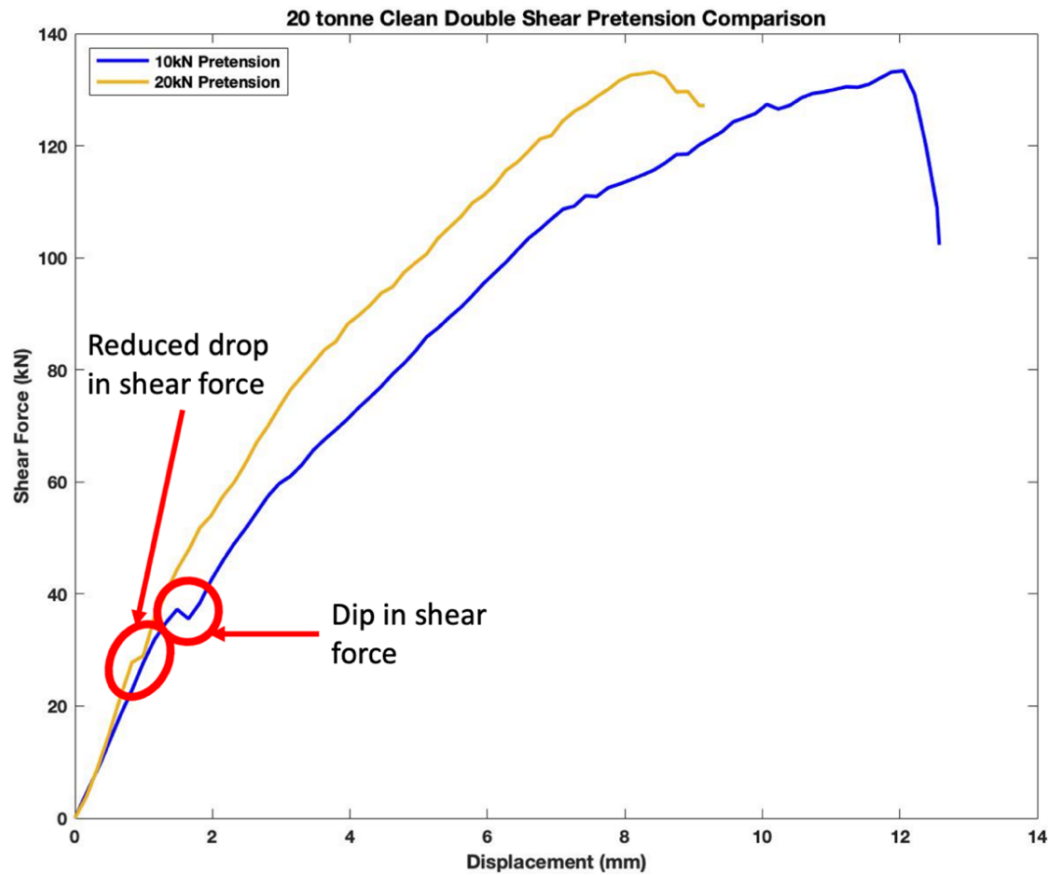


Figure 4.8: Change in recorded shear dip due pretension increase from 10kN to 20kN for 20-tonne rock bolts

The increase of the pretension setting also resulted in changes to the strain-softening stage of the defined shear profile. Samples subjected to pretensions greater than 10kN presented with a single linear representation of the rock bolts' strain-softening response to shear, highlighted in Figure 4.9. Conversely, the sample testing the impact of a 10kN pretension shown in Figure 4.9, demonstrated a strain-softening region comprised of two linear stages, with the later stage presenting with a smaller gradient. This reduction in gradient indicated the occurrence of a possible failure within the system. As previously outlined in this section, the induced system confinement as a result of the pretension strengthened the properties of the system materials. Therefore, it is likely that the cause of the second stage of strain-softening was due to a failure within either the grout, host material and/or interfaces between them. Lastly, the increase in pretension displayed no identifiable influence on the elastic stage of the shear profile of the tested rock bolts. It is argued that due to the samples transitioning out from the elastic region early in the shearing process, prior to the failure limits of the strata simulating materials, the elastic region was not significantly impacted by any increase in strength to defined materials.

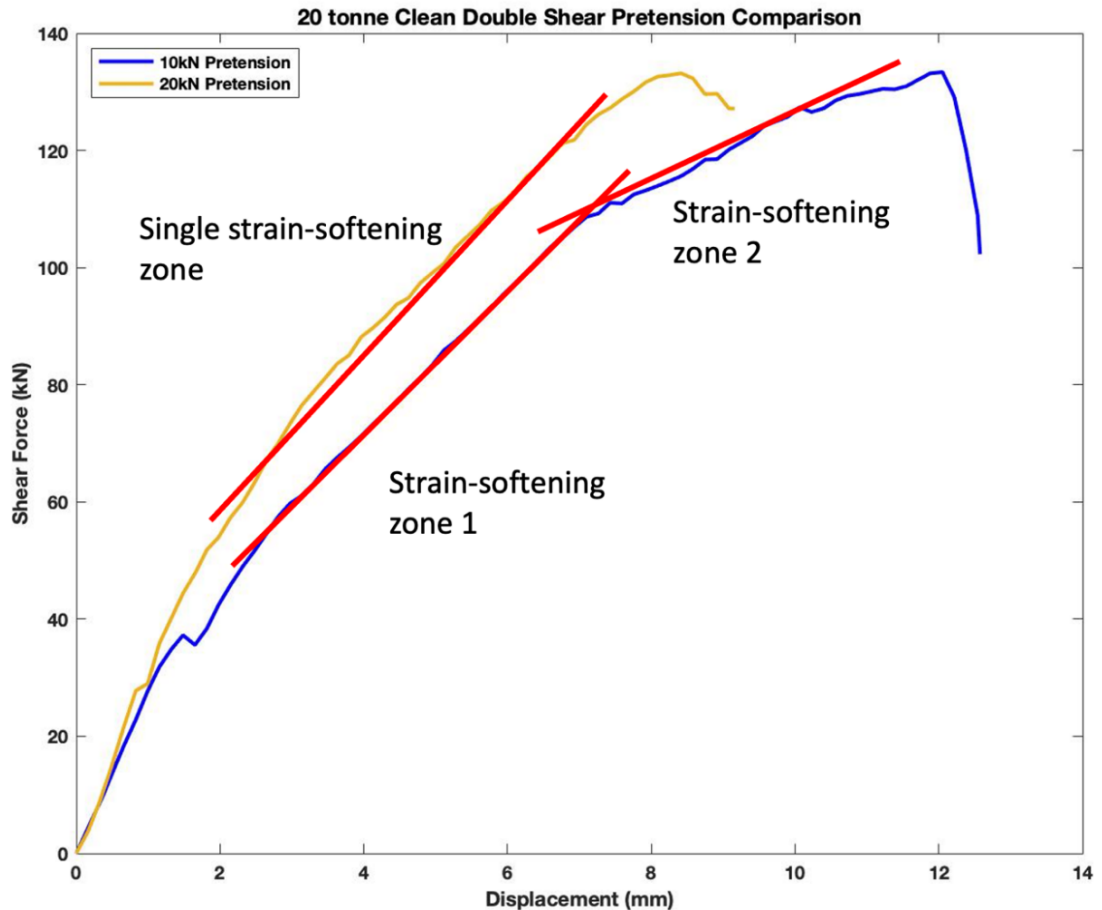


Figure 4.9: Changes to the strain-softening stage for 20-tonne rock bolts as a result of pretension

4.3.4 Failure characteristics

Post failure all samples were dismantled and notable failure characteristics were highlighted. These key characteristics included: the hinge point and interface damage. There was an observed correlation between the set pretension of the sample and the resultant hinge point at failure. Samples with higher pretensions recorded a greater degree of bending at the hinge point compared to samples of lower pretensions. The sample set to the lower pretension of 10kN resulted in an approximate angle of bending of 11° . This angle increased to approximately 14° for the sample tested at 20kN pretension as highlighted in Figure 4.10, Figure 4.11 and Table 4-2. The change in confinement forces due to the applied pretensions, as described in section 4.3.3, was the presumed cause of the observed change in hinge point properties. The resultant increase to the strength of the various interfaces surrounding the rock bolt caused the rock bolt to bend around the shear interface as opposed to pushing through and damaging the shear interface surface. The increase to the strength of the rock bolt,

grout and host rock interfaces caused by the higher initial pretension values, resulted in less damage to the rock bolt element extending internally from the shear plane as highlighted in Figure 4.11. Samples with a lower initial pretension value such as the 10kN sample, were subjected to fewer additional axial forces. The reduced axial forces resulted in a weaker shear plane and grout and host rock properties. This led to the rock bolt exhibiting a lower degree of bending at the location of failure as the surrounding material failed around the rock bolt throughout the shearing process.

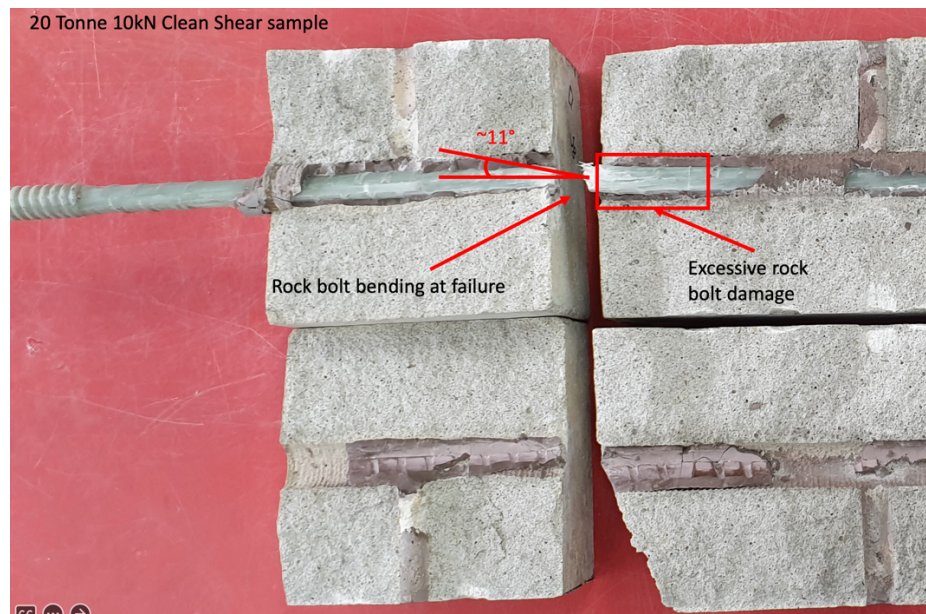


Figure 4.10: Angle of failure and rock bolt damage for 20-tonne 10kN pretension clean shear rock bolt

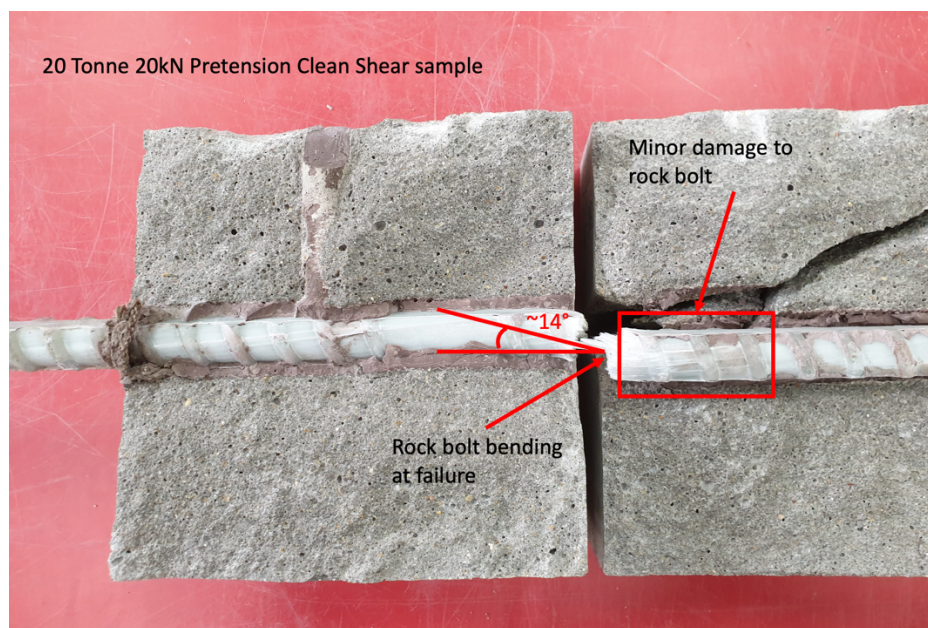


Figure 4.11: Angle of failure and rock bolt damage for 20-tonne 20kN pretension clean shear rock bolt

Increasing the initial pretension setting exhibited no change to the damage presenting in the vicinity of the point of shear and the surrounding material. As can be seen in Figure 4.12, samples prepared at both 10kN and 20kN pretensions respectively showed no signs of increased damage to the grout, simulated host rock and shearing surface. This could be due to the limited strength of the 20-tonne rock bolts in shear resulting in the rock bolt failing prior to subjecting damage to the surrounding materials. The large fracture present in the host material displayed in Figure 4.12 was a result of the processes used to split the samples post failure to enable this analysis.

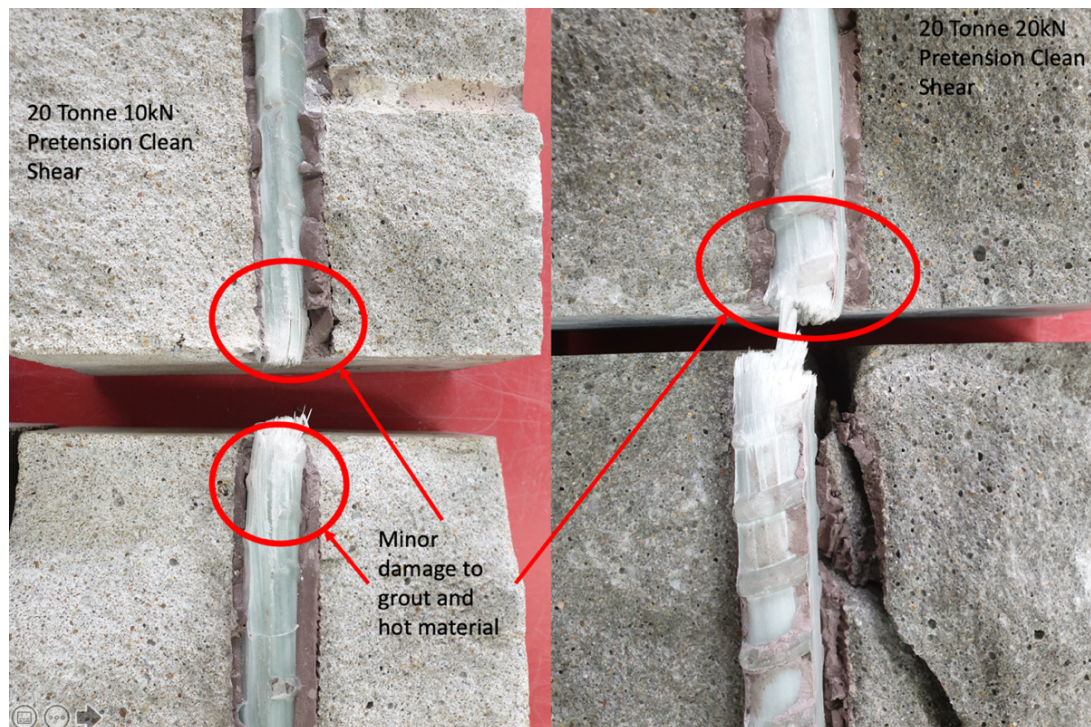


Figure 4.12: Damage caused to host material by the 20-tonne rock bolts of 10kN and 20kN pretensions

4.4 Results for 30-tonne rock bolts, double shear testing

4.4.1 Shear behaviour profile

The 30-tonne fibreglass rock bolts were subjected to pretensions ranging from 0kN to 20kN and clean shear joints were analysed for their response to applied shear loads. Similar to the previous 20-tonne samples, the results of the double shear tests were measured using the processes outlined in section 4.3.1. In addition, the axial forces were measured using a button load cell with the data recorded by the laboratory data acquisition system. After systematic tests were conducted under varying pretension

conditions, the shear load profiles could be described by the following three stages including elastic, strain-softening and failure as highlighted in Figure 4.13. The elastic stage occurred from the initial resting stage of the sample and continued to the elastic yield point when the system was no longer able to exhibit elastic deformation and any further displacement resulted in plastic deformation. Throughout the elastic region any deformation due to loading was temporary and reversible. The strain-softening stage began from the elastic yield point to the peak failure limit. Similar to the elastic region, the strain-softening stage also presented as linear, however at a reduced gradient when compared with the elastic stage. Most samples exhibited an instantaneous dip of between 2kN to 10kN in their recorded shear load either at the transition point from the elastic range to the strain-softening, or just after the transitioning into the strain-softening response as demonstrated by the highlighted section of Figure 4.14.

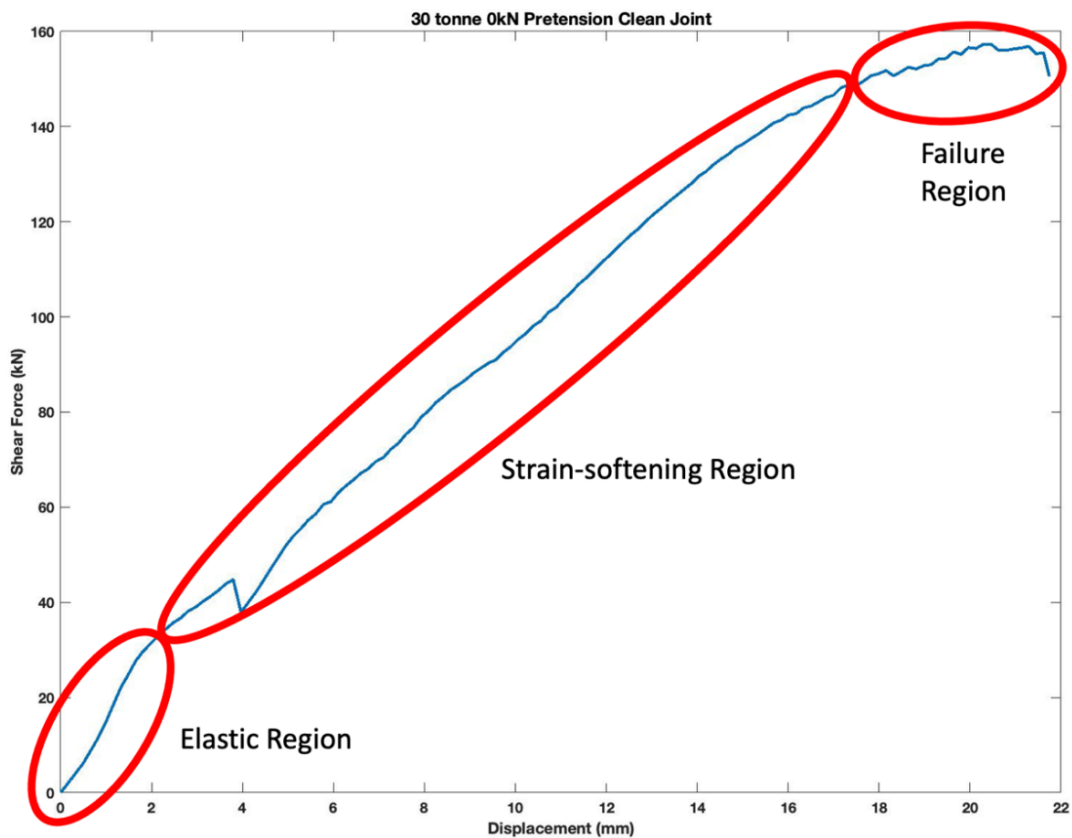


Figure 4.13: Example of the failure regions for 30-tonne rock bolt with a pretension of 0kN

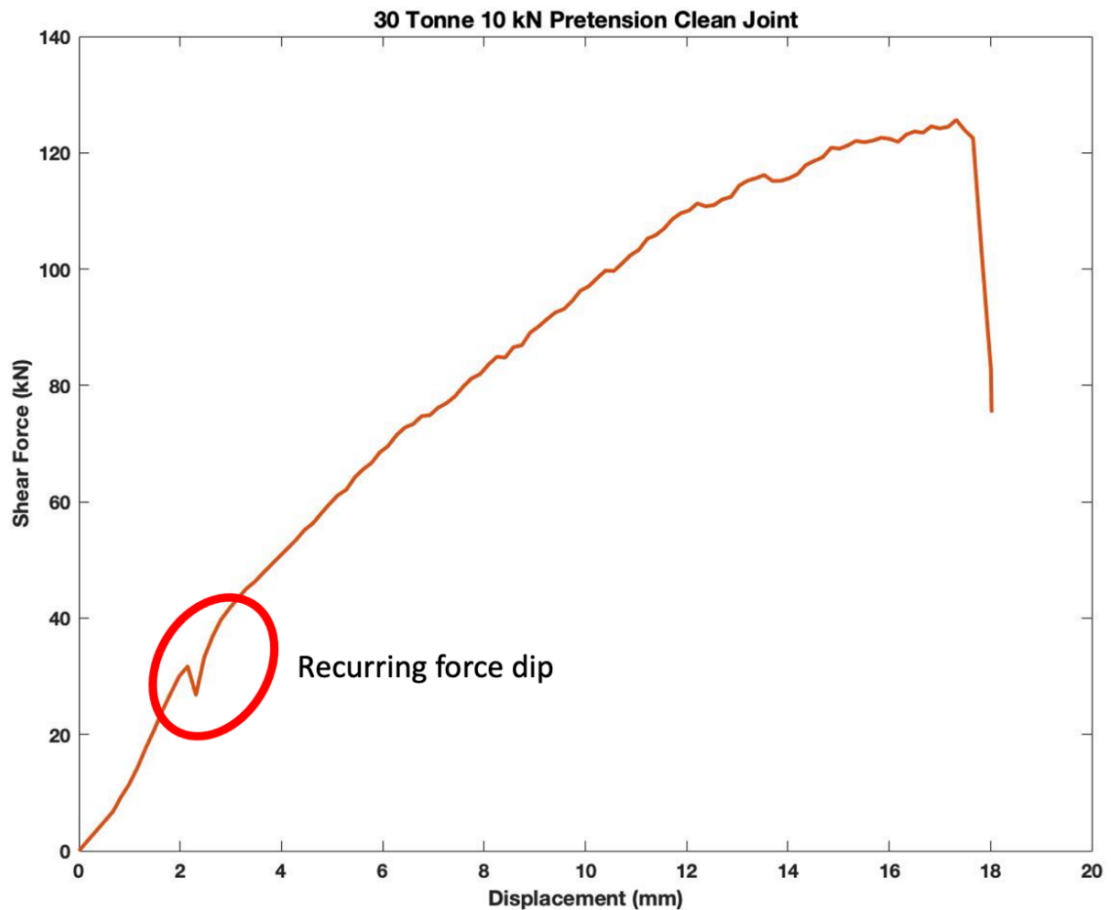


Figure 4.14: Example of the recurring reduction in shear force for the 30-tonne sample with 10kN pretension

The 30-tonne rock bolt sample subject to a pretension of 15kN was an outlier and while it maintained a similar failure profile overall, it did not exhibit what was identified as the typical load drop of 2kN to 10kN as highlighted in Figure 4.15. The transition into the strain-softening region marked the point where any deflection/deformation subjected to the sample became non-reversible. Upon inspecting the failed samples, the reduction in recorded shear load could be attributed to a combination of fibreglass strand delamination, grout compressive failure and host concrete compressive failure resulting in a momentary release of the applied load. The samples quickly recovered from the load change and proceeded to continue through the strain-softening stage until they reached their peak load. The samples' peak load was represented by the greatest shear load the samples could withstand based on the resistance of rock bolt and friction between concrete blocks prior to failure. The transition from strain-softening to failure was represented by the flattening of the curve when nearing the failure limit. Once the samples achieved their failure limits the fibres within the rock bolts failed abruptly resulting the shear load reducing to a residual value.

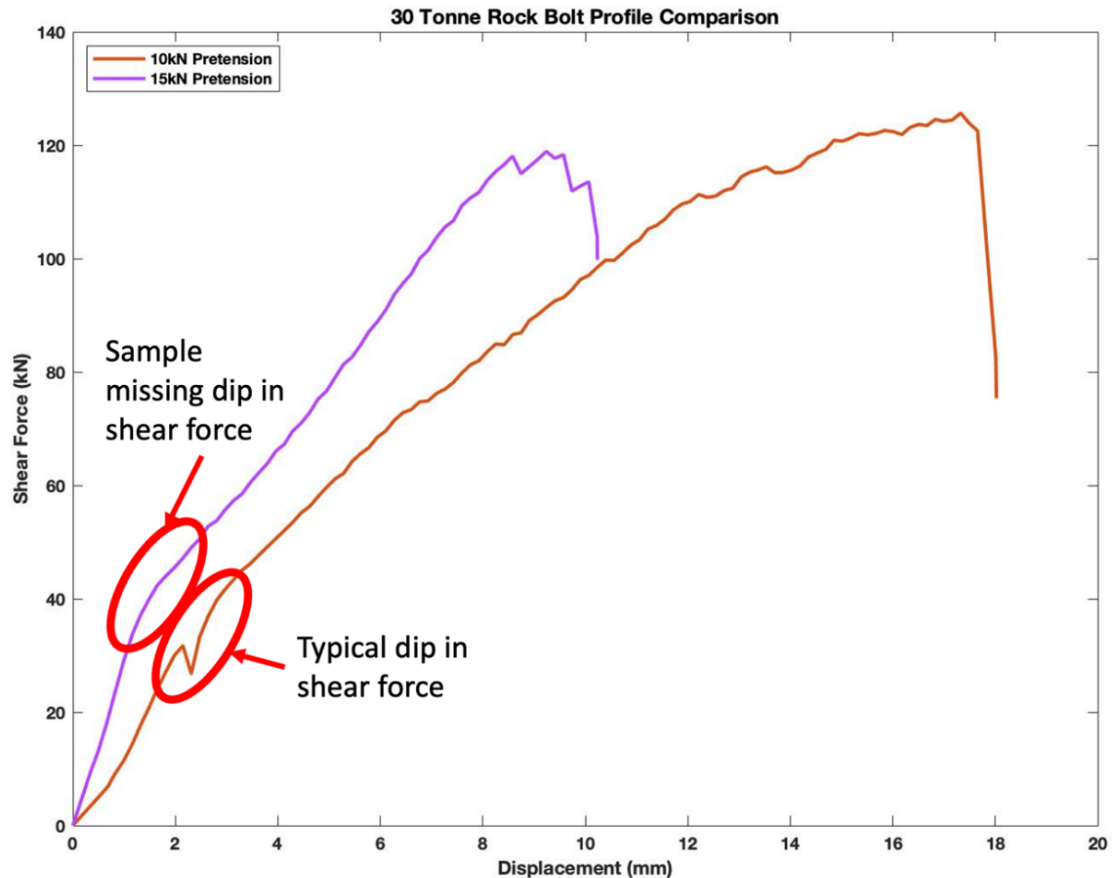


Figure 4.15: Comparison of 30-tonne rock bolt profile with and without shear force dip.

4.4.2 Pretension profile

The pretension profile observed during testing was the result of shearing forces transferred through the load ram and to the subsequent materials within the system. The recorded values demonstrated the transformation of shear load to axial load throughout the shearing process. The designed double shear system did not and was not intended to simulate a perfect shearing plane of the likes of the guillotine tests. Therefore, it was expected that as the rock bolt, grout and host material deformed and failed, the applied load would subsequently transform to an axial load. Each pretension axial force profile consisted of three stages: zones one, two and three as highlighted in Figure 4.16. The first zone was represented by a linear increase in axial force suggesting the applied shear load was transmitted through the system with proportional losses. This indicated little to no change of state to either of the interacting elements throughout the path of shear load transformation. While this did not signify whether zone one exhibited elastic or strain failure, it suggested that the interacting elements

of the system i.e. grout encapsulation and host material were in a state prior to failure. As the sample progressed into zone two, there was an evident overall increase in average gradient from zone one to zone two. In addition, the gradient throughout zone two gradually increased with displacement. This increase in gradient signified an increase in the transformation of shear forces to axial forces, which were then transmitted through the rock bolt. The increase of axial forces could be attributed to interface failures within the system, such that interacting zones were no longer able to withstand increasing loads. Some suggested interface failures could occur between the host material and grout as well as the grout to rock bolt interface. As these interfaces failed, the increasing loads were forced to transmit through the rock bolt. The final stage as denoted by zone three indicated the transition to total system failure. This zone was identified by a rapid drop in gradient where an increase in displacement no longer resulted in an increase in axial forces. This indicated that the fibreglass strands within the rock bolt were beginning to fail. The sample continued to progress through zone three until there was a catastrophic failure of all strands within the rock bolt.

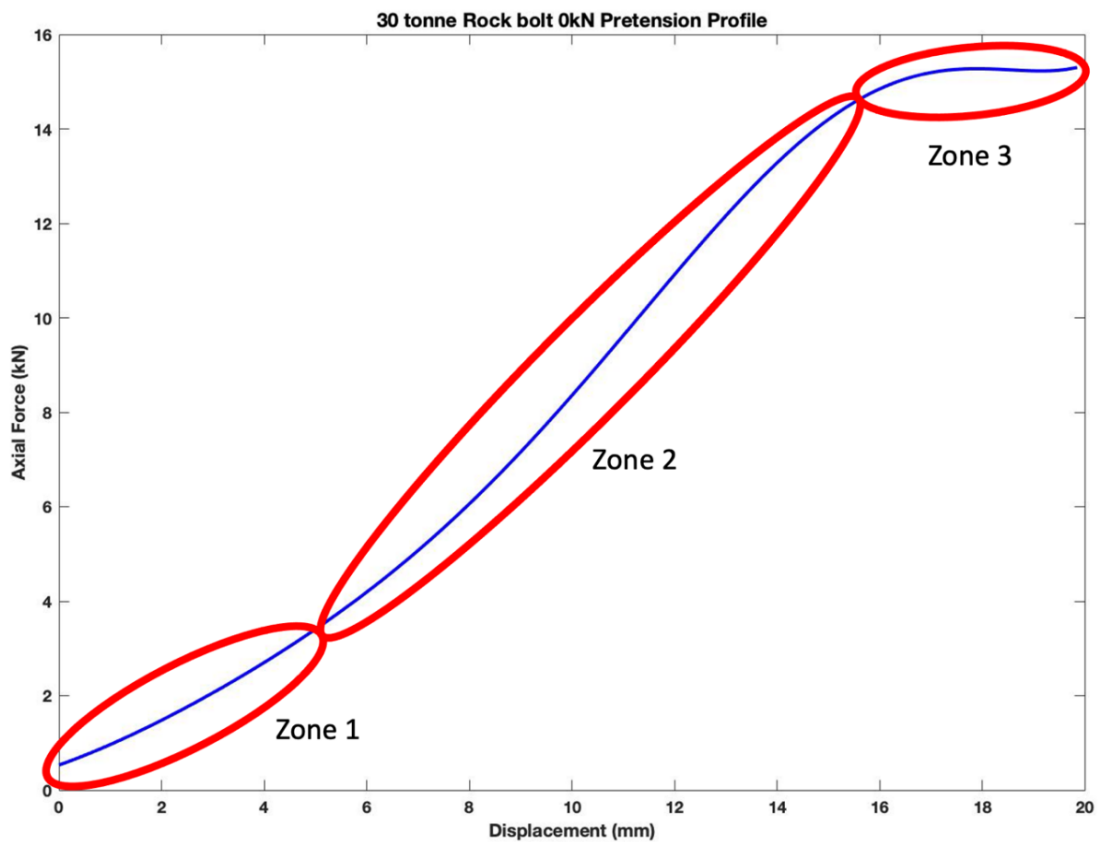


Figure 4.16: Illustration of the pretension profile zones under axial loads for 30-tonne rock bolt with 0kN pretension and clean shear interfaces.

Throughout testing of the rock bolts with increasing pretension values, certain patterns were evident. Increasing the initial set pretension subsequently increased the axial load at failure. However, this trend did not occur with each increase in pretension and was instead an overall increase from the initial 0kN pretension sample. Figure 4.17 shows samples with an applied initial pretension both achieving a peak failure of 24kN, while the sample representing the resting initial pretension only achieved a peak value of 15kN. The data set representing the initial pretension of 15kN was discarded from analysis due to inconsistencies during testing. In addition to the noted increase in peak axial load, there was also an observed decrease in displacement at failure. Unlike the peak load's single response to increased pretension, the displacement at failure reduced with each increase to initial pretension. Figure 4.17 demonstrates the reduction in failure displacement where the 0kN pretension sample reached a displacement of 20mm, the 10kN and 20kN pretension samples achieved failure displacements of 16.5mm and 9.5mm respectively. This suggested a correlation between initial pretension and failure displacement. It is noted that the samples experienced load fluctuations during curing, resulting in variability from the designed pretension setting.

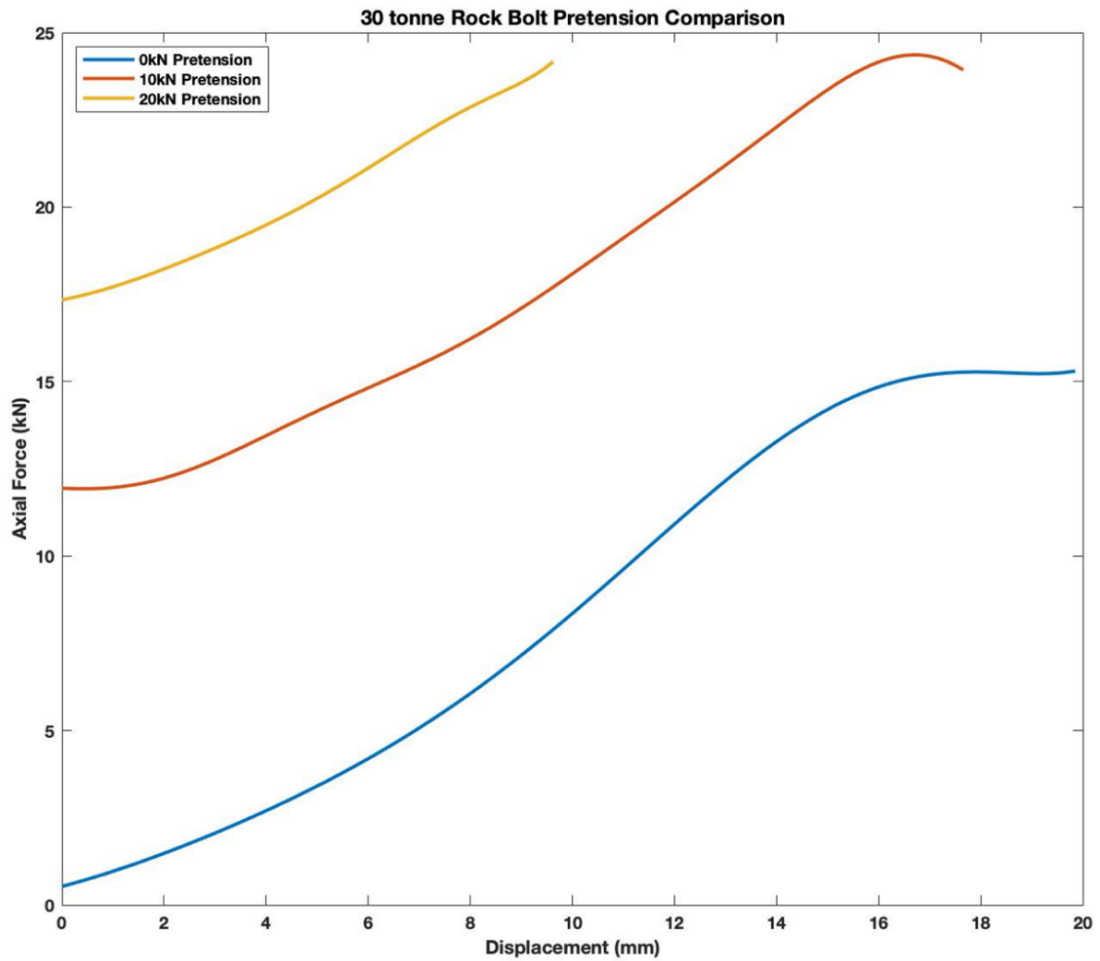


Figure 4.17: 30-tonne rock bolt clean pretension profile comparison

4.4.3 Impact of pretension on shear strength

The application of pretension to the 30-tonne clean shear samples had significant impact on several shear performance elements of the rock bolts including: peak shear force, failure displacement and shear profile. The two most significant impacts to the rock bolts' performance were from the increase in pretension and was: the reduction in peak shear force and displacement as highlighted by Figure 4.18. Increasing pretension resulted in an immediate reduction to the peak shear force of the tested rock bolts. However, this reduction presented as an individual phenomenon from the first pretension increase of 0kN to 10kN, resulting in an approximate 20% reduction of the rock bolts' peak shear capability. Each subsequent increase in pretension presented limited new peak shear force losses. As such, the 10kN, 15kN and 20kN pretension samples all reached similar peak shear forces of between 120kN to 125kN.

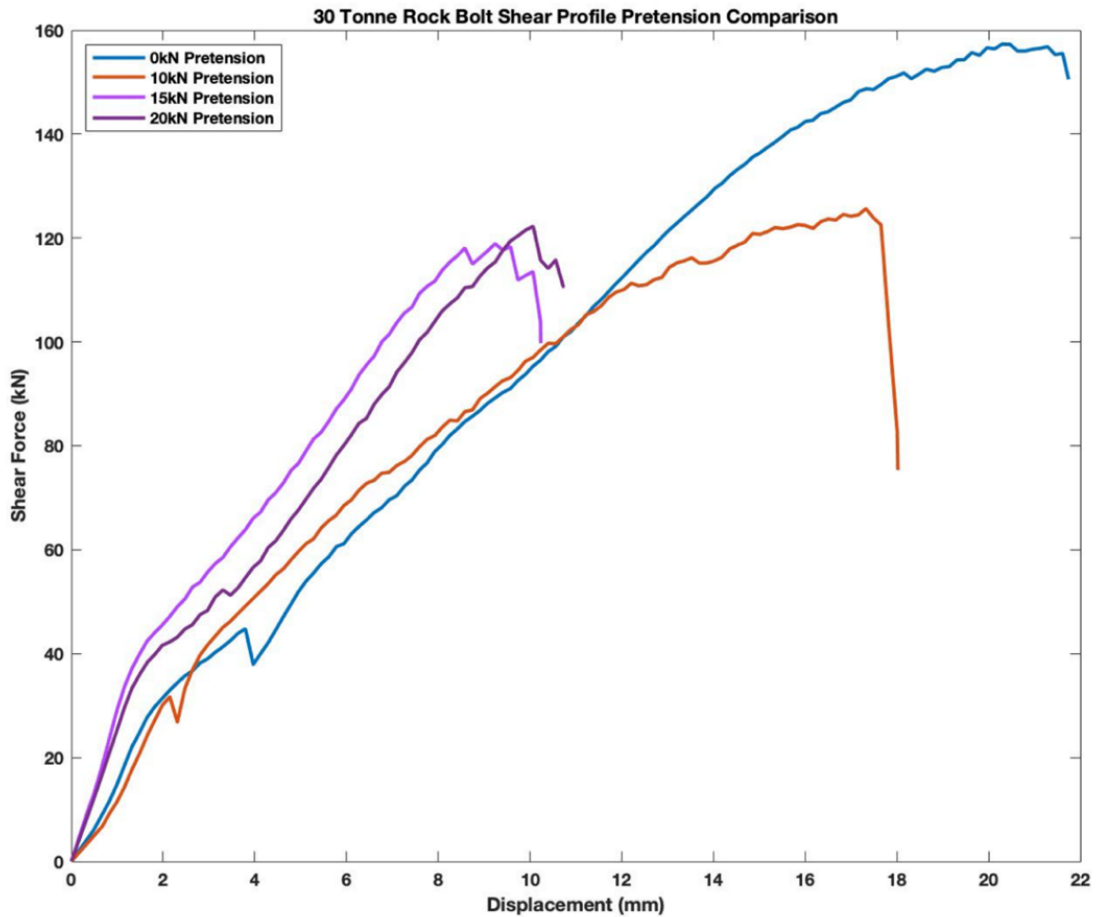


Figure 4.18: Impact of pretension on the overall shear performance of 30-tonne rock bolts with clean shear interface

Unlike the one-off impact to the peak shear force, the increase in pretension resulted in incremental decreases to the samples' failure displacement with the most significant decreases occurring between the 0kN, 10kN and 15kN samples. The 0kN sample achieved a failure displacement in excess of 20mm, while the 10kN and 20kN samples reached failure displacements of 17mm and 9mm respectively as illustrated in Figure 4.18. This incremental reduction in shear displacement may be attributed to a tightening of the shear planes imparted through the increased axial loads caused by the application of pretension. As the axial forces increased and caused artificial confinement of the shear planes, the failure limits of the elements within the systems such as the grout interface and host material increased. This resulted in reduced load losses throughout the system as previously attributed to interface failures. This was further justified by the gradual elimination of the dip in shear force experienced within the strain-softening region, as explained in section 4.4.1. Figure 4.19 highlighted, that the sample subjected to a pretension of 15kN no longer exhibited the negative spike in

shear force as experienced by the 0kN pretension sample. Furthermore, there was a notable reduction in spike intensity as well as displacement with each increase in pretension, until it was eliminated as shown in Figure 4.20. Figure 4.20 illustrates in detail how the 10kN pretension sample exhibited a reduced negative spike of approximately 5kN occurring at a displacement of 2mm-2.5mm, as opposed to the 0kN sample experiencing a negative spike of approximately 8kN at a displacement of 3.5mm-4mm. Finally, the sample subjected to 15kN exhibited no discernible spike in shear force.

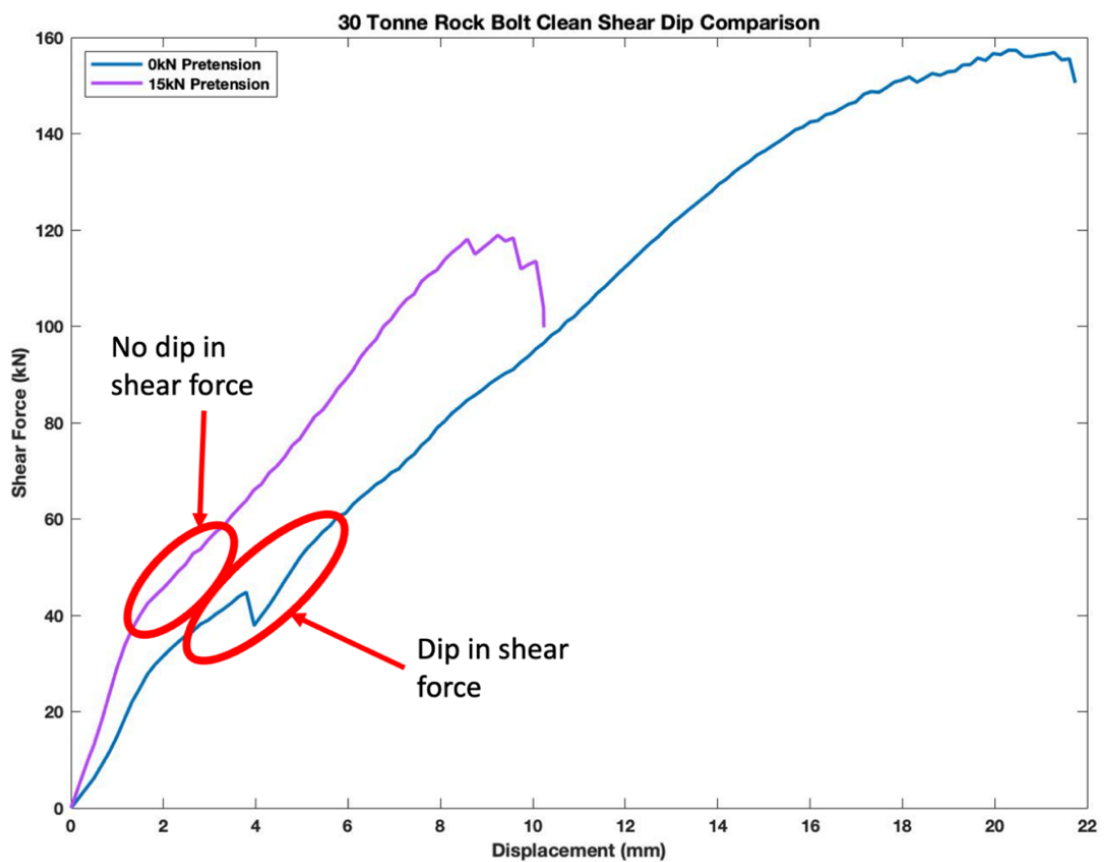


Figure 4.19: Impact of pretension on shear force dip for 30-tonne rock bolts tested in clean shear system

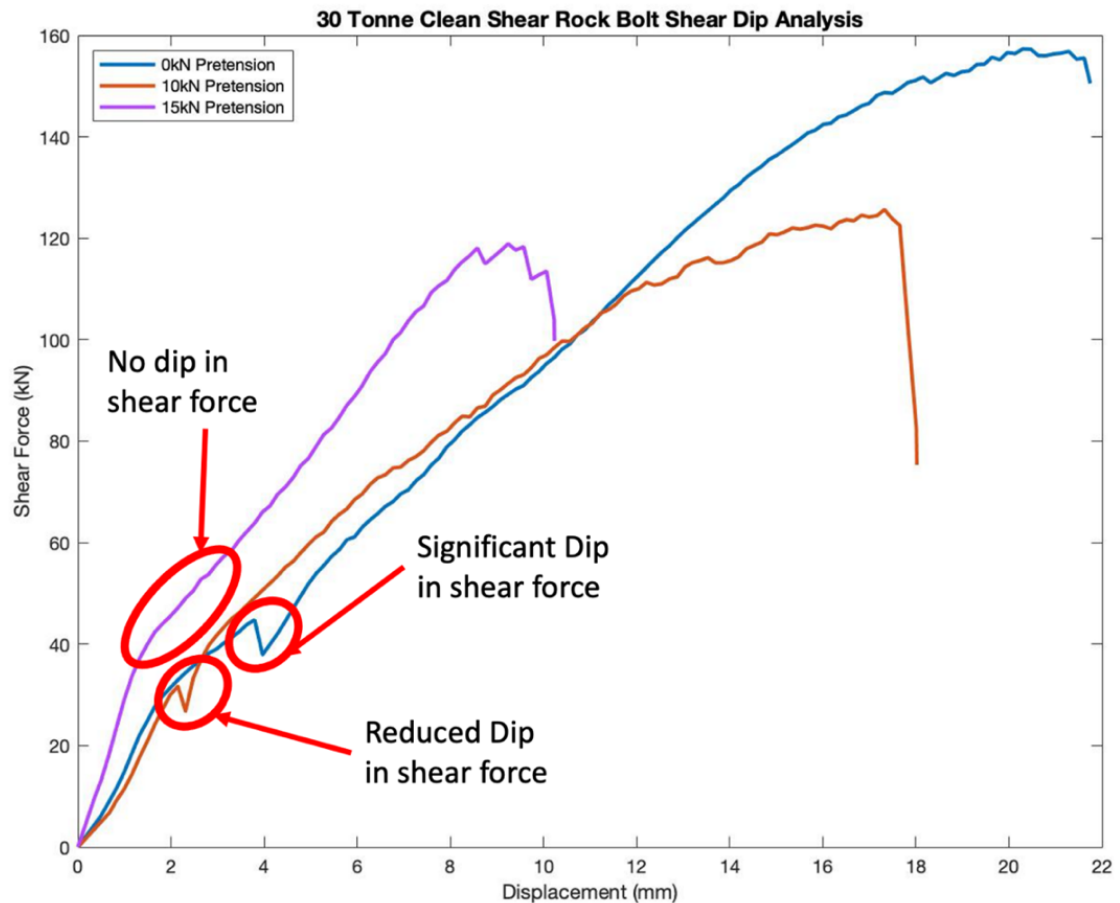


Figure 4.20: The effect of pretension on dip in shear force for 30-tonne rock bolts with pretensions of 0kN, 10kN and 15kN

The application of pretension also had significant impacts on the elastic stage and strain-softening stage of the shear profile. The subsequent changes to pretension had an unexpected impact on the rock bolts' elastic failure response where the elastic failure force increased after the application of pretension. This increase in elastic limit occurred once and then stabilised for all subsequent increases in pretension. Additionally, there were minor incremental decreases to the displacement range of the region.

Lastly, the increase in pretension was observed to have a significant and proportional impact on the stiffness and strain-softening response to loading as demonstrated in Figure 4.18. The subsequent increase in slope gradient throughout the strain-softening region indicated an increase in rock bolt stiffness. While each succeeding increase in pretension resulted in an increase in shear stiffness, there appeared to be no new significant impact on the peak shear performance of each rock bolt.

4.4.4 Failure characteristics

Upon dismantling each sample, notable failure characteristics were highlighted including: the hinge point, interface damage and shear surface damage. When analysing the hinge point across all the tested pretensions, it was identified that an increase in pretension resulted in changes to the total bending experienced at the hinge point. Figure 4.21 and Figure 4.22 illustrate the bending at failure for the samples subjected to 0kN pretension and 20kN pretension respectively. The 20kN pretension sample recorded a hinge point bending of approximately 13° , an increase of 3° from the 10° recorded from the 0kN pretension sample. This increase in angle could be attributed to an increase in confinement forces and thereby an increase to the strength of the surrounding interfaces, forcing the rock bolt to rotate around the shear plane's edge. This increase in confinement forces for the grout and host rock interfaces also resulted in less damage propagating through the rock bolt element from the shear plane as highlighted in Figure 4.21. Unlike the samples with an applied pretension, the 0kN sample had no additional axial forces applied. This lack of axial force resulted in a relaxed shear plane and interface confinement. As a result, the rock bolt experienced a lower degree of bending at the location of failure as the rock bolt forced through the surrounding material throughout the shearing process. This caused the rock bolt to experience fractures and delamination propagating from the shear plane and extending deep within the system as highlighted in Figure 4.22.

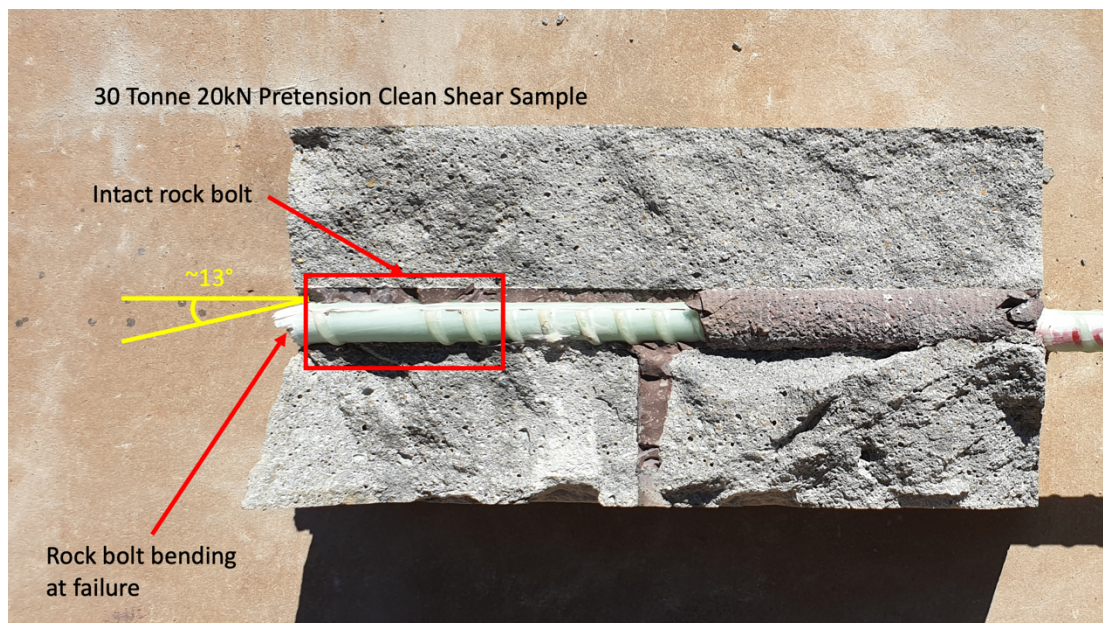


Figure 4.21: Angle of failure for 30-tonne rock bolt with 20kN pretension with clean shear conditions

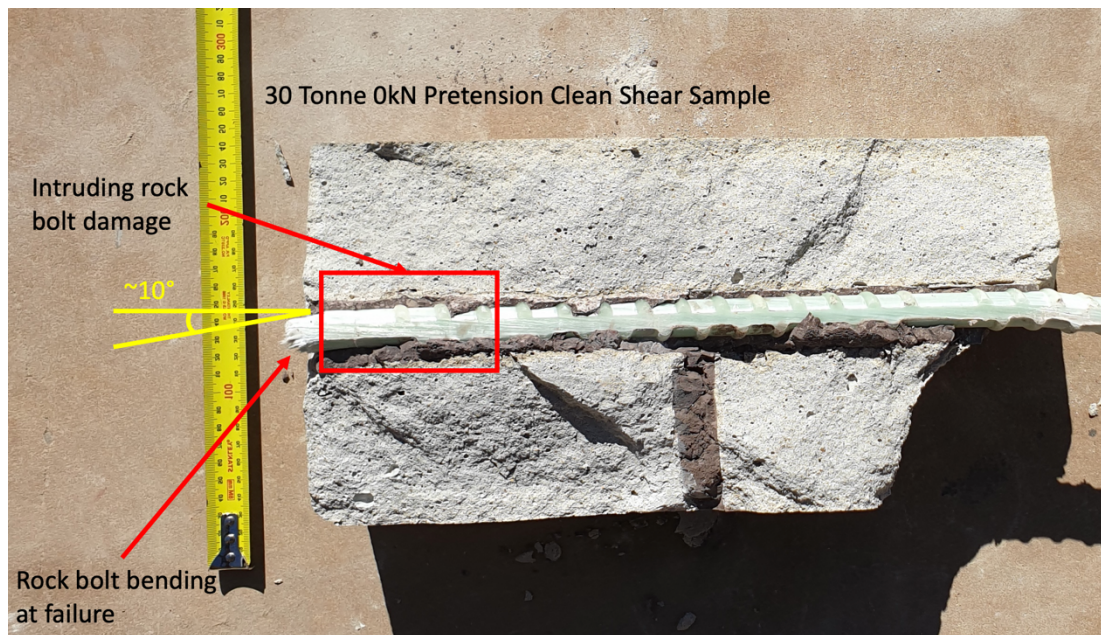


Figure 4.22: Angle of failure for 30-tonne rock bolt with 0kN pretension with clean shear conditions

With the increase in pretension, there appeared to be a change in the damage experienced by the surrounding material. Samples exposed to greater pretension forces caused increased damage to the shearing surface. This was due to the pretension forces creating a clamping effect across the shear planes and producing the protruding curved edge of the hinge point, evident in Figure 4.21. The curved failed edge of the rock bolt cut away a significant amount of host material from the adjacent shear plane surface. In comparison, the 0kN samples did not share this phenomenon as the failure of the rock bolt was less aggressive and there were no confining forces forcing the rock bolt into the adjacent shear surface, as illustrated in Figure 4.23.

As previously outlined, the sample subjected to a pretension of 0kN did not experience any additional confining forces similar to the samples with an applied pretension. This lack of additional axial forces resulted in intrinsic interface confinement pressures. Under these conditions the introduction of shear forces along the rock bolt element caused the grout and host rock interfaces to fail, evidenced by the observed damage around the element in Figure 4.24. In contrast, samples with an applied pretension contained additional axial forces, causing an artificial increase in confinement pressures. As demonstrated in Figure 4.24, the fibreglass rock bolt was unable to overcome the increased strength of the grout and host material resulting in significantly less damage around the rock bolt at the shear plane interface when compared to the sample with 0kN pretension.

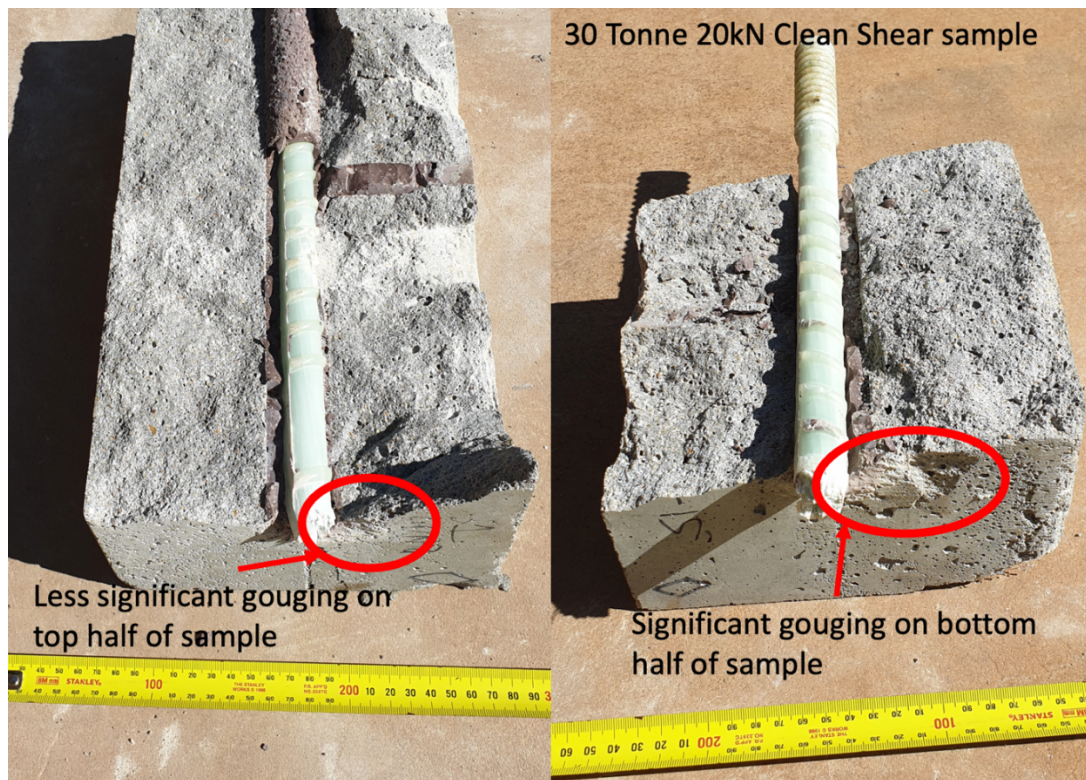


Figure 4.23: Damage caused by 30-tonne rock bolt to host material with 20kN pretension

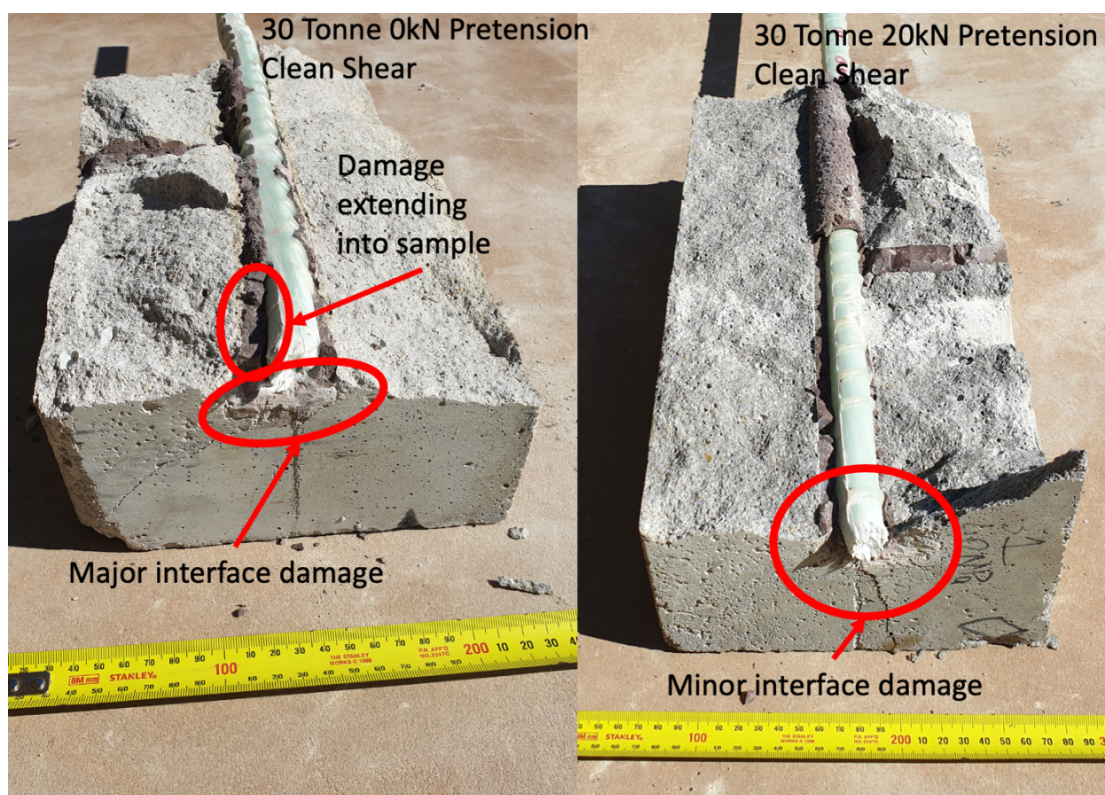


Figure 4.24: Shear interface comparison 0kN pretension and 20kN pretension

4.5 Comparison between 20-tonne and 30-tonne rock bolts

4.5.1 Shear behaviour profile

Throughout the completion of this study two products were tested: the 20-tonne and 30-tonne tensile rated fibreglass rock bolts. The shear behaviour properties for these bolt types were described in detail in sections 4.3 and 4.4 respectively. The following comparative analysis outlines the similarities and differences between the shear performance of the 20-tonne and 30-tonne rock bolt types. As the results of the 20-tonne 0kN pretension rock bolts have been discarded, the comparison has been conducted on the 10kN samples for both 20-tonne and 30-tonne rock bolts. It was previously identified that each type of rock bolt samples demonstrated a three-stage shear profile including the elastic, strain-softening and failure regions. Comparing the elastic region across the 20-tonne and 30-tonne samples it was evident that the elastic region observed for each bolt type was similar with respect to both plotted profile as well as their peak elastic forces. Both samples transitioned into the strain-softening stage at approximately 38kN, as highlighted in Figure 4.25. However, these elastic regions presented with differing gradients suggesting dissimilar strain responses. The profile for the elastic region of the 20-tonne rock bolts consistently recorded a gradient of approximately 88° , somewhat steeper than the 30-tonne rock bolt with 10kN pretension, which recorded gradients of approximately 86° , highlighted in Table 4-2. This suggested that the 20-tonne rock bolts experienced a stiffer response to shear forces. The gradients observed over the elastic region of the 20-tonne samples were all greater than the gradients of the 30-tonne rock bolts. However, samples with a pretension of 15kN and higher recorded similar results of 88.1° and 88° for the 20-tonne and 30-tonne sample respectively. Similar to the elastic region, the strain-softening stage of the shear profile demonstrated a stiffer response to shearing for the 20-tonne samples than the 30-tonne samples, with the exception of the 15kN pretension samples. As highlighted in Table 4-2, the 20-tonne 15kN pretension sample experienced a negligible decrease in gradient from the 10kN sample, while in the same scenario the 30-tonne sample experienced a gradient increase of 2.9° , suggesting the 30-tonne 15kN sample had a stiffer strain-softening region compared to the equivalent 20-tonne sample. Unlike the previous two stages, the final failure stage did not record an interference from changes in pretension, resulting in uniform gradients across each

pretension. In the case of the 20-tonne samples, each failure zone presented with increased gradients to that of the 30-tonne samples.

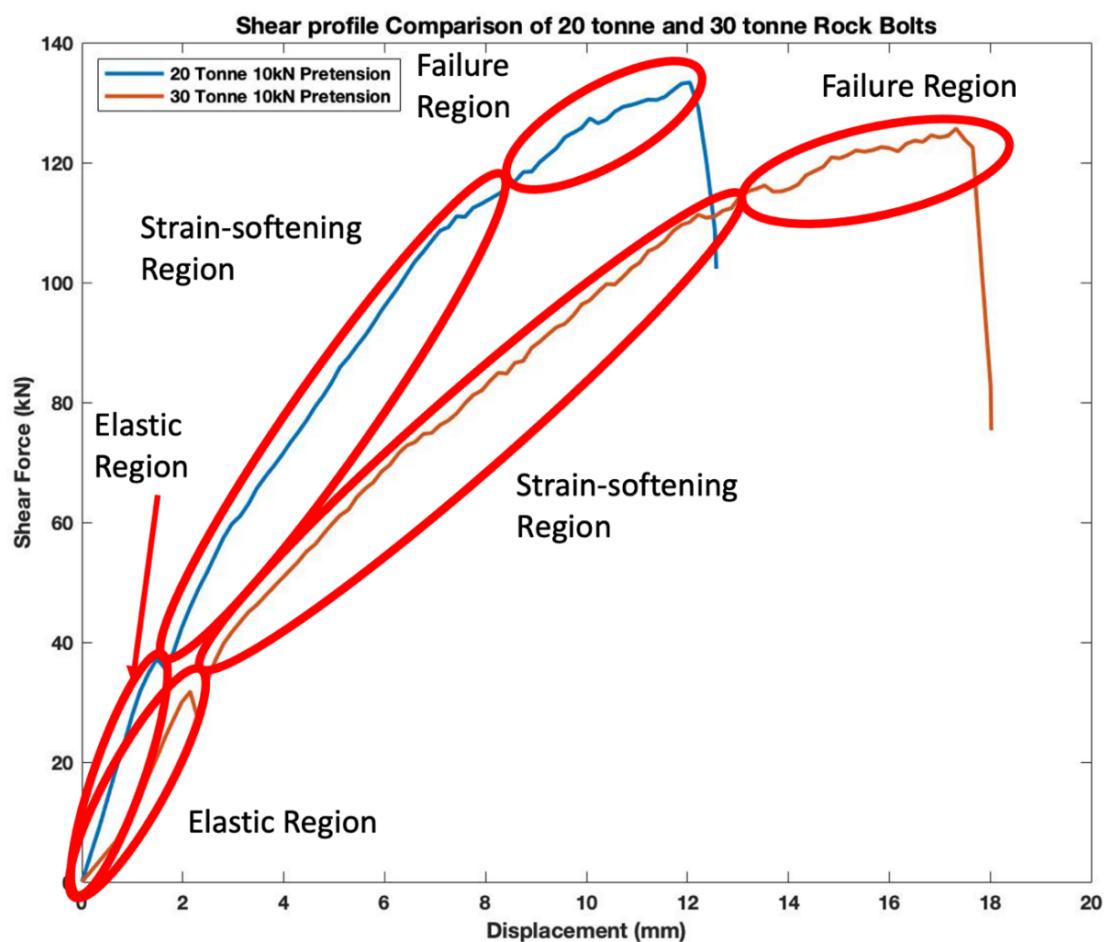


Figure 4.25: Shear profile comparison of 20-tonne and 30-tonne rock bolts.

Table 4-2: Summary of gradients at each stage of the shear profile curve and angle at the hinge point post failure

Rock Bolt	Elastic Gradient (°)	Strain-Softening Gradient (°)	Failure Gradient (°)	Angle at Hinge Point (°)
20T 0kN	Invalid	Invalid	Invalid	Invalid
20T 10kN	87.7	84.8	78.7	11.0
20T 15kN	88.1	83.7	76.0	12.5
20T 20kN	88.1	85.9	76.0	14.0
30T 0kN	86.2	82.9	63.4	10.0
30T 10kN	86.2	81.9	63.4	10.5
30T 15kN	88.0	84.8	71.6	12.5
30T 20kN	88.0	84.8	63.4	13.0

Table 4-3 shows that the peak shear forces achieved by the 20-tonne samples subjected to pretensions of 10kN, 15kN and 20kN varied by approximately 3kN, while the equivalent 30-tonne samples recorded a variance of approximately 6kN. In addition to differences in stiffness, this resulted in the 30-tonne samples achieving greater displacements at failure. While the 30-tonne 0kN pretension drastically outperformed all the other samples for peak shear, it also achieved the greatest peak displacement. However, the peak displacements achieved by the 30-tonne samples at a low pretension declined faster with each increase in pretension as opposed to the 20-tonne samples at which point the 30-tonne 15kN and 20kN pretension samples matched the displacements of the 20-tonne samples. While there was an observed decrease in peak shear force for the 30-tonne 0kN pretension to the 10kN pretension, it was not possible to comment on potential similarities to the 20-tonne samples as the 0kN sample was discarded due to inconsistencies. The 20-tonne and 30-tonne samples presented similar shear displacement trends with each increase in pretension. As identified in Table 4-3 each rock bolt type experienced a decrease in shear displacement when the pretension was increased. Finally, as previously shown in Table 4-2, the 20-tonne and 30-tonne samples exhibited similar hinge point trends as well as similar recorded values. It was observed that increasing the pretension resulted in incremental increases in bending at the hinge point post failure. Both samples experienced hinge point bending ranging from approximately 10° to 14°. It was impossible to determine an exact value for the hinge point bending as some of the less damaged strands recovered slightly after failure, therefore an average value was determined over the width of the failure zone.

Table 4-3: Summary of peak forces and shear stresses of all samples

Bolt Type	Peak Shear Force (kN)	Displacement at Peak Shear (mm)	Peak Shear Stress (GPa)
20T0kNC	Invalid	Invalid	Invalid
20T10kNC	133.3	12.1	0.42
20T15kNC	136.3	11.9	0.43
20T20kNC	133.4	8.4	0.42
30T0kNC	157.9	20.5	0.50
30T10kNC	125.5	17.3	0.40
30T15kNC	119.6	9.2	0.38
30T20kNC	122.6	10.1	0.39

4.5.2 Pretension profile

Throughout the testing program it was identified that all samples shared similar pretension properties. One of the fundamental outcomes of monitoring the pretension was to determine a pretension profile for shearing. Sections 4.3.2 and 4.4.2 discussed in detail the pretension profile properties for both the 20-tonne and 30-tonne rock bolts respectively. Through the analysis it became apparent that both types of tested rock bolts exhibited similar axial properties during shearing as well as displaying some key differences. Both rock bolt types achieved axial pretension profiles of the same properties and both the 20-tonne and 30-tonne rock bolts' pretension profiles could be defined by three zones as shown in Figure 4.26. However, throughout the testing program it was identified that there were differences within each zone. The 20-tonne samples consistently presented as the stiffer option evident by the samples' failures at lower displacements when compared to the 30-tonne samples. This recorded stiffness difference translated to the pretension profiles. Zones one and two displayed a difference in stiffness as evident by the comparison of the 10kN pretension samples in Figure 4.26. While zone one's gradient was consistent across the samples, there was a significant difference in its displacement range, with the 20-tonne samples exhibiting a consistently longer zone.

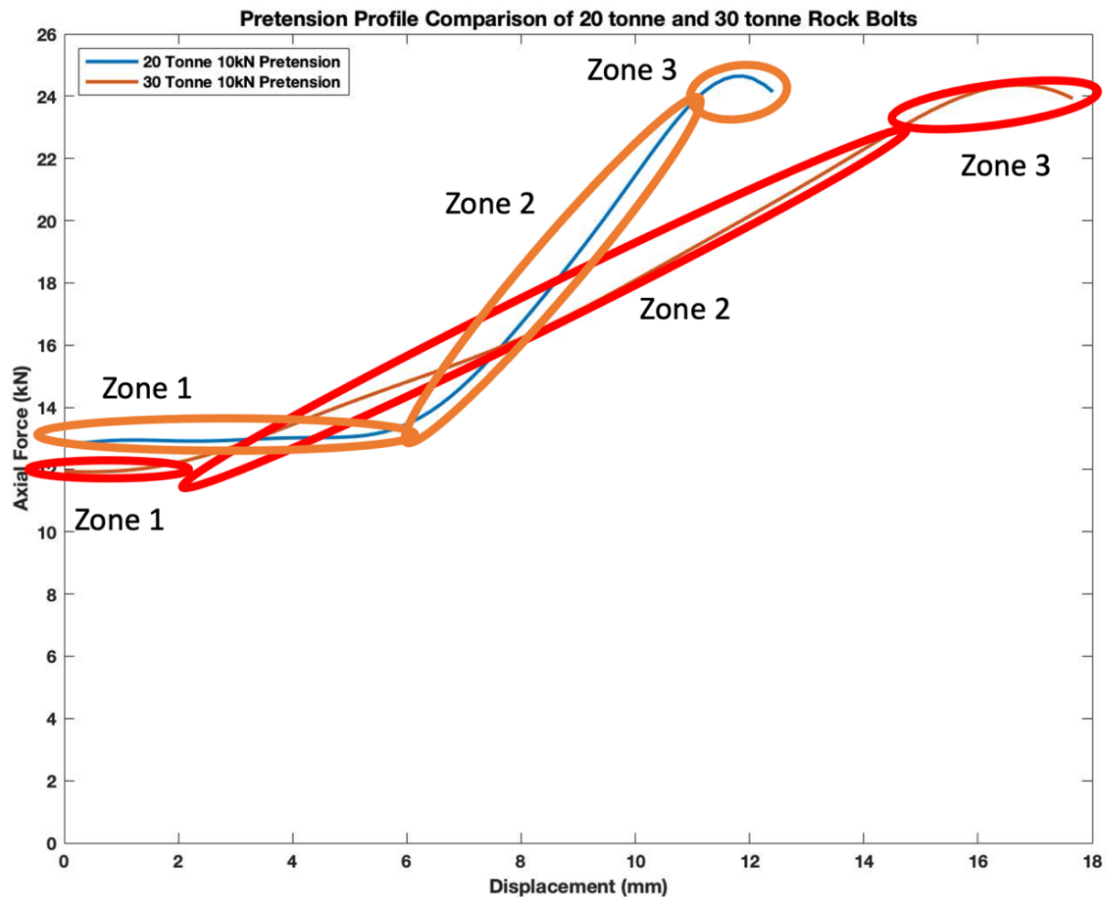


Figure 4.26: Comparison of the axial force profile for both 20-tonne and 30-tonne 10kN pretension samples

Zone two of the pretension profile for the 20-tonne sample recorded steeper gradients at the lower 10kN and 15kN pretensions when compared to the 30-tonne rock bolts as displayed in Table 4-4, with the exception of the 20kN sample. The gradient difference for the 20kN samples was potentially a result of the axial forces for the 30-tonne sample relaxing prior to testing as evident from its lower initial pretension as outlined in Table 4-1. Despite differences in gradients, both rock bolt types experienced similar consistent reductions to the zone two gradients in relation to increased pretension. In addition to the differences with zone two, zone one displayed variations across the rock bolt types, such as differing gradients and the previously mentioned length of the zone. All 20-tonne samples recorded a similar gradient, albeit lower when compared to the 30-tonne samples, throughout zone one of approximately 5.7° despite the 20-tonne sample presenting as the stiffer rock bolt. In addition, the 30-tonne rock bolt also experienced a reduction in gradient from the 0kN pretension sample to the 10kN pretension sample and then later recovered the gradient following the 15kN pretension sample. No comments could be made to compare the gradients for zone three as there

was too much variation with residual forces and data system cut-off limits. However, the final peak values were successfully recorded. There appears to be little to no correlation between rock bolt type and peak axial force. Both the 20-tonne and 30-tonne rock bolts recorded the same peak values of 24.5kN, suggesting there is no correlation between the tensile and shear capabilities of the rock bolts. It is noted though, that the 30-tonne sample also recorded the two lowest peak pretension results. This could be due to the system performing a more efficient shear therefore preventing the shear load from transforming to an axial load, potentially due to over-strengthened host concrete.

Table 4-4: Gradient profiles for zones one, two and 3 and peak axial force for all samples

Bolt Type	Zone 1 Gradient (°)	Zone 2 Gradient (°)	Zone 3 Gradient (°)	Peak Axial Force (kN)
20T0kNC	-	-	-	-
20T10kNC	5.7	64.5	-11.3	24.5
20T15kNC	5.7	45	-5.7	20.6
20T20kNC	5.7	11.3	0	21.6
30T0kNC	26.6	1.2	11	15.7
30T10kNC	11.3	50.2	5.7	24.5
30T15kNC	11.3	38.7	0	16.7
30T20kNC	21.8	35	0	24.5

4.5.3 Impact of pretension on shear strength

The application of pretension influenced both the 20-tonne and 30-tonne rock bolts similarly for both shear strength and shear displacement response. To ensure sample consistency throughout testing, pretensions were applied using identical methods for each sample as per the procedure outlined in Chapter 3.3. Despite the careful measures adopted to ensure the integrity of each sample, the 20-tonne 0kN pretension sample displayed inconsistent results and was removed from further analysis. Unfortunately, due to time constraints and casting complexities, it was not possible to replace the sample for analysis within this study. Therefore, the changes that occurred from the increase in pretension of 0kN to 10kN for the 20-tonne samples will not be discussed, however, similarities observed from the 10kN pretension across the 20-tonne and 30-tonne samples will be detailed. As outlined in 4.4.3, there was an observed reduction

for both peak shear force and displacement with respect to the 30-tonne samples which amounted to approximately 25kN and 5mm respectively, when the pretension was increased to 10kN as outlined in Table 4-3 and further illustrated in Figure 4.27. The reduction of shear force experienced by the 30-tonne sample resulted in the subsequent samples achieving similar results to the equivalent 20-tonne samples. Figure 4.27 demonstrated that the new peak shear force of the 30-tonne sample now closely resembled the shear force of the 20-tonne sample with a variation of only 8kN. Despite the similar shear force values, the observed failure displacement was not in agreement. The 30-tonne 10kN pretension sample was displaced an additional 7.6mm at the moment of failure when compared to the 20-tonne equivalent sample. The failure displacement for the 20-tonne sample was considerably less than the 30-tonne sample, suggesting that the 20-tonne sample displayed a stiffer response to shearing compared to that of the 30-tonne sample. However, when comparing samples transitioning to 15kN pretension, the reverse could be said. Increasing the pretension further to 15kN resulted in a continued trend of reduction in shear force and displacement for the 30-tonne sample. As a result, the 30-tonne sample with a pretension of 15kN now failed with a shear displacement 1mm less than the 20-tonne sample of the same pretension and therefore presenting as the stiffer rock bolt option. This trend, however, did not continue as the two rock bolt types displayed two opposing peak displacement responses to increased pretension. While the 30-tonne samples demonstrated significant reductions to the peak displacement, this effect reduced with each increase in pretension resulting in very little variation between the peak displacements of the 15kN and 20kN samples as illustrated in Figure 4.28. In contrast, the reverse observation was made for the peak displacement of the 20-tonne rock bolts, where the initial change of pretension from 10kN to 15kN showing as a minor change of less than 0.5mm. However, the change from 15kN to 20kN pretension resulted in a much greater decrease of 3.5 mm in displacement for the 20-tonne samples, as shown in Figure 4.28. The 20-tonne rock bolt with a pretension of 20kN was again the stiffer system when compared to the 30-tonne rock bolt of the same pretension.

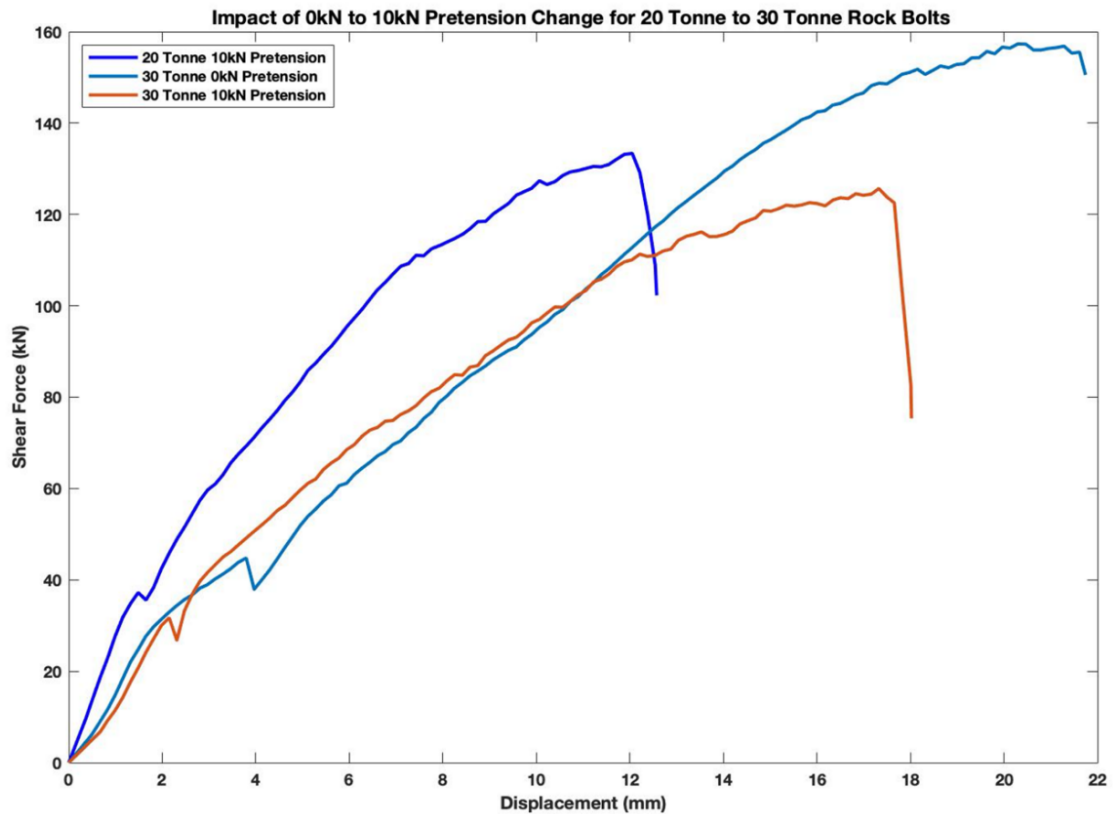


Figure 4.27: Influence of pretension increase from 0kN to 10kN on shear force for 20-tonne and 30-tonne rock bolts

Both 20-tonne and 30-tonne rock bolt samples exhibited the same ‘dip’ in shear force as outlined in sections 4.3.3 and 4.4.3 by observing Figure 4.27 and Figure 4.28, it was evident that each rock bolt type shared similar properties regarding this anomaly. For all samples, the shear force dip was observed to have occurred either at the end of the elastic region or just following the beginning of the strain-softening region, suggesting this phenomenon was a result of either the system as a whole or an intrinsic fibreglass response. Further testing would be required to determine the root cause. Overall, it was evident that the application of pretension had a positive impact on the reduction of the intensity of the dip and with a large enough pretension, the dip could be eliminated altogether. It was observed that each increase in pretension had a greater impact in reducing the dip in the 30-tonne samples, as opposed to the 20-tonne samples. A pretension of 15kN was required by the 30-tonne samples for the dip to be eliminated. However, the 20-tonne sample still presented remnants of the phenomenon with a pretension of 20kN as demonstrated in Figure 4.28.

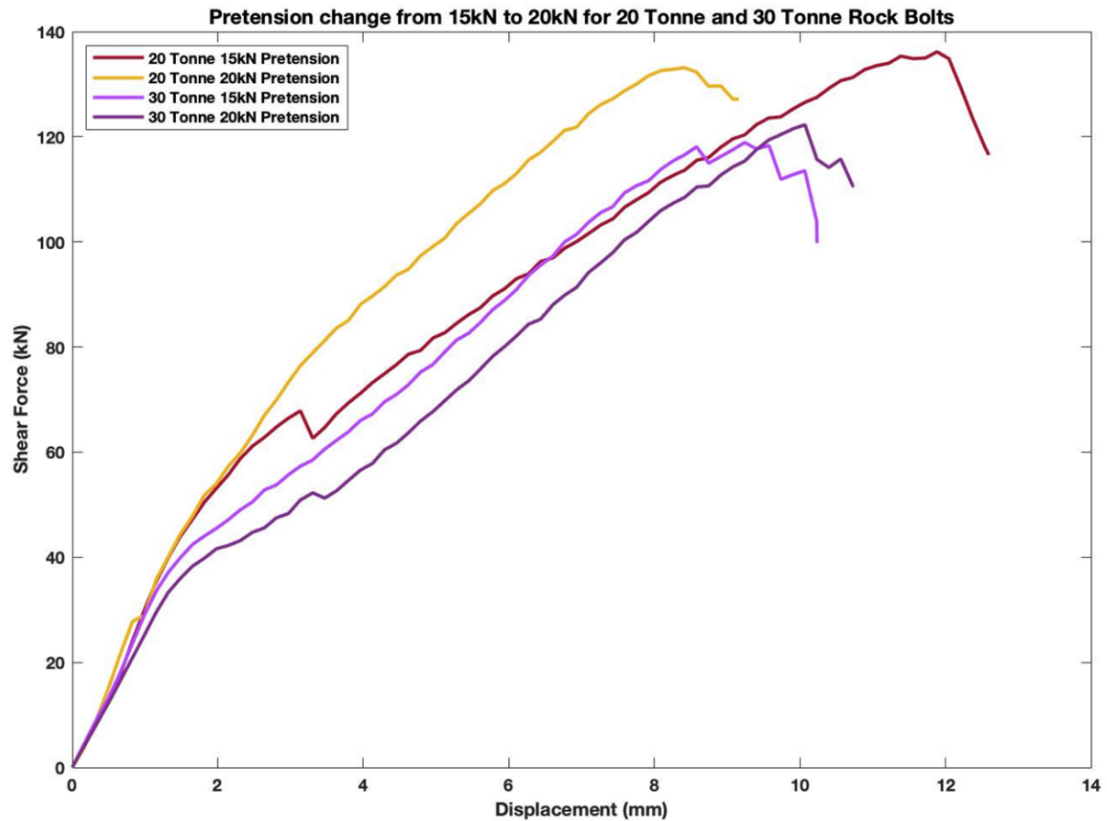


Figure 4.28: Influence of pretension increase from 15kN to 20kN on shear force for 20-tonne and 30-tonne rock bolts

4.5.4 Failure characteristics

The physical characteristics of all samples were analysed post failure to compare key characteristics between the 20-tonne and 30-tonne rock bolts. Sections 4.3.4 and 4.4.4 provide a detailed analysis of the failure characteristic of each rock bolt and highlight three key components of failure: the hinge point, the rock bolt structural damage and the shear surface damage. In the 10kN pretension samples it was evident that both the 20-tonne and 30-tonne rock bolt shared similar properties when analysing the hinge point. Both samples achieved similar failure angles with a difference of 0.5° as demonstrated in Figure 4.29. However, this was the only similarity for the 10kN pretension samples. When assessing the structural damage within the rock bolts, the 20-tonne sample displayed evidence of fractures propagating deeper into the sample. In contrast, the 30-tonne rock bolt displayed no internal fractures, as highlighted in Figure 4.29. Figure 4.30 shows that the 30-tonne rock bolts displayed the ability to damage the shear plane surface when there was an applied pretension of greater than 0kN. The damage depicted in Figure 4.30 was the result of the 30-tonne rock bolt

dragging across the surface. However, it can be seen that the 20-tonne rock bolt with the same 10kN pretension did not share this characteristic and as a result, no damage was observed on the shear plane. The 20-tonne rock bolt however exhibited signs of damage to the grout layer surrounding the rock bolt, unlike the 30-tonne sample as shown in Figure 4.29.

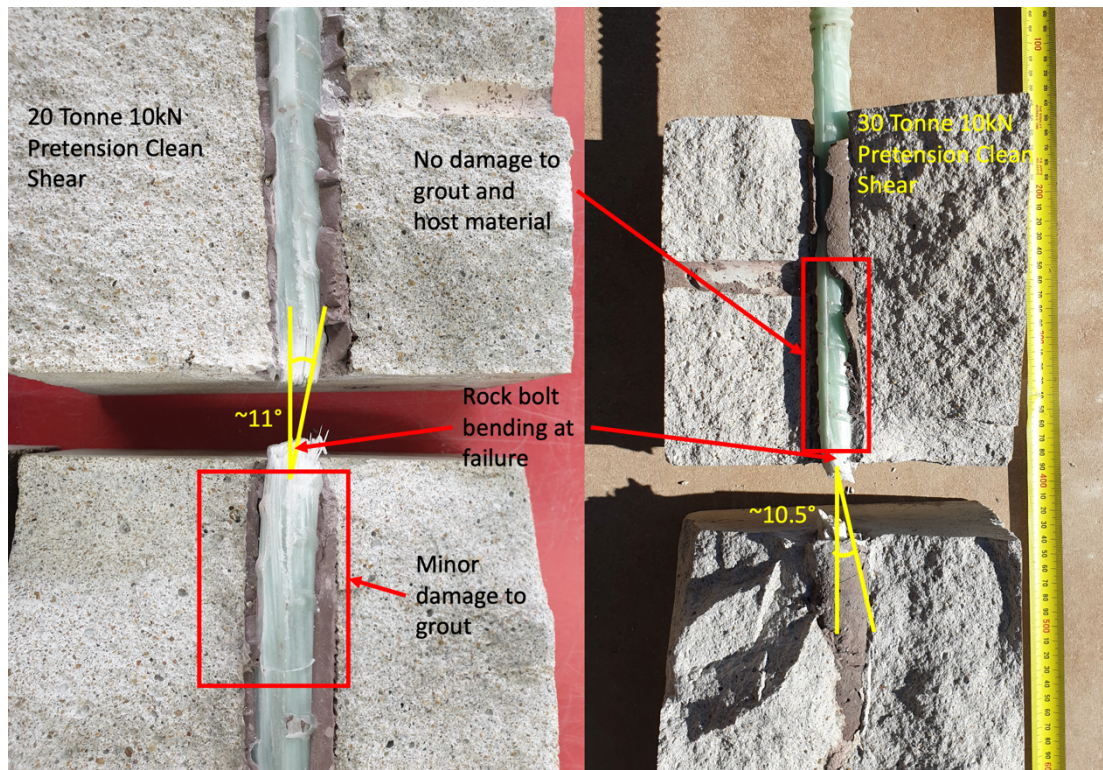


Figure 4.29: Comparing rock bolt structural damage for 20-tonne and 30-tonne rock bolts with 10kN pretension



Figure 4.30: Representation of shear plane damage for 20-tonne and 30-tonne rock bolts

The same comparative analysis was conducted for the 20-tonne and 30-tonne rock bolts subjected to the highest set pretension of 20kN, focusing on: the hinge point bending, rock bolt structural damage and shear plane damage. Similar to the 10kN pretension samples, both the 20-tonne and 30-tonne rock bolts, subjected to 20kN pretension, performed similarly when investigating the bending at the hinge point. However, the difference in recorded angles deviated further from the 0.5° recorded for the 10kN samples to 1° for the 20kN samples. While the difference in bending increased, the rock bolts performed similarly to the trends outlined in Table 4-2. Unlike the 10kN pretension samples, both of the 20kN pretension samples displayed similar structural performance and neither the 20-tonne or 30-tonne rock bolt displayed any propagating fractures from the zone of damage. Additionally, neither of the rock bolts displayed damage to the grout and host material interfaces due to the increased confinement as a result of the pretension.

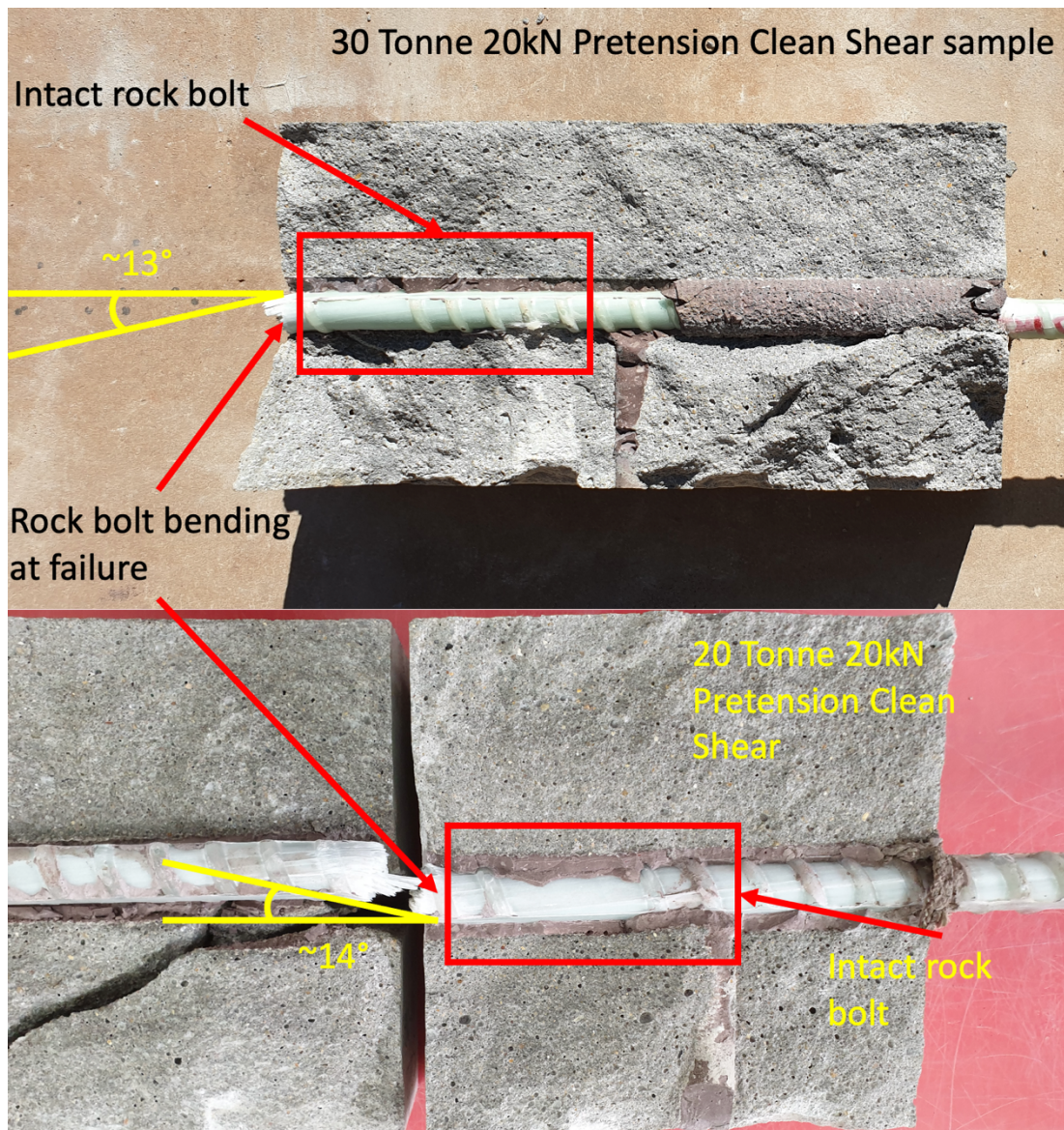


Figure 4.31: Comparing rock bolt structural damage for 20-tonne and 30-tonne rock bolts with 20kN pretension

Despite the 30-tonne samples causing damage to the shear plane through gouging across all of the tested pretensions during shearing, none of the 20-tonne samples presented with damage to the shear plane as a direct result of the rock bolt. Figure 4.31 highlights that even when the 20-tonne rock bolt is installed with the highest pretension setting of 20kN, no damage was sustained to the shearing surface. In contrast, Figure 4.32 highlights the damage sustained by the shear plane as a result of the 30-tonne rock bolt.

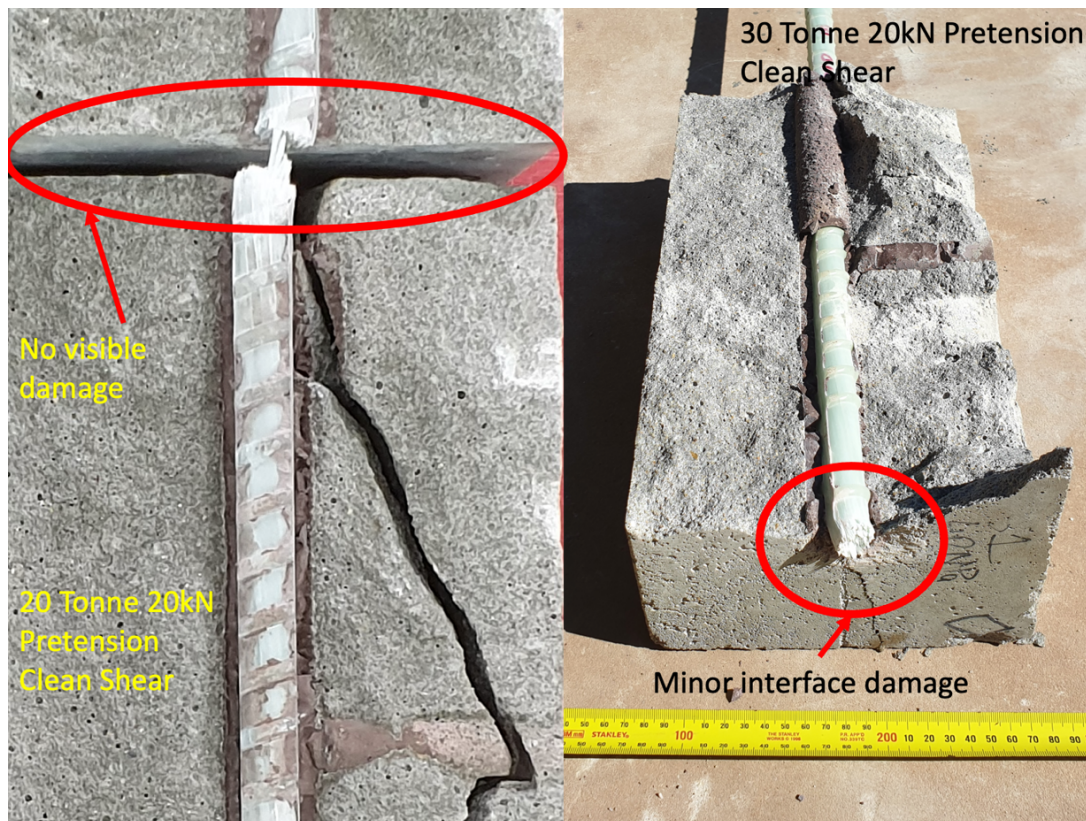


Figure 4.32: Comparing shear plane damage of 20-tonne and 30-tonne rock bolts

4.6 Understanding the behaviour of fibreglass rock bolts

4.6.1 Shear behaviour profile

To develop a comprehensive understanding of the shear performance of fibreglass rock bolts, tests were conducted to determine the true shear performance of the 20-tonne and 30-tonne fibreglass rock bolts. As outlined in Chapter 3.8.4, the rock bolt samples were subjected to the metal guillotine single shear test, eliminating external influencing factors such as applied pretension, converted axial forces, host rock interface and grout interfaces. This testing was undertaken to assist in understanding the rock bolts' performance during the double shear testing. The 20-tonne and 30-tonne rock bolts tested using the single shear testing method demonstrated comparable shear profiles containing the three regions as shown in Figure 4.33. The first region was the initial linear stage of the profile and was classified as the elastic region due to its apparent elastic response, therefore any failure occurring during stage one was reversible and caused no damage to the rock bolt. The second stage was identified by a positive nonlinear shear force increase with the increasing displacement. This

characteristic suggested the rock bolt experienced a form of hardening and therefore the region was aptly named the strain-hardening region. Strain-hardening was suspected to occur due to the single shear apparatus providing increasing axial confinement. Throughout the shearing action of the guillotine, the rock bolts' annulus decreased as the two halves of the shearing apparatus slid past each other as the displacement increased. Therefore, the rock bolt was forced to occupy a decreasing area at the shear face. This in turn provided increasing shear force transfer efficiency throughout the cross-section of the rock as forces were not able to dissipate through resin failure. This resulted in the observed increase in recorded shear force. The final region was identified as the failure region due to the reducing shear force response to displacement occurring through a mixture of significant instantaneous reductions in shear force as well as gradual declines. It was evident in both cases that the reducing shear force was a result of the fibres and resin structure failing and leading to complete rock bolt rupture. Both rock bolt samples performed similarly achieving similar peak shear forces and displacements. The main differences between the rock bolt types was the failure displacement and strain throughout each region. During the elastic and strain-hardening portions of the shear profile, the 20-tonne rock bolt demonstrated a stiffer response to shear, illustrated in Figure 4.33. The limits of each stage across the rock bolt types were similar, however the 20-tonne sample reached its peak shear force at lower displacements compared to that of the 30-tonne rock bolt. This resulted in the 20-tonne sample beginning the failure stage 1mm earlier than the 30-tonne sample. Despite achieving similar peak shear force values at differing displacements both rock bolts achieved ultimate failure within 0.2mm of each other. The post failure response of the 20-tonne rock bolt was drawn out over a longer period as evident by smaller decreases to the recorded shear forces. In contrast, the 30-tonne rock bolt demonstrated a greater number of significant and instantaneous decreases to the shear force.

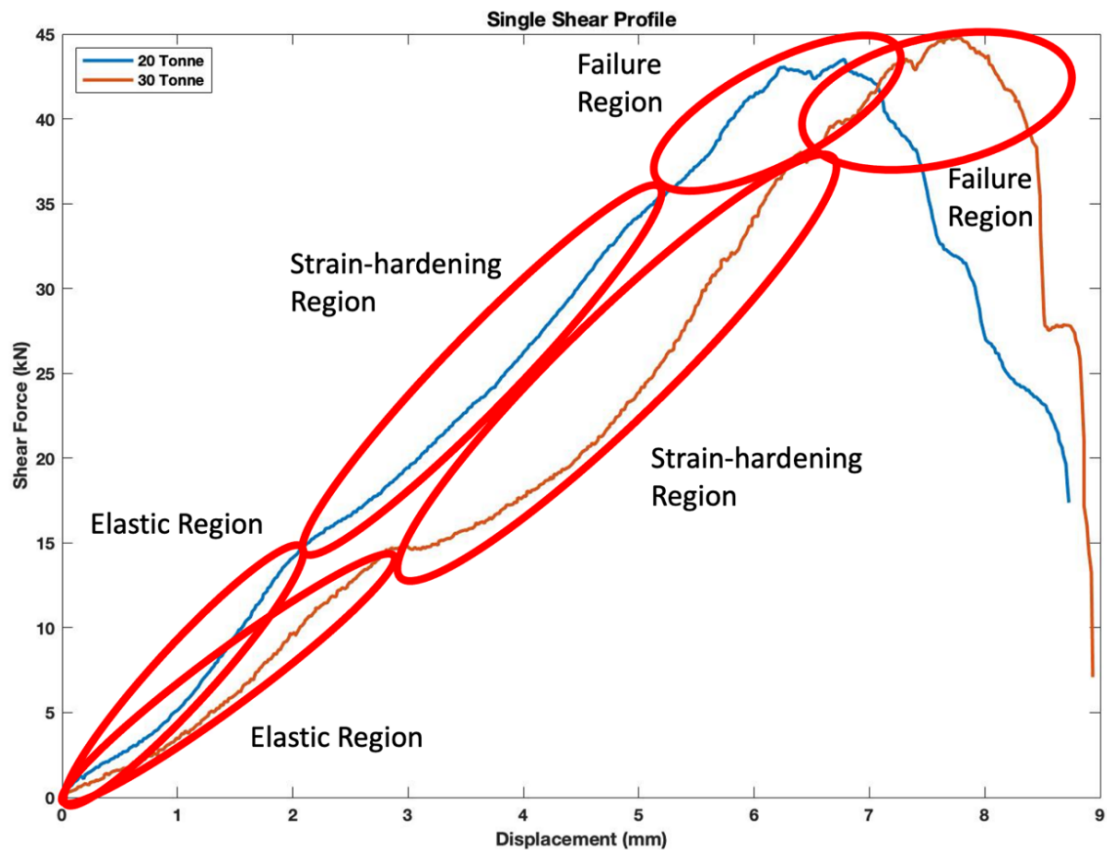


Figure 4.33: Stages of the single shear profile for 20-tonne and 30-tonne rock bolts

Throughout the completion of the double shear analysis, it became obvious that several key shearing behaviours experienced were also evident during the single shear tests, such as the shear profile and the difference in performance due to rock bolt type. The single shear and double shear testing methods both identified a shear profile consisting of three stages including the elastic region, a strain failure response region and finally the failure region, demonstrated in Figure 4.34. While the second stages identified opposite strain responses such that the double shear samples exhibited a strain-softening behaviour and therefore opposite to the strain-hardening behaviour of the single shear test. It was concluded that the strain response region was an intrinsic property of the rock bolt, whereas the type of strain response experienced was a function of the testing system. The double shear and single shear testing methods confirmed that the tensile rating of the rock bolts had a limited impact on their overall shear performance. The changes in confinement pressures because of the applied pretension, outlined in section 4.5, was an influencing factor for the performance differences between the rock bolt types impacting the strain response of the rock bolts. In section 4.4, increasing the pretension facilitated the efficient transfer of shear forces

directly to the rock bolt. This resulted in the decrease of the failure shear force and peak displacement of each rock bolt and with each increase in pretension the rock bolt's performance stabilised across the rock bolt types. The 20-tonne and 30-tonne samples exhibited increasing similar shear properties to that of the single shear samples.

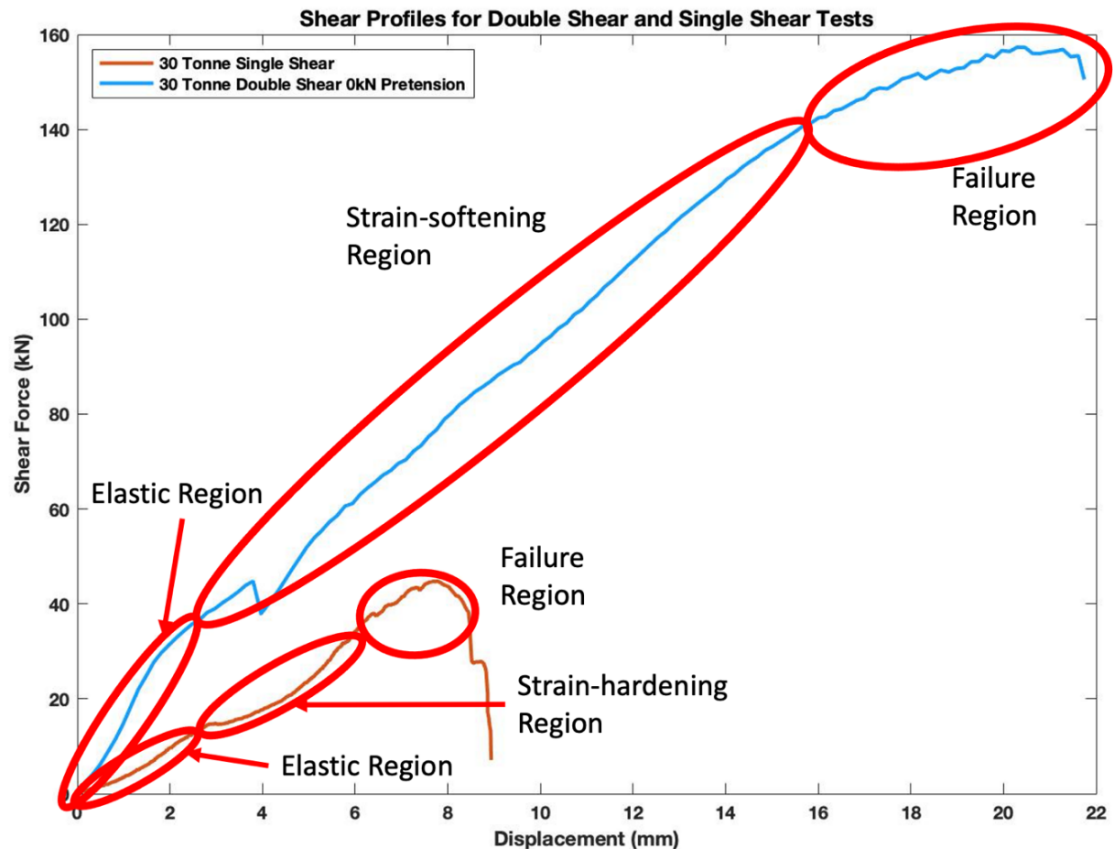


Figure 4.34: Shear behaviour of 30-tonne rock bolts outlining double shear and single shear stages

4.6.1.1 Single shear failure characteristics

The single shear samples were analysed post failure to determine the presence of outlying physical characteristics. As discussed in section 4.6.1, some assumptions were made regarding the physical influence the single shear apparatus had on the rock bolts. It was assumed that during the shearing process the lateral confinement subjected to the rock bolt at the shear plane increased due to the reducing volume within the chamber. At the beginning of the shearing process the shear plane was debris free and no lateral confinement was present, resulting in the clean shearing of the fibreglass strands as illustrated by the flat edges of the sheared surface in Figure

4.35. As shearing neared completion, the confinement at the shear plane increased, providing additional forces on the fibreglass rock bolt and forced the resin and fibreglass strands to crumble. The crumbling effect can be observed in Figure 4.35 across the centreline of the highlighted rock bolts. This progressed until the shear failure force was achieved and the sample split in two. It was observed that the damage caused by shearing was limited to within 5mm of the shear face. In contrast to the damage displayed by the 20-tonne and 30-tonne double shear tests outlined in sections 4.3.4 and 4.4.4, the single shear samples did not present with any additional crack propagation from the shear face. Finally, the failure face of the single shear samples was perpendicular to the orientation of the rock bolt, as shown in Figure 4.35. This shearing behaviour was in contrast to the samples tested using the double shear test system which exhibited varying degrees of bending.

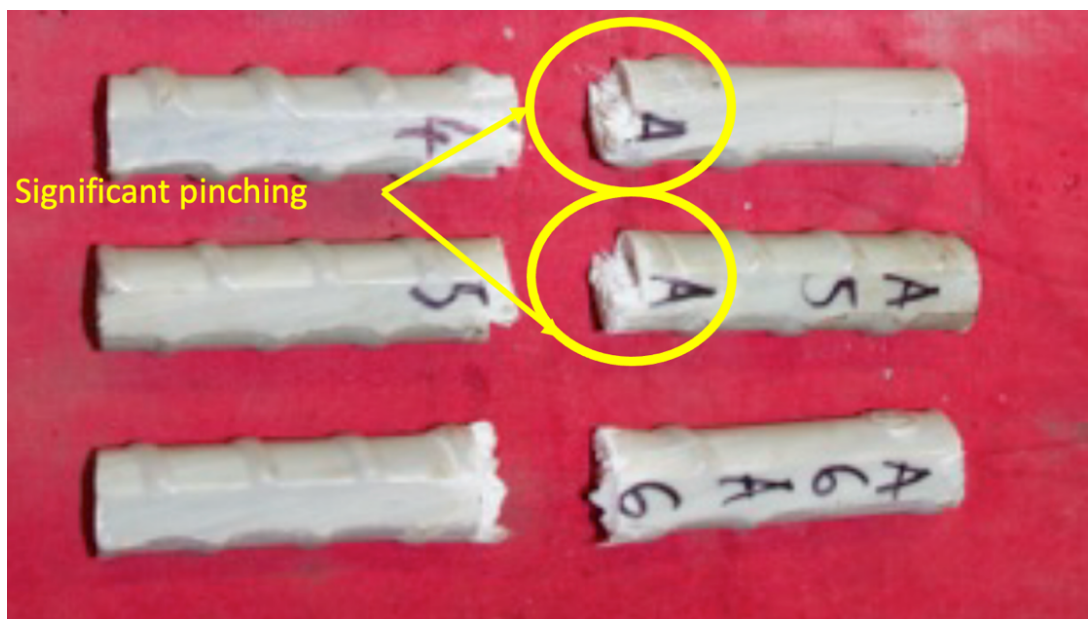


Figure 4.35: Single shear samples post failure highlighting pinch point

4.7 Summary

Two types of fibreglass rock bolts, the 20-tonne and 30-tonne rock bolts were tested utilising the modified double shear apparatus. The testing parameters included sample strength, pretension, and single shear performance. Throughout the double shear and single shear testing regime, 10 samples were tested for each of the 20-tonne and 30-

tonne rock bolts in order to study the effects of rock bolt strength. Upon completion of the testing regime, the following conclusions were made:

- The double shear performance profile of each of the tested fibreglass types could be described by three regions categorised as the elastic, strain-softening, and failure regions.
- The addition of increasing pretension values did not alter the regions of the shear profile for any of the tested samples. However, pretension did influence the peak failure shear force and failure displacement for the 30-tonne rock bolts. The 30-tonne rock bolts experienced a one-off failure shear force and failure displacement reduction when the pretension was increased from 0kN to 10kN. Any subsequent increase in pretension only resulted in minor variations to the rock bolts' performance.
- Due to the removal of the 20-tonne sample with a pretension of 0kN, no statement could be made regarding the influence of pretension on the sample.
- It was observed however that changes in pretension had little to no impact on the shear failure forces of the 20-tonne rock bolt samples. The increase in pretension did however impact the recorded failure displacement with each increase in pretension, resulting in up to a 4mm decrease in its failure displacement.
- Both the 20-tonne and 30-tonne samples registered a dip in recorded shear forces near the transition from the elastic region to the strain-softening region.
- Increasing the pretension of each rock bolt type resulted in a reduction in the severity of the recorded shear force dip. The applied pretension of 20kN completely removed the above phenomenon on the 30-tonne samples. The 20-tonne sample still presented the dip with an applied pretension of 20kN, however, the severity was considerably reduced.
- Each sample experienced bending of the fibreglass rock bolt at the shear plane, called the hinge point. Furthermore, the increase in pretension caused incremental increases to the amount of bending observed.
- The axial study of the pretension showed that the pretension profiles of the 20-tonne and 30-tonne rock bolt samples were identical, consisting of three zones. This was characterised by a linear zone one of ranging from a gradient of 5.7° to 11.3° , followed by significant gradient increases at zone two, suggesting

strain-hardening and finally zone three, represented by a reduction and then reversal of gradient indicating sample failure.

- The tensile rating of the rock bolts had a limited impact on their overall shear force performance. The single shear tests confirmed that both 20-tonne and 30-tonne samples displayed almost identical peak forces in response to shearing, with the key differentiator identified as the difference in strain response.
- The difference in strain response between the 20-tonne and 30-tonne rock bolts when subjected to pure shear directly impacted the recorded failure displacement, with the 30-tonne sample achieving approximately a 1mm increase to its failure displacement. This property was reflected by the double shear tests where the 30-tonne samples mostly outperformed the failure displacement of the 20-tonne samples.
- Post failure analysis of the rock bolts identified that increasing the applied pretension subsequently increased the confining pressure of the shear plane, resulting in reduced variability in the rock bolts' shear performance.
- The increased pretension resulted in less physical damage to the rock bolt propagating away from the shear plane. This supported the theory that the increase in pretension would result in increasingly efficient transfer of shearing forces to the rock bolt element, therefore resulting in less damage around the rock bolt element.

The double shear investigation is continued and expanded in Chapter 5 to explore the impacts of infilled shear planes on the 20-tonne and 30-tonne rock bolts. Chapter 5 continues to explore the rock bolts' double shear properties with pretension of 0kN, 10kN, 15kN and 20kN when subjected to the modified shearing conditions.

CHAPTER 5: RESULTS OF THE DOUBLE SHEAR TESTING OF FIBREGLASS ROCK BOLTS IN INFILLED JOINTS

5.1 Introduction

Host rock systems commonly encountered in both mining and civil projects requiring reinforcement are not only comprised of complex geometry but also include unique features that impact the effectiveness of rock bolts. Often these features are only identified after the section of strata has been destructively stripped for analysis. Therefore, targeting rock systems to study unique features is difficult and whether these features were targeted successfully can only be determined post failure. Additionally, attempting to isolate the impact of each rock system feature on the shear behaviour of rock bolts adds complexity and cost to the study and therefore reduces the confidence in the outcome. The developed double shear testing apparatus utilised in Chapter 4 was designed to accommodate the analysis of observed rock system features. When compared to the baseline determined in Chapter 4, the impact of each feature can be isolated to study their respective influence on the shear performance of fibreglass rock bolts.

The use of this versatile apparatus was extended to not only simulate the impact of various rock bolt testing conditions, but also the impact of the changes to the host rock system. As such, this chapter will expand on the double shear testing conducted in Chapter 4, to analyse the shear load transfer mechanism of fibreglass rock bolts. This was achieved by investigating the effect of infilled shear interfaces, containing sandy clay fill, have on the shear performance of fibreglass rock bolts at a range of pretensions.

The infilled joint double shear results were analysed in conjunction with the fibreglass rock bolts tested using the clean double shear testing study outlined in Chapter 4, to determine the shear behaviours of fibreglass rock bolts subjected to a rock system with infilled joints. The double shear tests were used to identify and compare the peak strength and displacement of 20-tonne, and 30-tonne dowels in a simulated multi-shear plane environment with interfaces containing sandy clay materials. To maintain consistency across testing schemes, this analysis was conducted utilising identical system properties to that of the clean interface testing scheme discussed in Chapter 4.

Therefore, the host material was set at a strength of 40MPa and pretensions applied ranging from 0kN to 20kN. To simulate the complex interference of infilled shear interfaces, 5mm layers of sandy clay fill was applied to the shear interfaces. A comparative analysis of the results was then undertaken to develop a comprehensive understanding of the shear behaviours of fibreglass rock bolts.

5.2 Overview of the testing process

As detailed in Chapter 3 and matching the parameters of Chapter 4, the testing was conducted on commonly used fibreglass rock bolts with design load capacity ratings of 20 and 30-tonnes. Similarly, samples were prepared utilising a host media strength of 40MPa. The fibreglass bolts were fastened using their respective nuts and washers. To create the infilled shear interfaces, smooth surfaces were created by utilising metal plates during casting. Once the concrete samples were cured, a mixture of sandy clay was applied to the shear planes to a thickness of 5mm, followed by the installation of the rock bolts with their corresponding pretension values of 0kN, 10kN, 15kN and 20kN. The system design properties, infill interface and rock bolt properties are outlined in Table 5-1. Key system properties included the designed pretension, achieved pretension, infilled thickness and rate of loading. As a result of casting experiences gained from the clean interface study from Chapter 4, the corresponding 20-tonne and 30-tonne samples achieved closer applied pretensions. Unfortunately, the application of pretension was difficult to control and resulted in each sample failing to achieve the designed pretension. To minimise the variance between the settled and designed pretensions the steps from Chapter 4 were implemented. Corrections were made for the beginning hour of the grout's curing process until the grout was sufficiently set. After the initial curing stage any additional adjustments would have minimal impact on the internal pretension of the system. Fortunately, through previous testing schemes, the variation of tested pretension between each sample had been minimised, but variations from the designed values were still present. Similar to the challenges from Chapter 4, some rock bolt samples experienced faster pretension settling rates than others, though by adopting the corrections, this minimised their impact on the final values. Recorded initial pretension values for all samples achieved values greater than the designed pretensions from 1kN to 2kN. As this was consistent across both the 20-tonne and 30-tonne rock bolts, testing system uniformity was maintained.

Table 5-1: Rock bolt properties for infilled shear system

Bolt Type	Rock bolt Dia. (mm)	Design Shear Capacity (t)	Designed Pretension (kN)	Applied Pretension (kN)	Tested Pretension (kN)	Infill Thickness (mm)	Rate of Loading (mm/min)
20T0kN INFILL	20	20	0	1.5	0.75	5	1
20T10kN INFILL	20	20	10	12	12.39	5	1
20T15kN INFILL	20	20	15	17	14.35	5	1
20T20kN INFILL	20	20	20	22	19.65	5	1
30T0kN INFILL	20	30	0	1.6	0.98	5	1
30T10kN INFILL	20	30	10	12	10.35	5	1
30T15kN INFILL	20	30	15	17	15.89	5	1
30T20kN INFILL	20	30	20	21	17.71	5	1

5.2.1 Double shear calculations

The double shear analysis conducted in Chapter 4 was carried forward and adapted to conduct the analysis on the infilled shear interface test schemes. Section 4.2.1 outlined the calculations used during testing and were adapted to develop an intimate understanding of the failure characteristics of the infilled double shear system.

5.3 Results for 20-tonne rock bolts, infilled double shear testing

5.3.1 Shear behaviour profile

Similar to the 20-tonne testing regime in Chapter 4, 20-tonne rock bolts were installed in the double shear system with varying levels of pretension applied including 0kN, 10kN, 15kN and 20kN. Unlike the tests conducted in Chapter 4, the following set of tests were conducted simulating a double shear environment with infilled discontinuities. As discussed in Chapter 3, a sandy clay material of 5mm thickness was selected to replicate infilled joints. Apart from the addition of the infilled joints, samples were set up and tested in an identical manner to that of the samples in Chapter 4, regarding pretension application, test system setup, test equipment, load application and data recording. Analysis of the shear response as a result of loading indicated a commonality in the rock bolts' failure characteristics. As a result, a shear behaviour profile was defined and can be described by three stages. Similar to the 20-tonne rock

bolts tested in Chapter 4, the shear behaviour profile of the 20-tonne rock bolts with infilled shear interfaces were defined as the elastic, strain-softening and failure regions as demonstrated in Figure 5.1.

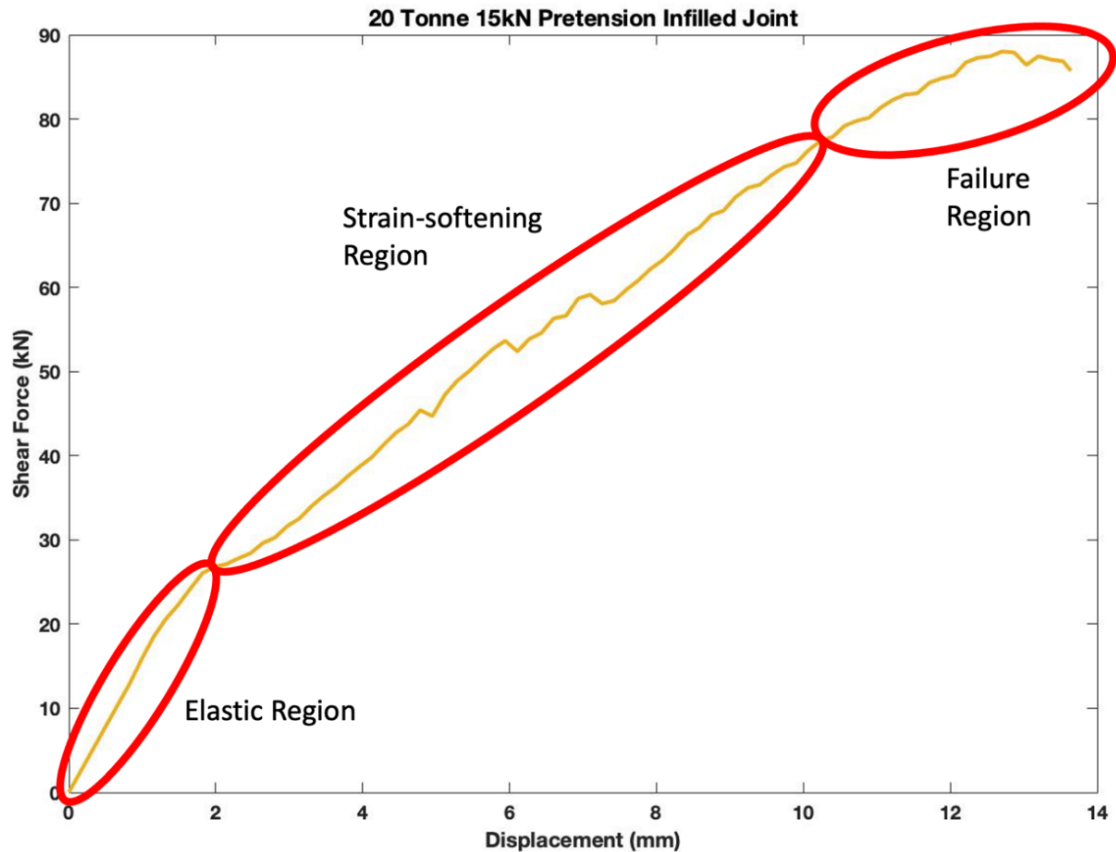


Figure 5.1: Example of the three failure regions for 20-tonne rock bolts with infilled shear interfaces.

The initial response to shear loading occurred within the elastic stage of the shear profile. The deformation occurring within this initial stage demonstrated elastic properties, resulting in the samples returning to their original state with no damage when the load was removed. Therefore, the rock bolts' response to loading within the elastic stage could be defined by the systems' modulus of elasticity. Continual loading resulted in the sample transitioning to the strain-softening stage. This stage was characterised by a reduced stiffness compared to that of the elastic stage and demonstrated physical indications of damage occurring within the sample as highlighted in Figure 5.2. The continual application of shear load within the strain-softening stage resulted in incremental increases in damage to the system. This increasing damage did not impact the rock bolts' stiffness throughout this stage and therefore the strain-softening stage could be represented by a constant stiffness value.

The damage can be seen in Figure 5.2, where each subsequent evidence of damage was more pronounced than the previous. The damage could be identified by the increasing intensity of the drops in recorded shear force, culminating in a drop of approximately 10kN. The sample was able to recover and continued to progress through the stage. As the rock bolt strands experienced increasing failures, the sample eventually transitioned into the final failure stage of the profile, which was characterised by a rapid reduction in the rock bolt's ability to resist the shearing forces.

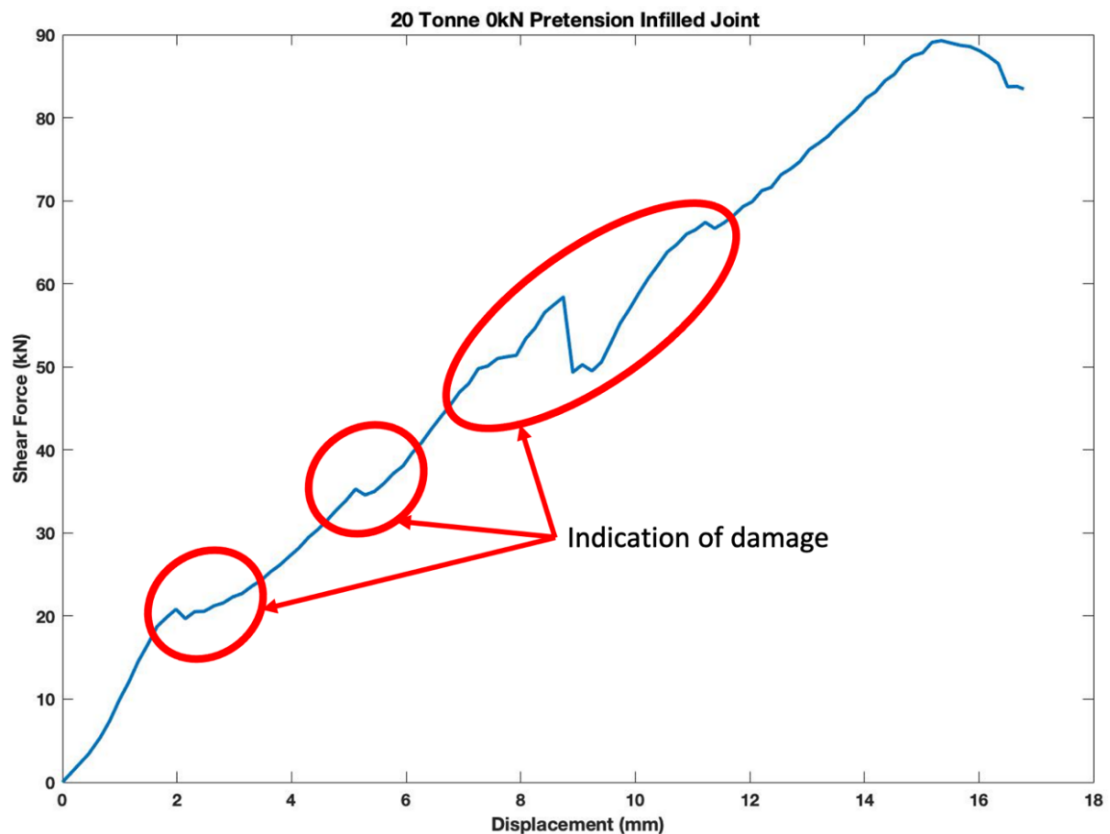


Figure 5.2: Indication of damage to sample during strain-softening stage for the 20-tonne double shear infilled sample

Unlike with the previous two stages, the final stage was identified by the incremental decrease in the rock bolts' stiffness response. Finally, the sample was no longer able to resist any shear forces and the rock bolt subsequently experienced total failure. The peak force recorded at failure represented the culmination of shear forces, interface friction and pretension confinement.

5.3.2 Pretension profile

As with the tests conducted in the clean shear interface scheme, the rock bolts were tested with initial pretensions of 0kN, 10kN, 15kN and 20kN. Additionally, to maintain consistency across the tests, the pretension application method was mirrored across all samples from both the clean interface and infilled interface testing schemes and utilised identical hardware. During testing the pretension was monitored using a load cell orientated to record axial forces along the rock bolt element and recorded with a complementing data acquisition system. The subsequent results were a representation of the shear forces as they transform to axial forces throughout the shearing process. The addition of infilled shear interfaces significantly altered the physical shear properties and added complexities to the shear interfaces, therefore altering how the applied shear forces transformed to axial forces. Unlike the clean shear system where the interfaces were in contact as one plane, the inclusion of the infilled material increased the spacing of the interfaces from 0mm to 5mm and altered the coefficient of friction of the interface. The coefficient of friction was now determined by the sandy clay infilled material as opposed to the host rock. Finally, the addition of the infilled material resulted in a doubling of the number of surfaces for each shear joint as each side of the infilled material was in contact with an interface. Like the clean shear scheme of Chapter 4, the transfer of shear force to axial force was a result of: failures within the grout, host rock and surface friction at the shear interface. However, for the infilled samples, the additional interfaces also influenced the transfer of shear force to axial force. The transformation of the shear forces through the host rock, grout and infilled material, in addition to the applied pretension, resulted in the infilled pretension profile illustrated in Figure 5.3. Throughout the shearing process it was identified that the rock bolts' axial performance could be defined by three zones. Zone one demonstrated a linear response of almost negligible increase in axial forces to the increasing displacement. This suggested that throughout zone one there was no transformation of shear forces to axial forces and as a result the axial force resembled that of the initially applied pretension. The failure of system materials at the shear interface was a key reason for the transfer from shear force to axial force. Therefore, the lack of increase of axial force in zone one indicated that no damage was experienced at the shear interface throughout the zone.

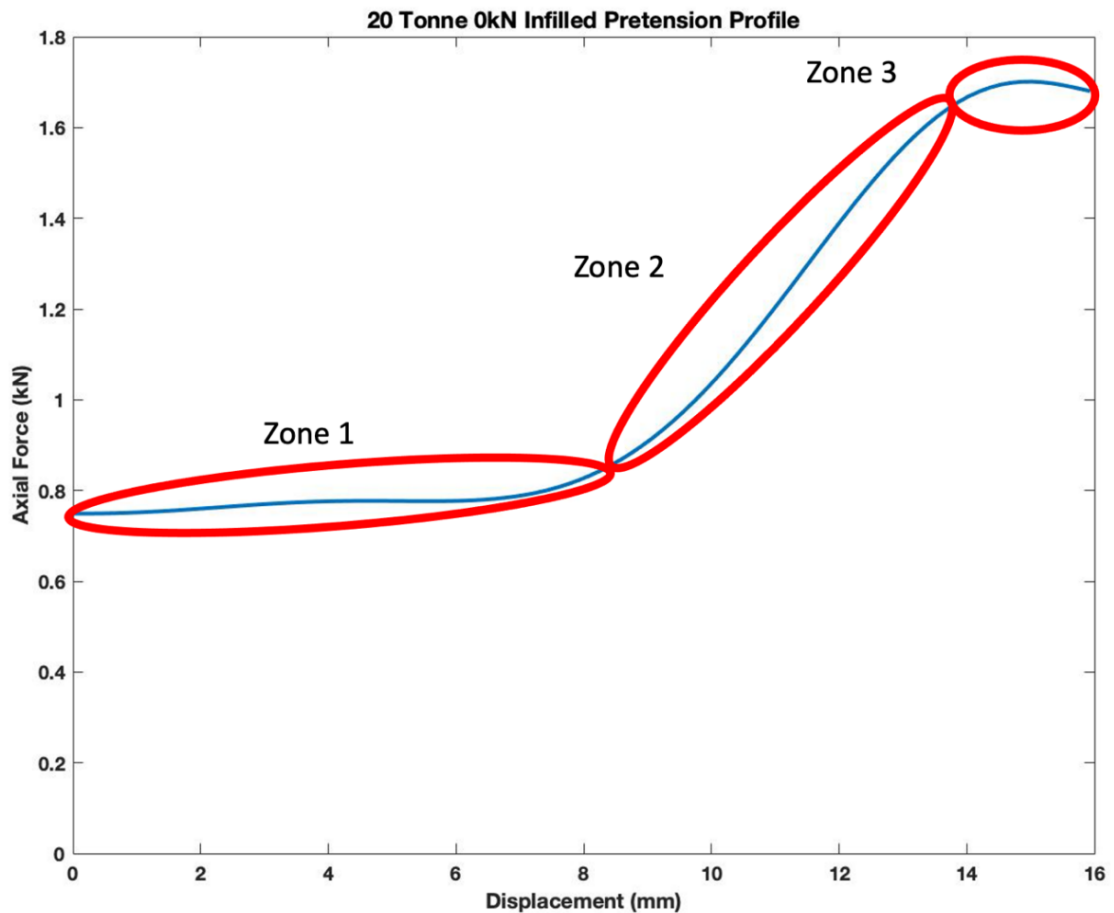


Figure 5.3: Example of pretension zones in axial force for 20-tonne infilled rock bolt with 0kN pretension

As with zone one, zone two was also represented by a linear curve profile, however, unlike with zone one, the rock bolt recorded a significant increase in axial force. The increase in axial force from the initial pretension value of 0.75kN to approximately 1.6kN indicated that the process of shear force to axial force transformation was in progress. It was therefore inferred that damage at the interface to either the grout, host rock and/or infilled material had commenced. As the axial force increased throughout zone two with no significant spikes or dips to the recorded value, it could be assumed that there was no change to the physical integrity of the rock bolt. Zone three was the final zone of the pretension profile and was initially defined by a lack of axial force increase, zone three continued as the axial force declined. This was the result of the rock bolt no longer able to withstand increasing axial forces, indicating that the force transfer path from shear to axial had been severed, suggesting the rock bolt had experienced rupture. The axial force profile categorised by zone three ultimately is a representation of rock bolt failure throughout the axial plane.

Throughout the completion of the 20-tonne infilled testing scheme the rock bolts' axial performance trends were identified to be a result of applied pretension. With the exception of the 0kN pretension sample, all other pretensioned samples recorded peak axial forces of approximately 19kN and within 1kN of each other, as shown in Figure 5.4. This suggests that although the 20-tonne rock bolts were pretensioned differently, they recorded similar peak forces. It is speculated that the 0kN sample did not achieve the same peak axial force due to the inherent differences during installation. Unlike the 10kN, 15kN and 20kN samples, the 0kN pretension sample had no initial tensioning as the sample was grouted with the rock bolt free floating as no nut installed. This was in contrast to the other samples, where their installation process required the nuts and washers to be installed and set to the required pretensions prior to grouting. This allowed the grout to set around a uniformly tensioned rock bolt. Unlike with the peak axial forces, there were incremental changes to the corresponding displacement values, highlighted in Figure 5.4. Samples with lower initial pretensions recorded peak axial forces at higher displacements, such as approximately 15mm for the 0kN pretension sample in comparison to the 10kN sample recording a displacement of 14.5mm. The displacement value continued to decrease, with the 20kN sample recording the lowest displacement of 9.5mm.

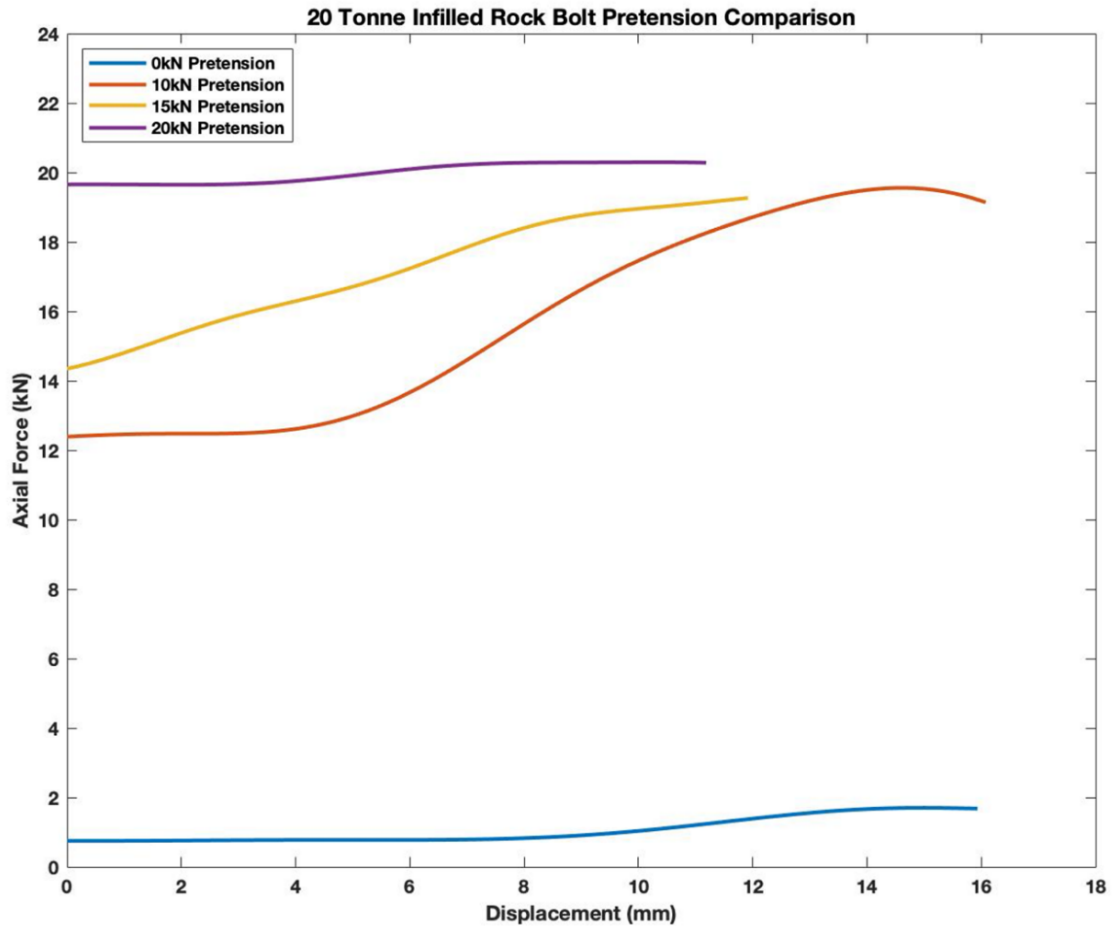


Figure 5.4: Comparison of 20-tonne infilled pretension axial force results

5.3.3 Impact of pretension on shear strength

Apart from the 20-tonne with 10kN pretension sample, the application of pretension had consistent impacts on several key properties of the 20-tonne infilled shear failure profile including the: peak shear force, failure displacement, elastic stiffness, and strain-softening stiffness. Increasing the initial pretension from 15kN to 20kN led to an increase in the shear resistance of the rock bolts by approximately 6kN, resulting in a peak shear force of 94.2kN. However, the increase in shear response was not observed until the highest initial pretension sample of 20kN, shown in Figure 5.5. Samples with the lower pretension values of 0kN and 15kN both recorded almost identical peak shear forces with a difference of 0.9kN. The 0kN pretension sample achieved a peak shear force of 89.3kN and the 15kN pretension sample achieved 87.9kN as shown in Table 5-2. The increase in pretension impacted the entire system as the axial forces were transferred by the grout interface, rock bolt nut and washer to the host materials. The inclusion of the sandy clay infilled material inhibited the

transfer of forces to the central block like a cushion and reduced the coefficient of friction between the interfaces. Therefore, increasing the pretension of the samples facilitated efficient transformation of shear forces to axial forces resulting in higher recorded peak shear forces at higher initial pretensions. The 0kN pretension 20-tonne sample however, did not follow to the same shear behaviours of the other samples and as a result recorded the highest peak shear value of 99.6kN, 5.4kN higher than the 94.2kN of the rock bolt with a pretension of 20kN, as shown in Figure 5.5 and Table 5-2. Unfortunately, due to time constraints, additional samples could not be manufactured to confirm the anomaly.

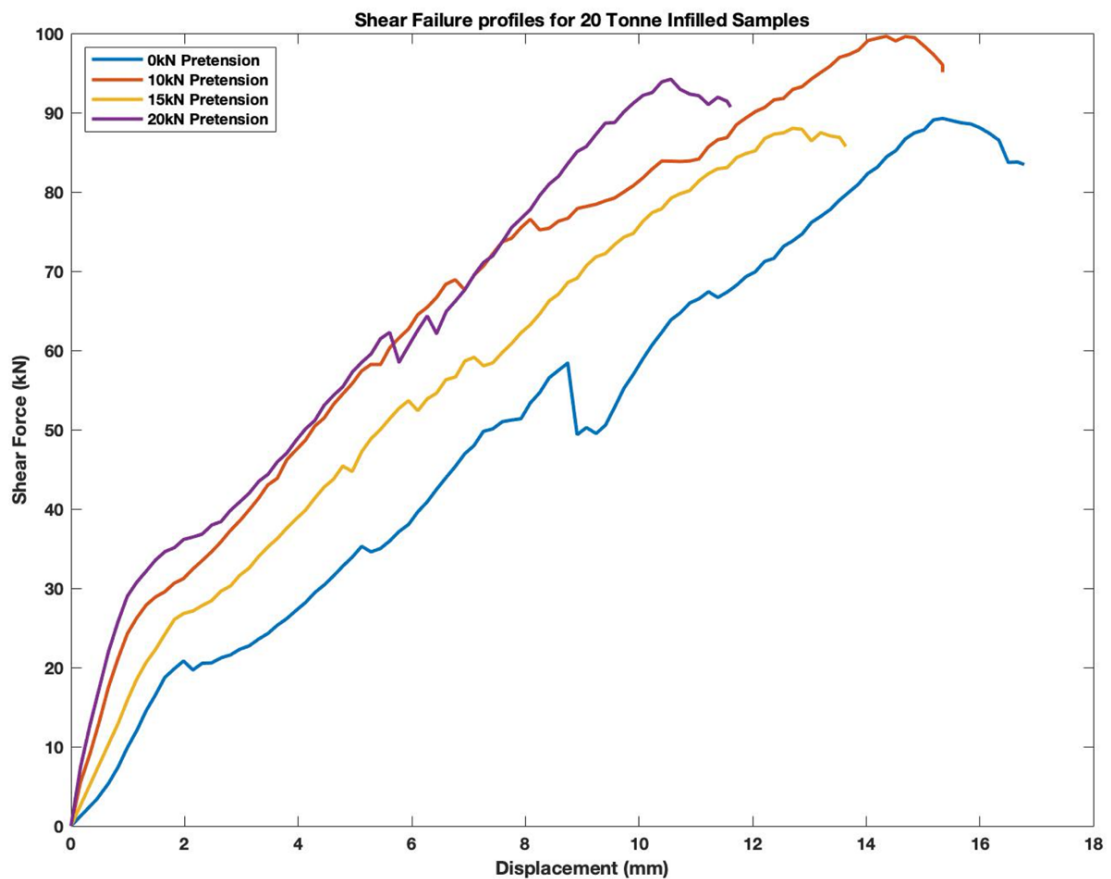


Figure 5.5: Shear force and displacement comparison of all 20-tonne infilled samples

The shear displacement recorded for each of the 20-tonne infilled samples demonstrated a proportional relationship to the sample's initial pretension. Increasing the applied pretension resulted in the samples achieving their peak shear force at lower displacement values, as shown in Figure 5.5, while the sample with the lowest pretension recorded the greatest displacement. Each subsequent increase resulted in an

increasing reduction in the samples displacement response to shearing, where the difference between the 0kN and 10kN pretension samples was a reduction of 0.9mm. As the pretension further increased, the displacement decreased with pretensions of 10kN, 15kN and 20kN, by 1.5mm to 2.4mm. As a result, there was a total of approximately 5mm difference in the peak shear displacement values between the 0kN pretension sample and the 20kN pretension sample. Overall, the observed range of peak shear displacement, as outlined in Table 5-2, was between 15.3mm and 10.5mm for the 0kN and 20kN pretension samples respectively. This was in part due to the increase in confining pressures at each interface. The inclusion of the infilled material facilitated an increasingly effective transfer of the shear force from the loading ram to the shear plain interface. This meant that less energy was dissipated through points of supplementary failure, such as grout and host rock interface. As a result, the rock bolts were able to have a stiffer response throughout both the elastic and strain-softening regions as outlined in Table 5-2.

Table 5-2: 20-tonne Infilled rock bolts failure properties.

Rock Bolt	Failure Displacement (mm)	Peak Shear Force (kN)	Elastic Stiffness (kN/mm)	Strain-Softening Stiffness (kN/mm)	Hinge Point (°)
20T0kN INFILL	15.3	89.3	10.9	5.1	15
20T10kN INFILL	14.4	99.6	16.8	5.9	11
20T15kN INFILL	12.9	87.9	14.6	6.0	12
20T20kN INFILL	10.5	94.2	26.5	6.9	10

In addition to the impact of pretension on the rock bolts' shear profiles, the increasing of pretension also appeared to have an impact on the rock bolts' shear performance partway through the strain-softening region. The 20-tonne infilled samples recorded a disturbance to the shear force, represented by a sudden drop in the applied shear force as shown in Figure 5.5. The increases in pretension resulted in a significant reduction in both the intensity of the shear force dip and its duration across the displacement. During the testing of the 0kN pretension sample, the shear dip presented as a minor drop in force at a displacement of 2mm however, reappeared four times while also

changing its intensity until the final dip occurred at a displacement of approximately 11mm. The third dip presented as most significant with a change in force of 9kN occurring over a displacement of approximately 1.3mm as highlighted in Figure 5.6. Incrementally increasing the initial pretension significantly improved the shear profile of the rock bolts by reducing the impact of this phenomenon. Comparing the samples with pretensions of 0kN and 20kN, it was observed that the increased pretension had not only reduced the intensity of the spike, but also its duration. The 20kN pretension sample recorded a single dip of only 3.8kN over a displacement range of 1mm.

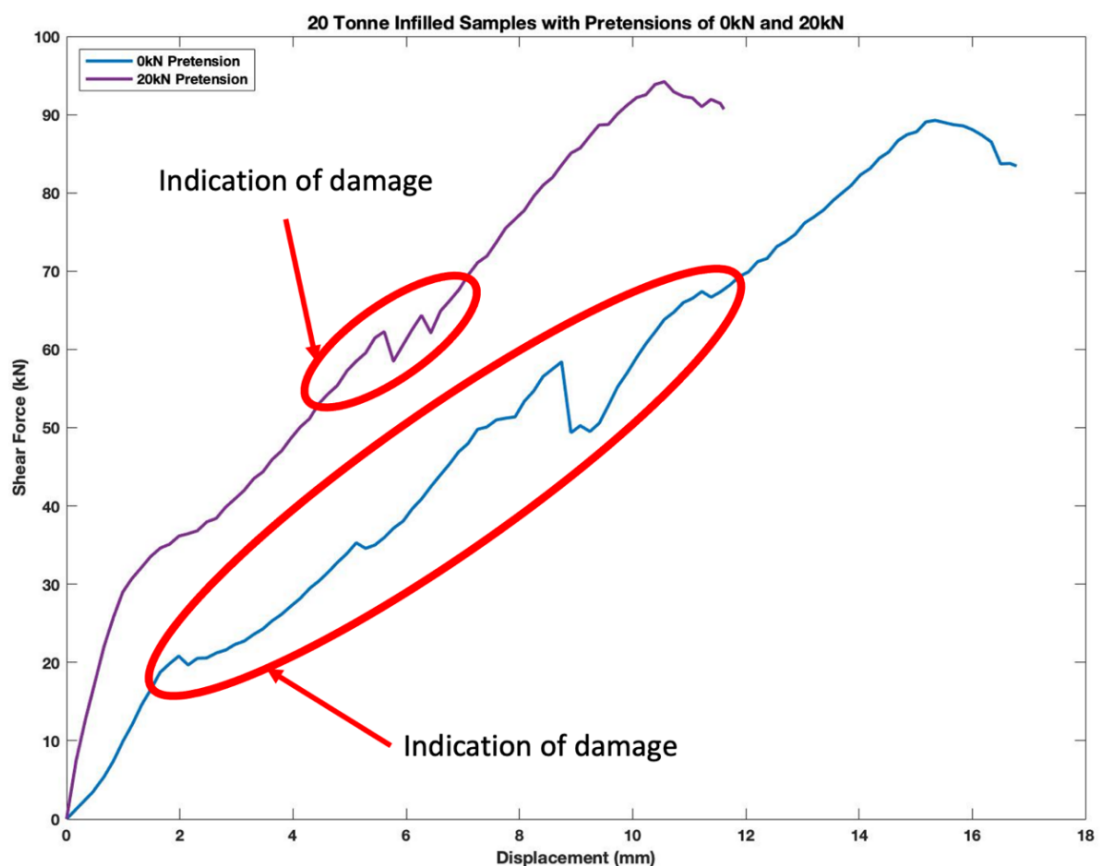


Figure 5.6: Change in recorded shear dip due to pretension increase from 0kN to 20kN for 20-tonne infilled rock bolts

5.3.4 Failure characteristics

Upon failure, samples were dismantled and analysed for any discernible issues that may have contributed to failure or were the result of the rock bolt failure. Areas of interest included the failure angle of the rock bolt known as the hinge point, damage to material interfaces in the vicinity of the rock bolt, damages to the shear surface and

structural damage within the rock bolt element. Observations were then compared across each 20-tonne infilled sample to determine the impact of pretension on the physical characteristics of the failed system.

The hinge point of each sample represented the bending experienced by the rock bolt at the shear interface. As shearing was induced, the rock bolt was bent about the shear plane at the boundaries of the grout and the host rock. The rock bolt did not bend about the infilled material as the sandy clay provided no additional strength to the system. Therefore, the amount of bending experienced was determined by the strength of the rock bolt to grout and grout to host rock interfaces. Figure 5.7 illustrates the imprint of the hinge point caused by the rock bolt. Figure 5.8 highlights the resultant hinge point on the rock bolt element.

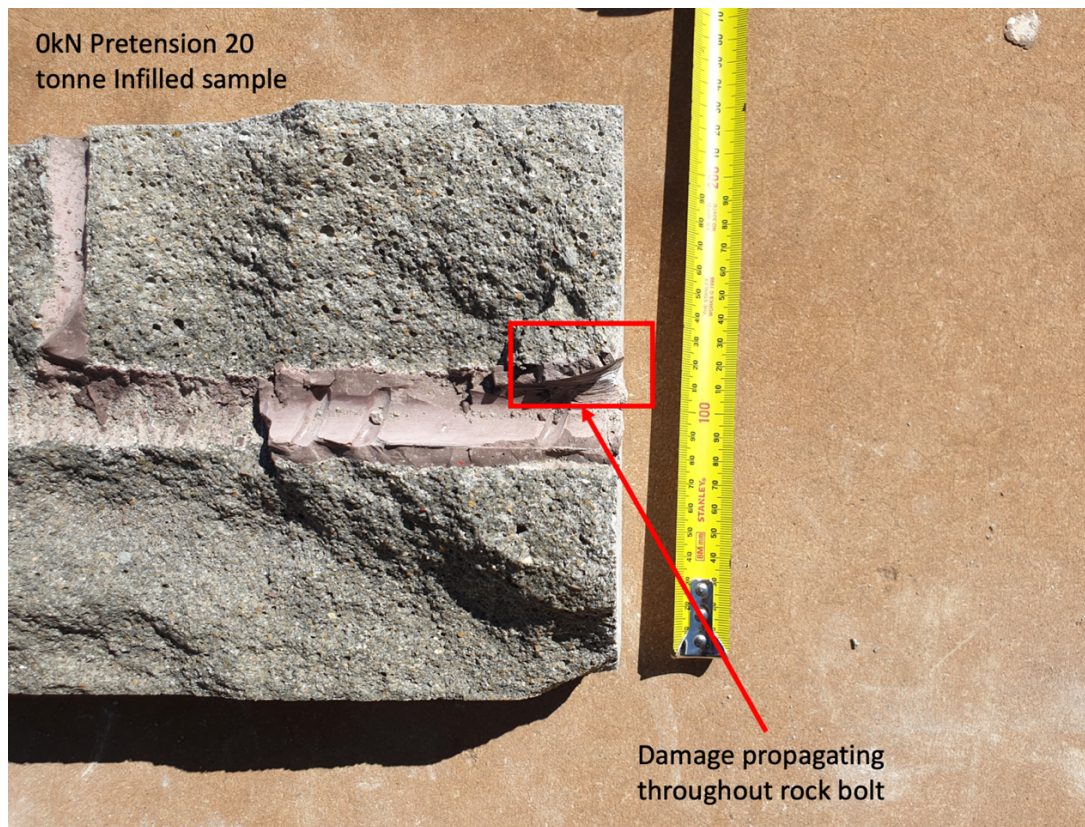


Figure 5.7: Angle of failure and damage to grout and host rock for 20-tonne 0kN pretension infilled rock bolt sample

With the application of pretension, additional confining pressures are added to the system materials and interfaces. Due to the compressive strength properties of the grout and host rock, the increase in pretension enabled these materials to withstand greater forces. The increase in pretension therefore reduced the bending at the hinge

point as failure of the system materials occurred in compression. Table 5-2 further highlighted this increase in strength as the 0kN sample recorded a 15° hinge point, while the 20kN samples experienced only 10°. It is noted that this reduction in hinge point bending was not uniform with the increase in pretension. Instead, the greatest change was experienced at 10kN. No significant change to the hinge point was observed when further increasing the pretension to 15kN, in fact the angle increased by approximately 1°. Finally, increasing the pretension to the highest setting of 20kN saw the lowest degree of hinge point bending. The sample achieved a decrease of approximately 17% from the 15kN sample and a 33% decrease from the 0kN sample. This decrease in the bending at the hinge point resulted in an increasingly direct shearing action on the rock bolt where less forces were dissipated throughout the system and therefore the system was increasingly performing closer to a perfect shear, as highlighted in Figure 5.9.

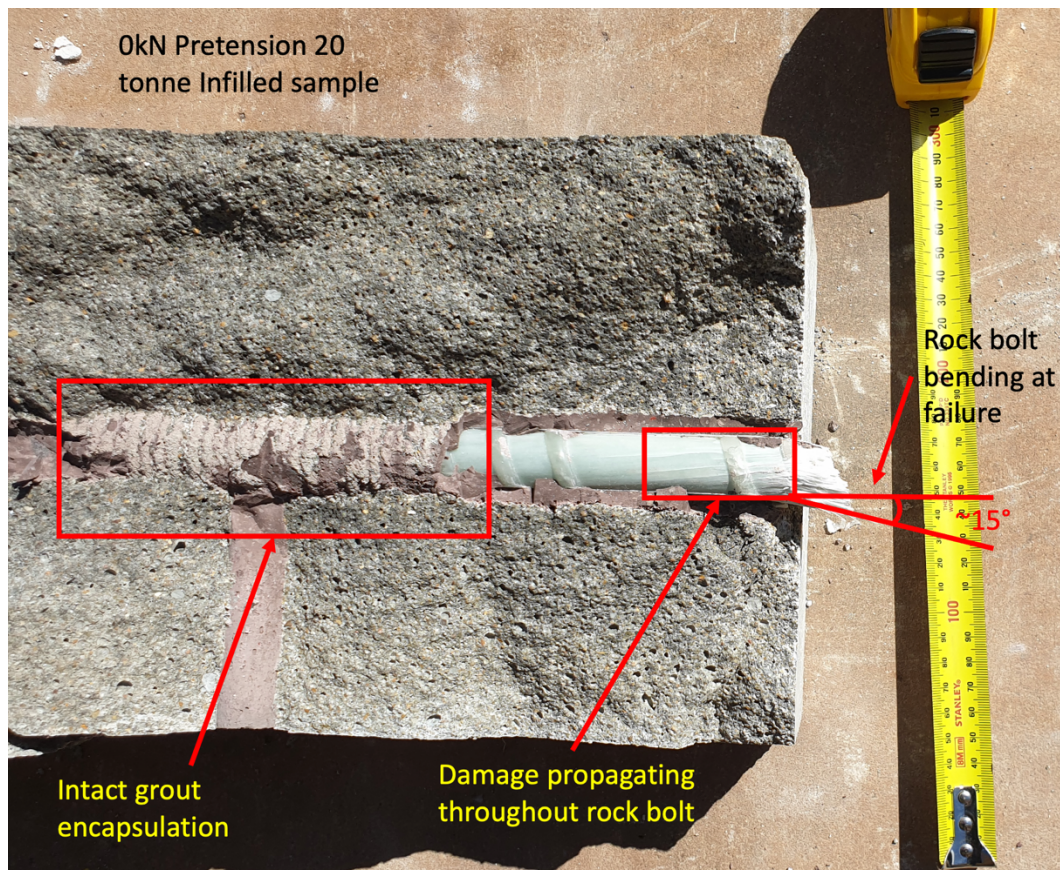


Figure 5.8: Angle of failure and rock bolt damage for 20-tonne 0kN pretension infilled rock bolt sample

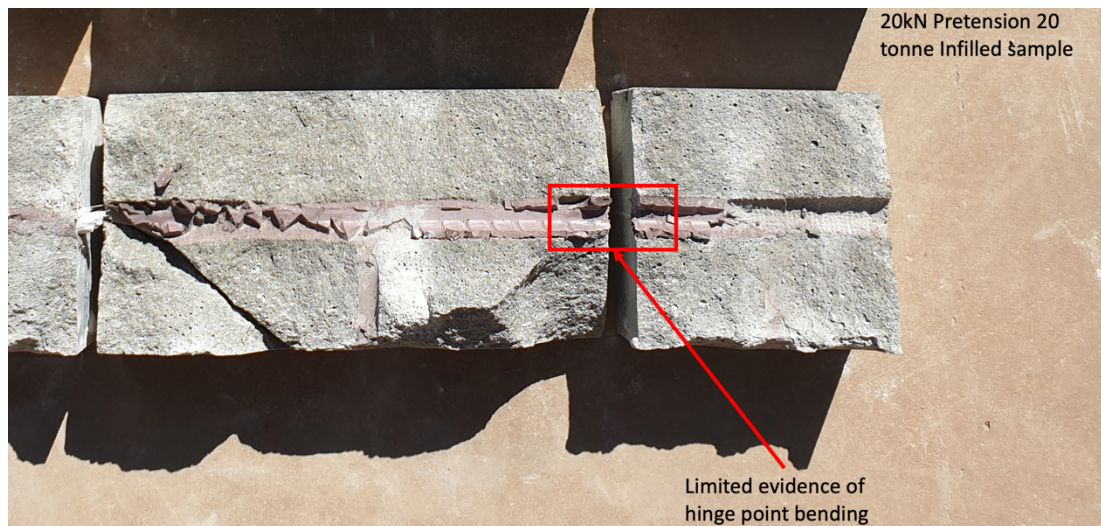


Figure 5.9: Limited evidence of bending at the hinge point for the infilled 20-tonne 20kN pretension sample

Further analysis of the samples also identified that the samples subjected to greater pretensions also suffered less damage propagating from the shear interface. When comparing the rock bolt subjected to 0kN pretension in Figure 5.8 and the 20kN pretension sample from Figure 5.10, the 20kN sample demonstrated significantly shorter fracture propagation away from the shear interface when compared to the 0kN sample. This supported the concept that increasing the pretension has a stiffening effect on the system.

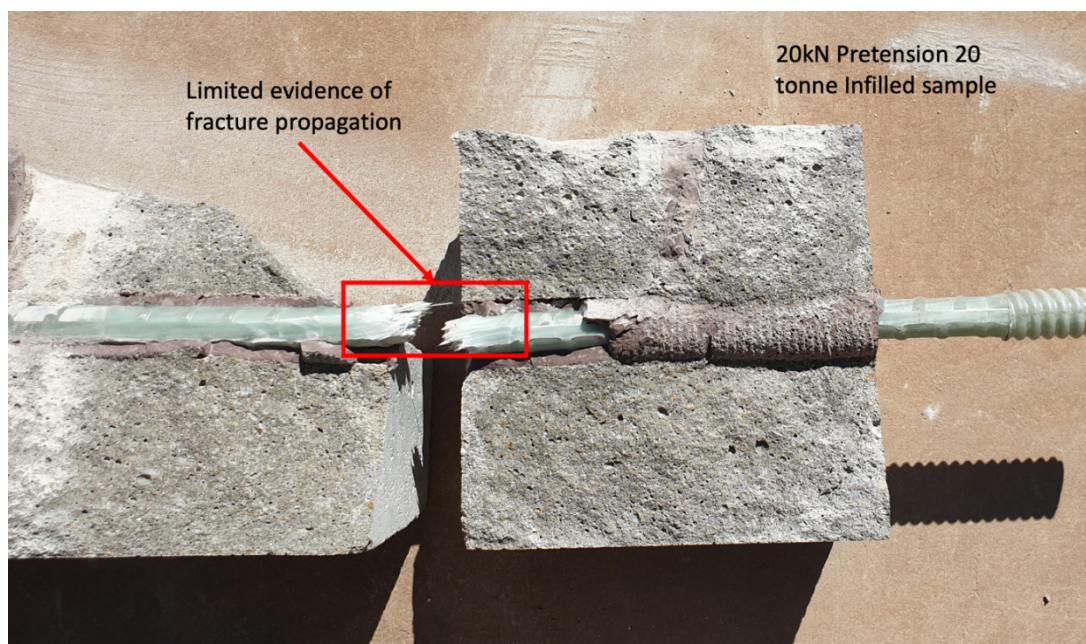


Figure 5.10: Infilled 20-tonne 20kN sample demonstrating limited fracture propagation along the rock bolt element

The addition of the infilled interface resulted in failure characteristics unique to samples subjected to the infilled testing scheme. The sandy clay material selected for the infilled interface was the weakest component of the shearing system and due to the lack of confinement, it could not take advantage of the strengthening effect of pretension. Instead, the infilled interface behaved as a lubricating and cushioning material. Throughout the shearing process, the infilled material was forced through the seams of the interface. Samples with higher pretensions generated enough force on the infilled material that there were limited areas remaining intact as highlighted in Figure 5.11. However, due to the disassembly process it was difficult to maintain the integrity of the infilled interface. As highlighted previously, the infilled interface provided a protective layer that prevented damage to the shear surface. Throughout the shearing process damage was subjected to the shear interface by both the formation of the hinge point as well as the splintering and final rupture of the rock bolt. With the inclusion of the sandy clay infill material, a sacrificial buffer zone was created. As the rock bolt strands failed, they came in contact with the infilled interface instead of the shear surface of the host rock. Infilled material was slowly removed preventing damage to the host material. Furthermore, as the sample failed completely, the lower coefficient of friction and the sacrificial nature of the infilled interface resulted in minimal damage to the host rocks' shear interface as the entire fractured edge of the rock bolt sheared past, highlighted in Figure 5.12.

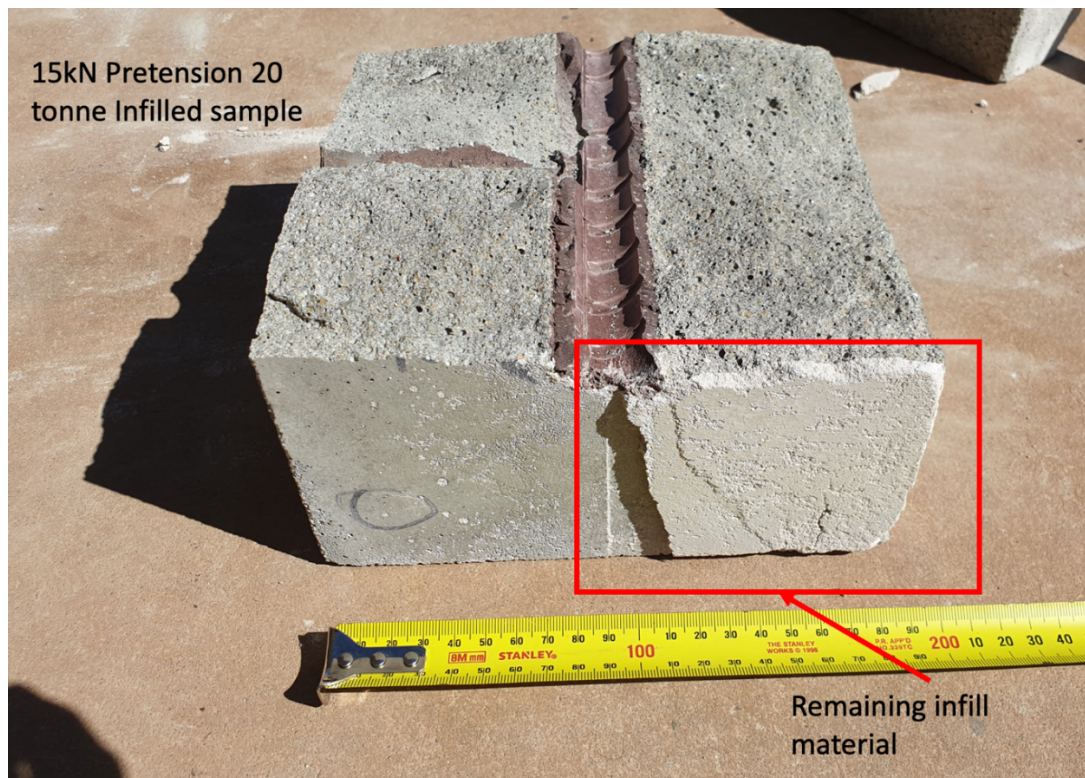


Figure 5.11: Infill material that remained after disassembly of the 15kN pretension infilled 20-tonne sample

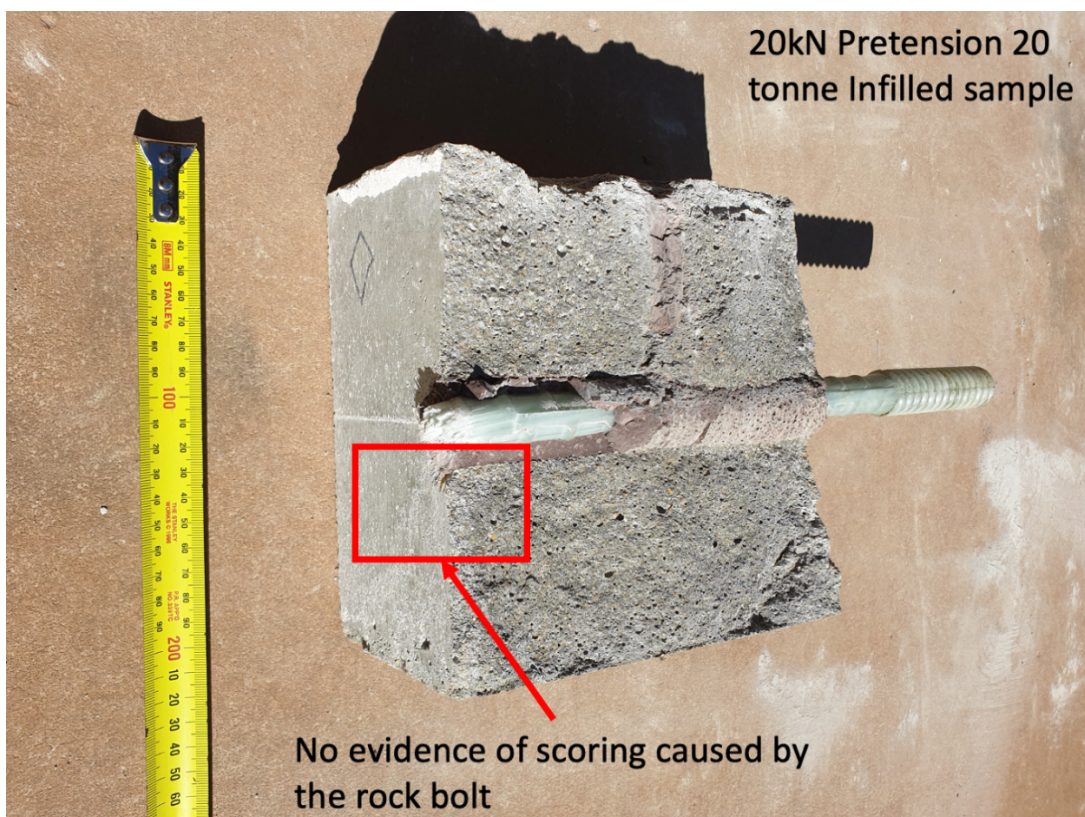


Figure 5.12: No evidence of scoring caused by dragging of the fractured rock bolt end on the 20-tonne 20kN infilled sample

5.4 Results for 30-tonne rock bolts, infilled double shear testing

5.4.1 Shear behaviour profile

Continuing with the infilled testing scheme, the 30-tonne rock bolts were tested at different pretension values with shear interfaces modified with a sandy clay infill. Mirroring the previous 20-tonne samples, the 30-tonne samples were testing with pretensions set to 0kN, 10kN, 15kN and 20kN. Shear was achieved through the application of constant displacement to the centre block. Forces were recorded using the same methods outlined in Chapter 4 section 4.3.1. It was identified that the sample's failure profile was comprised of the same three regions identified in the previous test schemes of Chapter 4 and Chapter 5 section 5.3.1, highlighted in Figure 5.13. The elastic region was characterised by a linear shear response to the increase in displacement and in all samples presented as the smallest region, spanning approximately 1.5mm to 2.5mm, representing 8% to 20% of the samples' total shear displacement. Additionally, the elastic region for each sample presented as the most consistent region with the least visible variations to the recorded shear forces, further reinforcing that minimal damage has been sustained to any of the systems' components. As damage started to present, the sample transitioned into the strain-softening region.

Strain-softening occurred when the sample recorded a reduction in the increase of the recorded shear force for a constant increase in displacement. The strain-softening range alternated as the largest and second largest region, however, there was minimal correlation with pretension. The transition from the elastic region to the strain-softening region was identified by an inflection in the shear response to displacement. The inflection suggested that the rock bolt initially experienced softening as little to no load increase was recorded over approximately 0.5mm, however, then transitioned to hardening before continuing as strain-softening, as outlined in Figure 5.14. The entire transition occurred over a displacement of approximately 1mm with the entire strain-softening range occupying from 36% to 52% of the shear displacement profile. The final region of each sample was the failure region, occurring when components of the system began to fail and were no longer able to withstand increasing shear forces. This region culminated in the complete failure of the rock bolt as indicated by the sudden significant drop in the recorded shear force.

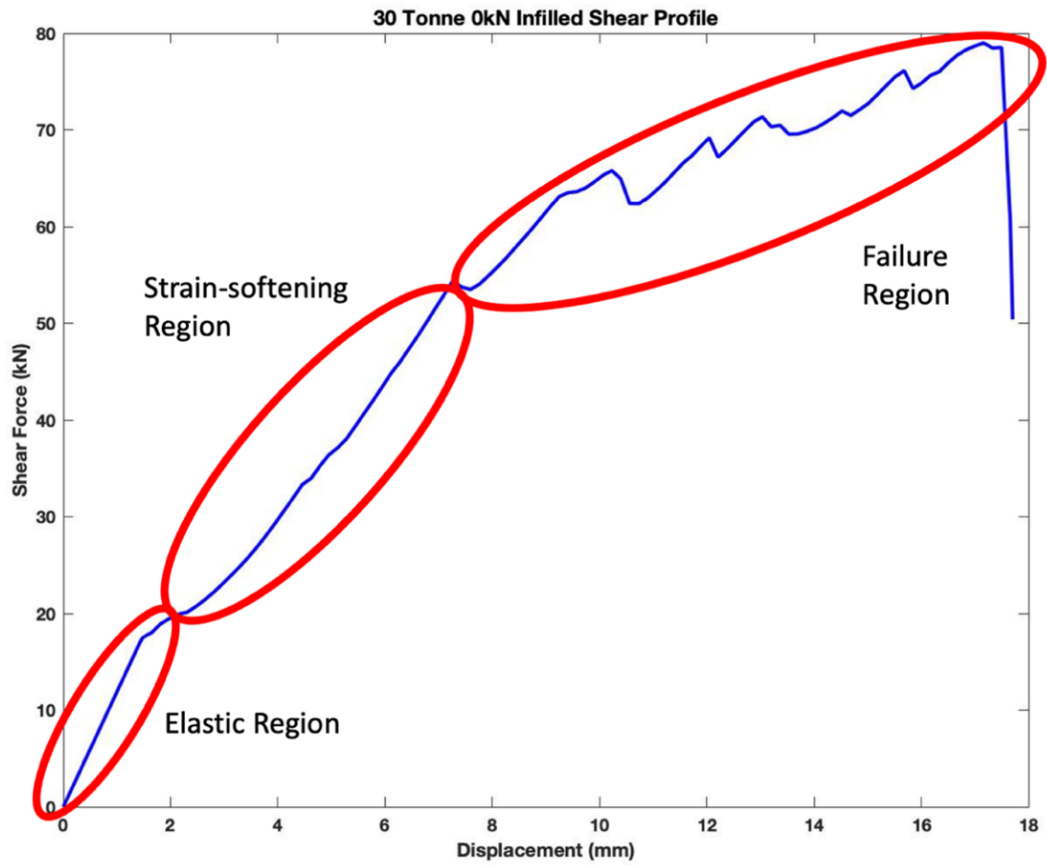


Figure 5.13: Example of the failure regions for the 30-tonne infilled rock bolt with a pretension of 0kN

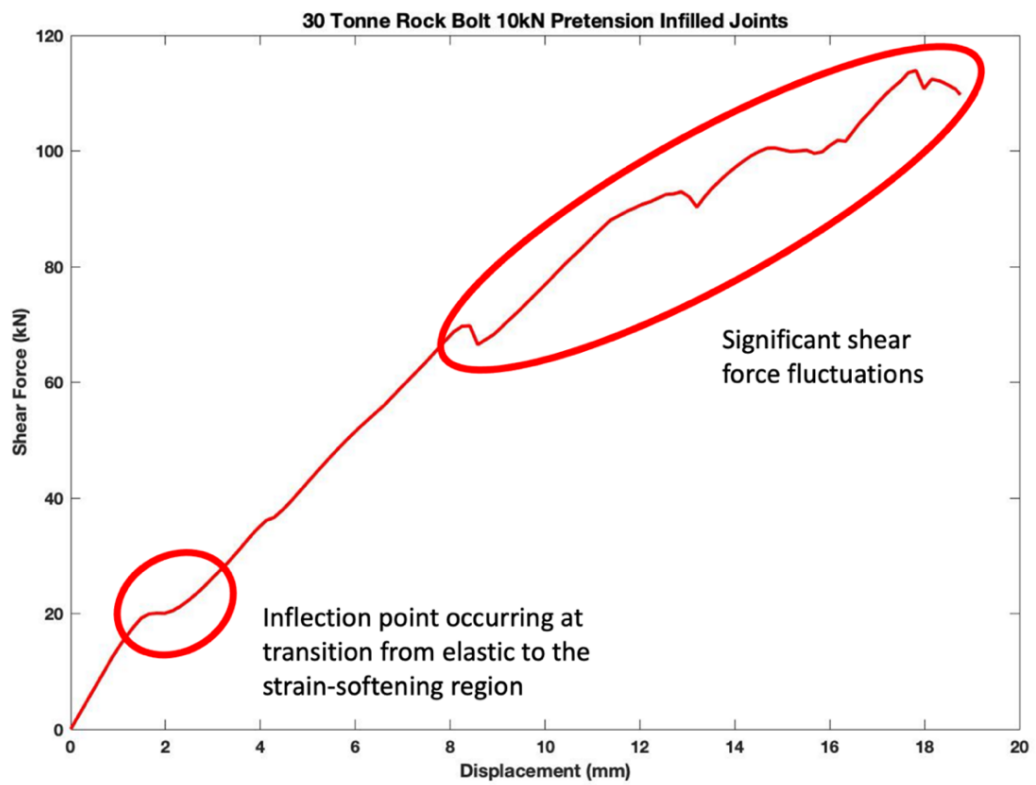


Figure 5.14: Example of the inflection and fluctuations in shear force for the 30-tonne sample with 10kN pretension

The failure of the rock bolt did not occur as a single event and was in fact foreshadowed by a series of comparatively minor failures as indicated by the series of dips in the recorded shear forces throughout the failure region in Figure 5.14. The failure region presented across approximately 20% to 63% of the total displacement of the tests. These failures represented damage sustained to various elements within the system such as to the grout, grout interface, host rock, rock interface as well as some strand failure within the rock bolt element. As these failures occurred, the forces were transferred to the remaining intact components represented by periodic smoothening of the curve. However, as the number of intact components decreased, this caused increasing stress concentrations that eventually resulted in the cascading failure of the system.

5.4.2 Pretension profile

Similar to the analysis conducted on the shear curve profile, the axial forces were recorded for each test to determine the pretension profile for the 30-tonne rock bolt samples with infilled joints.

Axial forces increased due to the shear forces interacting with the system components such as the concrete and the grout. These interactions resulted in a portion of the applied forces being converted to axial forces. The recorded axial forces were analysed to determine the pretension profile for the 30-tonne rock bolts with infilled joints. Figure 5.15 highlights how the pretension profile was represented by three zones. The first zone represented a pre-failure state, where the shear system was able to resist against the applied shear force. The axial force throughout zone one remained unchanged and linear with increasing displacement which indicated that no component of the shear system had begun to fail and the shear forces remained unaltered. Zone one represented a small portion of the pretension profile with the transition to zone two occurring at approximately 22% of the total displacement. Zone two was the largest component of the axial profile covering approximately 55% of the total displacement of the sample. Unlike zone one, zone two was characterised by an increasing linear force response to displacement. This indicated that during zone two, the rock bolt began loading axially due to a conversion of the shear force, additionally, the linear increase in axial force suggested that the rate of conversion was constant. Zone three was the final zone of the pretension profile and occurred at the beginning of system failure. The transition was characterised by the recorded incline in axial

force reducing until a peak force was achieved. Once the sample achieved its peak value, the subsequent readings decreased for each change in displacement until the test reached completion.

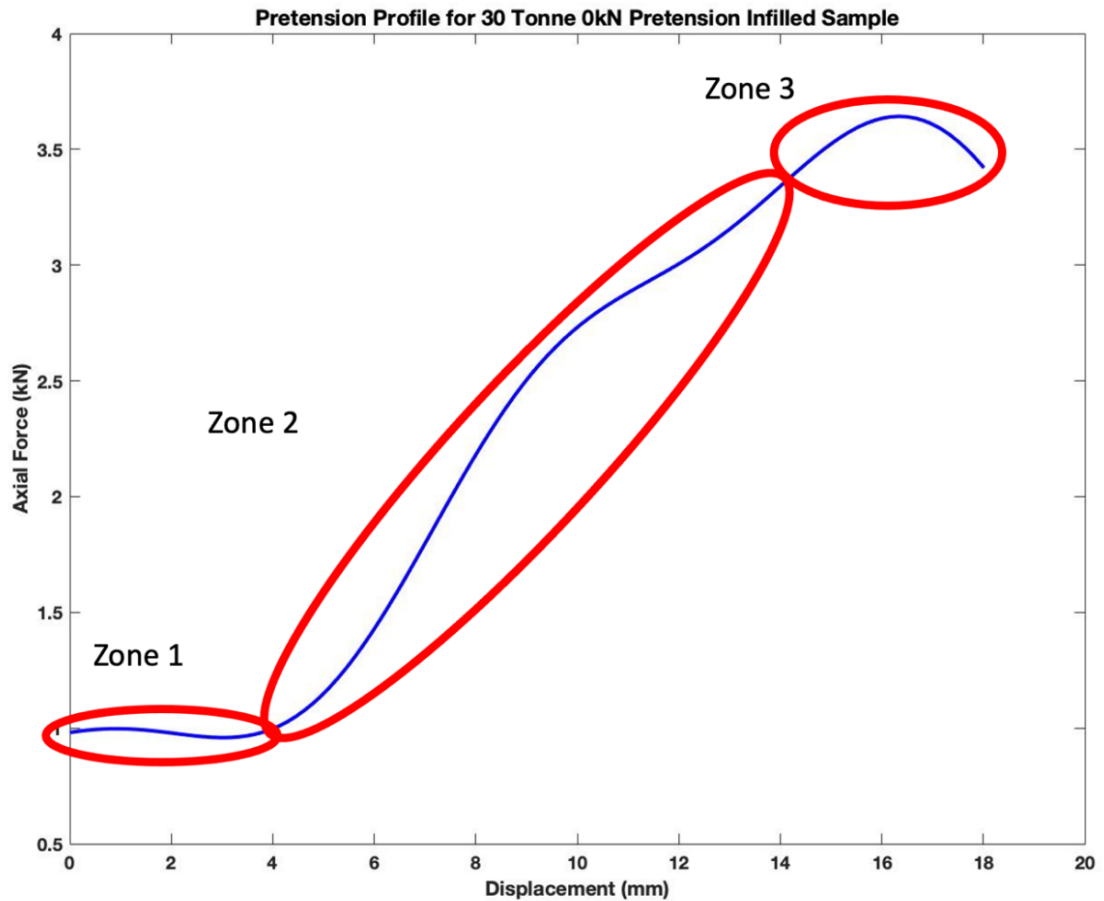


Figure 5.15: Illustration of the pretension profile zones for the 30-tonne 0kN pretension infilled sample

Samples were tested using pretension settings of 0kN, 10kN, 15kN and 20kN, allowing the determination of the 30-tonne rock bolts' axial force characteristics. Despite the changes to the initial pretension, the samples achieved peak values of approximately 2.6 and 3.6 times the initial reading. The 20kN pretension sample had an initial axial force of 17.7kN and a peak axial force of 44.3kN as can be seen in Figure 5.16, resulting in the peak force multiplier of approximately 2.6 times the initial value. Similarly, the 10kN sample also performed with an increase of 2.6 times the initial pretension value. The sample set to a pretension of 0.98kN failed with a peak axial force of 3.63kN, 3.6 times the initial pretension. The 15kN pretension sample on the other hand did not record any substantial increase in axial force from the initial

pretension value. Unfortunately, there was insufficient time and resources to repeat the test. The load cell did not present with any damage or faults, so it was suspected to be an issue with the tested sample. All samples, except the 15kN pretension sample performed with similar behaviours when analysing their profiles. Despite differences in the recorded axial forces, each sample transitioned from each zone at similar displacements. All samples transitioned from zone one to zone two at a displacement of approximately 4mm. While transitioning at similar displacements, the transition from zone two to zone three was achieved at increasing displacements for samples with higher pretensions. It can be seen in Figure 5.16 that the transition to zone three occurred at approximately 14mm, 15mm and 16mm for the samples with pretensions of 0kN, 10kN and 20kN respectively. Like the transition from zone two to three, each increase in pretension from 0kN to 10kN and finally to 20kN resulted in an increase in displacement where each sample achieved peak axial force at 16.5mm, 17.3mm and 18.6 respectively.

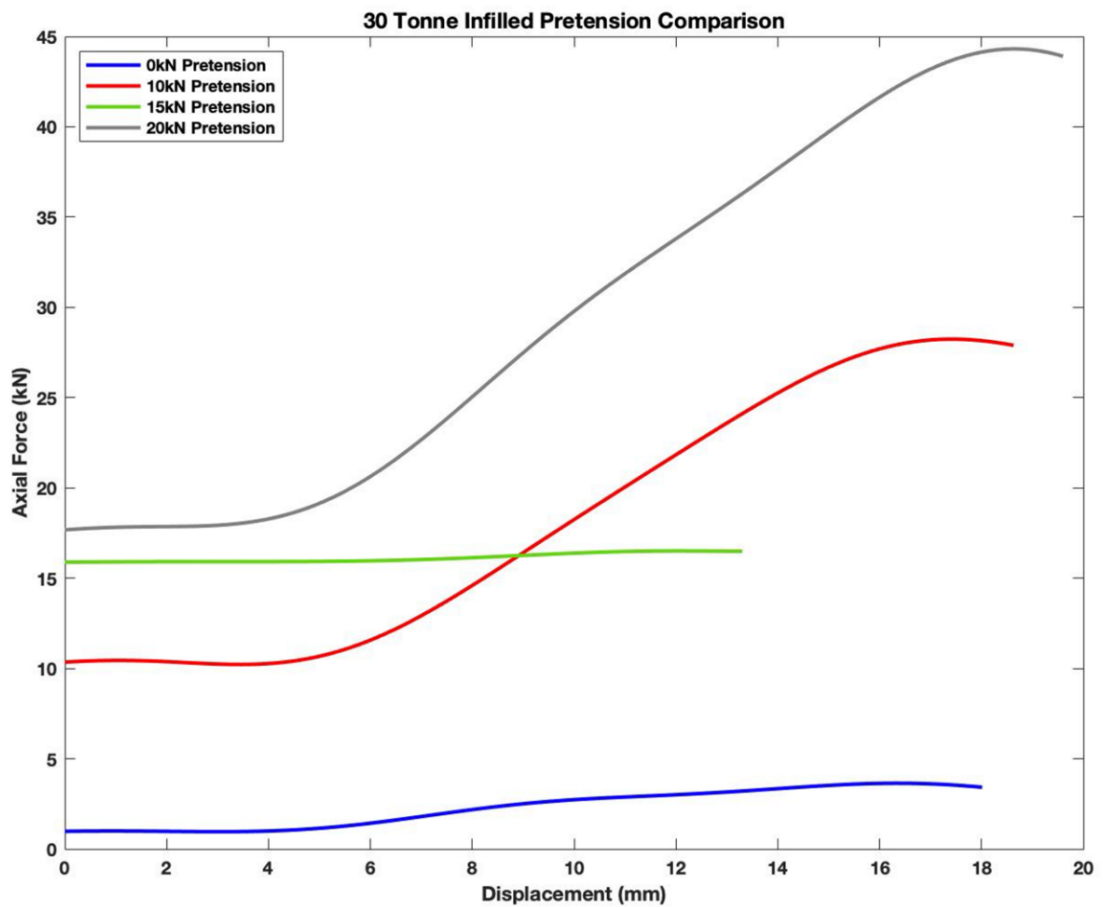


Figure 5.16: 30-tonne rock bolt infilled pretension profile comparison

5.4.3 Impact of pretension on shear strength

In addition to the development of the pretension profile, it was clear that the applied pretension also impacted the overall shear performance of the rock bolts. The impact of pretension was most prominent with two key properties: the peak shear force and the displacement at peak shear force. By testing samples at a range of pretensions it was identified that increasing the initial pretension of the sample increased the maximum shear force the sample was able to withstand prior to failure. Figure 5.17 highlights how the sample with a pretension of 0kN achieved a peak shear force of approximately 79kN, while the samples with a pretension of 10kN and 20kN reached shear forces of approximately 114kN. The 15kN sample however, did not perform as expected with its recorded shear force only reaching approximately 68kN. This was more than 10kN less than the 0kN sample and approximately 46kN less than the other samples. The disparity in the results indicated that there may have been an inherent issue with the 15kN sample. Similar to the effect pretension had on the shear force, samples demonstrated an increase in the recorded displacement at the recorded peak shear force. With the exception of the 15kN sample, the peak shear force displacement increased from 17.1mm to 17.8mm between the 0kN and 10kN samples respectively. Unlike the pretension phenomenon where the peak shear force presented with only one increase, there were continual increases in displacement for each set pretension, such that the 10kN and 20kN recorded an increase in displacement from 17.8mm to 18.3mm.

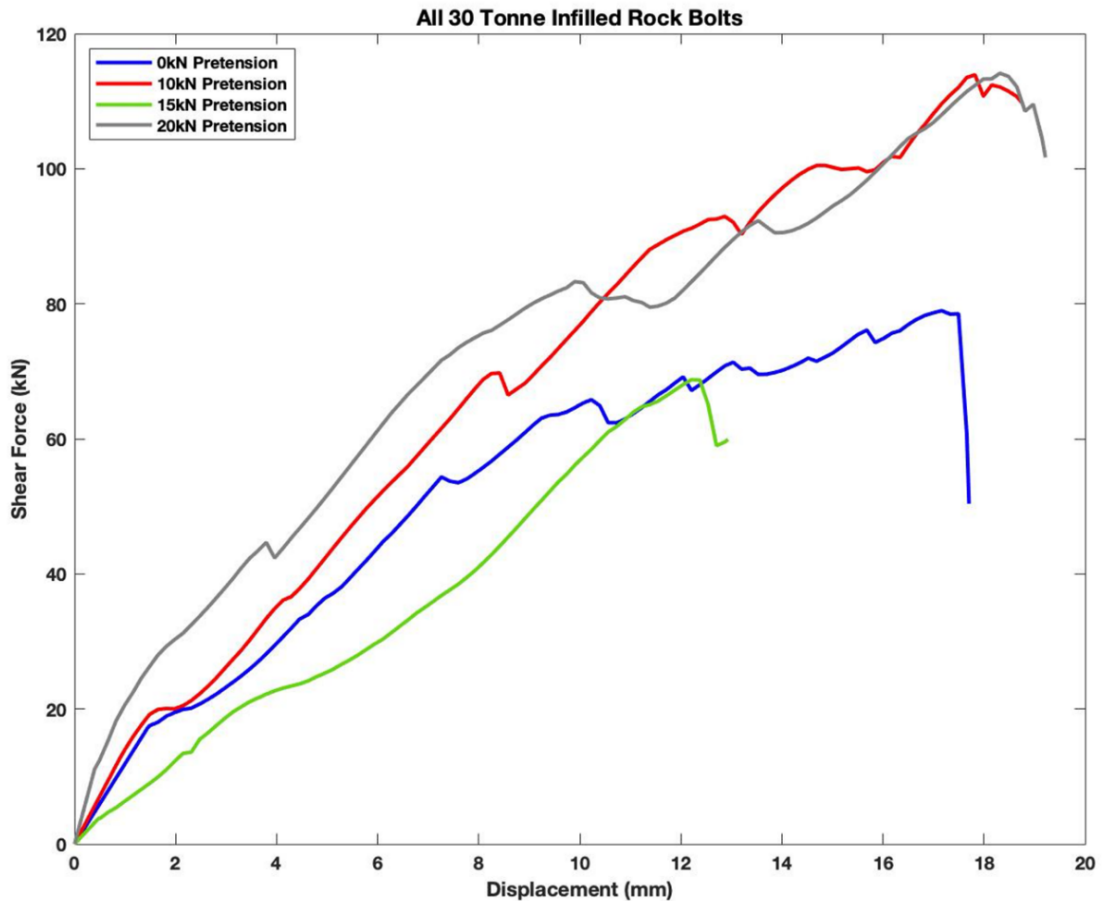


Figure 5.17: Impact of pretension on the overall shear performance of 30-tonne rock bolts with infilled shear interfaces

In addition to the pretensions' impact on the peak shear force and displacement, the pretension also impacted the way samples transitioned from the elastic region. As shown in Figure 5.18, the sample with the lowest initial pretension presented with an inflection in the shear force plot immediately after the end of the elastic region. Samples with the pretensions of 0kN, 10kN, and 15kN all demonstrated the shear force inflection response. The sample with the highest pretension however, did not demonstrate any shear force inflection at any point after the elastic region and continued to progress through to the next region. This was considered to be due to increased confinement pressure about the shear interfaces causing each component of the system to immediately resist the applied shear force. The inflection in the samples with lower pretensions suggested that there was less confinement forces at the shear interface. This was the consequence of the softer infilled material resulting in a portion of the shear curve flattening. As the displacement passed this inflection shear response and entered the next region, the recorded shear force resumed the typical behaviour as

observed with the other tested samples. All of the 30-tonne infilled samples except for the 20kN pretension sample presented with some degree of inflection at the elastic region transition, as evident in Figure 5.17. Therefore, it is suggested that a pretension of more than 15kN may be required to create a scenario where there is enough confinement on the rock bolt to facilitate a seamless transition from the elastic region. However, if the system design requires displacement flexibility to allow some displacement to occur without increasing the forces on the rock bolt, then a pretension of 15kN or less is recommended.

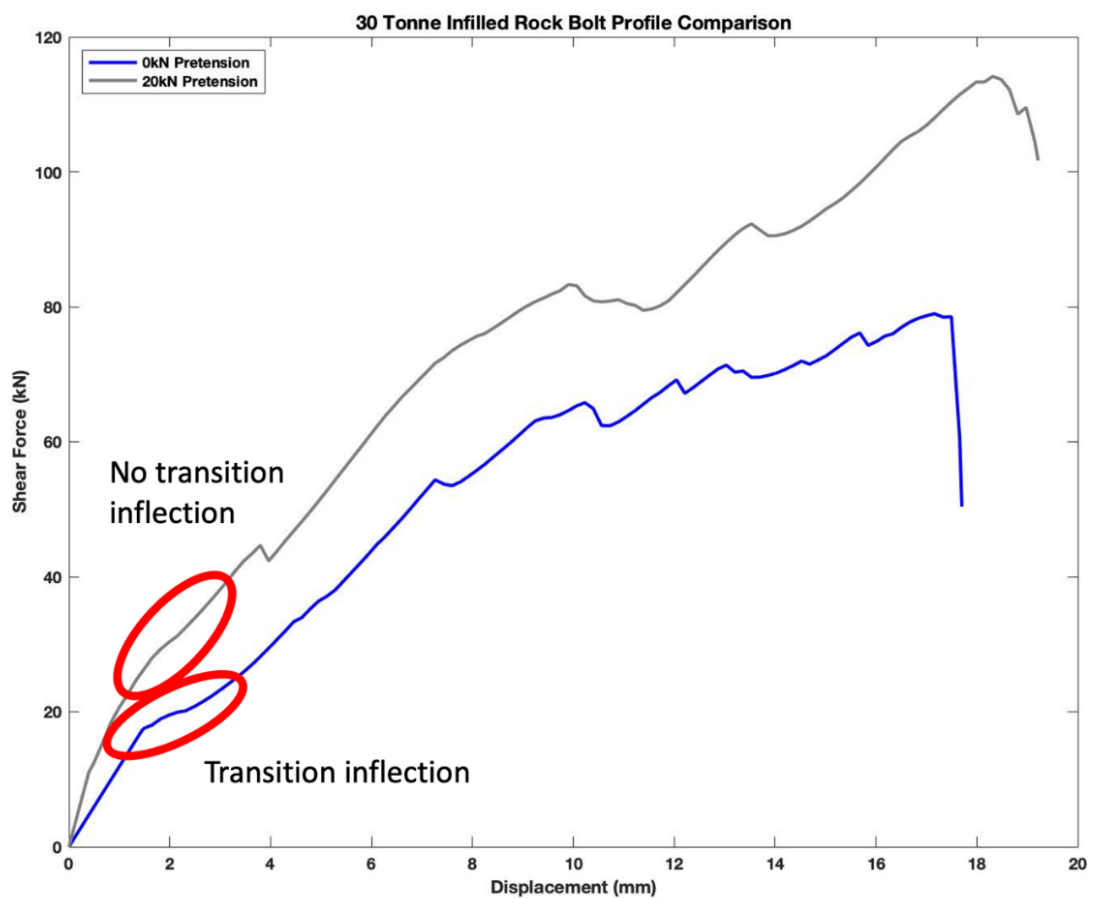


Figure 5.18: Impact of pretension on the elastic to strain-softening region for 30-tonne rock bolts tested with infilled shear joints

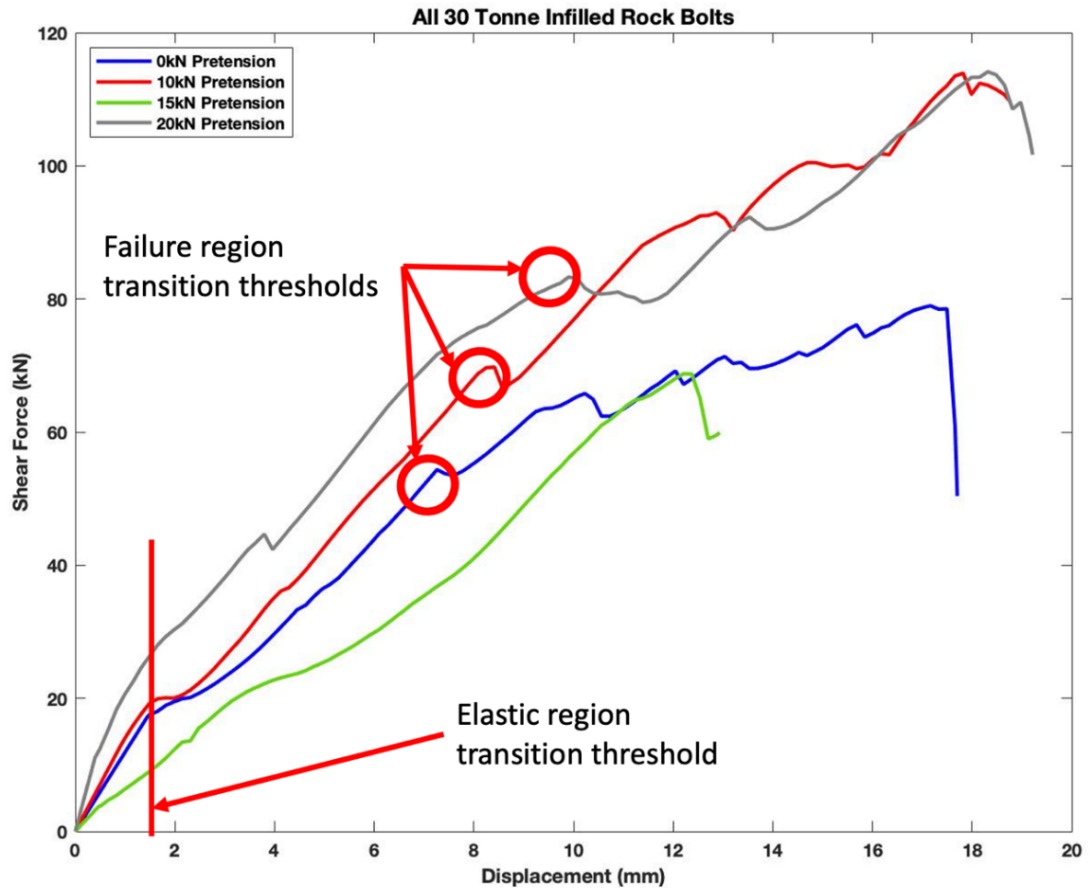


Figure 5.19: The effect of pretension on the elastic region transitions for the 30-tonne rock bolts with infilled joints.

The application of pretension also demonstrated unique properties regarding the location of the transition thresholds between each region. As shown in Figure 5.19 and with the exception of the 15kN pretension sample, all other samples demonstrated near identical displacement thresholds for the transition from the elastic region, despite differences in the type of transition present. As the 15kN sample failed to meet many of the other characteristics displayed by the other samples it is assumed that the sample did not represent a typical 15kN failure. Therefore, it was concluded that pretension had no impact on the transition threshold for the elastic region.

Conversely, analysing the transition to the failure region revealed that increasing the pretension resulted in an increase in both transition shear force and displacement. It was found that increasing the pretension from the 0kN sample to the 10kN sample resulted in an increase of 28% and 14% for the shear force and displacement respectively. Additionally, the increase from the 10kN pretension to the 20kN pretension saw increases of 20% for both the shear force and displacement. This

consistent increase in the transition threshold was indicative of gradual increases in the confinement pressures at the shear interface, where the greater the confinement pressures the more efficient the load transfer became.

5.4.4 Failure characteristics

Each sample was dismantled post failure to determine defining characteristics that were the result of the shearing process and shed light on the process of shearing. Like the previous samples tested with the infilled testing scheme, the samples were analysed for the following properties: hinge point, shear interface damage and rock bolt element damage. The utilisation of pretension resulted in recordable changes to the appearance of the hinge point. As the pretension increased, so did the angle of the hinge point from 9° to 11.5° for the 0kN and 10kN pretension samples respectively and then to 12° for the 20kN pretension sample. The 0kN and 20kN samples were displayed in Figure 5.20 and Figure 5.21, as they best highlighted the described changes to the hinge point. The incremental changes to the hinge point were due to the change in confinement pressures at the shear interfaces. When the pretension was increased, greater pressures were imparted to the shear surface, resulting in the bending of the rock bolt occurring over a shorter length of the bolt and therefore forming hinge points of greater angles. Another characteristic that was evidently altered by increasing the pretension was the extent to which damage propagated through the rock bolt away from the shear interface. With each increase in pretension, it was found that the extent of damage propagation decreased. The differences in damage propagation of the 20kN and 0kN pretension samples are highlighted in Figure 5.21 and Figure 5.22.

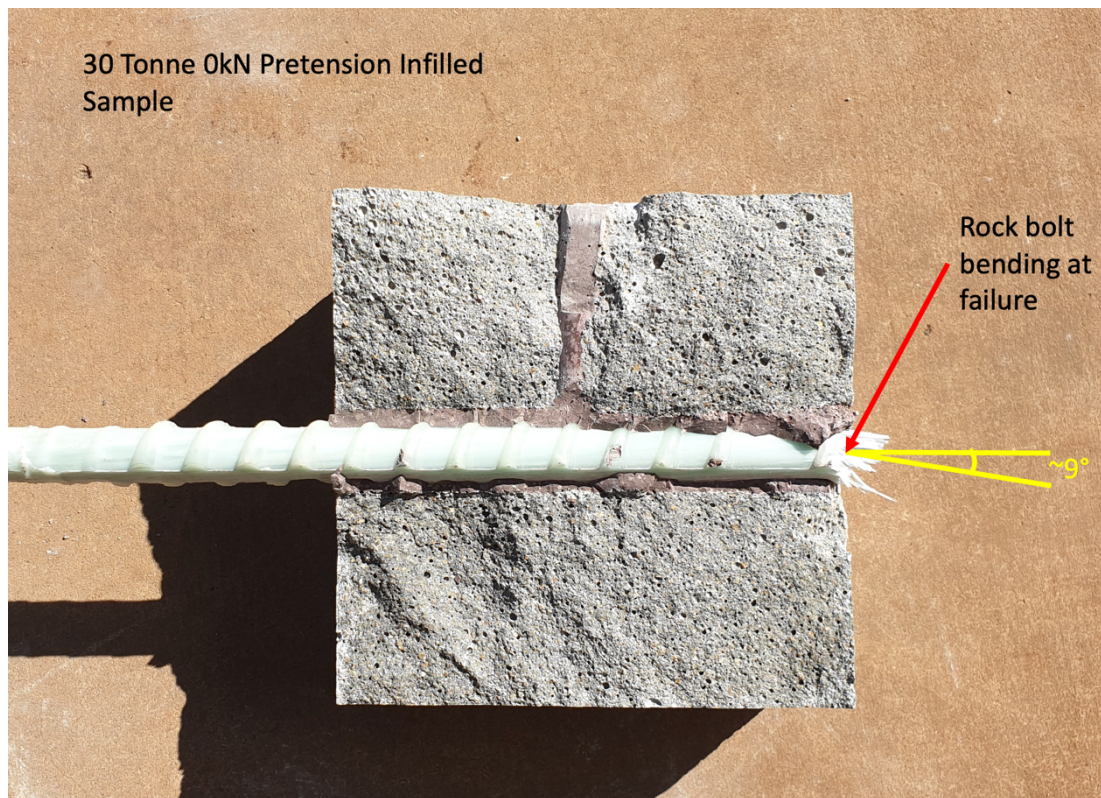


Figure 5.20: Angle of failure for 30-tonne rock bolt with 0kN pretension with infilled shear conditions

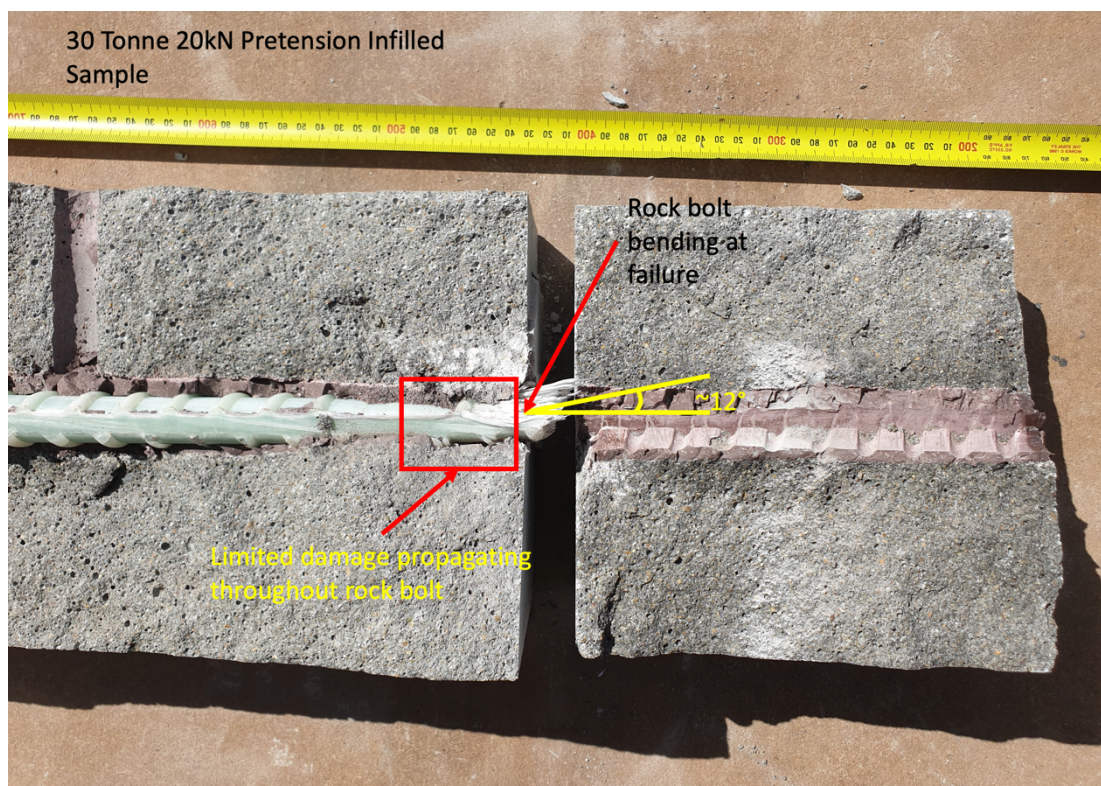


Figure 5.21: Angle of failure and damage propagation for 30-tonne rock bolt with 20kN pretension with infilled shear conditions



Figure 5.22: Damage propagating through element for 30-tonne rock bolt with 0kN pretension with infilled shear conditions

The presence of damage propagation was closely related to the bending experienced at the hinge point. Samples with smaller hinge point angles experienced greater damage propagation as opposed to samples with larger hinge point angles. The correlation with the hinge point and pretension was most likely due to the material properties of fibreglass. Fibreglass typically responds poorly to forces that induce bending, generally resulting in crack formations and fibre/resin delamination. This was evident in the tested samples where the increase in pretension reduced the length of the rock bolt that experienced bending. Additionally, increasing the pretension meant that the fibreglass experienced more direct shearing and therefore the internal strands were severed either at or close to the shear plane before there was a chance for cracks to propagate.

5.5 Comparison between 20-tonne and 30-tonne rock bolts

5.5.1 Shear behaviour profile

To understand the behaviour of the two rock bolts, the 20-tonne and 30-tonne rock bolts have been compared. Each aspect of the tested rock bolts, described in section 5.3 and section 5.4, have been analysed for their similarities and differences. For each rock bolt type, it was identified that their failure response to shearing occurred over

three regions: the elastic region, strain-softening region and finally the failure region. When analysing the shear profile for each rock bolt type as highlighted in Figure 5.23, it was evident that the 20-tonne and 30-tonne rock bolts with infilled shear discontinuities, presented with similar failure responses. The similarities in failure responses could be attributed in part to the similarities in the fibreglass properties of the two rock bolt types. As demonstrated in Figure 5.23 the samples exhibited similar shear profile characteristics such as the inflection present at the transition from the elastic region. However, the presence of the inflection was not mirrored for each rock bolt type. It was identified that the 30-tonne samples with a pretension of 20kN did not exhibit any inflection at the elastic transition. Figure 5.24 demonstrated that the 20-tonne samples retained the inflection properties from samples with lower pretensions. This indicated that the added strength of the 30-tonne rock bolt sample and the pretension of greater than 15kN may be required to overcome the shear interface weakness resulting from the infilled shear joints. In addition to the difference of the elastic region, compared samples also demonstrated differences regarding the displacement duration of the failure region. It was found that the 20-tonne infilled samples presented with a failure region occurring over a shorter displacement range when compared to the 30-tonne samples. Figure 5.24 highlighted that the 30-tonne rock bolt with a pretension of 20kN recorded a failure region over approximately 8.5mm as opposed to 2.5mm for the 20-tonne sample with the same pretension. The displacement ranges fluctuated across all samples, preventing clear correlation with pretension, although the 30-tonne samples recorded longer failure range displacements. Figure 5.23 also highlighted an increase of 2.2mm in the 30-tonne's failure displacement range compared to the 20-tonne's failure region when comparing samples with 10kN pretension. It was however evident that between the 20-tonne and 30-tonne samples the failure region commenced at similar displacements. The longer displacement range for the 30-tonne rock bolts may be attributed to the material properties of the rock bolt as well as the compressive strength of both the grout and the concrete. These components experienced increased shear forces due to the additional strength of the 30-tonne samples, resulting in greater forces being transferred over a longer duration before culminating in rock bolt failure.

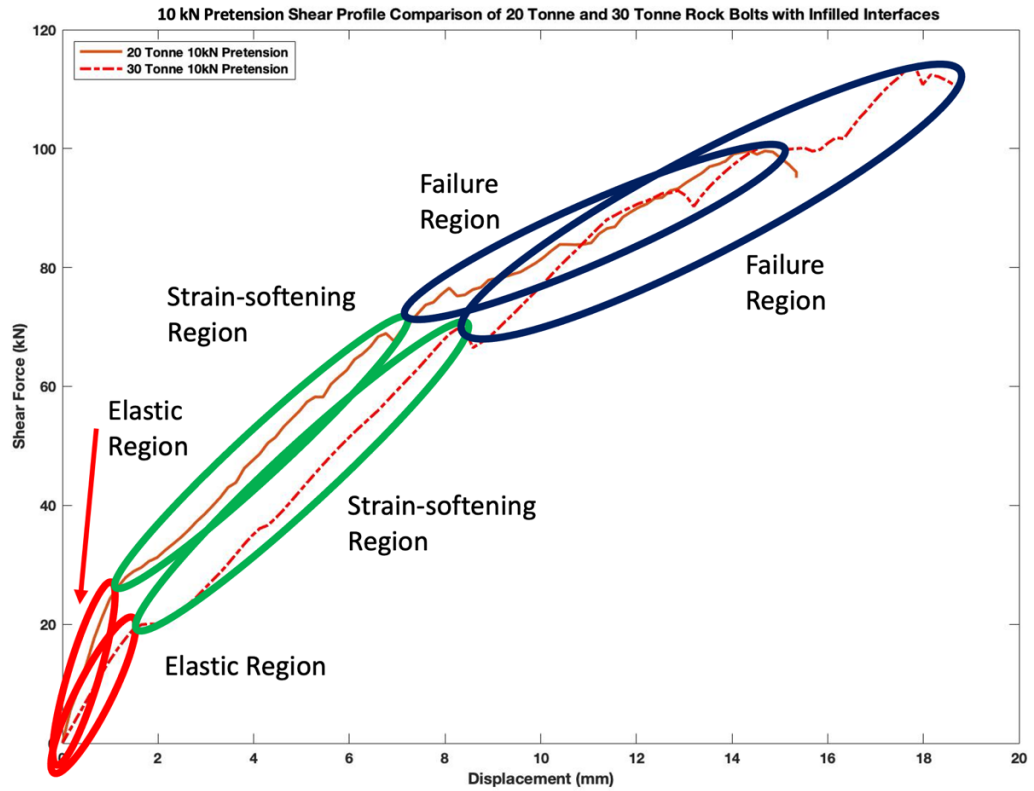


Figure 5.23: Shear profile comparison of 10kN pretension 20-tonne and 30-tonne rock bolts with infilled interfaces.

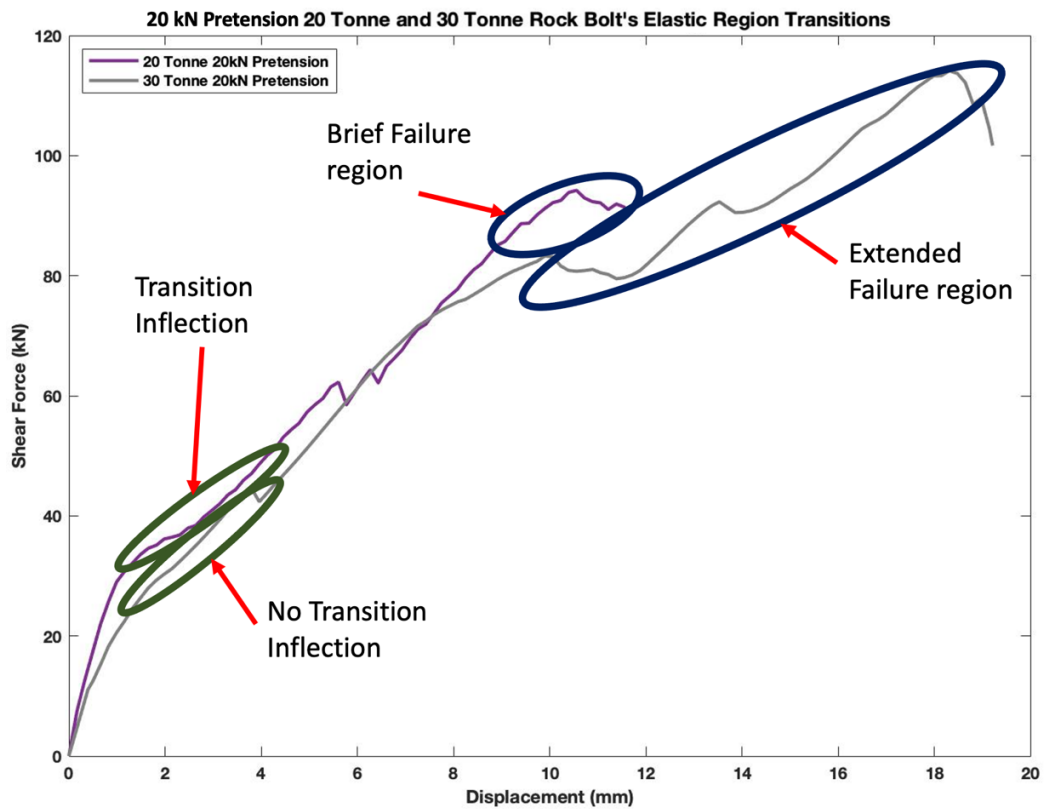


Figure 5.24: Comparison of the elastic region transition and the failure region of the 20kN pretension 20-tonne and 30-tonne rock bolts with infilled shear planes

Comparing the peak shear performance of each sample presented some similarities and differences on the rock bolts' responses to shear with infilled discontinuities. It was found that while the peak shear force values between the 20-tonne and 30-tonne samples varied, they were however, consistent. Both rock bolt types demonstrated no correlation between peak shear force and applied pretension, with the 20-tonne samples performing within a consistent range of 88kN to 100kN as shown in Table 5-3. The 30-tonne samples also showed no correlation between shear force and pretension, although the samples demonstrated significant shear force variability with a performance ranging from 69kN to 114kN. The lowest performing samples were the 0kN and 15kN pretension samples as shown in Table 5-3. This indicated that despite the shear forces transferring to axial forces during the shearing process, there was no mechanism for the reverse to occur. Additionally, pretension didn't indicate any shear strengthening properties.

Unlike with the shear force however, the 20-tonne samples demonstrated a clear correlation between the applied pretension and the peak failure displacements. As the pretension increased, the displacement at which failure occurred decreased incrementally. The initial 0kN sample failed at 15.3mm and the final 20kN sample failed at just 10.6mm as highlighted in Table 5-3. However, this trend was not evident with the 30-tonne sample. The 30-tonne samples showed no correlation between the initial pretension and the displacement at failure. Both the 0kN and 20kN samples failed within 1mm of each other and the 15kN sample presented as a potential outlier due to its 5mm to 6mm lower peak displacement. Additionally, the total displacement difference between the 0kN and 20kN samples was also just 1mm.

Table 5-3: Summary of peak forces and shear stresses of all infilled samples

Bolt Type	Peak Shear Force (kN)	Displacement at Peak Shear (mm)
20T0kNINFILL	89.3	15.3
20T10kNINFILL	99.6	14.7
20T15kNINFILL	87.9	12.8
20T20kNINFILL	94.2	10.6
30T0kNINFILL	78.5	17.3
30T10kNINFILL	113.9	17.8
30T15kNINFILL	68.8	12.2
30T20kNINFILL	114.1	18.3

5.5.2 Pretension profile

The pretension profile was analysed and compared across all tested infilled samples. While there were variations in the peak displacements and peak axial forces, all samples followed the sample three zone profile outlined in sections 5.3.2 and 5.4.2. Each of the samples progressed through the same zones throughout shearing beginning with zone one represented by the initial flat section of the curves. During this section each sample maintained the initial pretension value and experienced no increase in axial force. This suggested that there was no internal conversion of the shearing force to axial force. The key difference in the case of the 0kN pretension samples was that the 30-tonne sample maintained zone one over a shorter displacement range, approximately 50% of the 20-tonne samples', as illustrated in Figure 5.25. This could be attributed to the extra strength of the 30-tonne sample resulting in earlier internal damage that could facilitate the transition from shear force to axial force.

Conversely, it was also observed that the 30-tonne samples maintained zone two for a longer displacement when compared to the 20-tonne samples. As zone two was where a majority of the shear forces were converted to axial forces, the increased duration of this zone for the 30-tonne samples also resulted in the 30-tonne samples achieving higher axial forces. Figure 5.25 also demonstrated that the additional duration of zone two resulted in greater axial forces.

Zone three however, remained consistent across all samples. Zone three encompassed the failure portion of the rock bolt and as all samples were comprised of similar fibreglass, the failure mechanism of the core materials in the rock bolt remained constant. It was not possible to compare displacements of zone three as this was heavily influenced by the completion of the testing process. Hence, the zone three displacement was dependent on the point in time when the equipment detected failure and stopped applying shear. Despite significant variations to the recorded peak axial forces, in the case of the 30-tonne sample with 0kN pretension, the sample experienced more than double the axial force of the 20-tonne sample with 0kN pretension. The overall peak axial forces were influenced by the rock bolts' performance in zone two. When samples reached the zone three failure stage of the profile, only a minor increase in axial force was recorded before the samples quickly lost the ability to resist shear displacements.

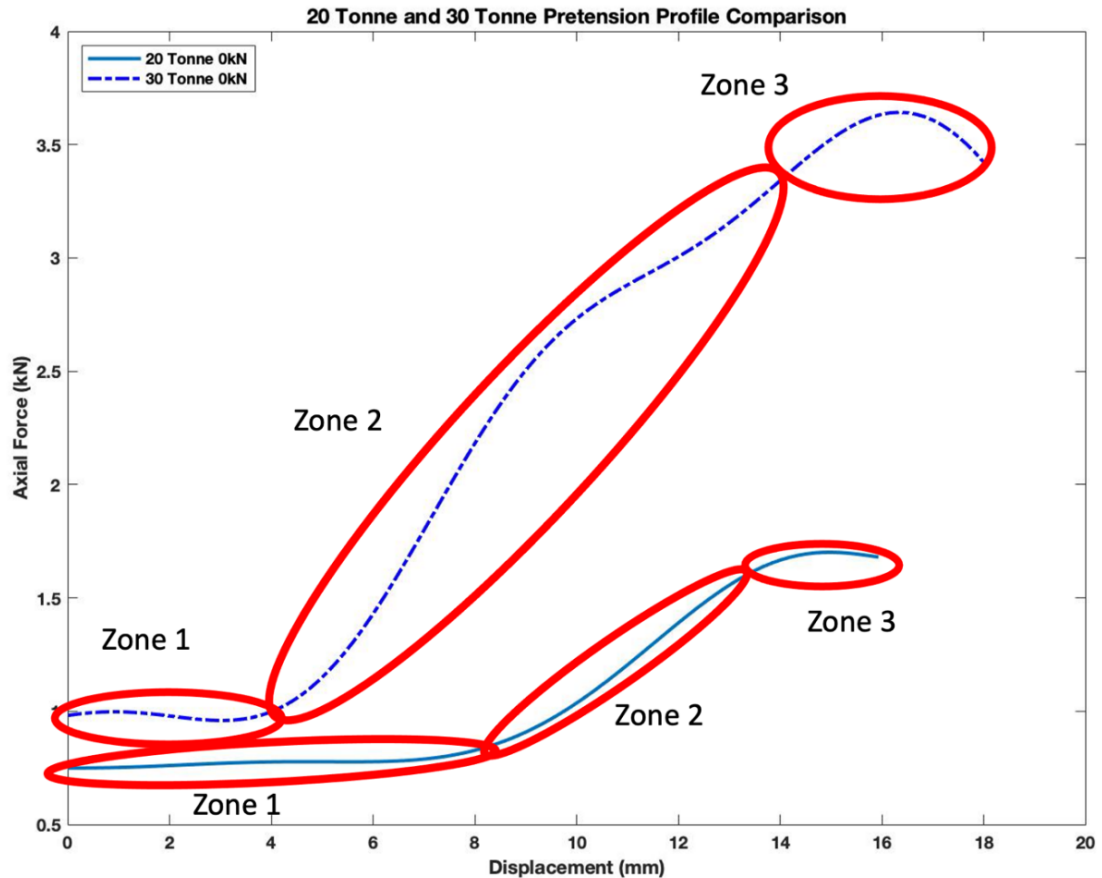


Figure 5.25: Comparison of the axial force profile for both 20-tonne and 30-tonne 0kN pretension samples with infilled shear planes

5.5.3 Impact of pretension on shear strength

The application of pretension had differing impacts on the performance of the 20-tonne and 30-tonne rock bolts. These differences impacted the peak shear force of the samples as well as their failure displacements. To ensure the accuracy of the comparison, both rock bolt types were prepared using the same techniques and tested under the same infilled testing scheme with the applied pretensions of 0kN, 10kN, 15kN and 20kN. However, due to complexities of the sample preparation process there were some variabilities between each sample set. The differences to the applied pretension were recorded in Table 5-1. Both rock bolt types presented with different responses to the applied pretensions with their performance summary outlined in Table 5-3. The application of pretension had the greatest consistent impact on the performance of the 20-tonne rock bolts, despite the 30-tonne rock bolts recording the greatest changes. The increase from 0kN pretension to 10kN pretension saw a gradual increase of 11% for the failure shear force of the 20-tonne sample while the 30-tonne

sample recorded an increase of 45% as evidenced in Figure 5.26. Both rock bolt types recorded similar magnitude of change to their failure displacement response. The 30-tonne samples recorded an increase of 3% in its failure displacement, while the 20-tonne samples recorded a decrease of 4%. This was due to the 20-tonne sample's inherent weaker strength. The addition of the pretension incrementally increased the strength of the system components due to increased confinement and as such, reduced the rock bolt's ability to resist shear displacement. On the other hand, the 30-tonne rock bolts were inherently stronger than the 20-tonne rock bolts and as a result were under-utilised in scenarios with lower pretensions. This was evident through the significant increase in shear force resistance and the increase in the failure displacement between the 0kN and 10kN samples. The 30-tonne rock bolt however, did not perform consistently with the increase to a pretension of 15kN, which saw a decrease in both failure shear force and failure displacement. This could be the result of a faulty sample as well as the strength of the rock bolt being an ineffective match to the test system's design. Poorly matching of a rock bolt type to the environment could result in inefficient transfer of forces through the element. The inefficient transfer of forces could present as a decrease in overall rock bolt performance, despite the greater design strength of the rock bolt. In this situation of small-scale testing, an over strengthened rock bolt could divert shear force to continually damage components within the system and can be characterised by an extended failure region. This could also result in increased bending within the element, reducing its effective strength due to the poor bending properties of the intrinsic fibreglass matrix.

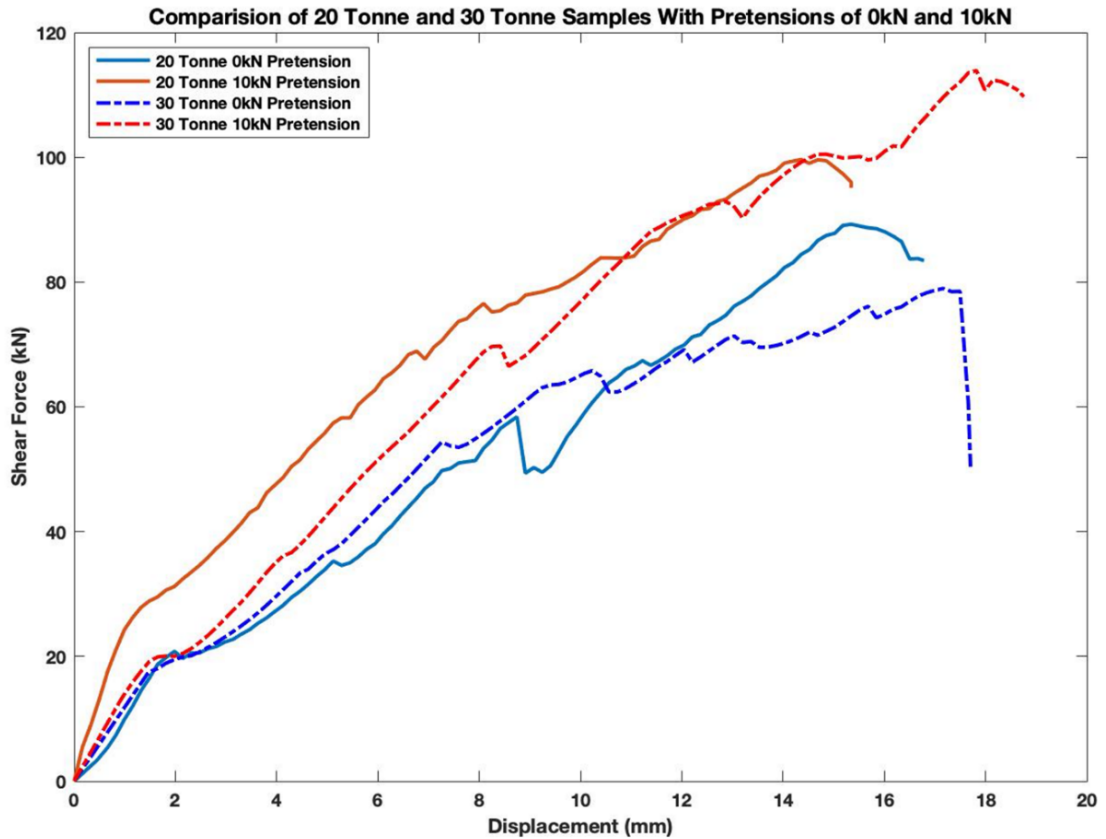


Figure 5.26: Influence of pretension increase from 0kN to 10kN on shear force for 20-tonne and 30-tonne rock bolts with infilled joints

Similarly, the rock bolts' response to an increase from 0kN pretension to 10kN both samples exhibited similar trends when increasing the pretension from 15kN to 20kN as shown in Figure 5.27. The 20-tonne samples recorded an increase in the failure shear force of 7% with an overall increase of 5.5% from the 0kN sample to the 20kN sample. The 20-tonne samples also maintained a consistent decrease in failure displacement with a decrease of 20% between the 15kN and 20kN samples. The 20-tonne sample recorded an overall decrease of 30% in its failure displacement when comparing the 0kN and 20kN samples. The 30-tonne samples also maintained their performance with variable failure shear forces and failure displacements. Increasing the pretension from 15kN to 20kN saw similarly large changes in shear failure forces with an increase of 40%. This was due to the 15kN sample performing significantly lower than the other samples. In a similar manner the failure displacement also recorded an increase of 50% for the same reason. Overall, the 30-tonne sample recorded a significant 45% increase in failure shear force when comparing the samples of the extreme ends of the pretension scale of 0kN and 20kN. Interestingly, the 30-

tonne sample only recorded an increase in 6% for the failure displacement further reinforcing its variable performance. Finally, it was found that overall the increase in pretension had a more significant impact on the 20-tonne rock bolts' failure displacement performance, while the 30-tonne sample experienced a greater impact on its peak shear force.

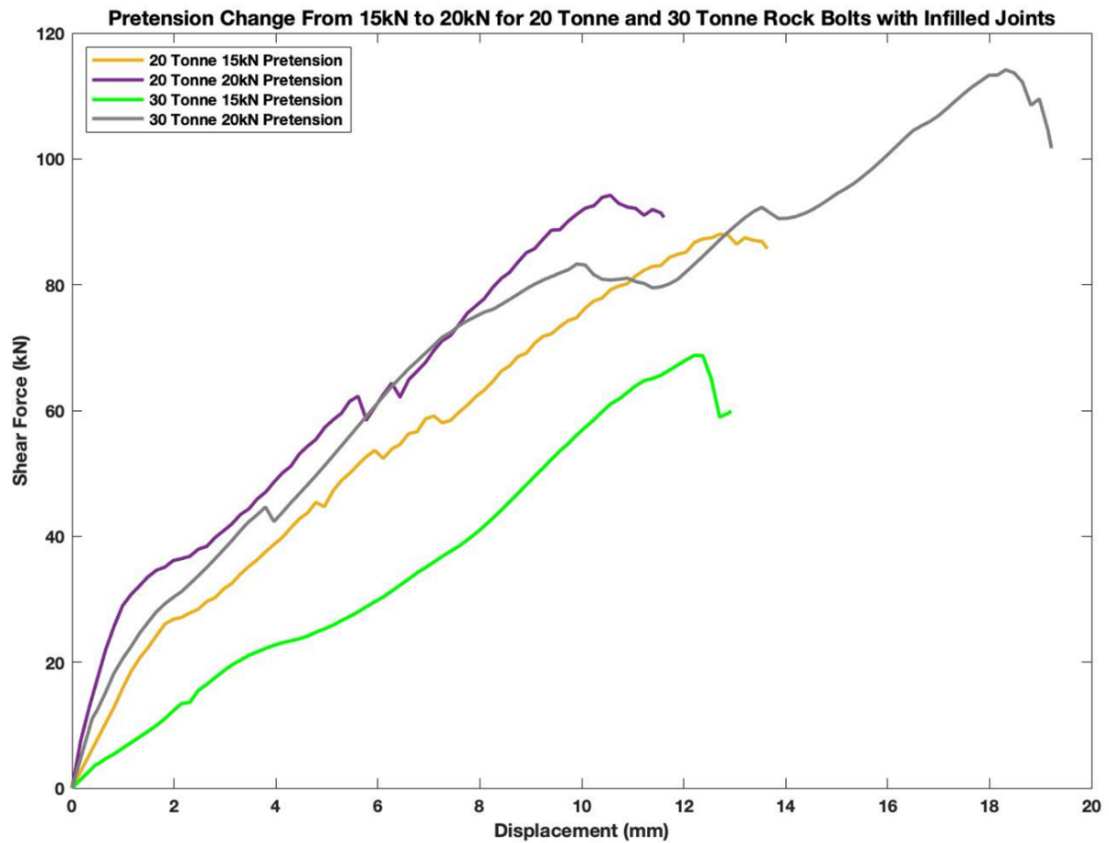


Figure 5.27: Influence of pretension increase from 15kN to 20kN on shear force for 20-tonne and 30-tonne rock bolts with infilled joints

5.5.4 Failure characteristics

The physical failure characteristics of the 20-tonne and 30-tonne rock bolts with infilled joint surfaces were compared based on the detailed analysis provided in Sections 5.3.4 and 5.4.4. As previously observed, the rock bolts experienced three key modes of failure: the hinge point, the rock bolt structural failure and the shear surface failure.

Unlike the clean interface samples, both the 20-tonne and 30-tonne rock bolt infilled interface shear samples experienced different degrees of bending when the hinge

points were analysed. At a pretension of 0kN, the 20-tonne experienced a greater degree of bending by approximately 6° when compared to the 30-tonne rock bolt as shown in Figure 5.28. Furthermore, both rock bolt types exhibited different responses to the increase in pretension. The 20-tonne rock bolts recorded a decrease to the degree of bending when pretension was increased from 0kN. On the other hand, the 30-tonne rock bolts recorded an increase to the amount of bending experienced at the same change in pretension.

Failure differences were also recorded when analysing the condition of the rock bolt element post failure. With a pretension of 0kN the 20-tonne rock bolt experienced a significant amount of damage propagating along the rock bolt away from the shear interface. This failure was only partially present on the 30-tonne rock bolt samples, with the rock bolt experiencing damage on one half of the shear interface as shown in Figure 5.29.

Neither rock bolt recorded shear interface gouging thanks to the lubricating effects of the sandy clay infill. The 20-tonne rock bolt however, experienced damage at the shear interface at 0kN as a result of the greater hinge point bending. In comparison the 30-tonne rock bolt recorded little to no damage to the shear interface due to the lower degree of bending as shown in Figure 5.30. Additionally, at low pretension settings, the infilled material did not fill all the shear interface voids for either of the 20-tonne and 30-tonne rock bolts as seen in Figure 5.30.

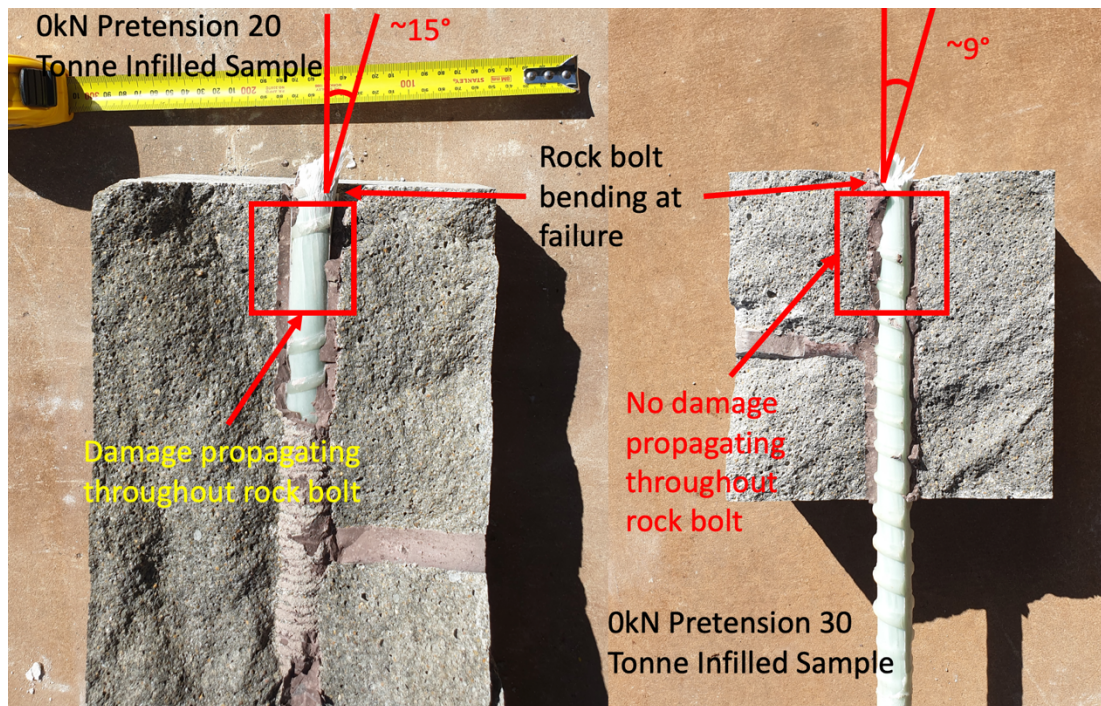


Figure 5.28: Comparing rock bolt structural damage for 20-tonne and 30-tonne rock bolts with 0kN pretension and infilled shear interfaces

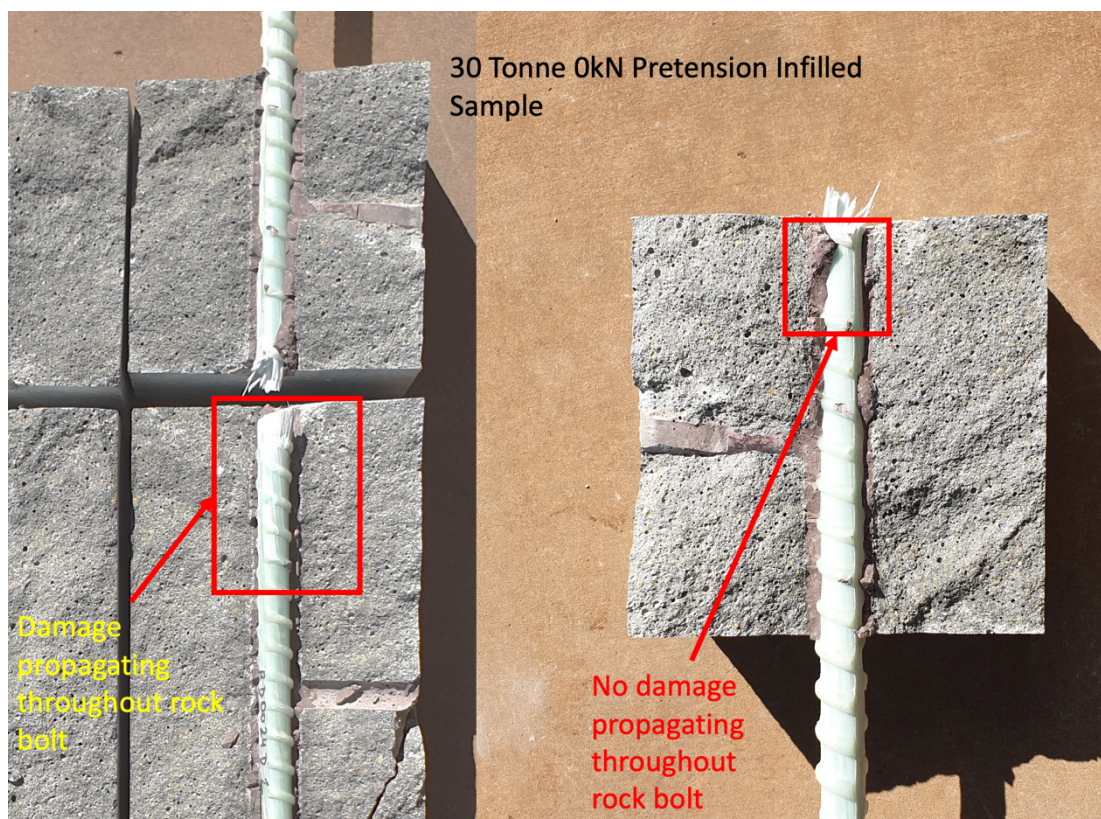


Figure 5.29: Representation of rock bolt damage for 30-tonne rock bolt with infilled shear interfaces and 0kN pretension

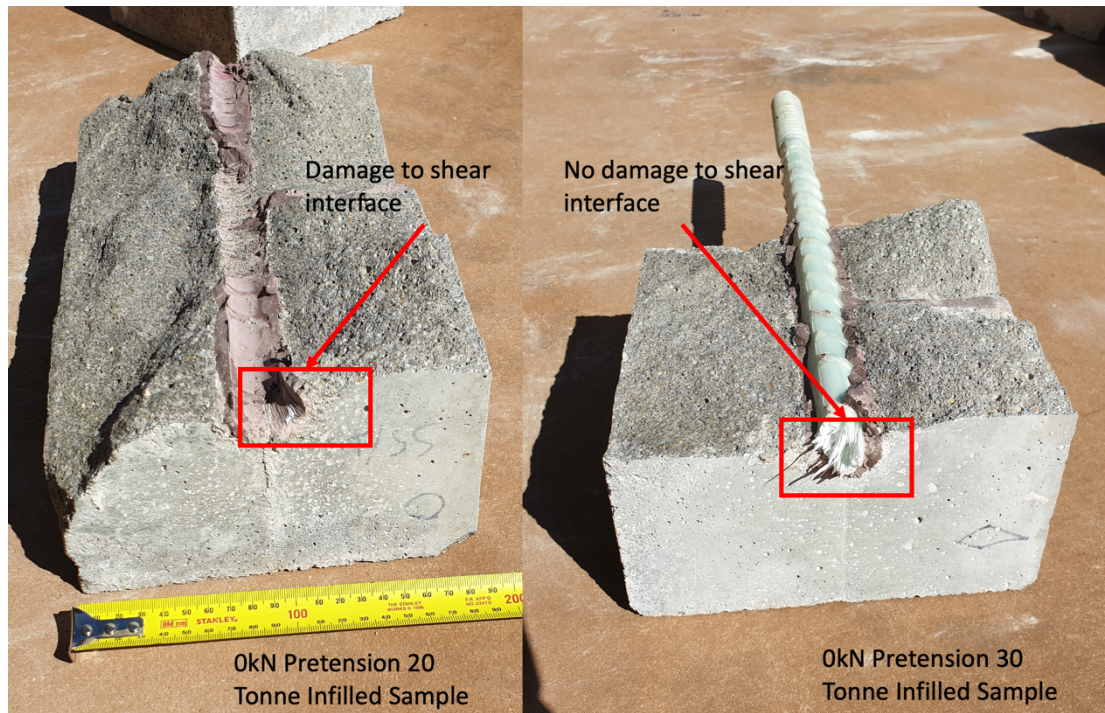


Figure 5.30: Comparing shear plane damage of 20-tonne and 30-tonne rock bolts with infilled shear interfaces and 0kN pretension

Increasing the pretension to 20kN resulted in two opposite failure trends for the 20-tonne and 30-tonne rock bolts. As the pretension was increased, the 20-tonne rock bolts experienced a reduction in the severity of bending at the hinge point, while the 30-tonne rock bolt recorded an increase in bending when compared to the 0kN samples. Despite this difference, the 20-tonne and 30-tonne rock bolts experienced similar amounts of bending with 20kN of pretension. The similar magnitudes of bending at the hinge point resulted in the two rock bolts experiencing similar degrees of damage propagating from the shear plane as shown in Figure 5.31.

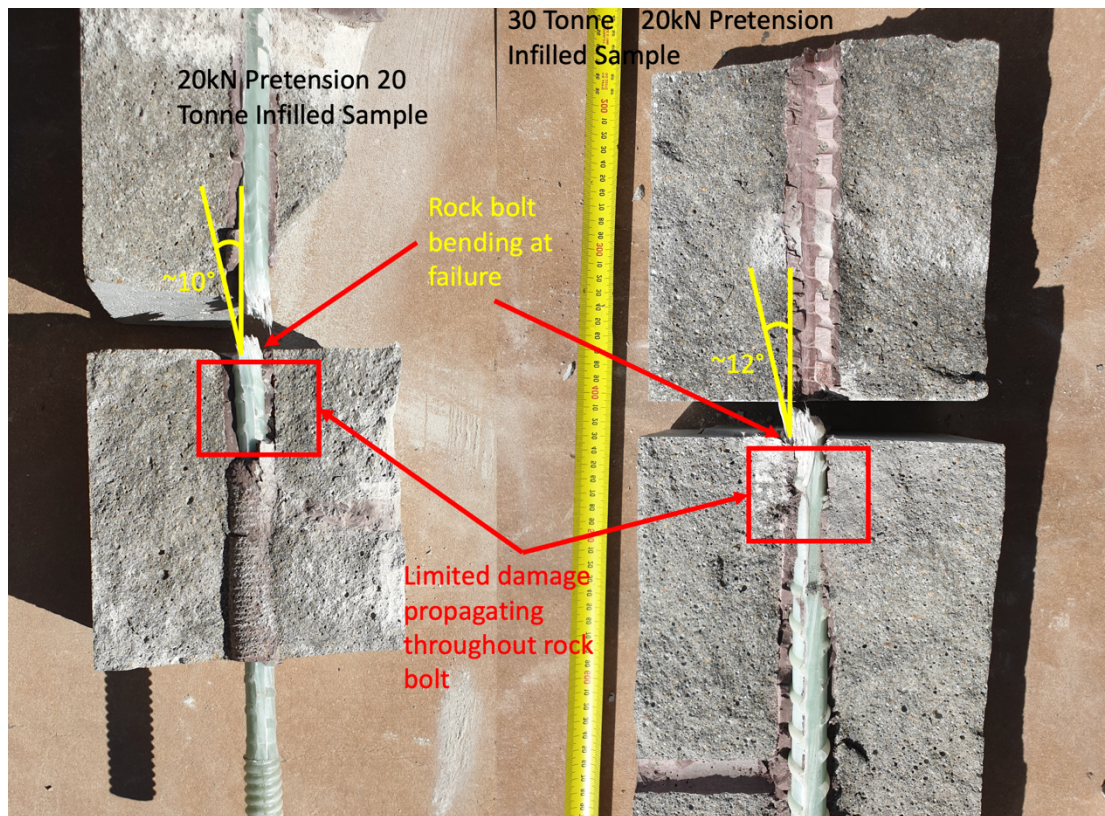


Figure 5.31: Comparing rock bolt hinge point and rock bolt damage for 20-tonne and 30-tonne rock bolts with 20kN pretension and infilled shear interfaces

Figure 5.32 shows that despite increasing the pretension to 20kN, neither the 20-tonne or 30-tonne samples experienced damage to the shear interface. The infilled material behaved as a protective barrier to the shear interface. Additionally, increasing the pretension resulted in more of the voids on the shear surface being filled by the infill material as shown in Figure 5.32.

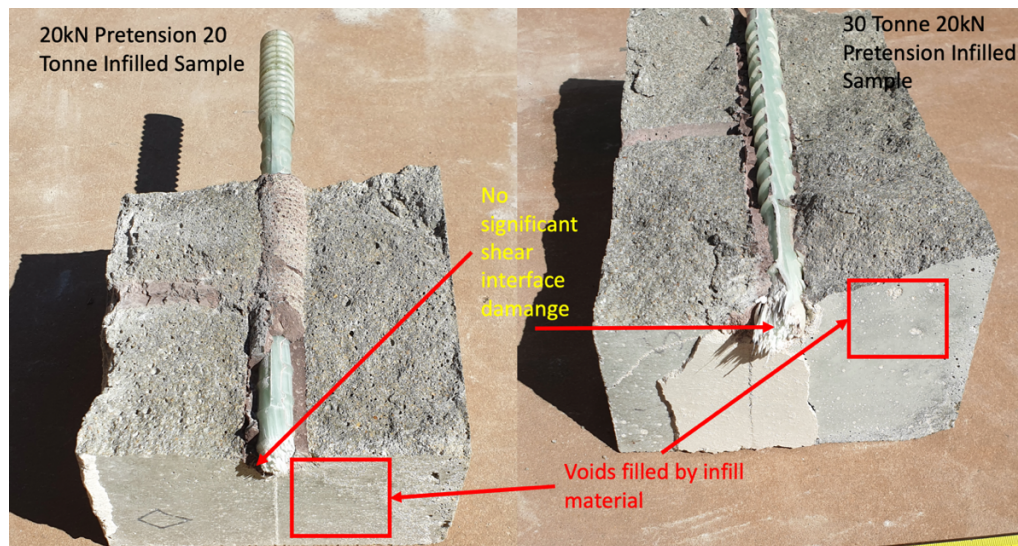


Figure 5.32: Comparing shear plane damage of 20-tonne and 30-tonne rock bolts with 20kN pretension and infilled shear interfaces

5.6 Summary

The traditional method of testing was modified to account for different shear interface conditions. The 20-tonne and 30-tonne rock bolts were tested to determine their shear performance when the shear interface had been modified through the inclusion of infilled material. Each rock bolt type was tested over a range of pretensions including 0kN, 10kN, 15kN and 20kN with a total of eight samples tested. Each test was analysed for their shear profile performance, pretension performance and impacts and physical attributes of failure. The following findings were noted:

- Upon evaluating the shear profile for each sample, it was found that all samples followed a three-part failure profile comprised of an elastic region, strain-softening region and failure region.
- Additionally, it was found that the infilled shear planes had no impact on the overall shear profile of the 20-tonne and 30-tonne rock bolts.
- The 20-tonne and 30-tonne rock bolts exhibited differing responses to the increase in applied pretension. The 20-tonne rock bolt saw a significant overall decrease of approximately 30% in its failure displacement response as opposed to the 30-tonne samples' which saw a 6% increase.
- When comparing the peak shear force of the 20-tonne and 30-tonne samples, it was found that the 30-tonne samples outperformed the 20-tonne rock bolts by up to 30% irrespective of initial pretension settings.

- The 20-tonne rock bolts maintained greater consistency of the achieved peaks, with an approximate variability of 10% as opposed to the 30-tonne samples recording peak shear force values with up to 40% variability.
- Increasing the pretension to 20kN for the 30-tonne samples resulted in a change to the transition from the elastic region of the shear profile. Rock bolts tested with a pretension of 15kN and less exhibited an inflection in their shear force as the sample exited the elastic region. Increasing the pretension past 15kN saw elimination of this inflection. The inflection was not evident in the 20-tonne samples.
- 30-tonne rock bolts maintained resilience to the impact of pretension with the samples maintaining a failure displacement of approximately 18mm. The 15kN was the exception and instead matched the displacement of the 20-tonne 15kN sample.
- Similarly, the shear profile of all tested samples maintained the same pretension failure profile despite changes to the shear interface and pretension settings. All samples followed a three-zone pretension profile.
- The 30-tonne samples exhibited an extended failure region when compared to the 20-tonne samples. This extension was due to the sample achieving higher shear forces and as such, maintained a level of integrity as components of the shear system began to fail.
- Comparing the physical failure characteristics of the samples found that both the 20-tonne and 30-tonne samples exhibited the same response to increased pretension. As pretension increased, the angle experienced at the hinge point also increased incrementally.
- Additionally, as the pretension was increased, less damage propagating down the rock bolt element was evident.

Chapter 6 introduces the use of numerical modelling and finite difference modelling in order to model the experimental results. MATLAB and FLAC3D were utilised to create double shear models which were then calibrated against the experimental results in Chapter 4 and Chapter 5. The models were then used to conduct a series of simulations and sensitivity analysis to model the shear performance of rock bolts without the need for cumbersome laboratory testing.

CHAPTER 6: ANALYTICAL AND NUMERICAL MODELLING OF ROCK BOLTS IN DOUBLE SHEAR

6.1 Introduction

The safe design of strata reinforcing systems is a core requirement of excavation projects the world over. These can take the form of surface excavation or tunnelling for both the civil and mining industries. As the use of rock bolts for strata reinforcement span various designs and implementation constraints, a comprehensive understanding of their rock reinforcing properties is required. Typically, experimental testing is conducted to determine the rock bolts' response under various conditions. Often these tests are limited to individual samples and strata simulations that often portray a uniform environment and conditions. These conditions are imposed on the experimental test systems as it is often too time consuming, logistically challenging and costly to represent complex shear systems. In this study, various models were adopted to simulate rock bolt behaviours using both analytical and numerical approaches. The analytical model used to determine rock bolt performance was a combination of expansive functions in the form of Fourier series and the energy balance theory. To accomplish the numerical modelling, finite difference was adopted by using the Fast Lagrangian Analysis of Continua software (FLAC3D) to simulate the shear performance of fibreglass rock bolts in double shear systems. This chapter extends the testing scheme of the fibreglass rock bolts from Chapter 4 and Chapter 5 by incorporating analytical and numerical modelling to:

1. Develop an analytical model that can predict the shear performance of fibreglass rock bolts subjected to clean and infilled joints at various stages of shearing,
2. Simulate the shear behaviour of fibreglass rock bolts using FLAC3D and conduct sensitivity analysis for various shearing conditions and rock bolt properties.

The outcomes of the analytical and numerical modelling were calibrated utilising the results of the single shear, double shear with clean joints and double shear with infilled joints testing schemes outlined in Chapters 3, 4, and 5. All initial models were created to replicate the physical design constraints of the experimental system to ensure validity of calibration. Due to model design limitations all simulated samples were

conducted with 0kN of pretension and therefore all subsequent simulations were based on scenarios with no pretension. Despite this limitation, the axial force of the rock bolts could be computed. A comprehensive analysis of the subjected shear simulations was undertaken to develop a broad understanding of the performance of fibreglass rock bolts subjected to various shearing environments.

6.2 Analytical modelling of shear behaviour of fibreglass rock bolts

6.2.1 Requirement for a new analytical model

The development and implementation of models simulating the various properties of rock bolts and cable bolts were outlined in Chapter 2. The previous discussion focused on their development, theory and reporting for both pure element failure as well as strata simulation. While there have been significant accomplishments in simulating strata supporting elements, their suitability and reliability need to be carefully considered for each implementation. Past simulations were limited to specific conditions, with models simulating the pure element with great accuracy, yet unable to model the element within an environment. Unfortunately, these approaches were optimised for the structure of metallic rock bolts and were therefore unsuitable for use with fibreglass rock bolts. Unlike in metallic rock bolt production, manufacturers have the ability to significantly alter the properties of fibreglass rock bolts by changing the composition of the binding resin, strand density as well as strand orientation. Other models including Aziz et al. (2015a) determined the shear stress of cable bolts utilising the Mohr Coulomb criterion and as a result was inherently limited to determining only the peak shear values of the cable bolts. In addition, the Aziz et al. (2015a) model was unable to predict the shear forces at each stage of the cable bolt failure. Simulations of this nature were calibrated for the purpose of testing metallic cable bolts only.

As there are a wide variety of rock bolt products available, some researchers have developed models to address the growing demand for composite rock bolts. One of the early representations of the composite rock bolt behaviours was the shear lag theory. This method adopted assumptions that were not well understood and over idealised (Cai et al., 2004), with one such assumption including the lack of slip at the interfaces. Additionally, unknown parameters were assumed using stress distribution matrices. Cai et al. (2004) modified the shear lag theory application to address many of its shortcomings. The outcome of Cai et al. (2004) study was the development of an

analytical model that expressed the pull-out force of the rock bolt. Ultimately, the shear lag theory's suitability was limited to modelling the pull-out capabilities of the rock bolt.

A more recent study conducted by Wen-qiang et al. (2022) attempted to address current limitations of the analytical modelling of rock bolts in shear. Wen-qiang et al. (2022) proposed that one of the main limitations of analytical modelling was that it assumed a linear force behaviour for the host material. Therefore, a new model incorporating joint dilation, axial force, joint displacement and transverse shear was developed.

Despite the comprehensive representation of the rock bolts' shear behaviour, the model does not account for the interaction of the shear joint properties with the shear performance of the rock bolt. Therefore, negating the impacts of joint friction angle, impact of pretension and the impacts of infilled materials. As a result, and to the best of this authors knowledge, the current analytical models fail to incorporate key system properties of fibreglass rock bolts.

6.2.2 Development of analytical model

The proposed model was developed to address the identified shortcomings of the current adopted models. The inadequacies outlined in section 6.2 included: the inability to model each of the regions of the shear curve, the impact of pretension, and the influence of various joint properties including friction angle and presence of infill. As such, a new approach was adopted to fill this gap. During shearing it was discovered that all the tested samples progressed through three regions: the elastic, strain-softening and finally the failure region as outlined in Figure 6.1.

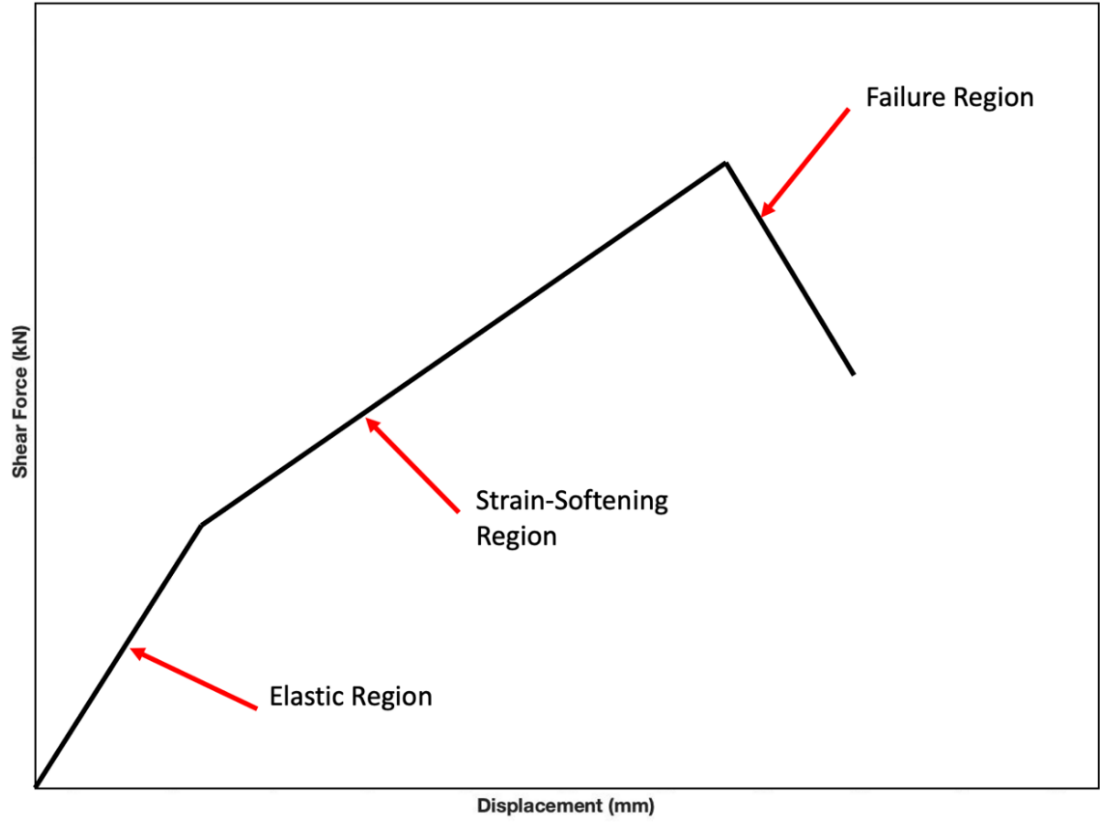


Figure 6.1: Illustration of shear regions

Therefore, it was deemed essential that this was incorporated to the foundations for the model development. In an attempt to achieve an accurate three region model, limits were adopted for each region. The elastic region was forced to comply with the limit denoted in equation 6.1 where u was the displacement and u_{yield} was the displacement at the elastic yield force.

$$u \leq u_{yield} \quad (6.1)$$

With a similar approach to the elastic region, the limit expressed by equation 6.2 was applied to the strain-softening region. By limiting the model between the displacement at the elastic yield force u_{yield} and the displacement at the peak shear force u_{peak} it was ensured that the results were constrained with no overlap.

$$u_{yield} < u < u_{peak} \quad (6.2)$$

The final limit used was to ensure the simulation of the failure region was clipped between the displacement at peak shear force and sample failure. Equation 6.3 demonstrates this by ensuring the displacement was greater than the displacement at peak u_{peak} and yet less than displacement at failure $u_{failure}$.

$$u_{peak} < u < u_{failure} \quad (6.3)$$

Once the regions were identified, unique models were created to best represent the rock bolts behaviour within each limit.

6.2.2.1 Elastic Region

Upon analysis of the experimental results, it was evident that the first region experienced by the fibreglass rock bolts could be described by linear elastic theory. Whereby any deformation imposed by the applied displacement was linear and reversible. As such, the following linear equation 6.4 was developed where K_e was the constant denoting the rock bolts elastic stiffness coefficient in Newtons per metre and where u represented the displacement in metres.

$$\tau_e = K_e u \quad (6.4)$$

6.2.2.2 Strain-softening region

When the applied force exceeded the elastic response of the rock bolt, the rock bolt transitioned into the more complex non-linear plastic response. Due to the increased forces exerted on the samples after the transition into the strain-softening region, the influence of the applied pretension took effect. In order to develop a reliable model of these responses, two key theories were adopted, the energy balance theory and Fourier transform. The energy balance theory was adopted to represent the overall behaviour of the rock bolt system. The theory states that the total energy within the system must remain constant and that the energy can only experience a change of state. Additionally, any energy entering the system, ΔU , will make changes to the original energy of the system, Q , minus the work done by said system, W , as represented by equation 6.5 and forming the basis of the force equilibrium equation.

$$\Delta U = Q - W \quad (6.5)$$

In the case of the investigation of the double shear testing scheme, energy was added to the system through the application of a force at a constant displacement. This increase in energy interacted with the double shear system through several components such as the final value of the initial elastic region, the rock bolt, pretension and interface properties. Due to the application of pretension having a limited impact on the physical properties of the rock bolt, its contribution to the force equilibrium equation was interrelated, such that, the initial applied pretension could be defined by the constant α . The coefficient α was an arbitrary value for each pretension that was determined through an iterative process. The remaining factors expressing the rock bolt's properties comprised of K_p , denoting the plastic stiffness and finally the systems shear displacement u . As the strain-softening region was an extension of the elastic region, the displacement needed to account for the displacement occupied by the elastic region. The rock bolts' strain-softening region's representation of displacement was described by $(u - u_y)$. Therefore, the rock bolts' work contribution to the force equilibrium equation could be defined by equation 6.6.

$$\tau_{RB} = K_p \alpha (u - u_{yield}) \quad (6.6)$$

The final component of the force equilibrium expression determined the contributions of the shear interface on the shear performance on the rock bolt. The shear interface properties were separated into the following components: influence of pretension, surface cohesion, friction angle and surface area of the shear interface. In contrast to the influence of pretension on the rock bolt element, its influence on the shear interface was complex, whereby the recorded axial force experienced multiple inflection points, as highlighted in Figure 6.2, in addition to linear portions of varying lengths.

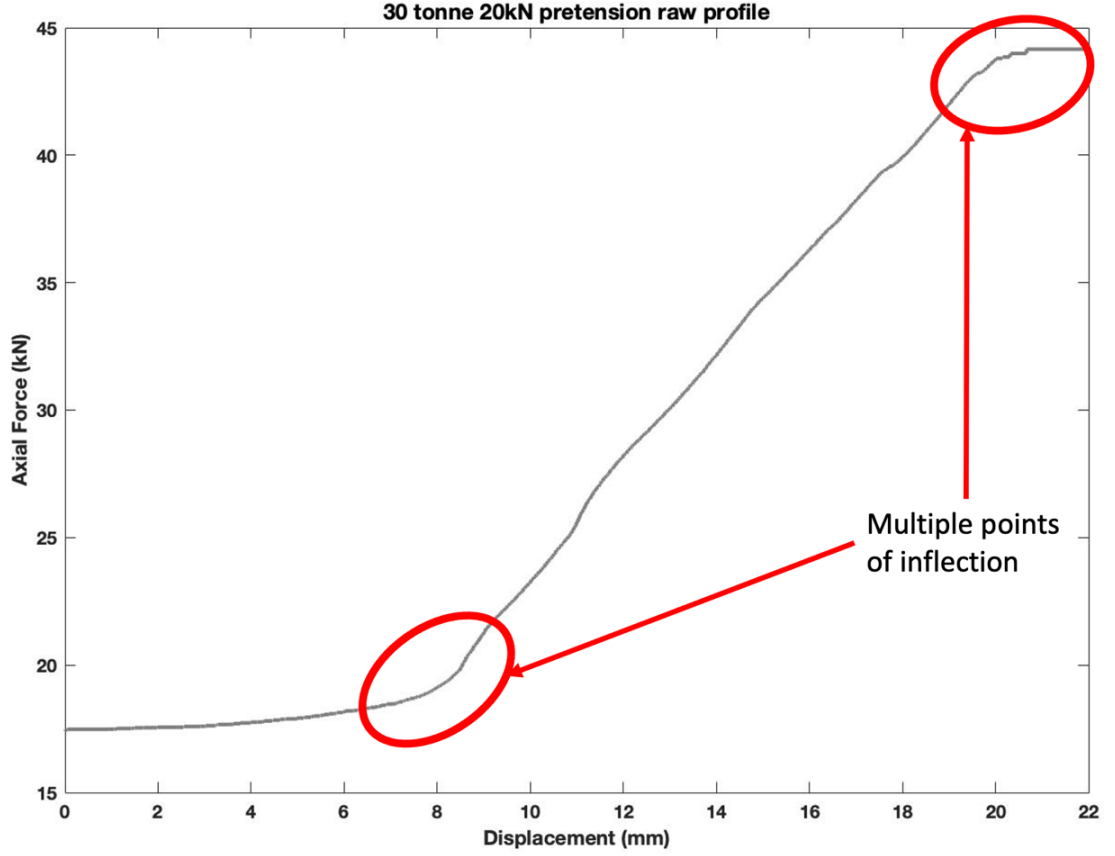


Figure 6.2: Demonstration of complex raw pretension profile for infilled 30-tonne 20kN pretension samples

Therefore, to account for the contributions of the pretension on the shear interface, this required the development of a Fourier transform to replicate the complex waveform of the axial component of the shear system. The Fourier series decomposed the pretension signal to its sine and cosine components and can be represented by the equation 6.7. To automate and simplify the calculation of the Fourier transforms for all tested samples, a subroutine program was written utilising MATLAB.

$$y = a_0 + \sum_{i=1}^n a_i \cos(iwx) + b_i \sin(iwx) \quad (6.7)$$

Figure 6.3 demonstrates close agreement between the MATLAB derived Fourier approximation and the raw pretension data set. As such, the matrix containing the output of the Fourier transform was denoted by σ_n and was the factor representing the pretension contribution of the shear interface.

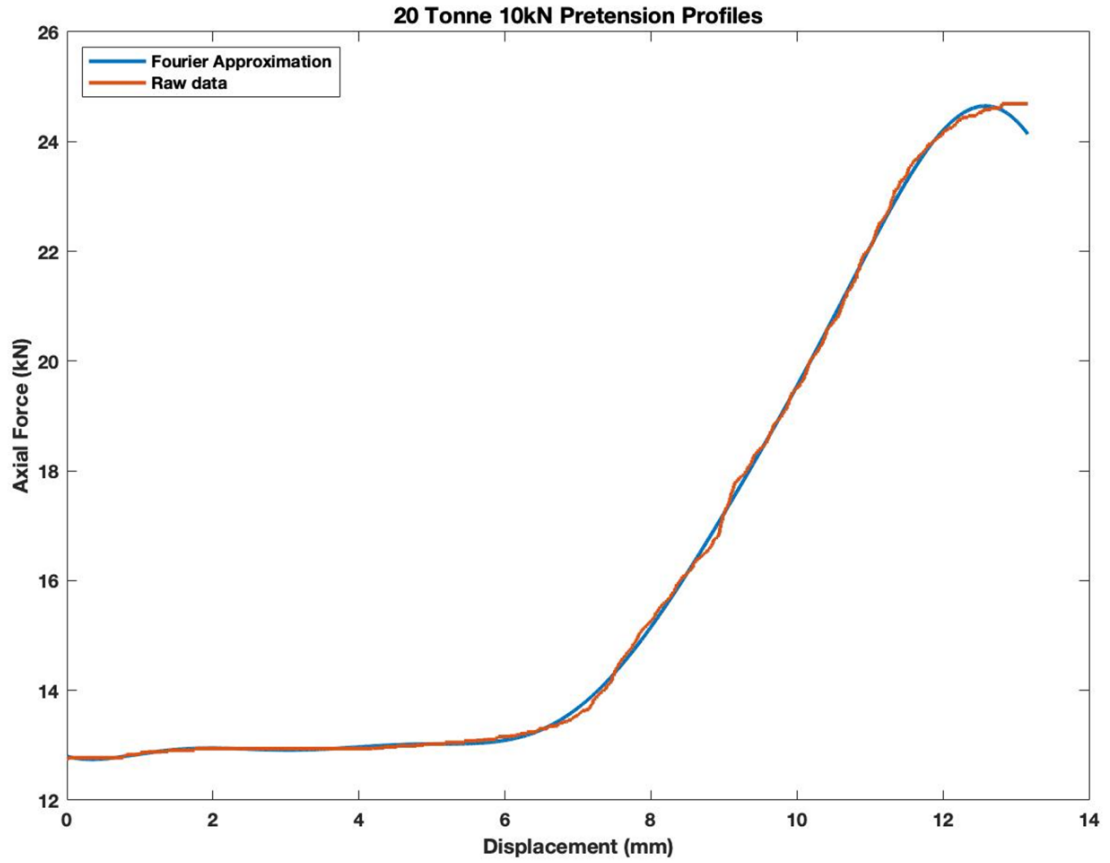


Figure 6.3: Comparison of the Fourier transform approximation to the raw data of the clean shear 20kN rock bolt with 10kN pretension

The remaining three components of the shear interface portion of the equation were determined by the system design such as the shear surface area, represented by A_s and laboratory testing. Values for the friction angle and cohesion of both clean and infilled surfaces were determined via direct shear testing as outlined in Chapter 3 and were denoted by ϕ and c respectively. Therefore, the shear interface contribution could be defined by equation 6.8, where for all clean jointed samples cohesion was set to 0. Therefore, the overall force equilibrium equation was expressed by equation 6.9. The initial condition of the region was represented by τ_e , the final value from the elastic region. The rock bolt contribution was denoted by τ_{RB} and finally the shear interface contribution denoted by τ_i .

$$\tau_i = A(\sigma_n \phi + c) \quad (6.8)$$

$$\tau_{ss} = \tau_e + \tau_{RB} + \tau_i \quad (6.9)$$

The shear load during the strain-softening region was derived from equations 6.4, 6.6 and 6.8 resulting in equation 6.10. Where the values for τ_{ss} , τ_e , σ_0 and σ_e were represented in Newtons, A_s in metres squared, ϕ in degrees, c in Pa, u_e and u_n in metres, K_p in Newtons per metre and finally α as a dimensionless constant.

$$\tau_{ss} = [\tau_e + A_s \phi (\sigma_0 - \sigma_e) - K_p \alpha u_e] + K_p \alpha u_n + A(\sigma_n \phi + c) \quad (6.10)$$

6.2.2.3 Failure region

The failure region denoted the final component of the analytical model and completed the trilinear expression. Similar to the initial elastic region the failure region was expressed utilising a linear expression bound to the limit outlined by equation 6.3. To create a transition from the strain-softening region, the initial shear force component was set to the peak shear force of the strain-softening region $\tau_{ss,p}$. To represent the now negative gradient due to the decreasing shear force values, the constant K_f with units Newtons per metre was incorporated to the linear expression and multiplied by the displacement u_n . Due to the inherent failure of the rock bolt for the duration of this region, pretension forces were no longer subjected to the system resulting in negligible contributions. As such, pretension coefficients and the related shear interface influences were ignored resulting in the representation of the failure region by equation 6.11 and completing the analytical model of rock bolts subjected to double shear.

$$\tau_f = K_f(u_n - u_{ss,p}) + \tau_{ss,p} \quad (6.11)$$

6.2.3 Model calibration for reinforcing clean joints

Upon developing the proposed analytical model, it was then calibrated against the experimental results for the clean joint testing scheme. This was to ensure model accuracy and suitability. Calibration was conducted in two stages; model setup and model tuning and was accomplished by developing an extensive MATLAB subroutine program. During the setup stage, the subroutine software loaded the experimental

results and conducted analysis to determine the shear profile properties K_e , K_p , and K_f . K_e and K_p . These properties were directly utilised for the gradient of the elastic and failure regions due to the simple linear theory. Additionally, the subroutine program allowed for the manual determination of the elastic to strain-softening transition as some samples experienced large transition zones making it difficult to automatically determine its location. The presence of subtle profile changes prevented the auto determination of the transition. Therefore, it resulted in the need to allow for manual selection. The subroutine programme mapped out potential turning points based on a chosen degree of certainty. Figure 6.4 demonstrates these potential turning points with the final point displaying good alignment with the actual region transition point as determined by experimental analysis.

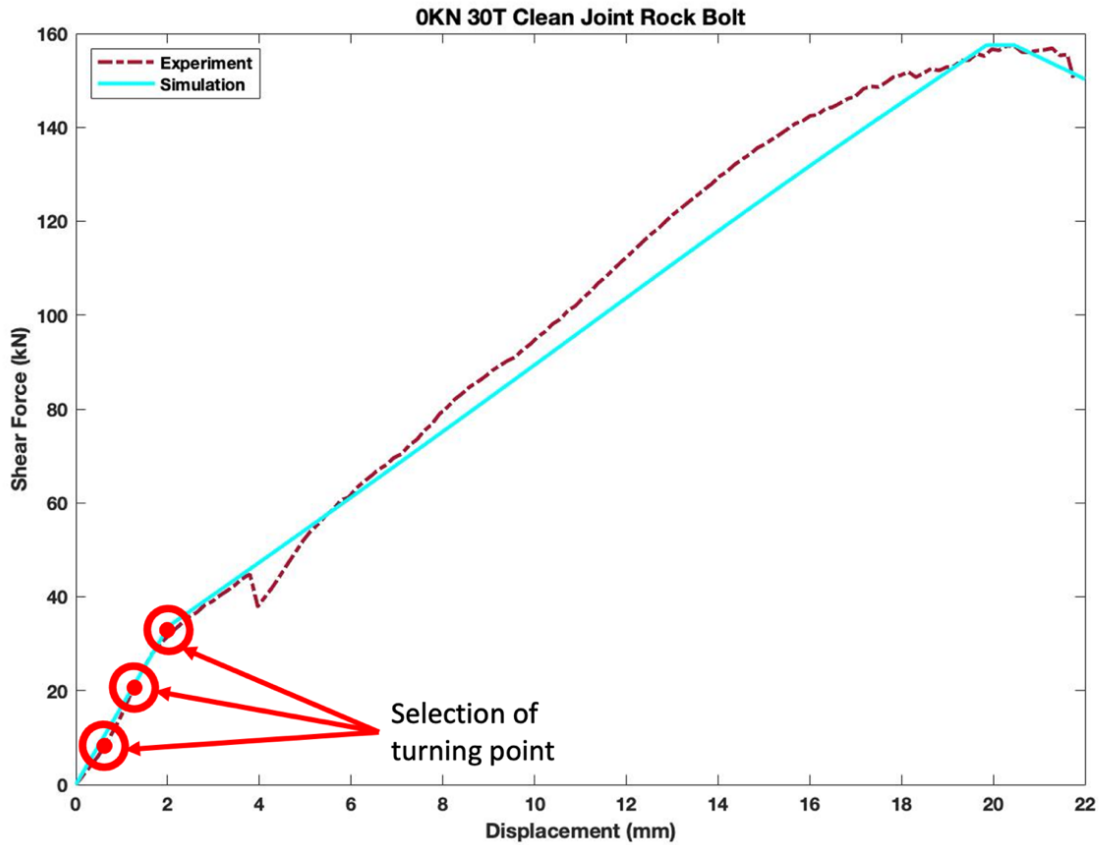


Figure 6.4: Determining the transition to the strain-softening region for clean samples.

Unlike the elastic region, the strain-softening region was comparably more complex to simulate due to the incorporation of pretension and shear interface properties. The K_p coefficient was utilised as the initial state, while α was then used as a tool to provide

fine tuning adjustment. The coefficient α was applied through an iterative process until there was an agreeable alignment between the model and the experimentally determined profile as highlighted in Figure 6.5. Figure 6.5 also demonstrates how adjusting α resulted in changes to both the gradient of the profile as well as its placement along the y -axis. α was either increased or decreased by increments of 0.0001 depending on the proximity of the simulated peak value to the experimental peak value. When the peak values were in agreement based on the defined error factor, the subroutine programme locked in the coefficient resulting in the profile highlighted in Figure 6.4.

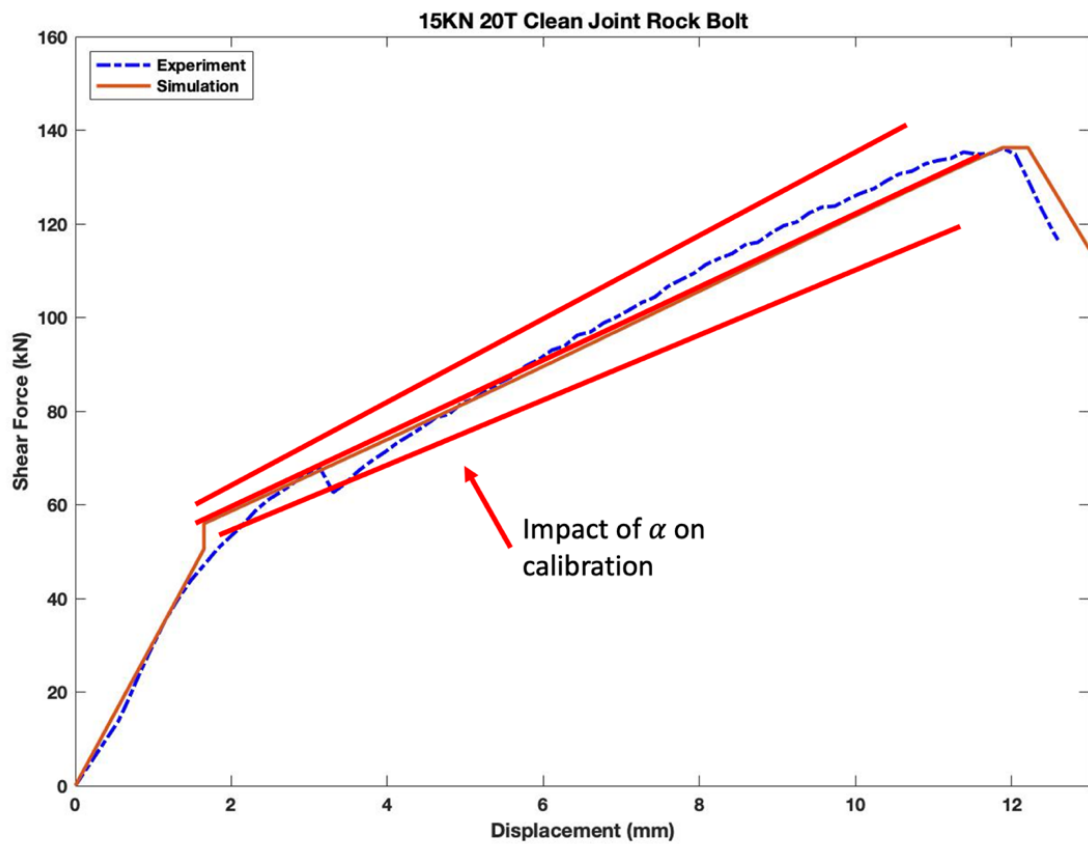


Figure 6.5: Calibration of the strain-softening region using the α constant to ensure model agreement.

Despite the calibration, process the model presented challenges in predicting the transition zones between the regions for some of the samples. Typically, the analytical models simulating the performance of 20-tonne rock bolt samples demonstrated a stepped transition between the failure regions. Figure 6.6 demonstrates how the simulation presented a vertical step when transitioning from the elastic region to the strain-softening region. A similar horizontal step was recorded when transitioning out

of the strain-softening region. This could be attributed to the additional calculation parameters of the strain-softening region including the complex pretension profile and calibration coefficients. The three regions required the adaptation of varying analytical models and through the calibration process the most appropriate agreement was adopted. While these transitions were visible, they had minimal impact on the overall performance of the model. Unlike the 20-tonne samples, the majority of the 30-tonne rock bolts subjected to the clean joints testing scheme presented with seamless transitions from region to region as highlighted in

Figure 6.7. The increase in rock bolt capacity appeared to result in the seamless transition from the elastic region to the strain-softening region. Some 30-tonne samples still presented with a minor step when transitioning to the failure region.

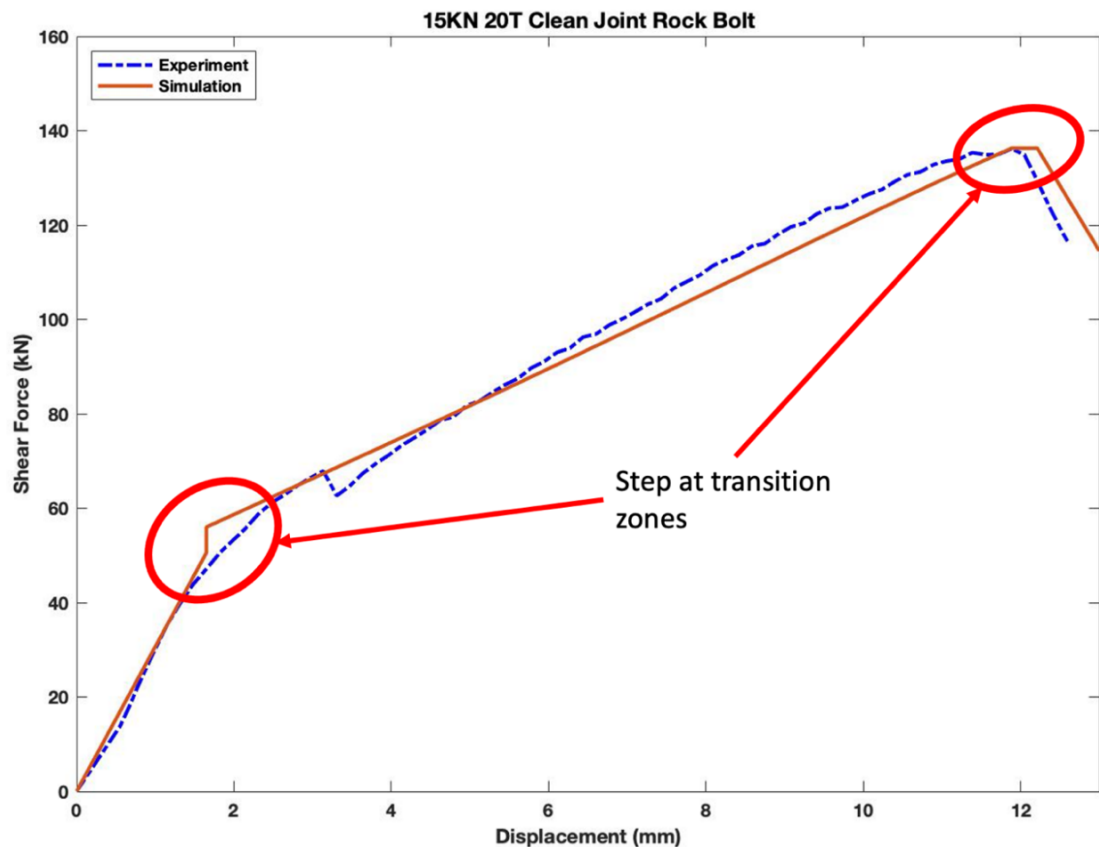


Figure 6.6: Challenges in simulating the transition zones between the regions for 20-tonne rock bolts with clean joints

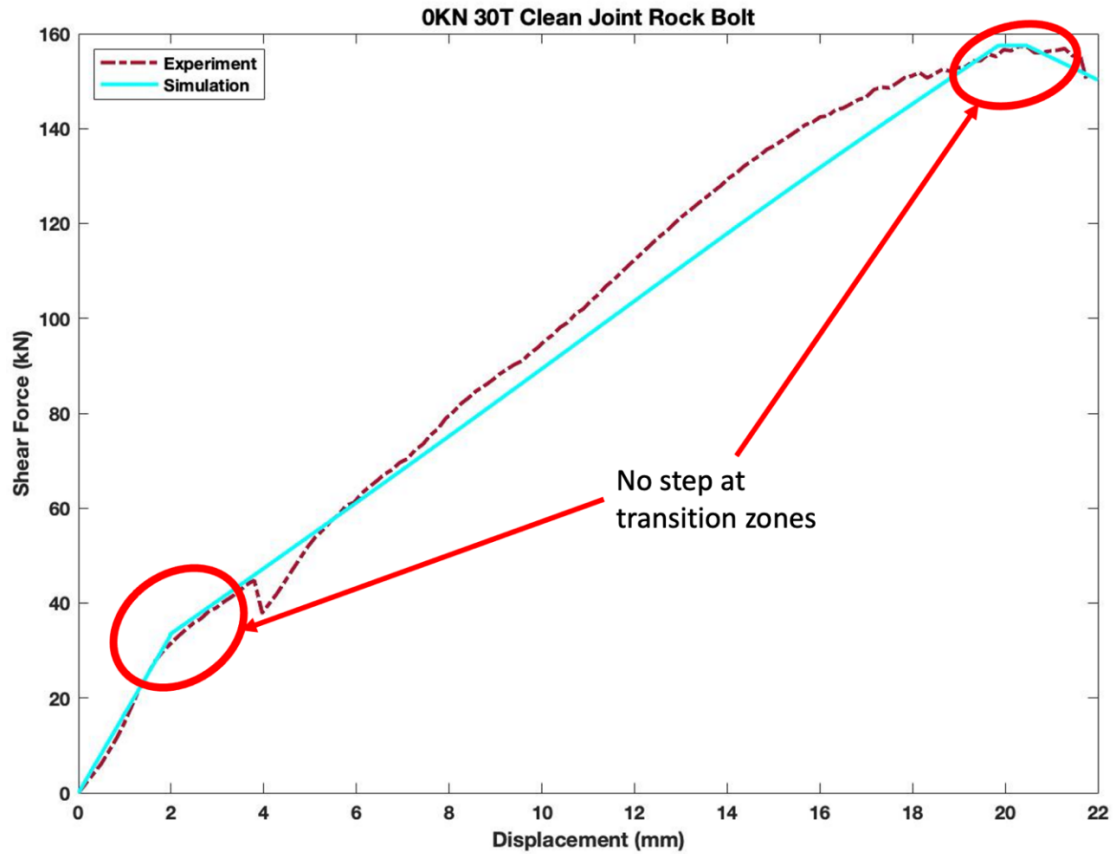


Figure 6.7: 30-tonne rock bolts with clean joints presenting with seamless transitions between regions.

All the clean joint sample scenarios were successfully modelled using the developed subroutine programme. One of the key outcomes of the simulation was to predict the rock bolts' shear profile as displacement increased. However, this model was unable to accurately predict each rock bolts' post-failure behaviour and therefore an approximation was adopted. Throughout the experimental phase of this study, it became clear that the post failure response would not be possible to accurately model as some samples instantly returned to a shear force of 0kN moments after failure while others retained a residual force. This was in part due the bending of the centre shearing block post failure, an outcome of the inability to achieve perfect symmetry. In an attempt to combat this variability, the simulated failure region was a linear approximation controlled by K_f and extended until the value intersected with the y -axis at 0kN as shown in Figure 6.8. As a result of the sample variability, the K_f coefficient also resulted in a significant range as shown in Table 6-1. Table 6-1 also presents K_e and K_p , forming the key portions of the shear profile. These values were of the same magnitude and presented with minor changes when compared to each sample in the

test scheme. Therefore, it could be deduced that they provided an accurate representation of the shear behaviour in those regions. Similarly, the gradual increase in the α coefficient was in agreement with the change to the applied pretension where, as the pretension was increased, the α coefficient also increased.

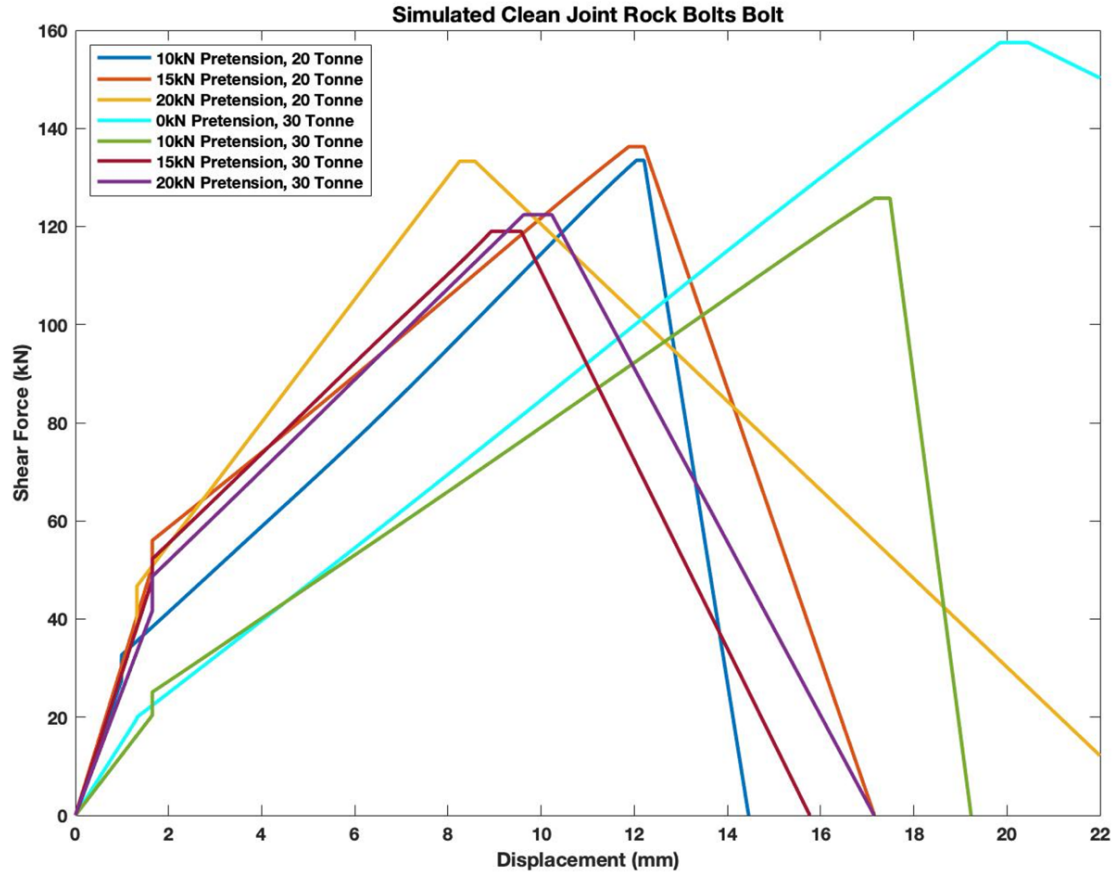


Figure 6.8: Analytical simulation results for clean joint testing scheme

The α coefficient was less sensitive to changes in samples with lower pretension values, suggesting that α has a stepped response to pretension. Additionally, the low pretension cut-off also varied between the 20-tonne and 30-tonne clean shear tested rock bolts. Therefore, the α pretension relationship could be considered as bi-linear with the turning point occurring after a pretension of 15kN for the 20-tonne rock bolt, whereas this point was reached at a pretension of 10kN for the 30-tonne samples.

Table 6-1: Analytical estimates of shear and displacement parameters for clean shear testing scheme

Rock Bolt Scenario	K_e (N/m)	Elastic Yield (kN)	K_p (N/m)	Peak Shear (kN)	K_f (N/m)	ϕ (°)	α
10KN20TC	27670	38.73	20900	133.6	-55430	10	0.422
15KN20TC	29830	41.46	20900	136.3	-28410	10	0.425
20KN20TC	31560	44.81	20900	133.7	-11290	10	0.600
0KN30TC	16680	37.02	20942	157.6	-1933	10	0.315
10KN30TC	13810	26.37	20942	125.8	-63200	10	0.308
15KN30TC	27760	51.64	20942	119.3	-14320	10	0.428
20KN30TC	25450	33.85	20942	122.5	-10790	10	0.483

6.2.4 Model calibration for reinforcing infilled joints

The outlined analytical model was also developed to simulate the shear response of rock bolts when subjected to infilled joints. To ensure consistency across all the test scenarios, the same subroutine program was utilised. As such, the development of the simulation went through the same stages as the 20-tonne clean joint samples with the exception of one key factor. The addition of the infilled material also added the requirement to account for its specific material properties. This was accomplished by changing the value of the friction angle, ϕ , and the addition of the cohesion parameter outlined in Table 6-2. These properties were determined through laboratory analysis of the infill material and were only valid for the tested double shear scenarios of this study.

Like the clean interface samples, the subroutine program required the input of the elastic region transition point, otherwise referred to as the turning point as depicted in Figure 6.9. This point had significant impacts on the estimations of the length of the elastic and strain-softening regions as well as the slope of the latter. Therefore, the experimental results were used to validate the selection of this point. Following the selection of the turning points, the subroutine programme adjusted the α coefficient in conjunction with error validation to ensure that the simulation accurately captured the slope and the peak shear value. Inadvertently, calibrating the slope and peak value intersect also resulted in a suitable approximation of the shear failure displacement. Figure 6.10 illustrates this impact of α on the outlined aspects of the shear failure profile.

Table 6-2: Analytical estimates of shear and displacement parameters for infilled shear interface testing scheme

Rock Bolt Scenario	K_e (N/m)	Elastic Yield (kN)	K_p (N/m)	Peak Shear (kN)	K_f (N/m)	ϕ (°)	Cohesion (Pa)	α
0KN20TINFILL	10370	25.94	20900	89.45	-5455	0.0963	2190	0.224
10KN20TINFILL	25230	35.32	20900	100.3	-4212	0.0963	2190	0.234
15KN20TINFILL	14350	33.15	20900	88.39	-1123	0.0963	2190	0.252
20KN20TINFILL	28890	44.2	20900	94.47	-4071	0.0963	2190	0.265
0KN30TINFILL	8007	25.78	20942	79.14	-45400	0.0963	2190	0.178
10KN30TINFILL	9570	25.17	20942	114.6	-5293	0.0963	2190	0.282
15KN30TINFILL	6203	18.11	20942	69.06	-25200	0.0963	2190	0.256
20KN30TINFILL	13840	39.99	20942	114.5	-12450	0.0963	2190	0.229

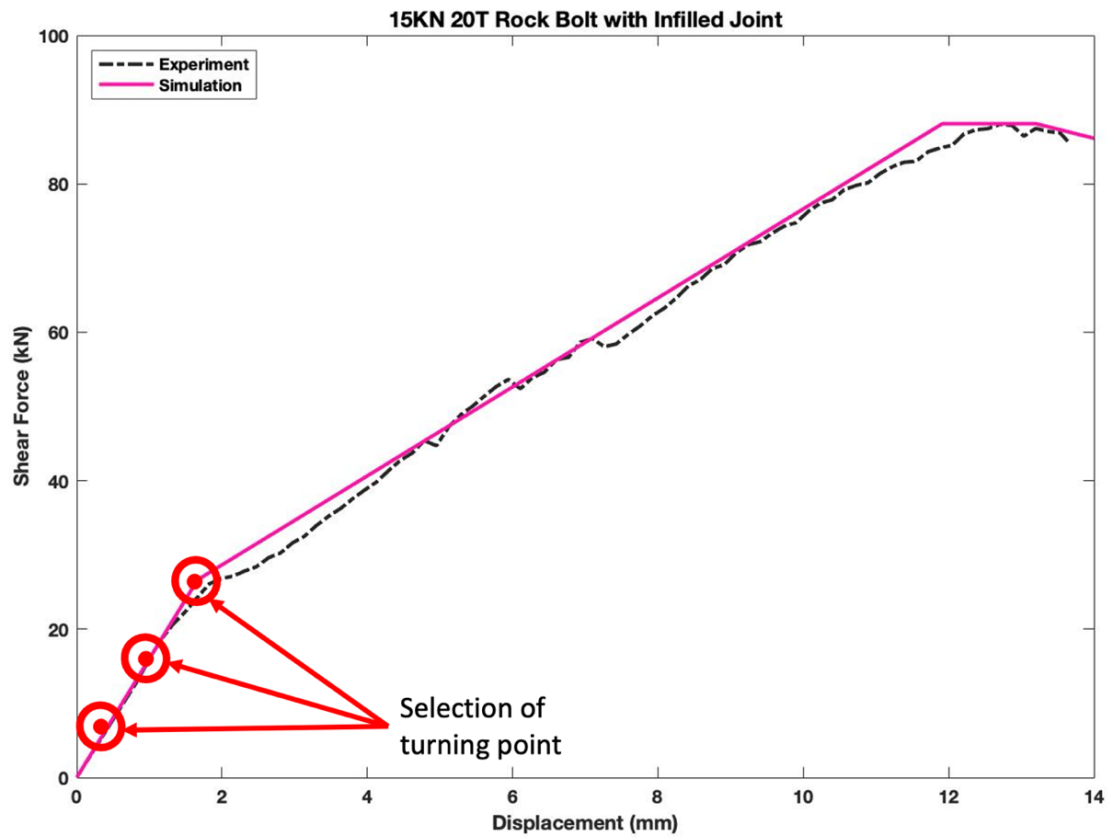


Figure 6.9: Determining the transition to the strain-softening region for infilled samples.

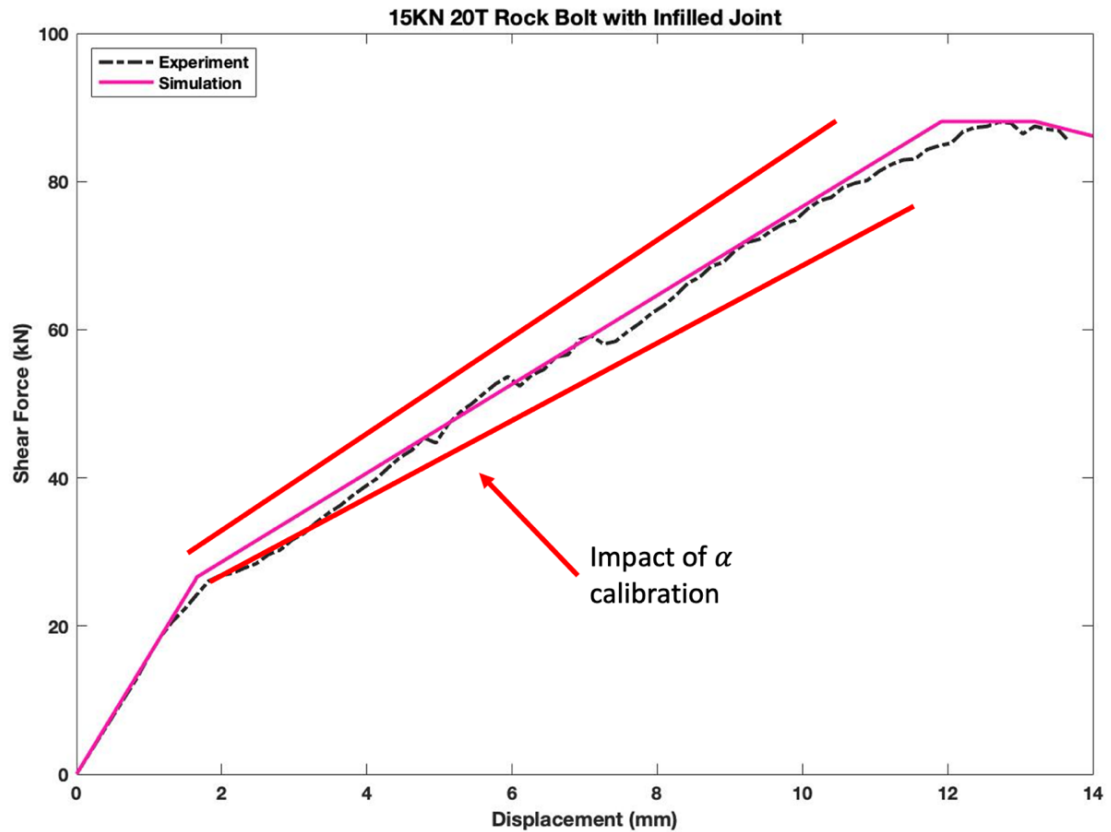


Figure 6.10: Calibration of the strain-softening region for samples with infilled shear interfaces using the α constant to ensure model agreement

Once the optimal simulation settings were established, they were recorded in Table 6-2 and the outputs highlighted in Figure 6.11. Similar to the experimental results outlined in sections 5.3 and 5.4, the simulation captured the influences of the rock bolts' strength and pretension for infilled samples. Despite the same analytical model utilised for both clean and infilled test scenarios, the infilled models presented with fewer plotted complexities. Unlike the clean joint models, the infilled joint models presented with no step between the elastic and strain-softening regions as highlighted in Figure 6.12. Infilled simulations also presented with a less pronounced step between the strain-softening and failure regions. Scenarios subjected to the clean joint testing scheme demonstrated notable differences between 20-tonne and 30-tonne samples when comparing the presence of vertical stepping at the transition point between the elastic and strain-softening regions. The infilled testing scheme however, demonstrated no such variations between the 20-tonne and 30-tonne samples. Additionally, the simulated samples presented with no step at the elastic transition point. The appearance of the step occurring at the failure transition zone was indicative

of the failure process. When the experimental samples reach their failure limit, the shear forces levelled out briefly before transitioning to their residual force. Hence why in Figure 6.12 the failure transition point was highlighted as not representing a transition step.

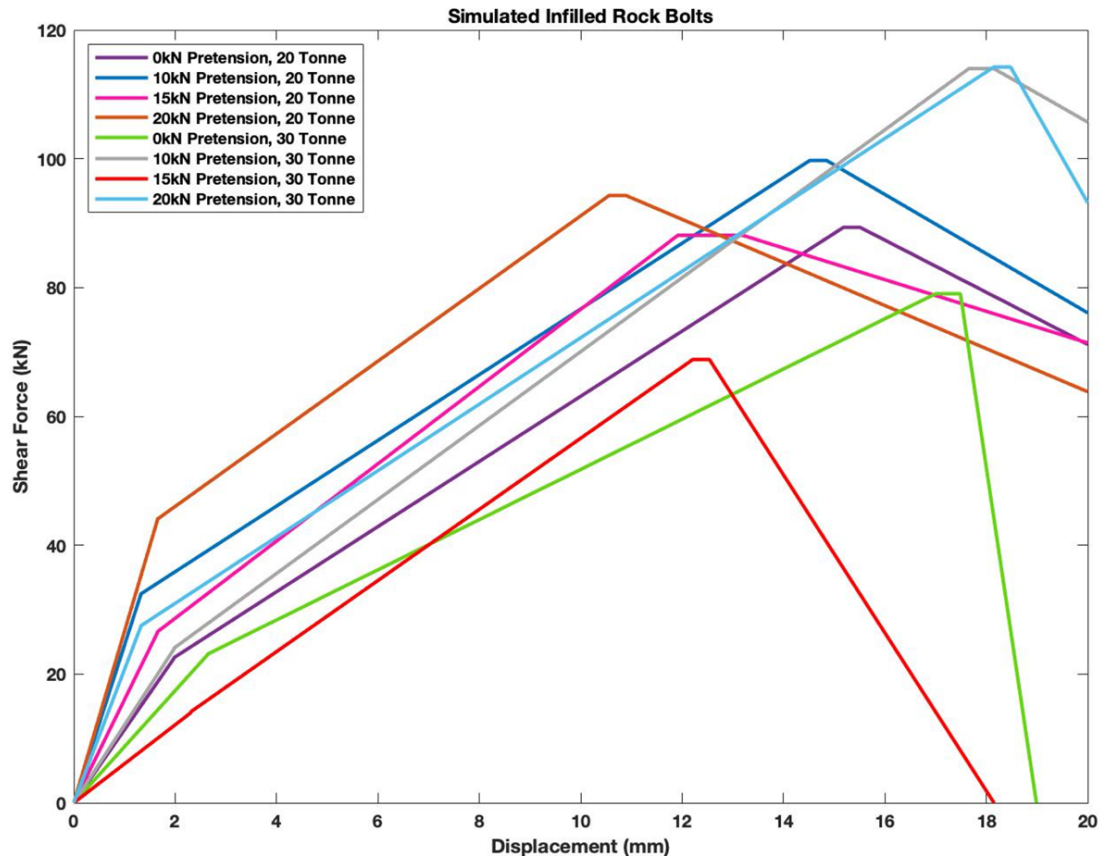


Figure 6.11: Analytical simulation results for infilled joint testing scheme

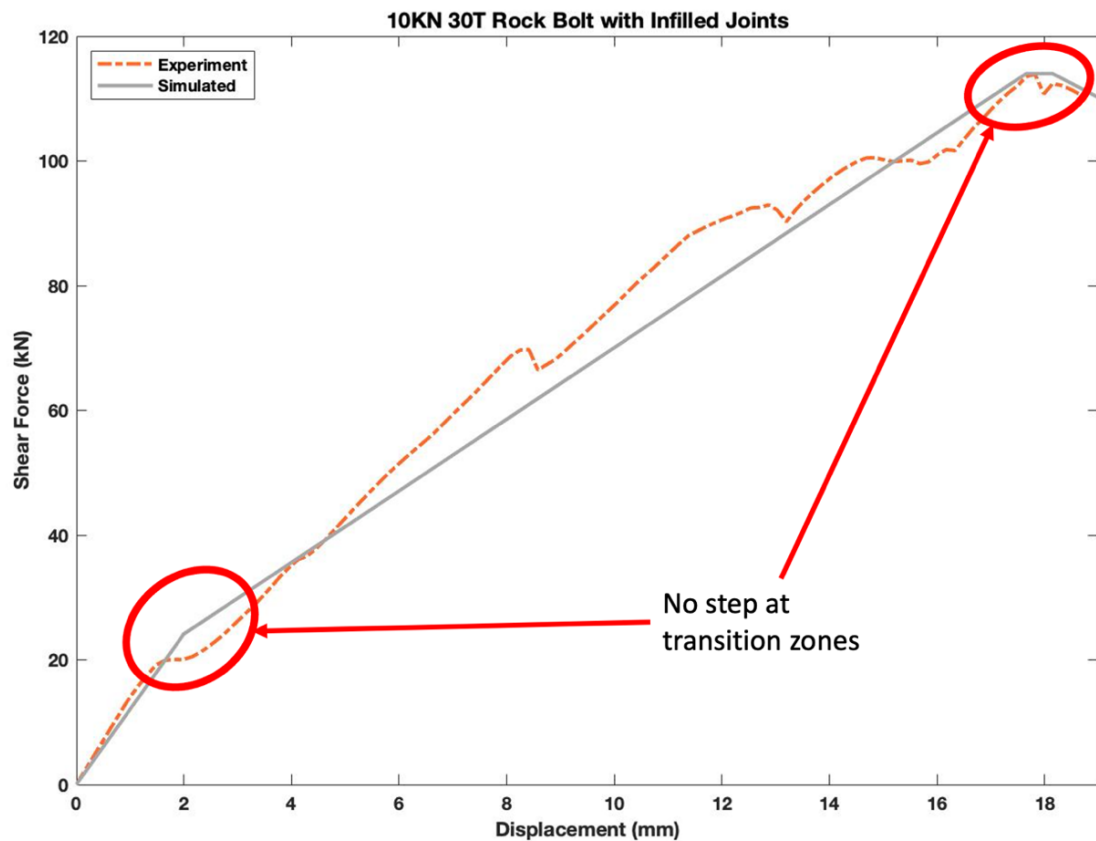


Figure 6.12: Challenges in simulating the transition zones between the regions for 30-tonne rock bolts with infilled joints

The analytical model can be used for simulating numerous scenarios outside its design. The input and output variables specified for this model were developed to accommodate user specific situations. By incorporating variables such as the α coefficient into the analytical model, the performance of samples with properties such as pretensions not directly tested in this study can be determined by approximation using functions such as Piecewise Linear Interpolation. This progressive design approach resulted in a robust analytical model that has the capability to simulate a host of scenarios subjected to fibreglass rock bolts.

6.3 3D numerical simulation

FLAC3D, the modelling software designed by ITASCA was utilised in this research to develop advanced numerical simulations due its widespread deployment within industry. Software such as FLAC3D are actively utilised tools to conduct advanced simulation analysis for civil and geotechnically related fields such as: ground water design and management, soil analysis, foundation design, tunnelling and slope stability. For the purpose of this study scheme, FLAC3D was used to simulate:

1. The single shear and double shear performance of rock bolts subjected to the same conditions as the experimental test scheme for data validation,
2. Sensitivity analysis of both single shear and double shear test scenarios focusing on variations to host environment, shear speed and installation angle.

FLAC3D was chosen due to its unique ability to conduct a wide range of geomechanical structural analysis. This software can analyse the interaction of arbitrary geometric structures with soil or rock masses (Itasca, 2005). Incorporated in the software's core functions are a variety of structural elements, constitutive models and material failure properties, allowing users to determine the most appropriate model group for their simulation.

6.3.1 Development of the rock bolt model

The pile structural element with the activated rock bolt flag was chosen for all test simulations. Unlike other elements such as the cable element, piles allow the user to utilise rock bolt specific properties such as resistance to bending moments resulting in a simulation that better represents the performance of rock bolts. Unfortunately, there is not one perfect element and therefore compromises were made. The most significant shortcoming of the selected rock bolt element was the inability to effectively apply pretension to the rock bolts. This property is inherent in the cable structural element. Attempts were made to modify the simulation, however no variation to the model yielded accurate results.

The FLAC developed rock bolt model is a highly versatile model adopting features from piles, beams and cable bolt elements. This allowed the rock bolt model to include both the normal and shear friction, stiffness matrix and plastic bending moment (Itasca, 2002). Rock bolt elements simulate the mechanical behaviour of the element by deconstructing the rock bolt into nodes. Each node is then separated by a series of springs also known as coupling springs, with one of each representing the axial stiffness, the shear stiffness and cohesive strength at each node as highlighted in Figure 6.13.

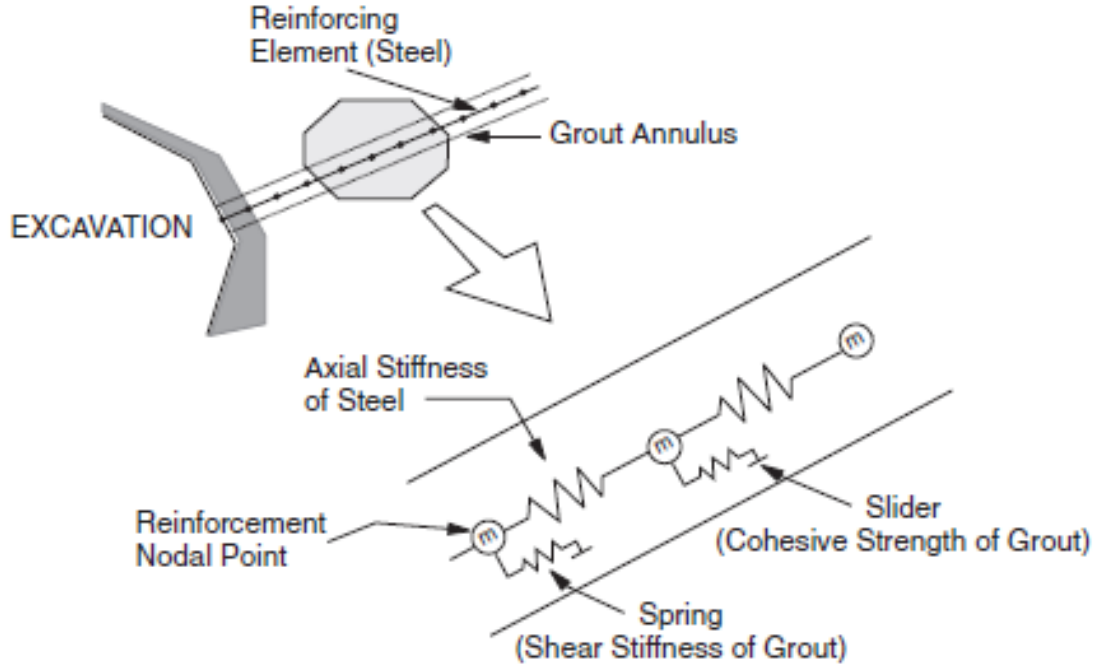


Figure 6.13: FLAC3D Coupling spring concept (Itasca, 2005)

The defined coupling springs convention facilitates a one-dimensional explanation for each of the defined behaviours. As such, the axial behaviour is reduced to its primitive relationship between the axial stiffness K as calculated across the rock bolts cross-sectional A , its Young's modulus E and lastly its length as outlined by equation 6.12.

$$K = \frac{AE}{L} \quad (6.12)$$

Similarly to the axial calculations, the shear behaviour of the rock bolt was simplified to an ideal state to facilitate computational simplicity. To achieve the desired outcome, the spring model outlined in Figure 6.13 was used to simulate a slider effect along the interface annulus. Therefore, the shear behaviour became a function of the coupling spring material and interface properties such as: stiffness k_s , cohesive strength c_s , friction angle ϕ_s and the rock bolt perimeter p as illustrated by Figure 6.14.

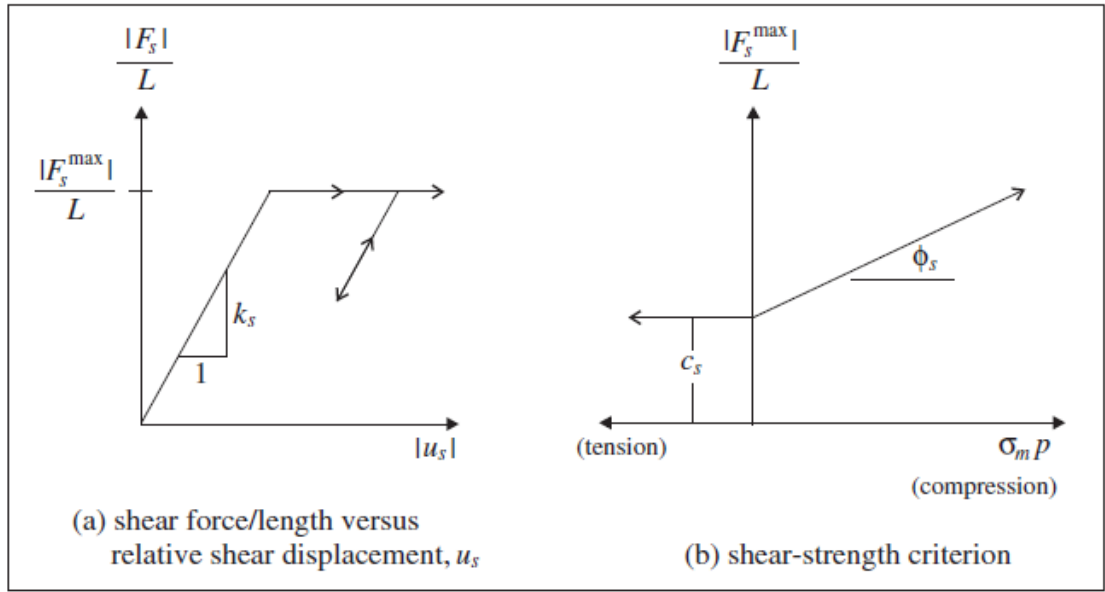


Figure 6.14: Shear behaviour of rock bolt elements (Itasca, 2005)

The overall mechanical behaviour of the rock bolts in the normal plane then become a function of the confining stress. Figure 6.14 further demonstrates the distinction between nodes in compression and in tension, where friction angle and cohesive strength are key drivers of the node's response respectively. The confining stress was calculated as a relationship between the principal stresses σ_1 and σ_2 and pore pressure p as defined by equation 6.13.

$$\sigma_m = -\left(\frac{\sigma_1 + \sigma_2}{2} + p\right) \quad (6.13)$$

The last key calculation component within the rock bolt property was the rock bolt extension otherwise defined as the tensile behaviour of the rock bolt. This property considered the axial and bending resistance of the simulated nodes unlike the cable simulation equivalent which only considered the axial resistance. As a result, this property was defined as the relationship between axial plastic strain ε_{pl}^{ax} , rock bolt diameter and length, d and L respectively and lastly θ_{pl} the elements average angular rotation. The calculation was expressed using equation 6.14 and defined within FLAC as the tensile failure strain.

$$\varepsilon_{pl} = \sum \varepsilon_{pl}^{ax} + \sum \frac{d}{2} \frac{\theta_{pl}}{L} \quad (6.14)$$

These rock bolt properties were implemented as part of the FLAC3D subroutine program and initiated prior to commencement of the simulation. Table 6-3 outlines each of the selected properties and their input values.

Table 6-3: 20-tonne and 30-tonne rock bolt simulation properties

Rock bolt Properties		
Rock Bolt Type	20-tonne	30-tonne
Youngs Modulus	69.4 x 10 ⁹ Pa	68.4 x 10 ⁹ Pa
Poisson Ratio	0.25	0.25
Cross-sectional Area	3.14 x 10 ⁻⁴ m ²	3.14 x 10 ⁻⁴ m ²
Perimeter	0.0628 m	0.0628 m
Ultimate Tensile Strength Properties		
Tensile Yield	6.75 x 10 ³	1.5 x 10 ⁴
Tensile Failure Strain	0.025	0.03
Plastic Moment	2.21 x 10 ³	2.9 x 10 ³
Moment of Inertia Y Direction	3.3 x 10 ⁻⁸	3.3 x 10 ⁻⁸
Moment of Inertia Z Direction	3.3 x 10 ⁻⁸	3.3 x 10 ⁻⁸
Polar Moment of Inertia	7.85 x 10 ⁻⁹	7.85 x 10 ⁻⁹
Coupling Cohesion Shear	5.15 x 10 ⁶	5.15 x 10 ⁷
Coupling Stiffness Shear	9.5 x 10 ⁷	6.12 x 10 ⁷
Coupling Cohesion Normal	5.95 x 10 ⁶	9.95 x 10 ⁷
Coupling Friction Normal	45	45
Coupling Stiffness Normal	3.75 x 10 ⁸	5.5 x 10 ⁸
Coupling Friction Shear	45	45

6.3.2 Developing the rock and joint model.

The construction of the shear environment required careful selection of the material constitutive models within the FLAC3D library due to the vast differences in their mechanical behaviours. The system was defined by the following four components:

1. The host rock,
2. The washers,
3. The infill material, and
4. The overall model environment.

Models were chosen based on their ability to replicate material performance for each system component as determined by the experimental results. A strain-softening model was applied to the concrete simulating the host rock. This enabled the model to

simulate the impacts of cohesion, friction and dilation during the shearing process as applied forces may either soften or harden the host rock.

For some components of the model this depth of data was unnecessary and a potential hindrance to the overall performance of the system. In the case of the washer, an elastic model was implemented as the material was homogeneous and isotropic and only required the simplest material representation.

The infill material manufactured for testing was a soil-clay derivative and as a result the Mohr-Coulomb model was applied as this provided an accurate representation of the shear failure of soils. Finally, mechanical damping was applied to the entire environment to compensate for system losses due to vibration. Without an applied damping, components within the simulation can begin to oscillate and distort results.

Table 6-4 outlines each of the selected properties and their input values for each of the system elements such as the strata, clean and infilled joints and the rock bolt washers.

Table 6-4: System properties for the strata, shear joints, infill material and washers

Strata Properties	
Density	2400 kg/m ³
Bulk Modulus	11 x 10 ⁹ Pa
Shear Modulus	10 x 10 ⁹ Pa
Cohesion	8.93 x 10 ⁶
Friction Angle	49.05
Tensile Strength	4.7 x 10 ⁶
Dilation	12
Washer Properties	
Normal Stiffness	1000 Pa
Shear Stiffness	1000 Pa
Friction	45
Cohesion	0
Clean Shear Interface	
Normal Stiffness	1000 Pa
Shear Stiffness	500 Pa
Friction	8.5
Cohesion	7.173 x 10 ³
Infilled Shear Interface	
Density	2000 kg/m ³
Bulk Modulus	20 x 10 ⁹ Pa
Shear Modulus	3.94 x 10 ³ Pa
Cohesion	2.19 x 10 ³
Friction Angle	5.5

6.3.3 Single shear conceptual model

A simulated test environment was created to determine the pure single shear performance of the 20-tonne rock bolts. The conceptual model highlighted in Figure 6.15 demonstrates the schematic design uploaded to FLAC3D where 'X' denoted planes fixed to the *y-axis* and 'V' denoted elements fixed to the *x-axis*. Fixing the host block to the *x-axis* ensured that the shearing force could be enacted while allowing the block to still experience dilation movement. Similarly, the rock bolt element was fixed to the *y-axis* at its outer most nodes to simulate the element being bolted to the extremities of the sample as well as preventing the simulation from pulling the element through the block. For simplicity, the model was created using rectangular block with a width and depth of 100mm and a height of 200mm. The properties of the blocks were set to arbitrarily high values to ensure a pure shearing action was achieved. To ensure accuracy of the simulation, various grid densities were trialled until one was found to provide simulation efficiency and accuracy. The selected grid density instructed the software the position where the calculation was to be completed, as well as the total number of calculation nodes draped across the model. Increasing the grid density resulted in increased accuracy in reaction force mapping. However, this also resulted in increased simulation runtime. This grid property was determined to be 10 x 10 x 10 as this provided the fastest simulation runtime while also providing adequate model accuracy. The node spacing along the rock bolt element was determined in a similar method along with the addition of the node's location to the shear interface. If the node spacings were too far apart they were unable to determine the rock bolts' behaviour at the shear interface. Therefore, 40 segments were identified to develop an ideal representation of the rock bolts' shear performance.

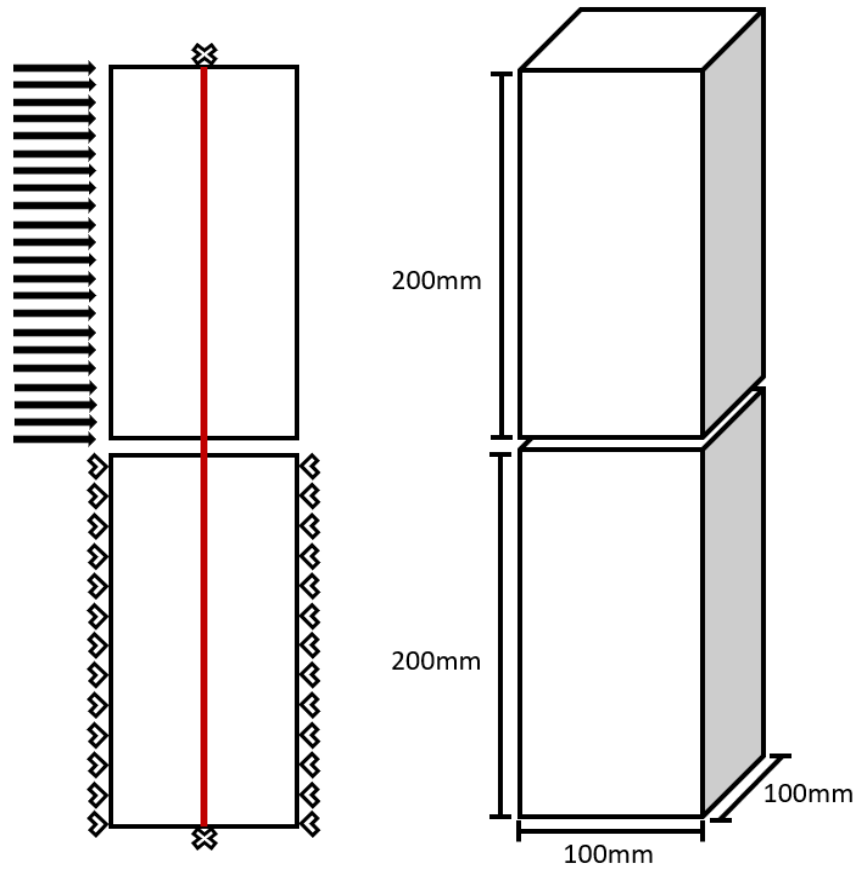


Figure 6.15: Single shear conceptual model (left) and model dimensions (right)

6.3.4 Numerical simulation of single shear

To simulate the single shear scenario, the conceptual model was uploaded to FLAC3D and the outcomes were compared to the experimental dataset as highlighted in Figure 6.16. While the model was able to accurately predict properties like the elastic transition trough, peak shear force, peak displacement and post failure response as demonstrated in Figure 6.17, it lacked agreement in predicting the shear forces at earlier displacements. This could be attributed to the simulation anticipating a perfect world scenario with little to no imperfections within the system. Such an assumption could result in the higher shear forces at low displacements as there are no imperfections to dampen the transfer of forces. As the shear forces increased, the experimental dataset showed closer alignment to the simulation as the forces were now great enough to overcome the damping effects.

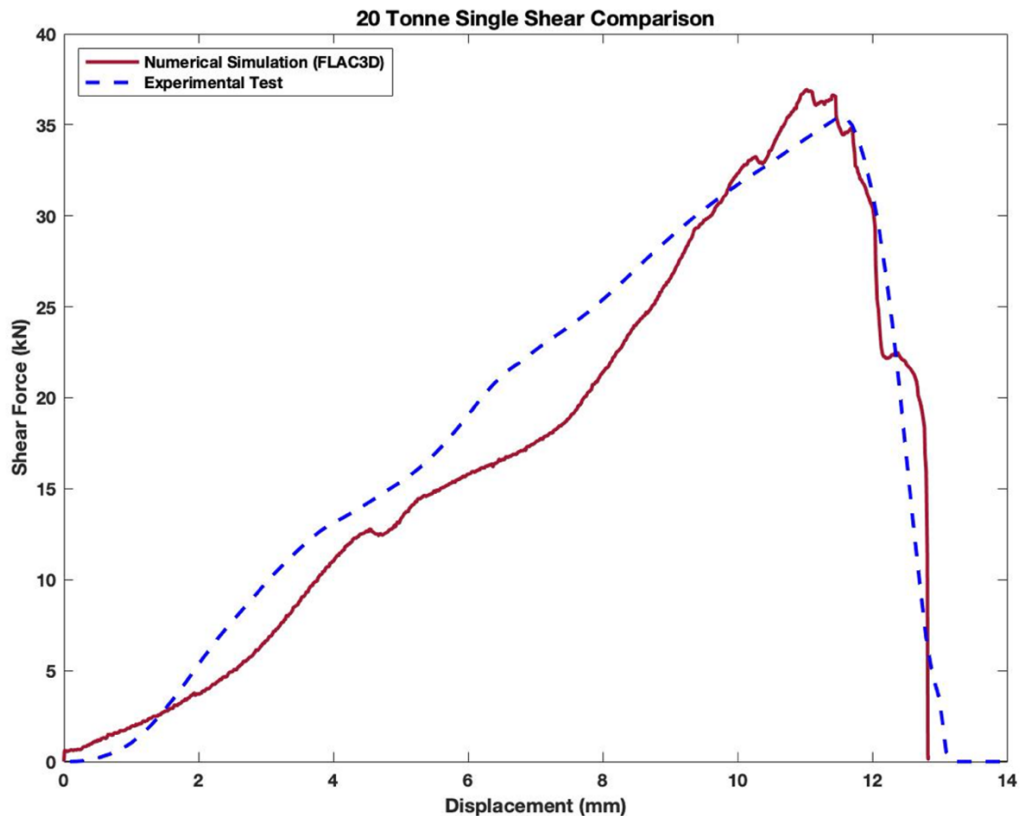


Figure 6.16: Results of the numerical simulation and experimental test for the 20-tonne rock bolt subjected to single shear.

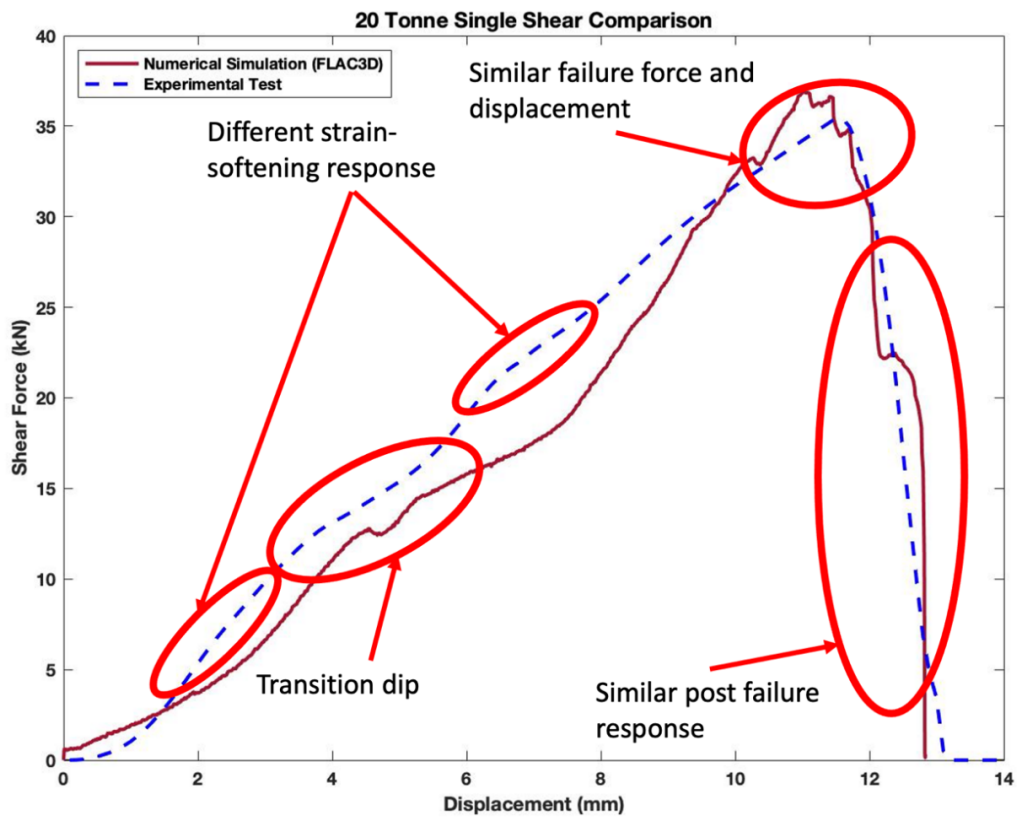


Figure 6.17: Comparison of the numerical simulation and experimental test for the 20-tonne rock bolt subjected to single shear.

6.3.5 Double shear conceptual model

A simulated test environment was also created to determine the double shear performance of the rock bolts. The conceptual model highlighted in Figure 6.18 demonstrates the schematic design uploaded to FLAC3D. Mimicking the experimental testing scheme, the outer two blocks were fixed in space with the centre block freed for shearing. A displacement equivalent to 1mm/minute was applied to the top surface of the block to simulate the shearing action. Additionally, to prevent the rock bolt pulling through the block and failing prematurely, the first and last node of the rock bolt were fixed in place in a similar fashion to utilising the nut. Unlike the single shear model, the double shear model was designed to replicate the design of the experimental tests. Therefore, the outer two blocks were created to the dimensions of 200mm by 200mm by 200mm and the centre block with dimensions of 200mm by 400mm by 200mm as illustrated in Figure 6.18.

Additionally, the material properties of the blocks were based on realistic material properties in accordance with the experimental study and were outlined in Table 6-4. The grid properties were determined by trial and error to identify the most accurate and efficient completion of each simulation. Selecting a grid as $1/20^{\text{th}}$ of the dimensions of the blocks resulted in fast computation with minimal change in results and therefore the final selected grids were 10 x 10 x 10 for the outer blocks and 10 x 20 x 10 for the centre block. Additionally, the rock bolt segments were required to match the double shear simulation and were unable to be transferred from the single shear simulations. Trialling various settings indicated that dividing the element into 70 segments provided the most suitable compromise.

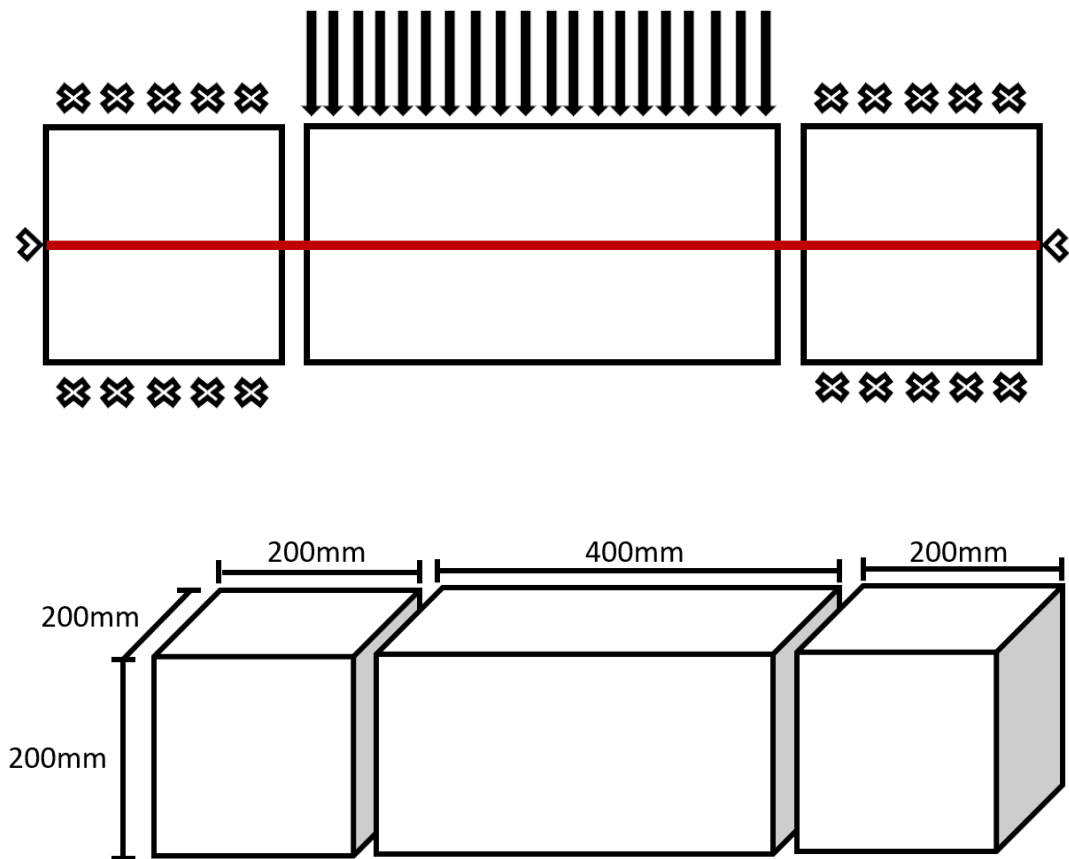


Figure 6.18: Double shear conceptual model (top) and model dimensions (bottom)

6.3.6 Numerical simulation calibration of double shear clean joints

The double shear simulation process underwent calibration against the experimental testing scheme to ensure model accuracy. Calibrating against known metrics ensured that the numerical simulation could then be utilised to simulate scenarios not addressed by the conducted physical tests as well as sensitivity analysis. Due to the differences in rock bolt performance, both the 20-tonne and 30-tonne rock bolts were calibrated separately. The numerical simulations were limited to passive 0kN pretension test schemes, as such the 20-tonne model was calibrated against the 20-tonne 0kN pretension infilled shear test as shown in Figure 6.19. The 30-tonne model was calibrated against the 30-tonne 0kN clean shear test as highlighted in Figure 6.20. Unfortunately, due to inconsistencies present with the 20-tonne 0kN pretension clean joint experimental results, they were not considered an accurate representation of the rock bolts' performance and as such could not be calibrated against.

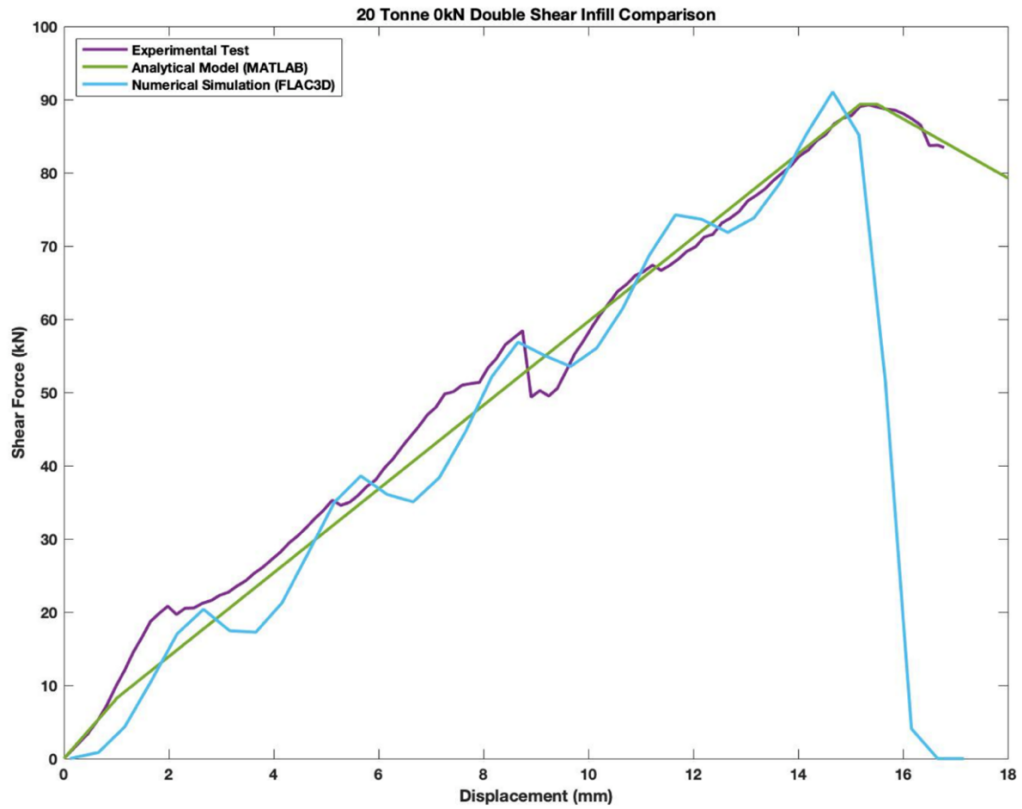


Figure 6.19: Experimental data, analytical model, and numerical simulation for 20-tonne infilled 0kN pretension sample.

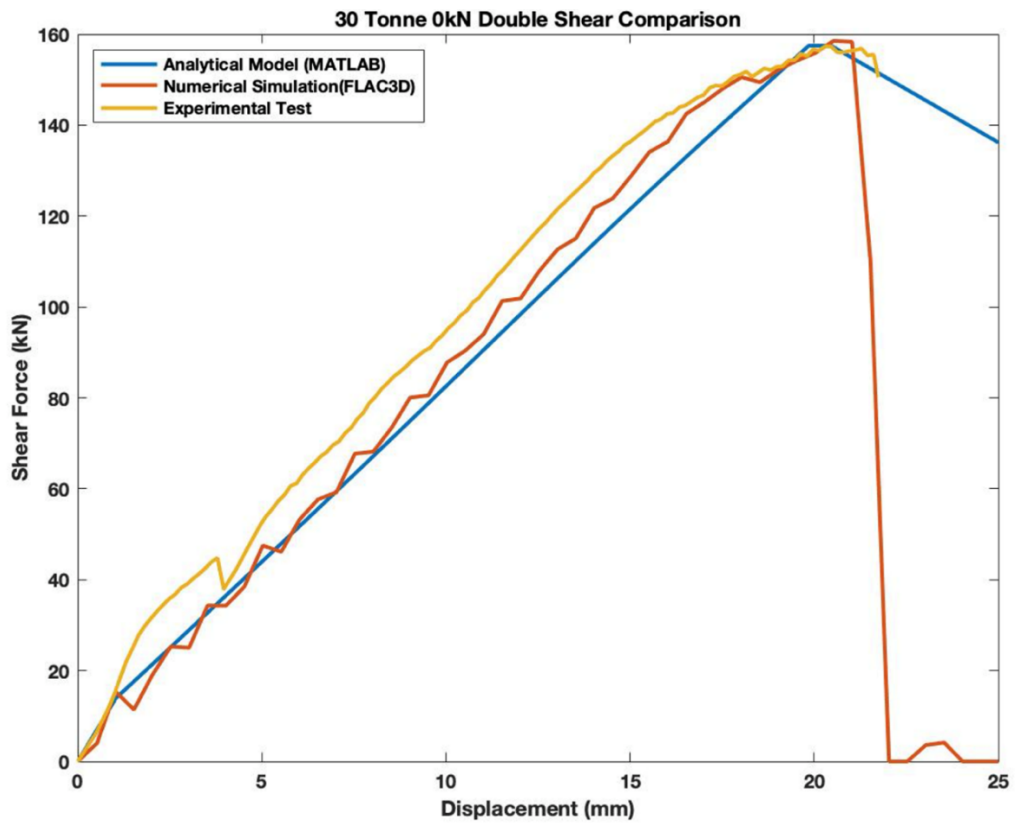


Figure 6.20: Experimental data, analytical model, and numerical simulation for 30-tonne clean joint 0kN pretension sample.

The chosen parameters resulted in successful calibration for the two rock bolt types with only minor variation between the three data types. The numerical model of the 20-tonne sample presented with good alignment to the experimental data set, most notably simulating similar transition zone properties, a feature not evident on the analytical model as shown in Figure 6.21. The simulation matched the undulating force response at the elastic transition zone with only a minor variation in displacement. The numerical model was also able to predict the various peaks and troughs during the entire shearing process. Despite some variance in the correlation with the experimental results, they provided an overall realistic representation of the shear/displacement response of the rock bolt. Throughout the numerical simulation, the recorded displacement for each stage of shearing did not align, however was consistently within 1mm of the experimentally tested samples. Additionally, the post failure portion of the model showed little correlation with the experimental data set. The numerical model indicated a steeper release of the shear force with almost no retained residual resistance 2mm after failure. The analytical and experimental results however indicated a retained shear force in excess of 90% presenting as residual forces 2mm post failure.

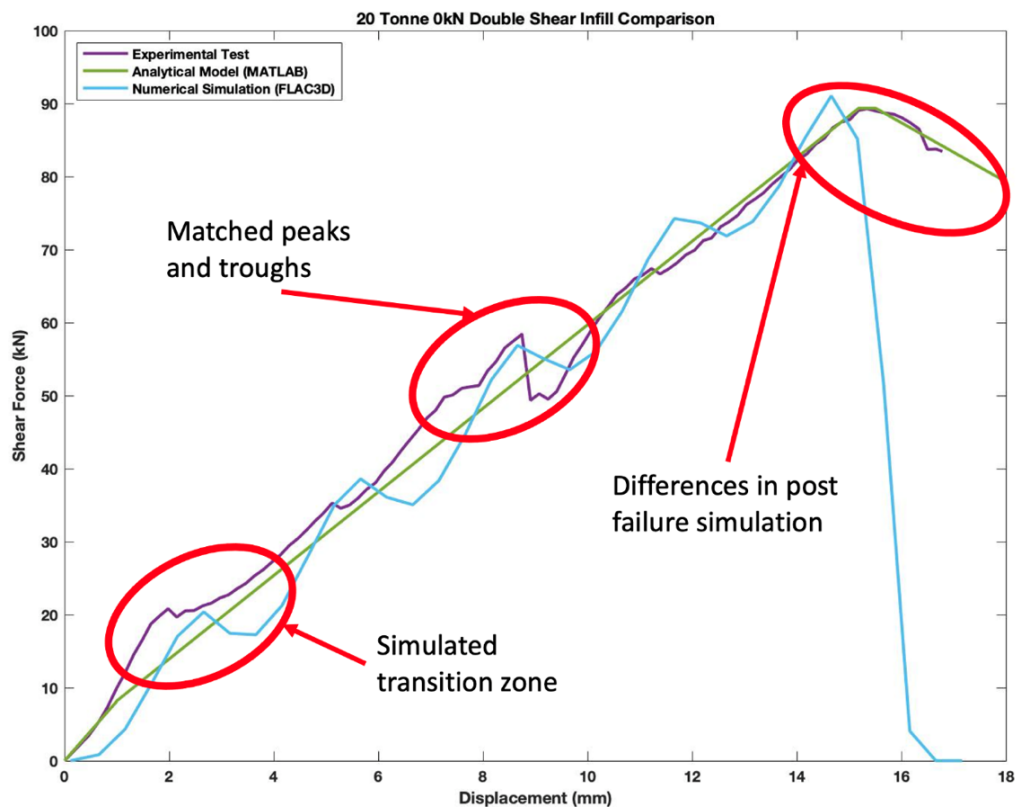


Figure 6.21: Comparison of experimental data, analytical model, and numerical simulation for 20-tonne infilled 0kN pretension sample.

The numerical simulation of the 30-tonne rock bolt with clean joint interfaces displayed similarities to both the analytical simulation and experiment confirming the model's ability to accurately replicate the shear response of the rock bolt. The FLAC3D based model was able to replicate key features of the shear profile such as the rate of increase of shear force, peak failure force and peak failure displacement. However, despite the overall agreement between the models and experimental results, there were several discrepancies with the shear profile as highlighted in Figure 6.22. While the numerical model was able to replicate various peaks and troughs throughout the shearing profile, they did not align with any present during experimental testing. This resulted in the inability to identify the transition point from the elastic region to the strain-softening region. Lastly, there was a disagreement between the numerical and analytical models with simulating the failure and post failure region of the shear profile. Despite this, the numerical model bore the closest resemblance to the experimental result with near identical peak failure displacement and failure force. Unfortunately, the post failure behaviour of the rock bolt could not be compared as the experimental result was cut off immediately after failure. The numerical simulation predicted an almost immediate release of shear resistance to a residual of 0kN, while the analytical predicted a gradual decline. While it was challenging to predict the actual behaviour of the post failure shear profile, the limited experimental data indicated similar trends to the numerical simulation, however further study would be required to confirm this.

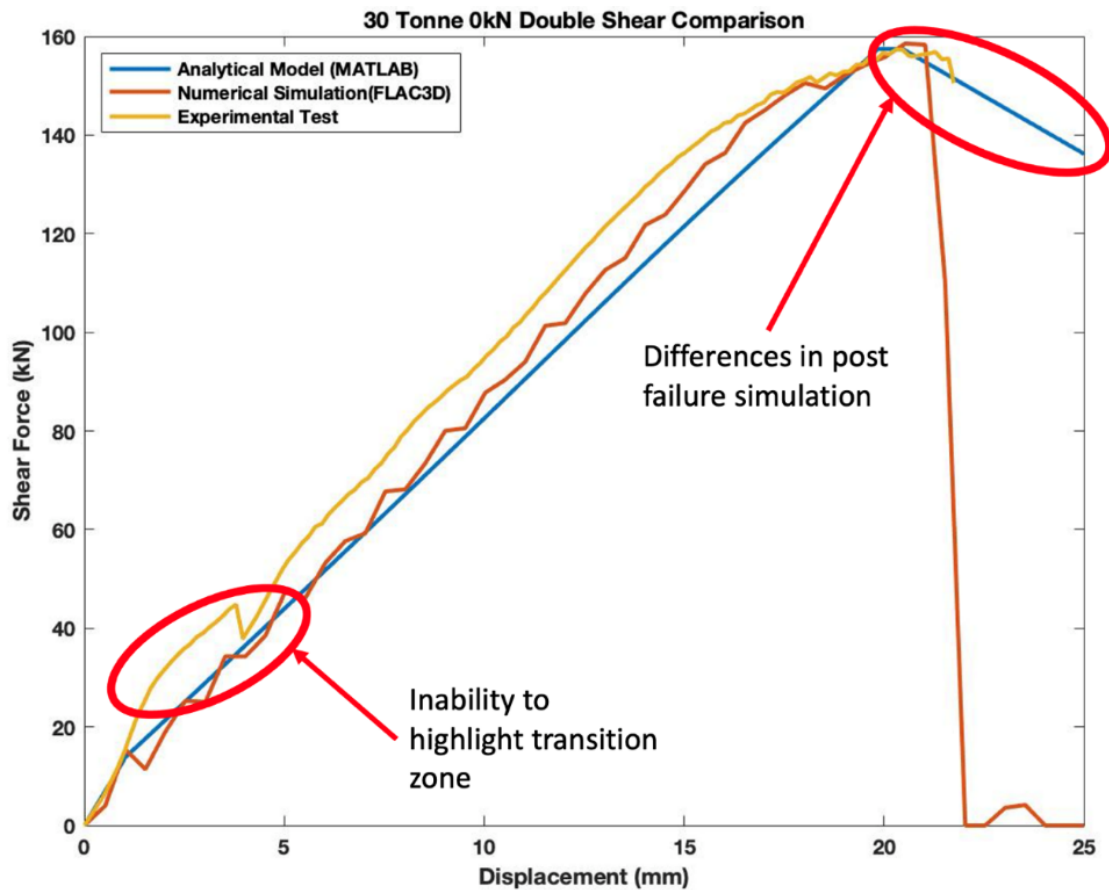


Figure 6.22: Comparison of experimental data, analytical, and numerical models for 30-tonne clean joint 0kN pretension sample.

6.4 Sensitivity analysis

The development of the above simulations enabled the determination of the rock bolts response to double shear forces under a range of conditions without the need to complete time consuming experimental studies. The validated numerical models were used to simulate the rock bolts' double shear response when subjected to a range of environmental variances such as host rock strength, speed of shear loading and rock bolt implementation to determine the rock bolts' sensitivity to changes within its system. For each scenario, the rock bolts were subjected to different parameters of interest such as: low to high strength host rock, slow, standard and fast shearing speeds and no angle and angled rock bolt installation. Their outcomes were then compared against the system parameters of the validated numerical simulation.

6.4.1 Host rock strength variation

Rock bolts can be installed in a variety of host rock types ranging in their parameters. Testing for these variations involve significant labour and time investments. Utilising the numerical model developed in this research allowed for the comprehensive testing of a range of host rock strengths for 30-tonne clean joint and 20-tonne infilled joint scenarios. Each scenario was repeated with rock UCSs of 20MPa, 30MPa, 40MPa and 60MPa. 40MPa was considered the baseline as it also directly reflected the experimental results. The 30-tonne clean and 20-tonne infilled scenarios demonstrated differing responses to changes in the host rock strengths, however for both rock bolt types, the initial differences were difficult to identify when analysing their full shear profiles. Both rock bolts needed to be examined closely to identify variances. The 30-tonne rock bolt samples looked identical initially as shown in Figure 6.23. However, upon closer investigation it was clear that increasing the UCS of the host rock impacted the shear force across the entire profile, while leaving the displacements unchanged. Figure 6.24 highlights the discrete increase of the shear force as well as features such as agreements, peaks and troughs. This impact of rock UCS on the performance of the rock bolt could possibly be attributed to 30-tonne rock bolts being able to outperform the host rock for shear resistance. Therefore, as the UCS increased, so did the rock bolt's ability to transfer the shear forces.

Similar to the 30-tonne rock bolts, the 20-tonne rock bolts also presented with negligible differences in their response to changes in the host rocks UCS as shown in Figure 6.25. However, unlike the 30-tonne rock bolt sample, the 20-tonne shear profile resulted in no discernible relationship to changes in host rock UCS. It is evident in Figure 6.26 that changing the host rock UCS had no impact on either the shear force response over the profile or its displacement. The variations observed were likely due to simulation variance and not as a direct result of the change in this parameter. This was likely caused by the weaker strength of the 20-tonne rock bolts. If the 20MPa host matched or outperformed the rock bolt's ability to resist shear forces, any increase would therefore result in no change to the rock bolts' shear profile as it was already performing to capacity.

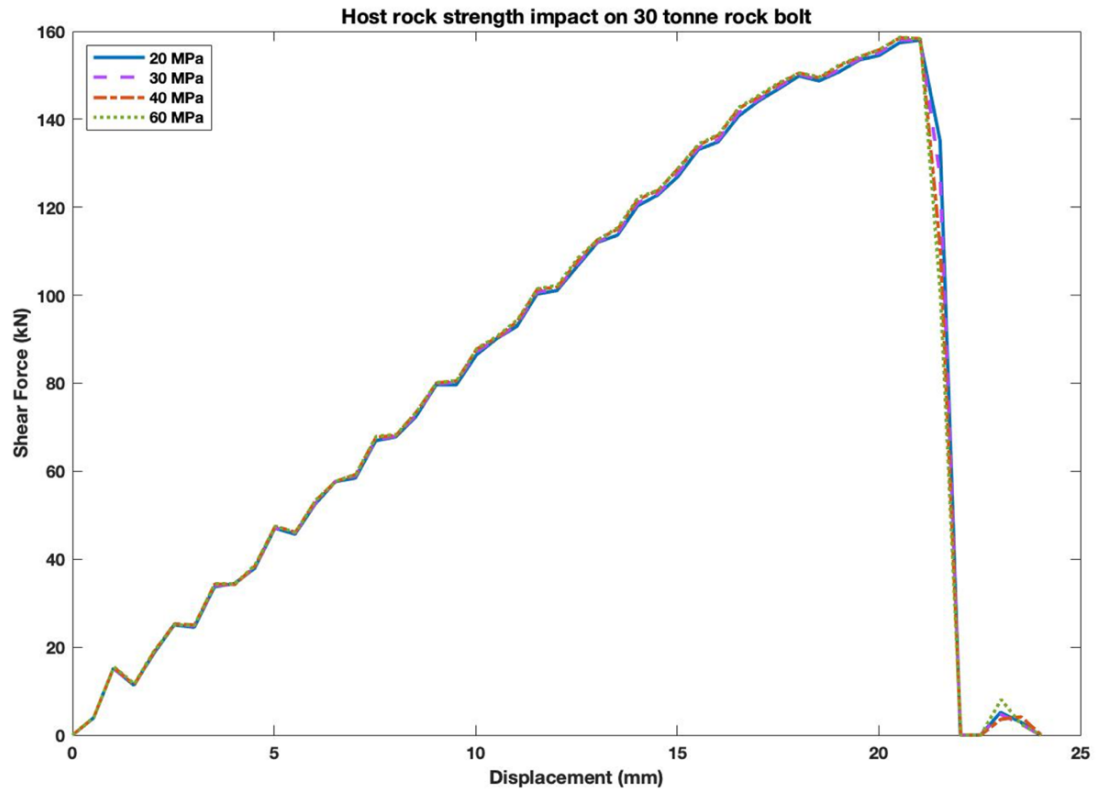


Figure 6.23: Results of changing the host rock UCS and its impact on the shear force of the 30-tonne rock bolt.

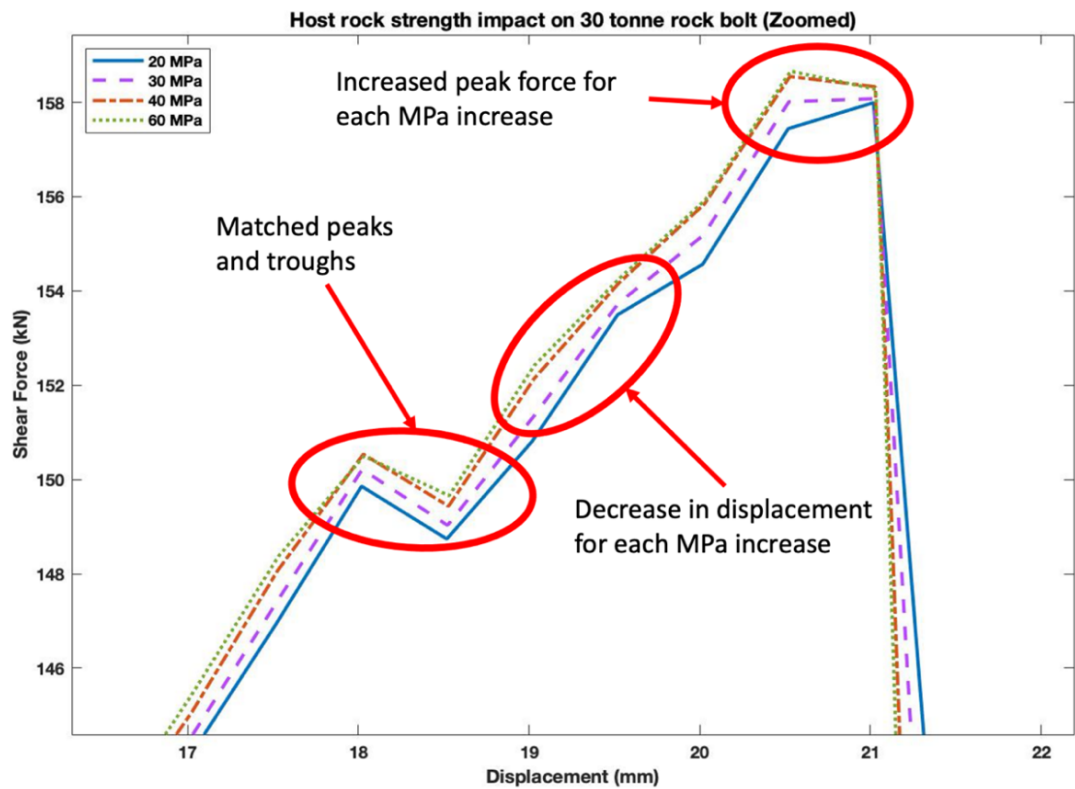


Figure 6.24: Zoomed in comparison of the effects of host rock strength on the shear force profile of the 30-tonne rock bolt.

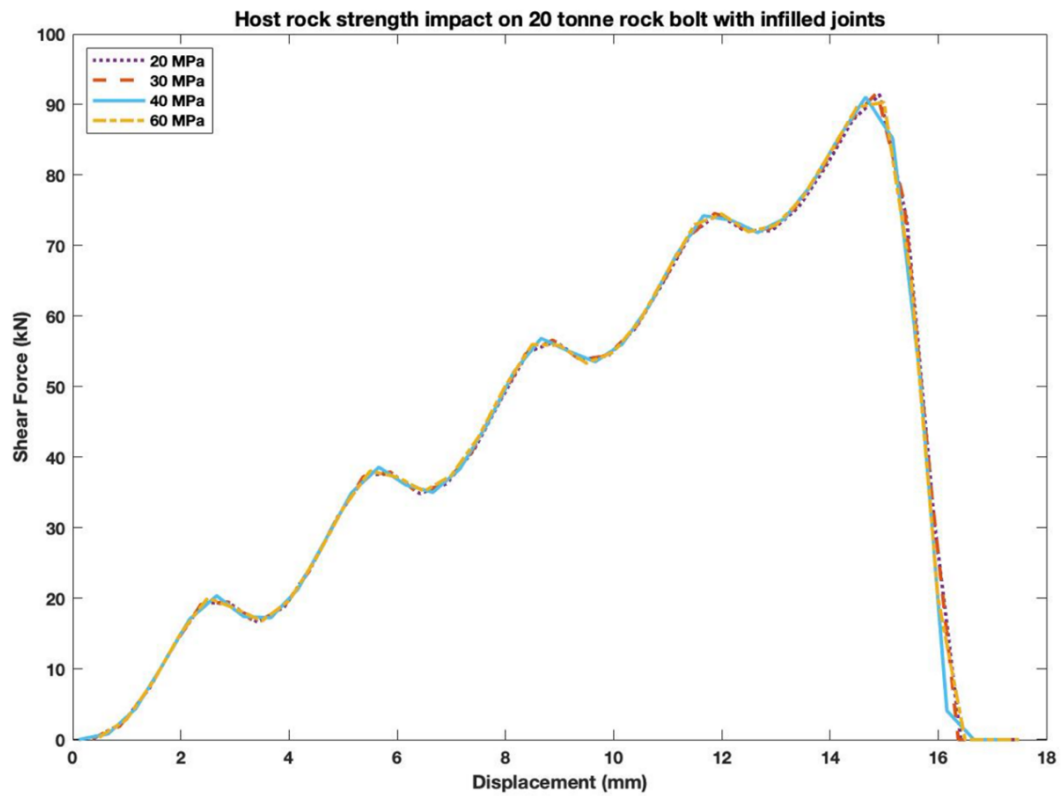


Figure 6.25: Results of changing the host rock UCS and its impact on the shear force of the 20-tonne infilled rock bolt

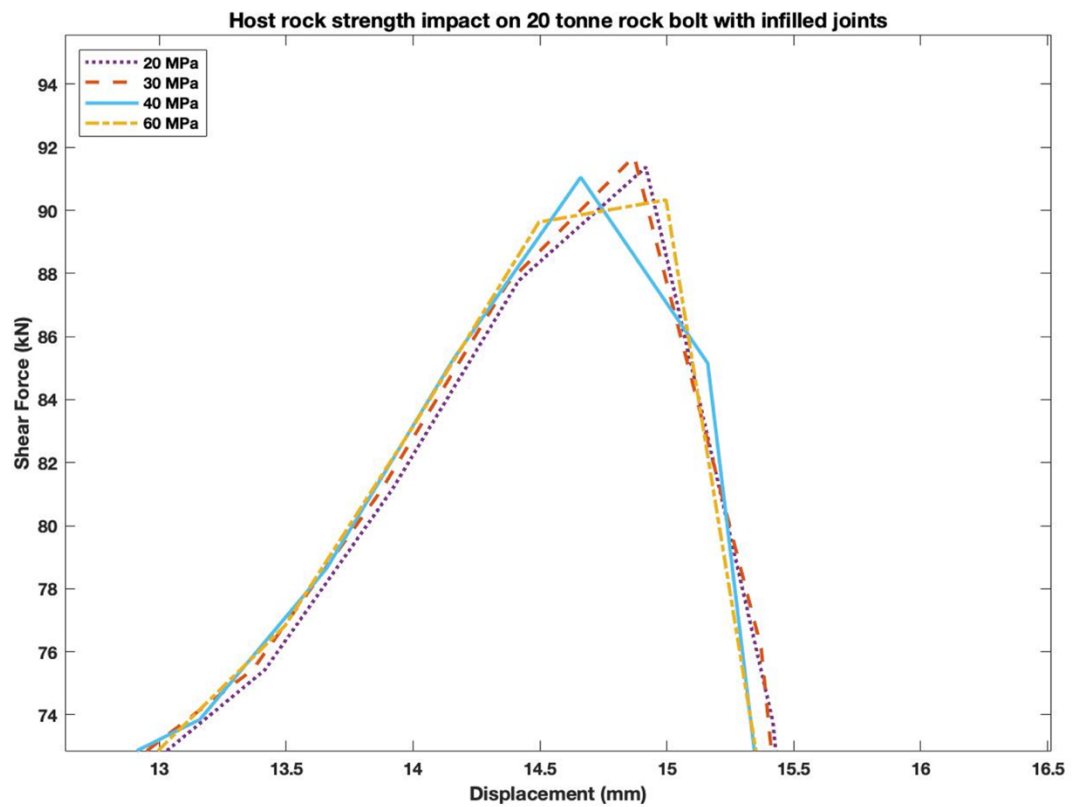


Figure 6.26: Zoomed in comparison of the effects of host rock strength on the shear force profile of the 20-tonne infilled rock bolt.

6.4.2 Rock bolt angle

The sensitivity analysis was extended to include the impact of the intercept angle of the rock bolt and shear joints. Shear joints are naturally occurring structures and are rarely uniform or perpendicular to the installed rock bolt. The numerical model was utilised to investigate the impact installing rock bolts at an angle other than 90 degrees to the shear interface. To accomplish this the modified conceptual model shown in Figure 6.27 was adopted.

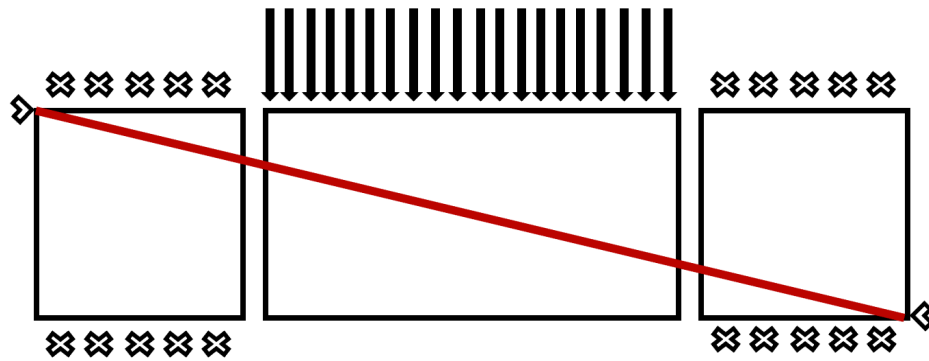


Figure 6.27: Conceptual model of the rock bolt installed at an angle.

The rock bolt was installed from the upper left to the lower right of the system to represent the most extreme angle possible within the tested design. All other properties of the system were retained to maintain consistency with the validated model. Greater angles could be accomplished but would require significant changes to the constitutive model requiring validation of a new model.

Both the 30-tonne clean joint and 20-tonne infilled samples presented with similar significant changes to the post failure responses of the rock bolts when compared with the experimentally verified model. Figure 6.28 and Figure 6.29 illustrates these differences as an immediate reduction to shear force post failure. The angled samples alternatively recorded a gradual reduction of shear forces until a residual load was achieved. This was most likely attributed to the one side of the rock bolt applying the shear force to a disproportionally small volume of the host rock, while the other half of the sample applying the same load to a disproportionally large volume segment. As a result complete shear only occurred at one of the shear planes resulting in the intact plane to carry the residual load.

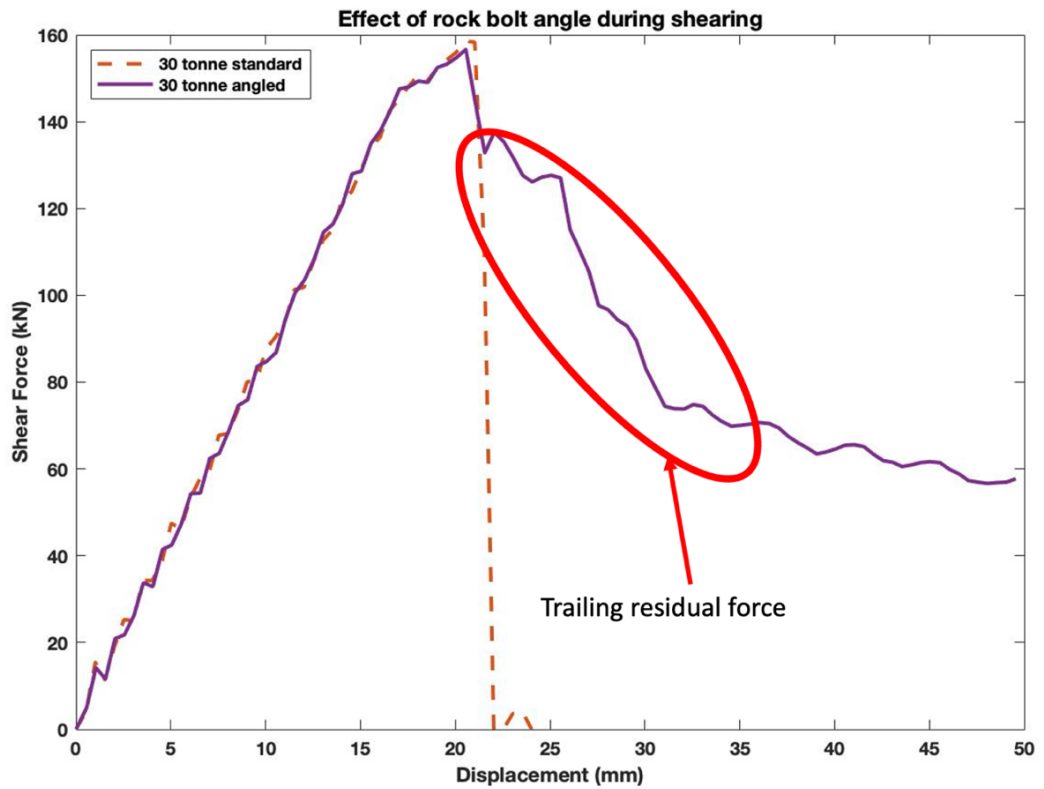


Figure 6.28: Impact of the shear force profile of a 30-tonne clean joint rock bolt installed at an angle compared to the original test parameter.

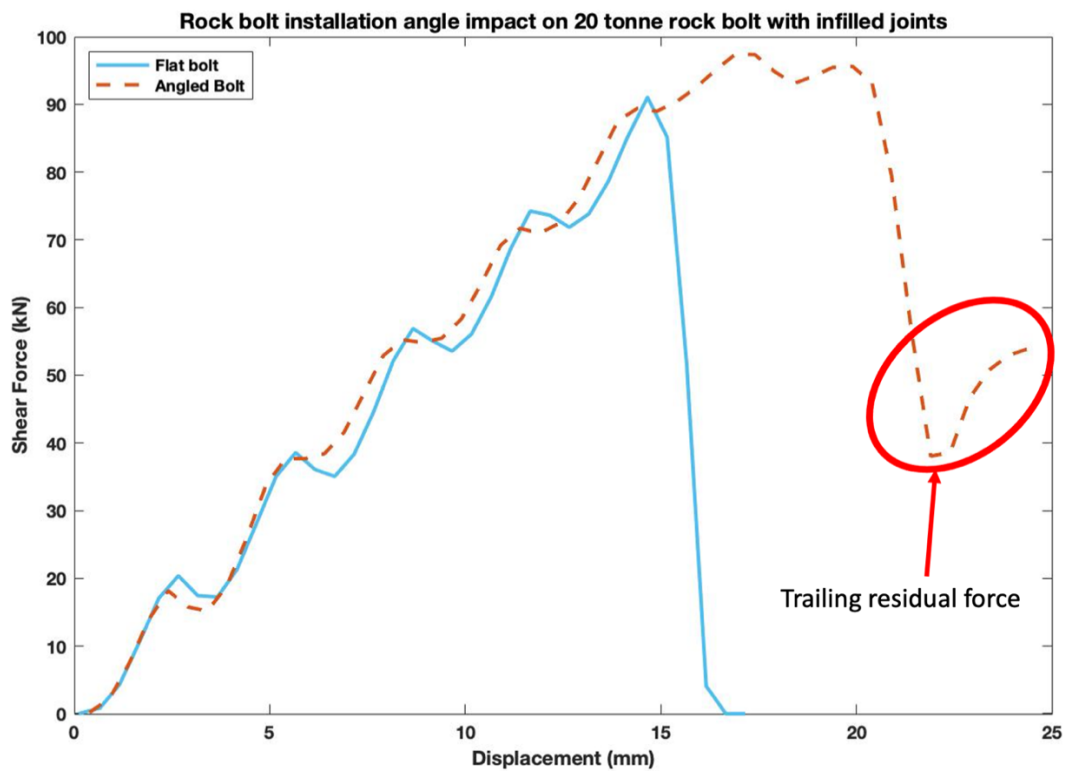


Figure 6.29: Impact of the shear force profile of a 20-tonne infilled rock bolt installed at an angle compared to the original test parameter.

6.4.3 Shear speed

The final system property tested for sensitivity was the rate of shear applied to the samples, reflecting the variations to shear that may be present in natural environments. The experimental shear property of 1mm/min was considered the baseline with samples then subjected to a slow speed scenario of 0.5mm/min and fast speed scenario of 1.5mm/min.

Changing the shear speed had profound impacts on the shear profile of the 30-tonne clean jointed rock bolt as highlighted in Figure 6.30. The impact of reducing the shear speed to 0.5mm/min was initially not evident on the overall profile, however, when zoomed in like in Figure 6.31, it was evident that the definition of shear profile was greatly improved. The jagged peaks and troughs were replaced with smoothed transitions. Increasing the shear speed to 1.5mm/min conversely resulted in a lower definition view of the shear profile with more significant exaggerations of the peaks and troughs. This change in the smoothness of the profile was most likely due to the slower shearing samples having more time to resolve variations in the absorption and repulsion of shear forces. Faster samples lacked the ability to find equilibrium to varying shear forces resulting in compounded peaks and troughs. Furthermore, increasing the shear speed completely altered the post failure response of the 30-tonne clean sample. Both the slow and baseline shearing samples experienced a dramatic release of shear forces to 0kN, while the fast-shearing sample experience a gradual decline in residual shear forces until it released to 0kN at a displacement double to that of the other two samples. As the 30-tonne sample was already determined to be stronger than the host rock environment, the increase in shear speed most likely caused failure within the rock structure preventing the rock bolt from achieving an absolute shear. Therefore, the sample relied on excessive displacement to achieve shear as opposed to applied shear force.

The 20-tonne sample however, presented with no notable responses to the change in shear speed. The sample presented with no change in profile definition and no changes to post failure response. This was most likely attributed to the weaker nature of the 20-tonne rock bolt and most importantly its weaker properties to that of the host rock. The 20-tonne sample was unable to overpower the host rock to achieve trailing residual forces as well as changes to the peaks and troughs of its shear profile.

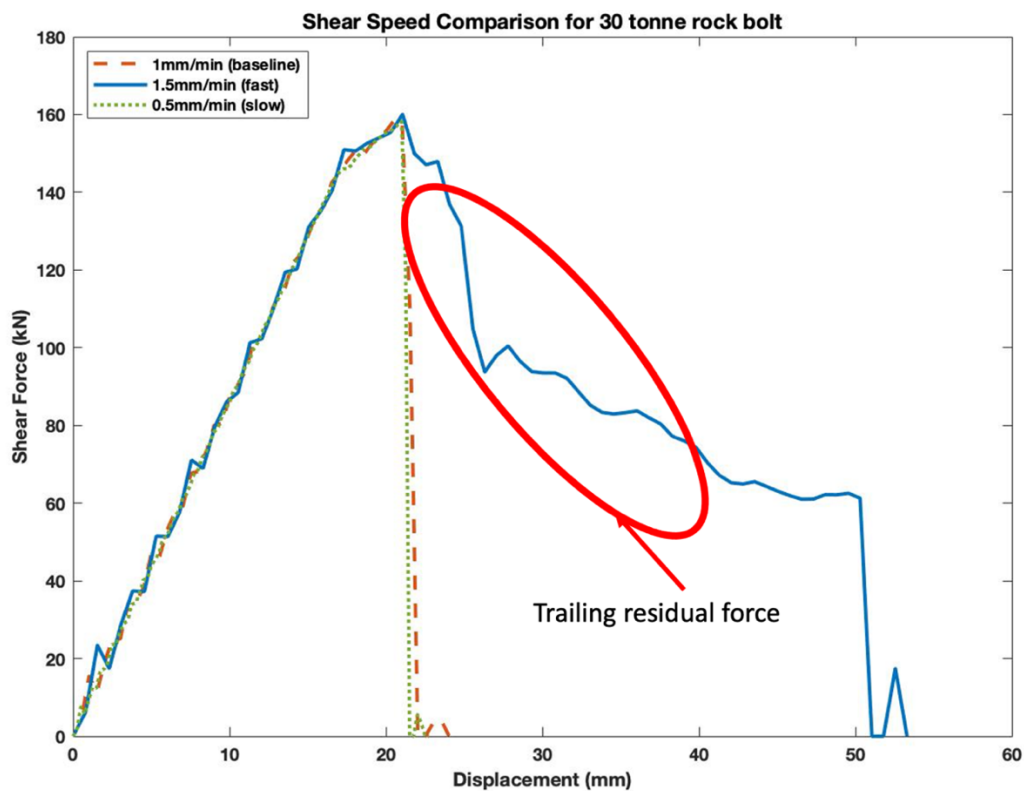


Figure 6.30: Impact of the shearing speed on the 30-tonne clean joint rock bolt compared to the original test parameter.

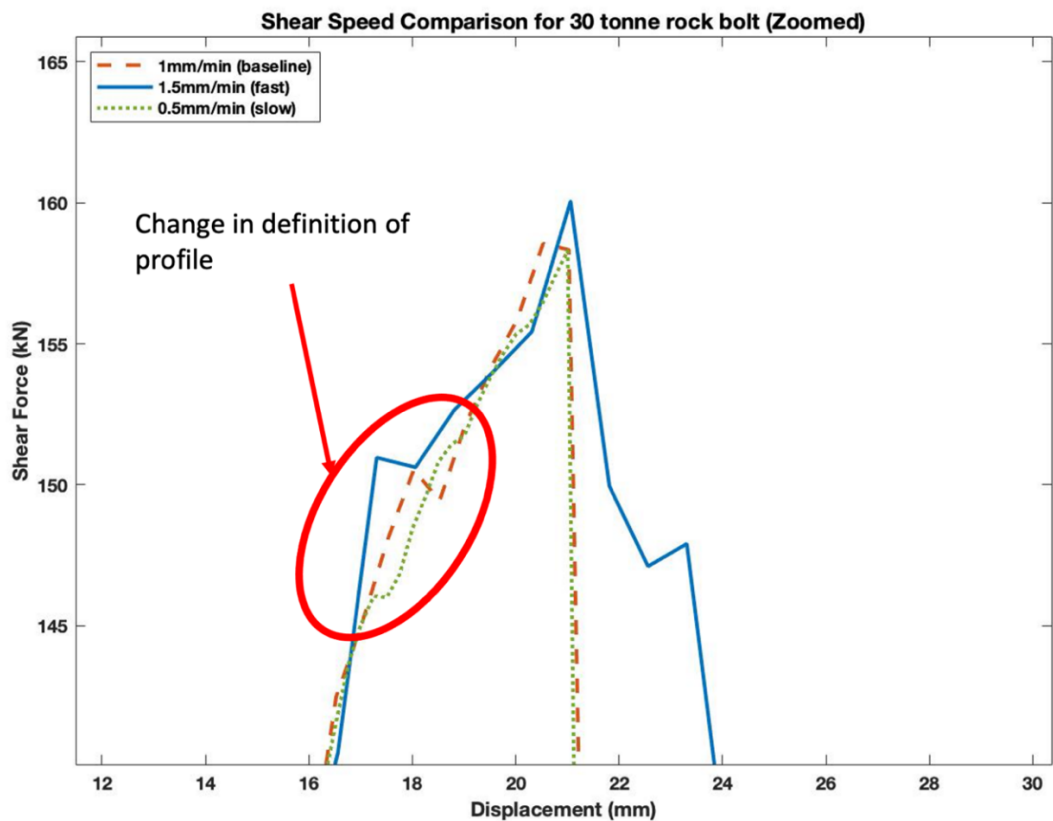


Figure 6.31: Zoomed in comparison of the impact of shearing speed on the 30-tonne clean joint rock bolt compared to the original test parameter.

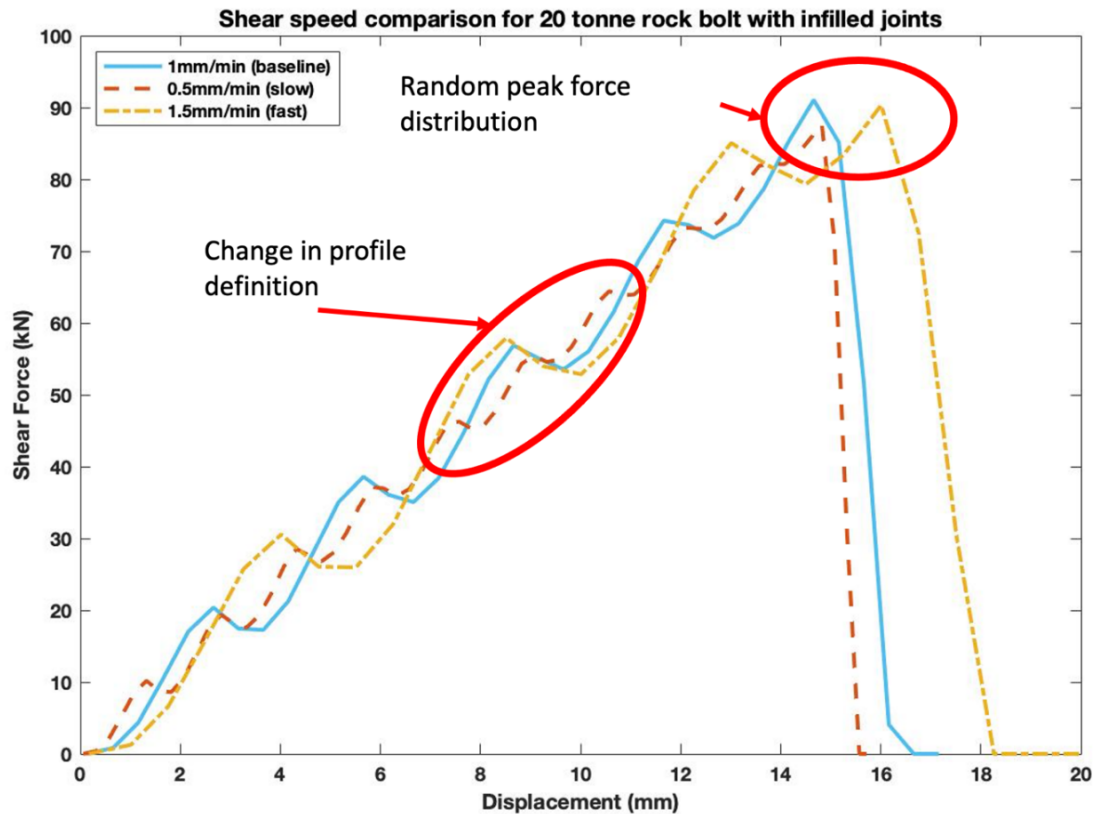


Figure 6.32: Impact of the shearing speed on the 20-tonne infilled rock bolt compared to the original test parameter.

6.5 Summary

Analytical and 3D numerical models were developed to accurately simulate the shear properties of the 20-tonne and 30-tonne rock bolts with clean and infilled rock joints. Models were compared and validated against the experimental 0kN sample testing scheme.

The analytical model was developed with adjustable coefficients to allow for fine tuning to the user's specific rock bolt properties. This method resulted in good agreement with the experimentally determined shear profiles and successfully represented the elastic, strain-softening, and failure regions of each sample. Despite the analytical model's ability to replicate each rock bolts' shear profile it had some shortcomings. Many of the simulated profiles presented with steps at the transition zones and while this did not have a dramatic impact on the reliability of the model it is a possible point for improvement.

The developed 3D numerical model was created utilising the FLAC3D software. The creation of this model required a new conceptual model representing the 3D properties

of the rock bolt system. This conceptual model was developed in alignment with the shear box constructed for the experimental testing scheme. The models were used to simulate the shear response of 20-tonne and 30-tonne rock bolts embedded in host rock with and without infilled shear joints. Benefits of the 3D numerical simulation were that sensitivity analysis could be conducted to determine the shear properties of the rock bolts in alternate scenarios. Simulations were conducted to determine the effect of host rock strength, shear speed and shear plane angle. To reduce the computation time, these scenarios were conducted on 20-tonne infilled samples and 30-tonne clean joint samples. Simulations as part of the sensitivity analysis were compared against the baseline dataset that represented the experimental test scheme. Notable variations occurred when 30-tonne samples were subjected to increased shear speeds resulting in an altered post failure response, a behaviour that was not present for the 20-tonne sample. Similar altered post failure responses were identified for both the 20-tonne and 30-tonne rock bolts subjected to angled shear joints.

Despite the versatility of the 3D numerical simulation, it was restricted by a limitation of the FLAC3D software which was unable to simulate any rock bolts with an applied pretension resulting in all simulations conducted as a passive 0kN set up.

CHAPTER 7: CONCLUSIONS AND RECOMMENDATIONS

7.1 Introduction

Despite the widespread use of fibreglass rock bolts within ground support systems, limited studies have been conducted on their failure mechanisms. Furthermore, the standards by which rock bolts are tested, have presented with significant shortcomings and design flaws that can negatively impact the test's outcome. Therefore, the aim of this research was to study the shear failure mechanisms of fibreglass rock bolts using the modified double shear testing apparatus.

In this study, experimental test schemes were developed to investigate the shear performance of fibreglass rock bolts. The test schemes employed different rock bolt tensile ratings, various pretension settings, clean and infilled shear interfaces and the development of an analytical representation of shearing. The double shear testing apparatus was modified to suit the test requirements, while also incorporating design improvements to minimise impacts on the test outcomes. Finally, a numerical model was developed to better understand the impact varying parameters also have on the shear performance of fibreglass rock bolts. This provided the opportunity to develop an understanding of the shear failure mechanisms of fibreglass rock bolts.

7.2 Key research outcomes

Six research objectives were developed to best address the fibreglass rock bolt shear research's shortcomings and testing method deficiencies.

7.2.1 Objective One: Critical review of research

A critical review of ground support systems was conducted by examining the different methods of ground supports, load transfer mechanisms and their properties. Four experimental test schemes were explored to determine the load transfer properties of rock bolts. These test schemes included: tensile, pull-out, single shear, and double shear test schemes. Much of the research focused on exploring the performance of both metal rock bolts and cable bolts. While some research explored the axial load transfer mechanisms of fibreglass rock bolts, there were limited studies researching the fibreglass rock bolts' shear load transfer mechanisms. Despite this, fibreglass rock bolts were studied utilising similar, if not the same, test methods to that of metal rock

bolts and cable bolts. Therefore, the study of rock bolt shear strength was accomplished by utilising single shear and double shear test methods. Through this investigation, shear apparatus shortcomings and design flaws were highlighted. The outcomes of the critical investigation identified the lack of research regarding fibreglass rock bolts and double shear test schemes, providing the foundations for this research.

7.2.2 Objective Two: Test scheme and experimental design

With the lack of research regarding fibreglass rock bolts outlined by the critical review, testing schemes were developed to systematically study the shear behaviour of fibreglass rock bolts. As a result of the investigation, it was determined that there were several system conditions that could impact the ultimate shear failure mechanisms of fibreglass rock bolts. System conditions included: the impact of pretension, host rock UCS, shear speed, installation angle, shear joint properties and rock bolt tensile ratings. Therefore, five testing schemes were developed to study how these conditions impacted the fibreglass rock bolts' shear performance. Experimental testing schemes were conducted for a select number of the shearing conditions, that were later utilised for the validation of the analytical models. Experimentally tested conditions included: subjecting rock bolts to a range of pretensions of 0kN, 10kN, 15kN and 20kN, testing rock bolts of two different tensile ratings of 20-tonne and 30-tonne and testing the impact of shear interface conditions such as clean and infilled interfaces. Modelling test schemes were also developed to map the test rock bolts' shear performance accurately three-dimensionally, and then extended to simulate the remaining identified system conditions: installation angle, shear speed and host rock strength. To conduct the tests a modified double shear testing apparatus was constructed, improving on previous shear test attempts. These improvements included the ability to test both clean and infilled samples, larger simulated host rock sizes to facilitate load transmission through the system and finally contactless apparatus modules preventing shear result interferences.

7.2.3 Objective Three: Clean interface shear study

The clean joint test scheme studied the shear performance of the fibreglass rock bolts with clean shear interfaces. To ensure a comprehensive study, experiments were also subjected to various system properties. These properties included fibreglass rock bolts

of 20-tonne and 30-tonne tensile ratings and pretensions of 0kN, 10kN, 15kN and 20kN. Great care was taken during sample preparation to ensure sample uniformity, however, achieving the specified pretensions proved to be a difficult task. Variability in the rock bolts' quality resulted in several discarded bolts during assembly and one discarded test sample. Despite the challenges introduced by the quality of the rock bolts, several shear behaviour characteristics were identified. Firstly, through the clean shear test scheme, the shear profile was categorised as elastic, strain-softening and failure regions. While it was found that all clean joint samples experienced these regions, the increasing pretension caused a reduction in the displacement and shear range of some of the rock bolts. The applied pretension resulted in increasing profile smoothing with respect to pretension value. Despite this, pretension had little to no impact on the recorded shear forces of the 20-tonne rock bolts. Additionally, the tensile load rating of the rock bolts did not influence the peak failure forces and instead impacted the systems' strain response, whereby the 30-tonne samples experienced failure at greater displacements. Lastly, clean joint samples subjected to increased pretension forces experienced a more efficient transfer of shear forces through the system and to the rock bolt, resulting in less damage propagating away from the rock bolt at the shear interface.

7.2.4 Objective Four: Infilled shear interface study

The infilled double shear testing scheme test also examined the shear performance of fibreglass rock bolts, largely mirroring the processes of the clean joint test scheme to enable system comparisons. Like the clean interface tests, the infilled interface study also examined the impact of rock bolt tensile strength and pretension settings on the shear performance of fibreglass rock bolts. Similarly, the infilled test scheme was impacted by the rock bolt's production variability during the pretensioning stage of sample preparations however, it did not result in any discarded samples. The infilled test scheme was conducted with 5mm thick sandy clay infilled shear interfaces. Like the clean joint test scheme, all tested infilled samples experienced the three-part failure profile comprised of the elastic, strain-softening and failure regions. Several exclusive shear behaviour characteristics were identified during the infilled test scheme. Firstly, both rock bolt types experienced a decrease to the shear failure displacement. The 20-tonne rock bolts experienced the greatest overall decreases. Contrastingly, the infilled shear system registered successive increases to the shear failure forces, with the 30-

tonne samples experiencing the greatest overall increases. Secondly, there was a notable increase in the shear force performance of 30-tonne rock bolts over the 20-tonne bolts. The 30-tonne rock bolts also showed strong correlations between increasing the pretension setting and decreasing failure displacement. Finally, both the 20-tonne and 30-tonne rock bolts experienced incremental increases to the hinge point angle with each pretension setting increase.

7.2.5 Objective Five: Analytical model

Complementing the experimental test schemes, the analytical model was developed to predict the shear performance of fibreglass rock bolts when subjected to clean and infilled shear interfaces. The model mimicked the design elements of each test scenario and were verified against the experimental results. The analytical model was developed by utilising several fundamental physical theories including: linear elastic theory, energy balance theory and Fourier transform. The combination of these theories resulted in the tri-linear expression that embodied the three-stage shear profile. To enable model calibration to different scenarios, each profile stage incorporated independently adjustable coefficients. Despite the model's close approximation to the sample's experimental performance, it proved challenging to accurately recreate the localised transition zones between each stage. This was typically represented by a vertical or horizontal step. However, through an iterative self-checking process, the model could provide close overall approximations and map the shear performance of fibreglass rock bolts subjected to the various shearing conditions.

7.2.6 Objective Six: Numerical model

A 3D numerical model was developed to model double shear test scenarios using a finite element method. Both the 20-tonne and 30-tonne 0kN pretension shear simulations accurately simulated both the peak shear and shear displacement of the samples. While the simulated rock bolts recorded similar gradients for the strain-softening region, there was a lack of attenuation resulting in an oscillating profile. The 20-tonne simulation was more susceptible to this oscillation resulting in significant peaks and troughs. Despite this, several of the oscillations aligned with the 20-tonne experimental results.

The sensitivity analysis conducted for the rock bolt installation angle and shear speed numerical models highlighted variations to the shear profile for both 20-tonne and 30-

tonne rock bolts. This suggested that these parameters were potentially significant to the rock bolt's performance. Increasing the shear speed from the experimental test baseline yielded substantial displacement increases to the post failure residual performance of the rock bolts. Changing the installation angle resulted in greater peak shear forces and long residual zones. The least significant impacts were observed when changing the host rock UCS, suggesting neither rock bolt was drastically impacted by weak or strong host rocks. Despite the success of the model, it was unable to simulate the impact of pretension on any of the scenarios due to software limitations.

7.3 Recommendations for future research

Fibreglass is a complex anisotropic composite material that has a wide range of uses. When incorporated into the rock bolt systems, its material properties add levels of complexity not observed in their metal counterparts. Despite this, they have the potential to greatly improve site safety in adverse conditions. As a result, their advantages and disadvantages must be deeply understood. The completion of this research study brought attention to several areas of possible investigation to both the designed test schemes as well as new areas of study that were not explored within the scope of this research. The following recommendations are suggested for the improvement of the experimental, analytical and numerical studies:

1. In this study, sample confinement was achieved by the securing of fixed sized external plates. This could potentially result in non-uniform confinement pressures across the length of the sample while also resulting in difficult replicability. It would be preferred to utilise an active confining system that has the ability to stabilise pressures across the length of the sample. A bladder type system that fits within the double shear apparatus would be ideal as this would also conform to the shape of the sample. This would eliminate the need for physically perfect samples and save time during assembly.
2. The clean joint and infilled test schemes used in this research could be extended to test additional aspects of rock bolt performance. Due to high variability in nature and rock formation processes, it would be highly valuable to study the impact of varying degrees of asperities on both clean joint and infilled joint samples.
3. It was identified through this research, the shear performance of rock bolts has the potential to be greatly impacted by their installation angle. It would be beneficial

to repeat the experimental test schemes of this study using various installation angles.

4. There is great variability in rock bolt installation environments from constant shear speed to dynamic shear loading. It is recommended that the impact of the shearing mode is studied to determine the influence of constant shear rates and dynamic shear rates on fibreglass rock bolts' shear load transfer mechanisms.
5. The developed analytical model presented with challenges when simulating the transition zones between each failure stage. As a result, it is recommended that additional studies are conducted to develop robust analytical representation of fibreglass rock bolts with the capacity to model transition zones.
6. The numerical model developed in this study was unfortunately unable to simulate shear scenarios which incorporated an applied pretension. It would therefore be recommended to explore numerical model methods that have the ability to simulate the impact of pretension on the fibreglass rock bolt's shear performance.
7. Lastly, the numerical model developed in this study was based off the experimental test scheme and therefore, does not represent any real-life scenario. To translate the findings from this research into real-life, models based on case studies simulating tunnel or slope support systems should be explored.

REFERENCES

1991. ASTM C-759. *Standard test method for compressive strength of chemical - resistant mortar, grouts, monolithic surfacing and polymer concretes*. Philadelphia PA: ASTM.
2009. BS 7861. *Strata reinforcement support system components used in coal mines - Part 1: Specification for rockbolting and Part 2: Specification for Flexible systems for roof reinforcement.*: BSI.
- AZIZ, N., CRAIG, P., MIRZAGHORBANALI, A. & NEMCIK, J. 2016a. Factors Influencing the Quality of Encapsulation in Rock Bolting. *Rock Mechanics and Rock Engineering*, 49, 3189-3203.
- AZIZ, N., CRAIG, P., MIRZAGHORBANALI, A., RASEKH, H., NEMCIK, J. & LI, X. 2015a. Behaviour of Cable Bolts in Shear; Experimental Study and Mathematical Modelling. *In: AZIZ, N. (ed.) 15th Coal Operators' Conference*. Wollongong: University of Wollongong.
- AZIZ, N., CRAIG, P., NEMCIK, J. & HAI, F. I. 2013. Rock bolt corrosion - an experimental study. *In: AZIZ, N. (ed.) Coal Operators' Conference*. Wollongong: The University of Wollongong.
- AZIZ, N., GILBERT, D., NEMCIK, J., MIRZAGHORBANALI, A. & BURTON, R. 2015b. The Strength properties of Fiber glass and other polymer based Dowels for Strata Reinforcement in Coal mines. *Third Australian Ground Control in Mining Conference*. Sydney, Australia: Ausimm.
- AZIZ, N., MIRZAGHORBANALI, A., NEMCIK, J., HEEMANN, K. & MAYER, S. 2015c. Shear strength properties of plain and spirally profiled cable bolts. *Canadian Geotechnical Journal*, 52, 1490-1495.
- AZIZ, N., MIRZAGHORBANALI, A., NEMCIK, J., LI, X., RASEKH, H. & WANG, G. Load transfer characteristics of plain and spiral cable bolts tested in new non rotating pull testing apparatus. *In: AZIZ, N., ed. Proceedings of the 16th Coal Operators' Conference, 10-12 February 2016* 2016b Wollongong. University of Wollongong, 32-39.
- AZIZ, N., MIRZAGHORBANALI, A., NEMCIK, J., RASEKH, H. & LI, X. 2016c. A Follow up to Study the Behaviour of Cable Bolts in Shear: Experimental Study and Mathematical Modelling. *In: AZIZ, N. (ed.) 16th Coal Operators' Conference*. Wollongong: University of Wollongong.
- AZIZ, N., NEMCIK, J., MIRZAGHORBANALI, A., FOLDI, S., JOYCE, D., MOSLEMI, A., GHOJAVAND, H., MA, S., LI, X. & RASEKH, H. 2014. Suggested methods for the preparation and testing of various properties of

resins and grouts. *In: AZIZ, N. (ed.) 14th Coal Operators' Conference.* Wollongong: University of Wollongong.

AZIZ, N., PRATT, D. & WILLIAMAS, R. 2003. Double Shear Testing of Bolts. *In: AZIZ, N. (ed.) Coal Operators' Conference.* Wollongong: The University of Wollongong, The Australasian Institute of Mining and Metallurgy.

AZIZ, N., RINK, O., RASEKH, H., HAWKINS, E., MIRZAGHORBANALI, A., YANG, G., KHALEGHPARAST, S., MILLS, K., JAN, N. & LI, X. 2017. Single shear testing of various cable bolts used in Australian mines. *In: AZIZ, N. (ed.) 17th Coal Operators' Conference.* Wollongong: University of Wollongong.

AZIZ, N. I. & JALALIFAR, H. 2005. Experimental and numerical methodology assessment of load transfer capacity of bolts. 24th International Conference on Ground Control in Mining, 2005 USA: University of West Virginia. West Virginia: University of West Virginia, 285-293.

BARTON, N. 1971. A relationship between joint roughness and joint shear strength. *Mécanique des Roches.* Nancy, France: Symposium Soc. Internat.

BARTON, N. 1973. A review of the shear strength of filled discontinuities in rock. *Bergmekanikk.* Oslo, Norway.

BARTON, N. & CHOUBEY, V. 1977. The shear strength of rock joints in theory and practice. *Rock Mechanics Felsmechanik Mécanique des Roches*, 10, 1-54.

BENMOKRANE, B., CHENNOUF, A. & MITRI, H. S. 1995. Laboratory evaluation of cement-based grouts and grouted rock anchors. *International Journal of Rock Mechanics and Mining Sciences & Geomechanics Abstracts*, 32, 633-642.

BERGMAN, G. 2001. Take the guesswork out of FRP corrosion. *Chemical engineering progress*, 97, 54-59.

BIGBY, D. 2005. Development of the Laboratory Short Encapsulation Pull Test for a Revised British Standard on Rock Reinforcement Components Used in Coal Mining. International Conference on Ground Control in Mining.

BLANCO MARTÍN, L., TIJANI, M., HADJ-HASSEN, F. & NOIRET, A. 2013. Assessment of the bolt-grout interface behaviour of fully grouted rockbolts from laboratory experiments under axial loads. *International Journal of Rock Mechanics and Mining Sciences*, 63, 50-61.

BRADY, B. H. G. & BROWN, E. T. 1985. Rock support and reinforcement. *Rock Mechanics: For Underground Mining.* Dordrecht: Springer Netherlands.

- CAI, Y., ESAKI, T. & JIANG, Y. 2004. An analytical model to predict axial load in grouted rock bolt for soft rock tunneling. *Tunnelling and Underground Space Technology*, 19, 607-618.
- CHANG, X., WANG, G., LIANG, Z., YANG, J. & TANG, C. 2017. Study on grout cracking and interface debonding of rockbolt grouted system. *Construction and Building Materials*, 135, 665-673.
- CHEN, J., HAGAN, P. C. & SAYDAM, S. 2016. Parametric study on the axial performance of a fully grouted cable bolt with a new pull-out test. *International Journal of Mining Science and Technology*, 26, 53-58.
- CHEN, J., SAYDAM, S. & HAGAN, P. C. 2015. An analytical model of the load transfer behavior of fully grouted cable bolts. *Construction and Building Materials*, 101, 1006-1015.
- CHUGH, Y., SINHA, S. & TINSLEY, J. 2016. *An Analysis of Short Encapsulation Bolt Pull Test (SEPT) Data from Interior Basin Coal Mines*.
- CLIFFORD, B., KENT, L., ALTOUNYAN, P. & BIGBY, D. 2001. Systems Used in Coal Mining development in Long Tendon Reinforcement. *20th International Conference on Ground Control in Mining*. West Virginia, USA.
- CLIFFORD, B. & KENT, L. K. 2000. Stability of Longterm Roadways. *RMT Report to HSE*.
- CONWAY, C. C. 1948. Roof Support With Suspension Rods. *Proceedings of the Illinois Mining Institute*. Springfield, Illinois: Mining Electrical Group.
- COON, R. & MERRITT, A. 1970. Determination of the in situ modulus of deformation of rock. *ASTM special technical publication*, 477, 154-173.
- CRAIG, P., AZIZ, N., NEMCIK, J. & MOSLEMI, A. 2013. *EVALUATING METHODS OF UNDERGROUND SHORT ENCAPSULATION PULL TESTING IN AUSTRALIAN COAL MINES*.
- DIGHT, P. M. 1982. *Improvements to the stability of rock walls in open pit mines [microform] / by Phillip M. Dight*, [Melbourne].
- DSI-UNDERGROUND. 2021. *Rock Bolts - FRP* [Online]. Online: DSI UNDERGROUND. Available: <https://www.dsiunderground.com.au/products/mining/rock-bolts/> [Accessed 2022].
- DSI-UNDERGROUND 2022. Ground Control Solutions. *Global Tunneling Edition*. Newcastle, NSW: DSI Underground.

- ELRAWY, W., ABDELHAFFEZ, G. & SALEEM, H. 2020. STABILITY ASSESSMENT OF UNDERGROUND OPENINGS USING DIFFERENT ROCK SUPPORT SYSTEMS. *Rudarsko-geološko-naftni zbornik*, 35, 49-63.
- FARMER, I. W. 1975. Stress distribution along a resin grouted rock anchor. *International Journal of Rock Mechanics and Mining Sciences & Geomechanics Abstracts*, 12, 347-351.
- FENG, X., ZHANG, N., LI, G. & GUO, G. 2017. Pullout Test on Fully Grouted Bolt Sheathed by Different Length of Segmented Steel Tubes. *Shock and Vibration*, 2017, 16.
- FORBES, B., VLACHOPOULOS, N., DIEDERICHS, M. S. & AUBERTIN, J. 2020. Augmenting the in-situ rock bolt pull test with distributed optical fiber strain sensing. *International Journal of Rock Mechanics and Mining Sciences*, 126, 104202.
- FRKETIC, J., DICKENS, T. & RAMAKRISHNAN, S. 2017. Automated manufacturing and processing of fiber-reinforced polymer (FRP) composites: An additive review of contemporary and modern techniques for advanced materials manufacturing. *Additive Manufacturing*, 14, 69-86.
- GAY, F. T. 1980. Engineering and Design: Rock Reinforcement. In: ENGINEERS, U. S. A. C. O. (ed.) Initial ed. Washington D.C.: U.S. Government Printing Office.
- GHADIMI, M., SHAHRIAR, K. & JALALIFAR, H. 2015. An Analytical Model to Predict Shear Stress Distribution in Fully Encapsulated Rock Bolts. *Geotechnical and Geological Engineering*, 33, 59-68.
- GHADIMI, M., SHAHRIAR, K. & JALALIFAR, H. 2016. Study of Fully Grouted Rock Bolt in Tabas Coal Mine Using Numerical and Instrumentation Methods. *Arabian Journal for Science and Engineering*, 41, 2305-2313.
- GILBERT, D., MIRZAGHORBANALI, A., LI, X., RASEKH, H., AZIZ, N. & NEMCIK, J. 2015. Strength Properties of Fibre Glass Dowels Used for Strata Reinforcement in Coal Mines. In: AZIZ, N. (ed.) *Coal Operators' Conference*. Wollongong: University of Wollongong.
- GORIS, J. M., MARTIN, L. A. & CURTIN, R. P. 1996. Shear behaviour of cable bolt supports in horizontal bedded deposits. *Cim Bulletin*, 89, 124-128.
- HAAS, C., CLARK, G. & NITZSCHE, R. 1974. An Investigation of the Interaction of Rock and Types of Rock Bolts for Selected Loading Conditions. Missouri: University of Missouri.

- HAAS, C. J. 1976. Shear resistance of rock bolts. *Journal Name: Trans. Soc. Min. Eng. AIME; (United States); Journal Volume: 260:1; Conference: AIME annual meeting, New York, NY, Feb 1975.* United States.
- HADJ HASSEN, F., THENEVIN, I. & JAHANGIR, E. 2015. Laboratory Testing Programme on rock-bolts and cable-bolts AMSSTED deliverable 3.2.1. Armines, Mines ParisTech.
- HAGAN, P., CHEN, J. & SAYDAM, S. The load transfer mechanism of fully grouted cable bolts under laboratory tests. 2014.
- HAQUE, A. & INDRARATNA, B. Experimental and numerical modelling of shear behaviour of rock joints. ISRM International Symposium, 2000. OnePetro.
- HARTMAN, W. & HEBBLEWHITE, B. 2003. Understanding the performance of Rock Reinforcement Elements under Shear Loading through Laboratory Testing - A 30-year History. *1st AGCM Conference.*
- HASSELL, R., VILLAESCUSA, E., THOMPSON, A. & KINSELLA, B. 2004. Corrosion assessment of ground support systems. *In: VILLAESCUSA, E. & POTVIN, Y. (eds.) Ground Support in Mining and Underground Construction.* London: Taylor and Francis Group, London.
- HOGG, P. & HULL, D. 1983. Corrosion and environmental deterioration of GRP. *Developments in GRP technology*, 1, 37-90.
- HOLDEN, M. & HAGAN, P. 2014. The size effect of rock sample used in anchorage performance testing of cable bolts. *Coal Operators' Conference.* Wollongong, NSW: The Australasian Institute of Mining and Metallurgy & Mine Managers Association of Australia.
- HUTCHINS, W., BYWATER, S., THOMPSON, A. & WINDSOR, C. A versatile grouted cable dowel reinforcing system for rock. *In: (AUSIMM), A. I. O. M. A. M., ed. AusIMM Proceedings 1990, 1990.* AusIMM, 25-29.
- HUTCHINSON, D. J. & DIEDERICH, M. S. 1996. *Cablebolting in Underground Mines*, BiTech Publishers.
- HYETT, A. J., BAWDEN, W. F., MACSPORRAN, G. R. & MOOSAVI, M. 1995. A constitutive law for bond failure of fully-grouted cable bolts using a modified hoek cell. *International Journal of Rock Mechanics and Mining Sciences & Geomechanics Abstracts*, 32, 11-36.
- HYETT, A. J., BAWDEN, W. F., POWERS, R., ROCQUE, P., QUEEN'S, U. & DEPARTMENT OF MINING, E. The nutcase cable bolt. International congress on mine design, Innovative mine design for the 21st century, 1993 Kingston; Canada. Balkema; 409-420.

- INDRARATNA, B. 1990. Development and applications of a synthetic material to simulate soft sedimentary rocks. *Geotechnique*, 40, 189-200.
- INDRARATNA, B., PERMADASA, W. N., NEMCIK, J. A. & JAYANATHAN, M. 2012. Shear strength model for sediment-infilled rock discontinuities and field applications. In: NARSILIO, I. G. A., ARULRAJAH, A. & KODIKARA, J. (eds.) *11th Australia - New Zealand Conference on Geomechanics: Ground Engineering in a Changing World*. Australia: Engineers Australia.
- ITASCA, F. 2002. Fast Lagrangian Analysis of Continua. Version 5.0 ed. Minneapolis. MN: Itasca Consulting Group, Inc.
- ITASCA, P. D. 2005. PFC3D. Minneapolis, MN: Itasca Consulting Group. Inc.
- IVANOVIC, A. 2001. *The dynamic response of ground anchorage systems*. University of Aberdeen.
- IVANOVIĆ, A. & NEILSON, R. D. 2009. Modelling of debonding along the fixed anchor length. *International Journal of Rock Mechanics and Mining Sciences*, 46, 699-707.
- IVANOVIC, A., NEILSON, R. D. & RODGER, A. A. 2001. Lumped parameter modelling of single-tendon ground anchorage systems. *Proceedings of the Institution of Civil Engineers: Geotechnical Engineering*, 149, 103-113.
- JAHANGIR, E., BLANCO-MARTÍN, L., HADJ-HASSEN, F. & TIJANI, M. 2021. Development and application of an interface constitutive model for fully grouted rock-bolts and cable-bolts. *Journal of Rock Mechanics and Geotechnical Engineering*, 13, 811-819.
- JALALIFAR, H. 2011. An analytical solution to predict axial load along fully grouted bolts in an elasto-plastic rock mass. *The Journal of The Southern African Institute of Mining and Metallurgy*, 111, 809-814.
- JENNMAR 2021. 32MM Fibreglass Torque Tension Bolt. Online: Jennmar Australia.
- JENNMAR 2022. Product Catalogue. *Coal Mining*. Smeaton Grange, NSW: Jennmar.
- JEREMIC, M. L. & DELAIRE, G. J. P. 1983. Failure mechanics of cable bolt systems. *CIM Bull.*; (Canada), Medium: X; Size: Pages: 66-71.
- KARAKUS, M., LIU, Y., ZHANG, G. & TANG, H. 2016. A new shear strength model incorporating influence of infill materials for rock joints. *Geomechanics and Geophysics for Geo-Energy and Geo-Resources*, 2, 183-193.

- LAMBERT, C. & COLL, C. 2014. Discrete modeling of rock joints with a smooth-joint contact model. *Journal of Rock Mechanics and Geotechnical Engineering*, 6, 1-12.
- LI, C. C. 2017a. Chapter Four - Mechanics of Rockbolting. *In: LI, C. C. (ed.) Rockbolting*. Butterworth-Heinemann.
- LI, C. C. 2017b. Principles of rockbolting design. *Journal of Rock Mechanics and Geotechnical Engineering*, 9, 396-414.
- LI, F., QUAN, X., JIA, Y., WANG, B., ZHANG, G. & CHEN, S. 2017a. The Experimental Study of the Temperature Effect on the Interfacial Properties of Fully Grouted Rock Bolt. *Applied Sciences*, 7, 327.
- LI, X., AZIZ, N., MIRZAGHORBANALI, A. & NEMCIK, J. 2016. Behavior of Fiber Glass Bolts, Rock Bolts and Cable Bolts in Shear. *Rock Mechanics and Rock Engineering*, 49, 2723-2735.
- LI, X., AZIZ, N., MIRZAGHORBANALI, A. & NEMCIK, J. 2017b. Comparison of the shear test results of a cable bolt on three laboratory test apparatuses. *Tunnelling and Underground Space Technology*, 61, 82-89.
- LI, X., NEMCIK, J., MIRZAGHORBANALI, A., AZIZ, N. & RASEKH, H. 2015. Analytical model of shear behaviour of a fully grouted bolt subjected to shearing. *International Journal of Rock Mechanics and Mining Sciences*, 80.
- MA, S., NEMCIK, J. & AZIZ, N. 2013. An analytical model of fully grouted rock bolts subjected to tensile load. *Construction and Building Materials*, 49, 519-526.
- MA, S., NEMCIK, J. & AZIZ, N. 2014. Simulation of fully grouted rockbolts in underground roadways using FLAC2D. *Canadian Geotechnical Journal*, 51, 911-920.
- MAEKAWA, K. & QURESHI, J. 1996. Computational Model for Reinforcing Bar Embedded in Concrete under Combined Axial Pullout and Transverse Displacement. *Doboku Gakkai Ronbunshu*, 1996, 227-239.
- MARANAN, G., MANALO, A., KARUNASENA, K. & BENMOKRANE, B. 2015. Bond Stress-Slip Behavior: Case of GFRP Bars in Geopolymer Concrete. *Journal of Materials in Civil Engineering*, 27, 04014116.
- MARK, C. 2017. DESIGN OF ROOF BOLT SYSTEMS. *In: LABOR, U. S. D. O. (ed.)*. Pittsburgh, PA: Pittsburgh Research Laboratory.

- MARTIN, L., HADJ HASSEN, F., TIJANI, M. & NOIRET, A. 2011. A new experimental and analytical study of fully grouted rockbolts. *45th US Rock Mechanics / Geomechanics Symposium*.
- MCKENZIE, R. & KING, B. 2015. Megabolt Shear Testing Program. *Mine Pressure and Strata Control*.: China University of Mining and Technology Press, Xuzhou, China.
- MEGA-BOLT 2021. High capacity strata support products and systems for underground mining. Online: MEGA BOLT.
- MINOVA 2021a. Grouted Cable Bolt - Versatility and Remarkable Performance. *Technical Data Sheet*. Georgetown, KY: Minova.
- MINOVA 2021b. Steel and Fibreglass. Online: MINOVA.
- MINOVA, NEWSON, S., CAMPOLI, A., SYKES, A., O'CONNOR, D. & SMITH, N. 2006. *The MINOVA Guide to Resin-Grouted Rockbolts*, Cambridge, UK, Piggott Black Bear.
- MIRZAGHORBANALI, A., ALENZEL, F., GREGOR, P., AZIZ, N., MCDOUGALL, K. & HELWIG, A. Shear strength of rock joints under constant normal loading conditions. Proceedings of the 2019 Coal Operators Conference, 18-20 February 2019a University of Wollongong. p188-195.
- MIRZAGHORBANALI, A. & AZIZ, N. 2017a. An experimental study of axial load transfer mechanisms of cable bolts using axially split embedment apparatus. *Journal of Mining and Environment*, 8, 131-137.
- MIRZAGHORBANALI, A., GHIRMIRE, B., RASTEGARMANESH, A., NOURIZADEH, H., MCDOUGALL, K. & AZIZ, N. 2022. Shear behavior of clayey infilled rock joints having triangular and sinusoidal asperities.
- MIRZAGHORBANALI, A., GREGOR, P., EBRAHIM, Z., ALFAHED, A., AZIZ, N. & MCDOUGALL, K. Strength properties of grout for strata reinforcement. Proceedings of the 2019 Coal Operators' Conference, 18-20 February 2019b. University of Wollongong, p196-202.
- MIRZAGHORBANALI, A. & NEMCIK, J. 2013. Numerical modelling of cyclic shear behaviour of rock joints under constant normal stiffness condition.
- MIRZAGHORBANALI, A., NEMCIK, J. & AZIZ, N. 2014. Effects of Cyclic Loading on the Shear Behaviour of Infilled Rock Joints Under Constant Normal Stiffness Conditions. *Rock Mechanics and Rock Engineering*, 47, 1373-1391.

- MIRZAGHORBANALI, A., RASEKH, H., AZIZ, N., YANG, G., KHALEGHPARAST, S. & NEMCIK, J. 2017b. Shear strength properties of cable bolts using a new double shear instrument, experimental study, and numerical simulation. *Tunnelling and Underground Space Technology*, 70, 240-253.
- MIRZAGHORNANALI, A., GREGOR, P., ALKANDARI, H., AZIZ, N. & MCDUGALL, K. Mechanical behaviours of grout for strata reinforcement. Proceedings of the 18th Coal Operators' Conference, 7-9 February 2018. University of Wollongong, p373-377.
- MOOSAVI, M., JAFARI, A. & KHOSRAVI, A. 2005. Bond of cement grouted reinforcing bars under constant radial pressure. *Cement and Concrete Composites*, 27, 103-109.
- MYERS, T. J., KYTÖMAA, H. K. & SMITH, T. R. 2007. Environmental stress-corrosion cracking of fiberglass: Lessons learned from failures in the chemical industry. *Journal of Hazardous Materials*, 142, 695-704.
- NEMCIK, J., GALE, W. J. & FABJANCZYK, M. W. 2006. Methods of Interpreting Ground Stress Based on Underground Stress Measurements and Numerical Modelling. In: AZIZ, N. (ed.) *Coal Operators' Conference*. Wollongong: University of Wollongong.
- O'GRADY, P., FULLER, P. & DIGHT, P. 1994. Cable bolting in Australian coal mines - Current practice and design considerations. 154, 63-69.
- OLIVEIRA, D. 2009. *An advancement in analytical modelling of soil-infilled rock joints and their practical applications*. Doctor of Philosophy, University of Wollongong.
- OLIVEIRA, D. & INDRARATNA, B. 2010. Comparison between models of rock discontinuity strength and deformation. *Journal of Geotechnical and Geoenvironmental Engineering*, 136, 10.
- PELLET, F. & EGGER, P. 1996. Analytical model for the mechanical behaviour of bolted rock joints subjected to shearing. *Rock Mechanics and Rock Engineering*, 29, 73-97.
- PENG, S. S. & TANG, D. H. Y. 1984. Roof bolting in underground mining: a state-of-the-art review. *International Journal of Mining Engineering*, 2, 1-42.
- PILE, J. D., BESSINGER, S. L., MARK, C. & TADOLINI, S. C. 2003. Short-Encapsulation Pull Tests For Roof Bolt Evaluation At An Operating Coal Mine. 2003.

- RAJAPAKSE, R. 2008. 25 - Soil Anchors and 26 - Tunnel Design. *Geotechnical Engineering Calculations and Rules of Thumb*. Burlington: Butterworth-Heinemann.
- RAJAPAKSE, R. 2016. 33 - Rock bolts, dowels, and cable bolts. *In: RAJAPAKSE, R. (ed.) Geotechnical Engineering Calculations and Rules of Thumb (Second Edition)*. Butterworth-Heinemann.
- RASEKH, H. 2017. *The shear performance of cable bolts in experimental, numerical and mathematical shear studies*. Doctor of Philosophy, University of Wollongong.
- RASEKH, H., AZIZ, N., MIRZA, A., NEMCIK, J., LI, X., YANG, G. & KHALEGHPARAST, S. 2017. Double Shear Testing of Cable Bolts with No Concrete Face Contacts. *Procedia Engineering*, 191, 1169-1177.
- RESERVE BANK OF AUSTRALIA. 2020. *Snapshot Comparison* [Online]. Webpage: Reserve Bank of Australia. [Accessed 2021].
- SAFE WORK AUSTRALIA. 2021. *Fatality statistics by industry* [Online]. Online: Safe Work Australia. [Accessed 2021].
- SCHMUCK, C. H. 1979. Cable bolting at the Homestake gold mine. *Mining Engineering*, 31(12), 1677-1681.
- SERBOUSEK, M. O. & SIGNER, S. P. 1987. Linear Load-transfer Mechanics of Full-grouted Roof Bolts. *In: INTERIOR, U. D. O. T. (ed.)*. United States: Bureau of Mines Report of Investigation.
- SHANG, J., ZHAO, Z. & MA, S. 2018. On the shear failure of incipient rock discontinuities under CNL and CNS boundary conditions: Insights from DEM modelling. *Engineering Geology*, 234, 153-166.
- SINGH, P. & SPEARING, A. 2021. An Improved Analytical Model for the Elastic and Plastic Strain-hardening Shear Behaviour of Fully Grouted Rockbolts. *Rock Mechanics and Rock Engineering*, 54, 1-17.
- SONG, M. K., CHOO, S. Y., KANG, S. S. & CHO, Y. D. 2008. A Comparison for Shear Resistant Behavior of Joints with Rock and Spiral Bolts Installed—A Numerical Approach. *Geosystem Engineering*, 11, 57-62.
- SPANG, K. & EGGER, P. 1990. Action of fully-grouted bolts in jointed rock and factors of influence. *Rock Mechanics and Rock Engineering*, 23, 201-229.
- SPEARING, A., MONDAL, K. & BYLAPUDI, G. 2010. The corrosion of rock anchors in US coal mines. *SME, Annual Meeting*. Phoenix: SME.

- STANDARD, T. B. 1996. Strata Reinforcement support system components used in Coal Mines - Part 1. Specification of rock bolting and Part 2: Specification for Flexible systems for roof reinforcement.
- TADOLINI, S. C. & DOLINAR, D. R. 2017. 10 - The use of cable bolts or ground control—current applications and future innovation A2 - Peng, Syd S. *Advances in Coal Mine Ground Control*. Woodhead Publishing.
- TANG, D. H. Y. & PENG, S. S. 1985. Reinforcement analysis and design of mechanical roof bolting systems in horizontally bedded mine roofs. *International Journal of Mining Engineering*, 3, 1-25.
- THENEVIN, I., BLANCO-MARTÍN, L., HADJ-HASSEN, F., SCHLEIFER, J., LUBOSIK, Z. & WRANA, A. 2017. Laboratory pull-out tests on fully grouted rock bolts and cable bolts: Results and lessons learned. *Journal of Rock Mechanics and Geotechnical Engineering*, 9, 843-855.
- THOMAS, R. 2012. The load transfer properties of postgroutable cable bolts used in the Australian coal industry. *Proceedings 31st International Conference on Ground Control in Mining*, 1-10.
- THOMPSON, A. & VILLAESCUSA, E. 2014. Case studies of rock reinforcement components and systems testing. *Rock mechanics and rock engineering*, 47, 1589-1602.
- THOMPSON, A. G., MATTHEWS, S. M., WINDSOR, C. R., S, B. & TILLMANN, V. H. 1987. Innovations in rock reinforcement technology in the Australian Mining Industry. *Sixth International Congress on Rock Mechanics*. Montreal, Canada.
- VANDEKRAATS, J. D. & WATSON, S. O. 1996. *Direct Laboratory Tensile Testing of Select Yielding Rock Bolt Systems*, New Mexico, United States. Department of Energy.
- WACLAWIK, P., RAM, S., KUMAR, A., KUKUTSCH, R. & MIREK, A. 2019. *Field and simulation study for rock bolt loading characteristics under high stress conditions*.
- WEN-QIANG, C. & YI-JIA, L. 2022. Analytical model of bolt shear resistance considering progressive yield of surrounding material. *SN Applied Sciences*, 4, 42.
- WINDSOR, C. & THOMPSON, A. 1992. Reinforcement design for jointed rock masses. *Proceedings of the 33rd US Symposium on Rock Mechanics*.
- WINDSOR, C. R. 1997. Rock reinforcement systems. *International Journal of Rock Mechanics and Mining Sciences*, 34, 919-951.

ZOHAIB, M., MIRZAGHORBANALI, A., HELWIG, A., AZIZ, N., GREGOR, P., RASTEGARMANESH, A., MCDOUGALL, K. & HELWIG, A. Shear strength properties of artificial rock joints. Proceedings of the 2020 Coal Operators' Conference, 18-20 February 2020. University of Wollongong.

Appendix A

MATLAB Data Preparation: Raw data cleaning

```
%% Double Shear Clean up %%
clear
clc

%% Load data %%
shear = load('double_shear_data.mat');
testname = fieldnames(shear);

%% Loop parameters %%

notest = 16;           % Number of tests
bolt = [20 30];       % Initiate bolt types
pt = [0 10 15 20];    % Initiate pre-tension
pret = 1;             % Pretention cycle count
k = 1;                % Bolt identifier for loop
i = 1;                % Turning point count
chk = 0;              % Check to determine which final turning point to use

correction = struct(); % Create structure to store altered data during loop
corrected = struct();  % Create structure to store altered data during loop

%% Loop to clean and extract required data %%
for t = 1 : notest      % Cycle all tests

    % if statement to choose bolt capacity
    if t <= 8
        k = 1;          % k = 1 identifies 20-tonne bolts
    else
        k = 2;          % k = 2 identifies 30-tonne bolts
    end

    % if statement to create temporary names and differentiate between clean and infill.
    if (t <= 4) || (t > 8) && (t <= 12)
        tempname = strcat(['SANS_',num2str(pt(pret)),'KN_',num2str(bolt(k)),'T_RAW']);
    else
        tempname =
        strcat(['SANS_',num2str(pt(pret)),'KN_',num2str(bolt(k)),'T_infill_RAW']);
    end

    tempnamestr = string(tempname); % Convert temporary names to string

    % Extract required load and disp data from the shear structure
    s = shear.(tempnamestr);
    % Adjust load values to kN
    s(:,1) = s(:,1)/1000;
```

```

%% Locate turing points in the data based on a set threshold %%
[TF,S1,S2] = ischange(s(:,1),'linear','Threshold',70);
% Create an array to store turning points
x = (1:length(s(:,1)))';
% Store all turning points
TP= x(TF==1);

% While loop to ensure last selected turning point is after peak load
while chk == 0
    i = i+1; % Cycle turning points from start
    [~,l] = max(s(:,1)); % Calculate and store peak load
    if l > TP(i) % Check if the peak TP value is greater than peak load
        chk = 0;
    else
        chk = 1;
    end
end

%% Cutting data %%
% If statement to determine when to cut starting tail of curve
if s(TP(1),1) < 10 % The 10 corresponds to 10kN
    line_x = s(x>=TP(2) & x<=TP(i+3),2); % Setting upper and lower cuts
    line_y = s(x>=TP(2) & x<=TP(i+3),1);
else
    line_x = s(x>0 & x<=TP(i+3),2); % Amending upper and lower cuts
    line_y = s(x>0 & x<=TP(i+3),1);
end

% Create structure to store usable data
correction(t).name = tempname; % Store test name
correction(t).data = [line_x,line_y]; % Store corresponding load and disp

%% Identify amended y and x intercept using y = m*x + b %%
m = (line_y(26)-line_y(6))/(line_x(26)-line_x(6));
b = line_y(1)-m*line_x(1);
% Find x when y=0
x_int = -b/m;
% Extend line to x-intercept
line_x = [x_int ; line_x]; % Add new first disp to start of array
line_y = [ 0 ; line_y]; % Add new first load to start of array
line_xc = line_x(:,1)-line_x(1); % Zero out the displacement data
corrected(t).name = tempname; % Store test name
corrected(t).data = [line_xc,line_y]; % Store corresponding data

%% Reset parameters for while loop %%
l = 0;
i = 1;
chk = 0;

```

```

% Cycle to next pretension
pret = pret+1;

% Reset pretension counter
if pret >4
    pret = 1;
end

%% Plotting %%
figure(t)
subplot(2,1,1)
plot(s(:,2),s(:,1),line_x,line_y,'*')
subplot(2,1,2)
plot(s(:,2),s(:,1),line_xc,line_y,'*')
legend('Data','Corrected','Location','south')
hold on

end

save('ds_corrected','corrected');

```

MATLAB Data Preparation: Data pairing

```
%% Double Shear Simulation %%
```

```

% Load data
raw = load('ds_corrected','corrected');
shear = raw.corrected;
rawpretension = load('fourier_pretension','pretension');
pretension = rawpretension.pretension;
% Loop parameters

notest = length(shear(1,:)); % Number of tests
bolt = [20 30]; % Initiate bolt types
pt = [0 10 15 20]; % Initiate pre-tension
pret = 1; % Pretention cycle count
k = 1; % Bolt identifier for loop
i = 0; % Turning point count
q = 0;
chk = 0; % Check to determine which final turning point to use

tests = struct(); % Create structure to store altered data during loop
cleaned = struct(); % Create structure to store final simulated results

% Loop to clean and extract required data
for t = 1 : notest % Cycle all tests

```



```

% if statement to choose bolt capacity
if t <= 8
    k = 1;                % k = 1 identifies 20-tonne bolts
else
    k = 2;                % k = 2 identifies 30- tonne bolts
end

% if statement to create temporary names and differentiate between clean and
infill.
if (t <= 4) || (t > 8) && (t <= 12)
    tempname = strcat(['SANS_',num2str(pt(pret)),'KN_',num2str(bolt(k)),'T_RAW']);
else
    tempname =
    strcat(['SANS_',num2str(pt(pret)),'KN_',num2str(bolt(k)),'T_infill_RAW']);
end

tempnamest = string(tempname);        % Convert temporary names to string

% Extract required load and disp data from the shear structure

tests(t).shear = shear(t).data;
tests(t).pretension = pretension(t).data;
div = 0.33;
disp = 0:div:65;                    % Create simulation displacement
disp = disp';
tests(t).name = tempnamest;          % Store test name

cleaned(t).name = tempnamest;        % Store test name

%Aligning peak pretension with peak failure

[maxsh,loc] = max(tests(t).shear(:,2));
[maxpt,locp] = max(tests(t).pretension(:,2));
if locp > loc
    corrindex = locp - loc;
    tests(t).pretension = tests(t).pretension(corrindex:end,1:2);
    tests(t).pretension(:,1) = tests(t).pretension(:,1) - tests(t).pretension(1,1);

else
    corrindex = loc - locp;
    fillarray(:,1) = tests(t).pretension(1:corrindex,1);
    fillarray(:,2) = tests(t).pretension(1,2);
    tests(t).pretension(:,1) = [fillarray(:,1),tests(t).pretension(:,1)];
    tests(t).pretension(:,2) = [fillarray(:,2),tests(t).pretension(:,2)];
end

lengthsh = length(tests(t).shear(:,2));
lengthpre = length(tests(t).pretension(:,2));

```

```

lengthfix = lengthsh-lengthpre;
if lengthsh > lengthpre
    addarray(:,1) = tests(t).pretension(end:lengthfix,1);
    addarray(:,2) = tests(t).pretension(end:lengthfix,2);
end

% Pretension Cleaning
test = 1;
for z = 1 : length(displacement)
    f = 0;
    g = 1;
    while f == 0
        if abs(displacement(z,1) - tests(t).pretension(g,1)) <=
test*abs(tests(t).pretension(g,1))
            cleaned(t).pretension(z,1) = tests(t).pretension(g,1);
            cleaned(t).pretension(z,2) = tests(t).pretension(g,2);

            f = 1;
        elseif g >= length(tests(t).pretension(:,1))
            cleaned(t).pretension(z,1) = tests(t).pretension(g,1);
            cleaned(t).pretension(z,2) = tests(t).pretension(g,2);
            f = 1;
        else
            g = g+1;
            f = 0;
        end
    end
end

% Shear Cleaning
test = 1;
for z = 1 : length(displacement)
    f = 0;
    g = 1;
    while f == 0
        if abs(displacement(z,1) - tests(t).shear(g,1)) <= test*abs(tests(t).shear(g,1))
            cleaned(t).shear(z,1) = tests(t).shear(g,1);
            cleaned(t).shear(z,2) = tests(t).shear(g,2);

            f = 1;
        elseif g >= length(tests(t).shear(:,1))
            cleaned(t).shear(z,1) = tests(t).shear(g,1);
            cleaned(t).shear(z,2) = tests(t).shear(g,2);
            f = 1;
        else
            g = g+1;
            f = 0;
        end
    end
end
end

```

```

% Cycle to next pretension
pret = pret+1;

% Reset pretension counter
if pret >4
    pret = 1;
end

end
save('ds_cleaned','cleaned')

```

MATLAB Data Preparation: Calculation of Fourier series

```
%% Fit using fouriers %%
```

```
%20-Tonne Clean%
```

```

f_20t_10kn = fit(Disp_20t_10kn,Load_20t_10kn,'fourier4');
f_20t_15kn = fit(Disp_20t_15kn,Load_20t_15kn,'fourier4');
f_20t_20kn = fit(Disp_20t_20kn,Load_20t_20kn,'fourier4');

```

```
%20-Tonne Infill%
```

```

f_20t_0kn_I = fit(Disp_20t_0kn_I,Load_20t_0kn_I,'fourier4');
f_20t_10kn_I = fit(Disp_20t_10kn_I,Load_20t_10kn_I,'fourier4');
f_20t_15kn_I = fit(Disp_20t_15kn_I,Load_20t_15kn_I,'fourier4');
f_20t_20kn_I = fit(Disp_20t_20kn_I,Load_20t_20kn_I,'fourier4');

```

```
%30-Tonne Clean%
```

```

f_30t_0kn = fit(Disp_30t_0kn,Load_30t_0kn,'fourier4');
f_30t_10kn = fit(Disp_30t_10kn,Load_30t_10kn,'fourier4');
f_30t_15kn = fit(Disp_30t_15kn,Load_30t_15kn,'fourier4');
f_30t_20kn = fit(Disp_30t_20kn,Load_30t_20kn,'fourier4');

```

```
%30-Tonne Infill%
```

```

f_30t_0kn_I = fit(Disp_30t_0kn_I,Load_30t_0kn_I,'fourier4');
f_30t_10kn_I = fit(Disp_30t_10kn_I,Load_30t_10kn_I,'fourier4');
f_30t_15kn_I = fit(Disp_30t_15kn_I,Load_30t_15kn_I,'fourier4');
f_30t_20kn_I = fit(Disp_30t_20kn_I,Load_30t_20kn_I,'fourier4');

```

```
%% Plot Fouriers %%
```

```
%20-Tonne Clean fit%
```

```

figure('Name','20Tonne Clean Fit')
plot(f_20t_10kn,Disp_20t_10kn,Load_20t_10kn)
hold on
plot(f_20t_15kn,Disp_20t_15kn,Load_20t_15kn)
plot(f_20t_20kn,Disp_20t_20kn,Load_20t_20kn)
hold off

```

```
%20-Tonne Infill fit%
```

```
figure('Name','20Tonne Infill Fit')
plot(f_20t_0kn_I,Disp_20t_0kn_I,Load_20t_0kn_I)
hold on
plot(f_20t_10kn_I,Disp_20t_10kn_I,Load_20t_10kn_I)
plot(f_20t_15kn_I,Disp_20t_15kn_I,Load_20t_15kn_I)
plot(f_20t_20kn_I,Disp_20t_20kn_I,Load_20t_20kn_I)
hold off
```

%30-Tonne Clean fit%

```
figure('Name','30Tonne Clean Fit')
plot(f_30t_0kn,Disp_30t_0kn,Load_30t_0kn)
hold on
plot(f_30t_10kn,Disp_30t_10kn,Load_30t_10kn)
plot(f_30t_15kn,Disp_30t_15kn,Load_30t_15kn)
plot(f_30t_20kn,Disp_30t_20kn,Load_30t_20kn)
hold off
```

%30-Tonne Infill fit%

```
figure('Name','30Tonne Infill Fit')
plot(f_30t_0kn_I,Disp_30t_0kn_I,Load_30t_0kn_I)
hold on
plot(f_30t_10kn_I,Disp_30t_10kn_I,Load_30t_10kn_I)
plot(f_30t_15kn_I,Disp_30t_15kn_I,Load_30t_15kn_I)
plot(f_30t_20kn_I,Disp_30t_20kn_I,Load_30t_20kn_I)
hold off
```

Appendix B

MATLAB double shear simulation code

```
%% Double Shear Simulation %%

% Load data
raw = load('ds_cleaned','cleaned');
raw = raw.cleaned;
shear = raw;

% Loop parameters

notest = length(shear(1,:)); % Number of tests
bolt = [20 30]; % Initiate bolt types
pt = [0 10 15 20]; % Initiate pre-tension
pret = 1; % Pretension cycle count
k = 1; % Bolt identifier for loop
i = 0; % Turning point count
q = 0;
chk = 0; % Check to determine which final turning point to use

simulation = struct(); % Create structure to store altered data during loop
simulatedtests = struct(); % Create structure to store final simulated results
disp = 0:0.33:50; % Create simulation displacement
disp = disp';

%Simulation Gradient Constants
kp20 = 20900; %Calculated from the plastic region of the guillotine experiments
kp30 = 20942; %Calculated from the plastic region of the guillotine experiments

% Loop to clean and extract required data
for t = 1 : notest % Cycle all tests

    % if statement to choose bolt capacity
    if t <= 8
        k = 1; % k = 1 identifies 20-tonne bolts
    else
        k = 2; % k = 2 identifies 30-tonne bolts
    end

    % if statement to create temporary names and differentiate between clean and
    infill.
    if (t <= 4) || (t > 8) && (t <= 12)
        tempname = strcat(['SANS_',num2str(pt(pret)),'KN_',num2str(bolt(k)),'T_RAW']);
    else
```

```

tempname =
strcat(['SANS_',num2str(pt(pret)),'KN_',num2str(bolt(k)),'T_infill_RAW']);
end

tempnamest = string(tempname);          % Convert temporary names to string

% Extract required load and disp data from the shear structure
s = shear(t).shear;

% Locate turing points in the data based on a set threshold
[TF,S1] = ischange(s(:,2),'linear','Threshold',0.1);
% Create an array to store turning points

x = (1:length(s(:,1)))';
% Store all turning points
TP= x(TF==1);
simulation(t).name = tempnamest;        % Store test name
simulation(t).TP = TP;
%Choose elastic region 0kn 20t clean

% While loop to isolate initial elastic portion
while chk == 0
    d = inputdlg('choose turning point','Choose turning point');
    i = str2double(d{1});
    simulation(t).TPi = i;
    line_x = s(1:TP(i),1);      % Setting upper and lower cuts
    line_y = s(1:TP(i),2)*1000;
    simulation(t).dataelasraw = [line_x,line_y];
    plot(s(:,1),s(:,2),'-
..',simulation(t).dataelasraw(:,1),simulation(t).dataelasraw(:,2)/1000,'-')
    ylabel('Shear Force (kN)')
    ylim([0 160])
    yticks(0:20:160)
    xlim([0 30])
    xticks(0:2:30)
    xlabel('Displacement (mm)')
    legend({'Experiment','Elastic Region'},'Location','northwest')
    b = inputdlg('Confirm turning point 0 = No, 1 = Yes','Confirm turning point');
    chk = str2double(b{1});
end

% While loop to isolate plastic portion
chk = 0;
q = i;
while chk == 0
    [~,l] = max(s(:,2)); % Calculate and store peak load
    if l > TP(q)          % Check ensure selection remains in linear zone
        chk = 0;
    end
end

```

```

else
    chk = 1;
    line_x = s(TP(i) : TP(q),1);    % Setting upper and lower cuts
    line_y = s(TP(i) : TP(q),2)*1000;
    line_px = shear(t).pretension(TP(i) : TP(q),1);
    line_py = shear(t).pretension(TP(i) : TP(q),2)*1000;
    simulation(t).dataplastraw = [line_x,line_y];
    simulation(t).preten = [line_px,line_py];
end
q = q + 1;    % Cycle turning points from start
end

% Extracting residual portion
line_x = s(TP(q) : TP(end,1),1); % Setting upper and lower cuts
line_y = s(TP(q) : TP(end,1),2)*1000;
simulation(t).dataresidraw = [line_x,line_y];

% Reset parameters for while loop
i = 0;
q = 0;
chk = 0;

%% Calculations for simulation %%
simulation(t).ke =
simulation(t).dataelasraw(end,2)/simulation(t).dataelasraw(end,1);
% Setting ke plastic value determined by bolt capacity
if t <= 8
    simulation(t).kp = kp20;    %Setting appropriate ke value for the tested bolt
capacity
else
    simulation(t).kp = kp30;    %Setting appropriate ke value for the tested bolt
capacity
end

[M,I] = max(simulation(t).dataplastraw(:,2));
max_x = simulation(t).dataplastraw(I,1);
simulation(t).kf = (simulation(t).dataresidraw(end,2)-M)...
/(simulation(t).dataresidraw(end,1)-max_x);
simulation(t).Uyeid = simulation(t).dataplastraw(1,1);
simulation(t).Upeak = simulation(t).dataplastraw(end,1);
simulation(t).Uresid = simulation(t).dataresidraw(end,1);
simulation(t).Phi = tand(5.5);    % degree
simulation(t).Coh = 2190;    % Pa
simulation(t).Area = 0.2*0.2;    % m^2
simulation(t).Alpha = 1;

% if statement to differentiate clean and infill coefficient.
if (t <= 4) || (t > 8) && (t <= 12)
simulation(t).Coh = 0;    % Pa (clean joint parameter)

```

```

simulation(t).Phi    = 10;    % degree (clean joint parameter)
else
simulation(t).Coh    = 2190;    % Pa (infill joint parameter)
simulation(t).Phi    = tand(5.5); % degree (infill joint parameter)
end
% Run simulation for elastic region
line_x1 = disp(disp <= simulation(t).dataelasraw(end,1)+0.5);
line_y1 = simulation(t).ke.*line_x1;
simulation(t).elast = [line_x1,line_y1/1000];

% Run simulation for plastic
line_x = simulation(t).preten(simulation(t).preten(:,1) >
simulation(t).elast(end,1) & simulation(t).preten(:,1) <=
simulation(t).dataplastraw(end,1));
[loca,locb] = ismember(line_x(:,1),simulation(t).preten(:,1));

line_y = (simulation(t).elast(end,2)*1000 + simulation(t).Area *
simulation(t).Phi * ...
(simulation(t).preten(1,2) -
simulation(t).preten(length(simulation(t).elast(:,1)),2))...
- simulation(t).kp * simulation(t).Alpha * simulation(t).elast(end,1)) +
...
simulation(t).kp * simulation(t).Alpha * line_x(:,1) + simulation(t).Area
* (simulation(t).Coh + ...
simulation(t).preten(locb,2) * simulation(t).Phi) ;

% simulation(t).plast = [line_x,line_y/1000];

reltest = 1e-3;
while chk == 0
[~,l] = max(line_y);
[~,M] = max(simulation(t).dataplastraw(:,2));
if abs(line_y(l)-simulation(t).dataplastraw(M,2)) <=
reltest*abs(simulation(t).dataplastraw(M,2))
chk = 1;
elseif line_y(l) < simulation(t).dataplastraw(M,2)
chk = 0;
simulation(t).Alpha = simulation(t).Alpha+0.0001;
elseif line_y(l) > simulation(t).dataplastraw(M,2)
simulation(t).Alpha = simulation(t).Alpha-0.0001;

end

line_y = (simulation(t).elast(end,2)*1000 + simulation(t).Area *
simulation(t).Phi * (
simulation(t).preten(1,2) -
simulation(t).preten(length(simulation(t).elast(:,1)),2)) - simulation(t).kp *
simulation(t).Alpha * simulation(t).elast(end,1)) + ...

```



```

simulation(t).kp * simulation(t).Alpha * line_x(:,1) + simulation(t).Area
* (simulation(t).Coh + ...
simulation(t).preten(locb,2) * simulation(t).Phi) ;
simulation(t).plast = [line_x,line_y/1000];

end

% Reset parameters for while loop
l = 0;
M = 0;
chk = 0;

% Run simulation for residual region
line_x = disp(disp >= simulation(t).dataplastrow(end,1));
xline = line_x - line_x(1);
line_y = (simulation(t).plast(end,2)*1000) + simulation(t).kf*xline ;
simulation(t).resid = [line_x,line_y/1000];

%Create name for each simulation
if (t <= 4) || (t > 8) && (t <= 12)
testname = strcat(['Simulated ',num2str(pt(pret)),'KN ',num2str(bolt(k)),'T Bolt']);
else
testname = strcat(['Simulated ',num2str(pt(pret)),'KN ',num2str(bolt(k)),'T Bolt
Infill']);
end

testnamestr = string(testname); % Convert test names to string

simulatedtests(t).name = testnamestr;
simulatedtests(t).simulation = [simulation(t).elast ; simulation(t).plast ;
simulation(t).resid]; % Concatenate simulations

%Store all coefficients to table for plotting
Scenario(t,1) = testnamestr;
ke(t,1) = round(simulation(t).ke,4,'significant');
Yeild(t,1) = round(simulation(t).elast(end,2),4,'significant');
kplast(t,1) = simulation(t).kp;
PeakShear(t,1) = round(simulation(t).plast(end,2),4,'significant');
kfail(t,1) = round(simulation(t).kf,4,'significant');
Phi(t,1) = round(simulation(t).Phi,4,'significant');
Cohesion(t,1) = round(simulation(t).Coh,4,'significant');
Area(t,1) = round(simulation(t).Area,4,'significant');
Alpha(t,1) = round(simulation(t).Alpha,4,'significant');
tablestore =
table(Scenario,ke,Yeild,kplast,PeakShear,kfail,Phi,Cohesion,Area,Alpha);
tablestore.Properties.VariableNames = {'Scenario','ke','Yeild','kPlastic','Peak
Shear','kFail','Phi','Cohesion','Area','Alpha'};

% Cycle to next pretension
pret = pret+1;

```

```

% Reset pretension counter
if pret >4
    pret = 1;
end

% Plotting
%figure(t)
plot(s(:,1),s(:,2),'-
.',simulatedtests(t).simulation(:,1),simulatedtests(t).simulation(:,2),'-')
title(testname)
ylabel('Shear Force (kN)')
ylim([0 160])
yticks(0:20:160)
xlim([0 30])
xticks(0:2:30)
xlabel('Displacement (mm)')
legend({'Experiment','Simulated'},'Location','northwest')
hold on

%print(ffigure(t),testname,'-dpng','-r1000')
writetable(tablestore,'Simulation Summary','Delimiter','');

end

```

Appendix C

Single shear numerical model of 20-tonne rock bolt using FLAC3D

model new

; Create Geometry/Zones Block 1

```
zone create brick point 0 (0, 0,0) point 1 (0.1, 0,0) ...
                point 2 (0, 0.1,0) point 3 (0, 0,0.2) ...
                size 10,10,10 ...
                group "box" slot "block1"
```

; Create Geometry/Zones Block 2

```
zone create brick point 0 (0, 0,0.2) point 1 (0.1,0,0.2) ...
                point 2 (0,0.1,0.2) point 3 (0, 0,0.4) ...
                size 10,10,10 ...
                group "box" slot "block2"
```

; Create joints for washers and plates

```
zone interface "S-Shear" create by-face separate range position-z 0.2
```

; Joint Properties

```
zone interface "S-Shear" node property stiffness-normal 10e3 ...
                                     stiffness-shear 10e3 ...
                                     friction 1e-5 ...
                                     cohesion 1e-5
```

; Create Zone/Face groups

Zone face skin

; Assign Constitutive Model

```
zone mechanical damping combined
```

; Assign Constitutive Models

```
zone cmodel assign elastic range group "box"
```

;Assign Properties for Concrete

```
zone property density 7700 ...
                bulk 210e9 ...
                shear 34.05e9 ...
```

```

Range Group                                "box"
; Block 1
zone face apply velocity-normal 0 range group    "box" slot "block1"
; Block 2
zone gridpoint fix velocity-z 0 range group      "box" slot "block2"
zone gridpoint fix velocity-y 0 range group      "box" slot "block2"
; Save Block
model save                                     "Single Shear"
; Step to Equilibrium
model largestrain                             on
zone mechanical damping combined
model solve
; Install Rock bolt
struct pile create by-line (0.05 ,0.05,0) (0.05, 0.05,0.4) segments 40
struct node group 'Bottom'  range position-z      0.0
struct node group 'Top'    range position-z      0.4
; Set Rock bolt Properties
struct pile property  rockbolt-flag              on  ...
        young                69.4e9  ...
        poisson              0.25  ...
        cross-sectional-area  3.14e-4  ...
        perimeter            0.0628

; Set ultimate tensile strength
struct pile property  tensile-yield              6.75e3  ...
        tensile-failure-strain  0.025  ...
        plastic-moment         2.2e3  ...
        moi-y                  3.3e-8  ...
        moi-z                  3.3e-8  ...
        moi-polar              7.85e-9  ...
        coupling-cohesion-shear 9.15e5  ...

```

coupling-stiffness-shear	4.1e9 ...
coupling-cohesion-normal	6.95e5 ...
coupling-friction-normal	45 ...
coupling-stiffness-normal	1.4e8 ...
coupling-friction-shear	45


```

; Set Shear test (Fix local nodal axes)
struct node fix system-local range group          "Bottom"
struct node fix system-local range group          "Top"

model solve

; Record results
fish define force
  local sum = 0.0
  loop foreach local gp gp.list
    if gp.isgroup(gp,'box','block1') then
      sum = sum + gp.force.unbal.x(gp)
    endif
  global force = sum
  endloop
end

fish define disp
  gp = gp.near(0.1,0.1,0.3)
  disp = gp.disp.x(gp)
end

; Set Histories
history interval 100

fish history name 'force' @force

```

fish history name 'disp' @disp

struct node history name 'move' displacement-x position (0.05,0.05,0.3)

; Set Shear velocity

zone face apply velocity-x 1e-6 range group "west2"

model step 14000

;Sensitivity

;Shear Rate

;young modulus

;tfs

;ty

;pmom

Appendix D

Double shear numerical model: 20-tonne rock bolt with clean shear interfaces and 20MPa host rock, using FLAC3D

model new

; Create Geometry/Zones Washer 1

```
zone create brick point 0 (0, 0,0) point 1 (0.2, 0,0) ...  
point 2 (0, 0.2,0) point 3 (0, 0,0.016) ...  
size 2,5,2 ...  
group "washer" slot "washer1"
```

; Create Geometry/Zones Washer 2

```
zone create brick point 0 (0, 0,0.816) point 1 (0.2, 0,0.816) ...  
point 2 (0, 0.2,0.816) point 3 (0, 0,0.832) ...  
size 2,5,2 ...  
group "washer" slot "washer2"
```

; Create Geometry/Zones Block 1

```
zone create brick point 0 (0, 0,0.016) point 1 (0.2, 0,0.016) ...  
point 2 (0, 0.2,0.016) point 3 (0, 0,0.216) ...  
size 10,10,10 ...  
group "concrete" slot "block1"
```

; Create Geometry/Zones Block 2

```
zone create brick point 0 (0, 0,0.216) point 1 (0.2, 0,0.216) ...  
point 2 (0, 0.2,0.216) point 3 (0, 0,0.616) ...  
size 10,20,10 ...  
group "concrete" slot "block2"
```

; Create Geometry/Zones Block 3

```
zone create brick point 0 (0, 0,0.616) point 1 (0.2, 0,0.616) ...  
point 2 (0, 0.2,0.616) point 3 (0, 0,0.816) ...  
size 10,10,10 ...  
group "concrete" slot "block3"
```

; Create Zone/Face groups

Zone face skin

```

;; Create joints for washers and plates
zone interface "Washer" create by-face separate range position-z 0.016;
zone interface "Washer" create by-face separate range position-z 0.816;
zone interface "Shear" create by-face separate range position-z 0.216;range group
"Top2" group "Bottom3"
zone interface "Shear" create by-face separate range position-z 0.616;
;; Define washer and load plate interface properties
zone interface "Washer" node property stiffness-normal      1000      ...
                                stiffness-shear      1000      ... ;shear modulus
                                friction      45      ...
                                cohesion      0

zone interface "Shear" node property stiffness-normal      1000      ...
                                stiffness-shear      500      ... ;shear modulus
                                friction      8.5      ...
                                cohesion      7.173e3

; Assign Constitutive Model
zone mechanical damping combined
; Assign Constitutive Models for Washer
zone cmodel assign elastic range group "washer"
; Assign Constitutive Models for Concrete
zone cmodel assign strain-softening range group "concrete"
; Assign Properties for Concrete
zone property      density      7700      ...
                bulk      210e9      ...
                shear      34.05e9      ... ; Shear modulus
                Range Group "washer"
zone property      density      2400 ...;
                bulk      11e9      ... ;
                shear      10e9      ... ; Shear modulus
                friction      49.05      ...; derived numerically

```



```

        cohesion    8.93e6    ...
        tension     4.7e6     ...
        dilation    12        ...; Taken from FLAC manual
    Range Group "concrete"

; Assign Boundary Conditions
; Washers
zone face apply velocity-normal 0 range group "washer" slot "washer1"
zone face apply velocity-normal 0 range group "washer" slot "washer2"
; Block 1
zone face apply velocity-normal 0 range group "concrete" slot "block1"
; Block 2
zone gridpoint fix velocity-z 0 range group    "concrete" slot "block2"
zone gridpoint fix velocity-y 0 range group    "concrete" slot "block2"
; Block 3
zone face apply velocity-normal 0 range group "concrete" slot "block3"
; Save Block
model save                                "Double Shear Clean"
; Step to Equilibrium
model largestrain                        on
zone mechanical damping combined
model solve

; Install Rock bolt
struct pile create by-line (0.1, 0.1, 0) (0.1, 0.1, 0.832) segments 70

struct node group 'Bottom' range position-z    0.0
struct node group 'Top'   range position-z    0.832
; Set Rock bolt Properties
struct pile property  rockbolt-flag            on ...
        young                69.4e9    ...
        poisson              0.25    ...

```

cross-sectional-area	3.14e-4 ...
perimeter	0.0628

; Set ultimate tensile strength

struct pile property	tensile-yield	6.75e3 ...
	tensile-failure-strain	0.025 ...
	plastic-moment	2.2e3 ...
	moi-y	3.3e-8 ...
	moi-z	3.3e-8 ...
	moi-polar	7.85e-9 ...
	coupling-cohesion-shear	3.15e5 ...
	coupling-stiffness-shear	1.5e9 ...
	coupling-cohesion-normal	2.95e5 ...
	coupling-friction-normal	45 ...
	coupling-stiffness-normal	4.7e8 ...
	coupling-friction-shear	45

; Set Shear test (Fix local nodal axes)

struct node fix system-local range group	"Bottom"
struct node fix system-local range group	'Top'

model solve

fish define force

```

local sum = 0.0
loop foreach local gp gp.list
if gp.isgroup(gp,'concrete','block1') then
    sum = sum + gp.force.unbal.x(gp)
endif
global force = sum
endloop
end

```

```
fish define disp
```

```
    gp = gp.near(0.1,0,0.416)
```

```
    disp = gp.disp.x(gp)
```

```
end
```

```
; Set Histories
```

```
history interval 500
```

```
fish history name 'force' @force
```

```
fish history name 'disp' @disp
```

```
struct node history name 'move' displacement-x position (0.1,0.1,0.416)
```

```
history export 'force' vs 'disp' file '40T 0kn 40MPa clean'
```

```
; Set Shear velocity
```

```
zone face apply velocity-x 1e-6 range group "West5"
```

```
model step 40000
```

Double shear numerical model: 30-tonne rock bolt with clean shear interfaces and 40MPa host rock, using FLAC3D

```
model new
```

```
; Create Geometry/Zones Washer 1
```

```
zone create brick point 0 (0, 0,0) point 1 (0.2, 0,0) ...
```

```
    point 2 (0, 0.2,0) point 3 (0, 0,0.016) ...
```

```
    size 2,5,2 ...
```

```
    group "washer" slot "washer1"
```

```
; Create Geometry/Zones Washer 2
```

```

zone create brick point 0 (0, 0,0.816) point 1 (0.2, 0,0.816) ...
    point 2 (0, 0.2,0.816) point 3 (0, 0,0.832) ...
    size 2,5,2 ...
    group "washer" slot "washer2"
; Create Geometry/Zones Block 1
zone create brick point 0 (0, 0,0.016) point 1 (0.2, 0,0.016) ...
    point 2 (0, 0.2,0.016) point 3 (0, 0,0.216) ...
    size 10,10,10 ...
    group "concrete" slot "block1"
; Create Geometry/Zones Block 2
zone create brick point 0 (0, 0,0.216) point 1 (0.2, 0,0.216) ...
    point 2 (0, 0.2,0.216) point 3 (0, 0,0.616) ...
    size 10,20,10 ...
    group "concrete" slot "block2"
; Create Geometry/Zones Block 3
zone create brick point 0 (0, 0,0.616) point 1 (0.2, 0,0.616) ...
    point 2 (0, 0.2,0.616) point 3 (0, 0,0.816) ...
    size 10,10,10 ...
    group "concrete" slot "block3"
; Create Zone/Face groups
Zone face skin
;; Create joints for washers and plates
zone interface "Washer" create by-face separate range position-z 0.016;
zone interface "Washer" create by-face separate range position-z 0.816;
zone interface "Shear" create by-face separate range position-z 0.216;range group
"Top2" group "Bottom3"
zone interface "Shear" create by-face separate range position-z 0.616;
;; Define washer and load plate interface properties
zone interface "Washer" node property stiffness-normal 1e5 ...
    stiffness-shear 1e5 ... ;shear modulus
    friction 45 ...

```

```

                                cohesion          0

zone interface "Shear" node property stiffness-normal    10000    ...
                                stiffness-shear        5000    ... ;shear modulus
                                friction                8.5      ...
                                cohesion                7.173e3

; Assign Constitutive Model
zone mechanical damping combined

; Assign Constitutive Models for Washer
zone cmodel assign elastic range group "washer"

; Assign Constitutive Models for Concrete
zone cmodel assign strain-softening range group "concrete"
;Assign Properties for Concrete
zone property    density    7700    ...
                bulk        210e9    ...
                shear       34.05e9    ... ; Shear modulus
                Range Group "washer"

zone property    density    2400 ...;    ...
                bulk        14.7e9    ... ;
                shear       13.4e9    ... ; Shear modulus
                friction    49.05    ...; derived numerically
                cohesion    8.93e6    ...
                tension     4.7e6    ...
                dilation    12    ...; Taken from FLAC manual
                Range Group "concrete"

; Assign Boundary Conditions
; Washers
zone face apply velocity-normal 0 range group "washer" slot "washer1"
zone face apply velocity-normal 0 range group "washer" slot "washer2"

; Block 1
zone face apply velocity-normal 0 range group "concrete" slot "block1"

```

```

; Block 2
zone gridpoint fix velocity-z 0 range group      "concrete" slot "block2"
zone gridpoint fix velocity-y 0 range group      "concrete" slot "block2"
; Block 3
zone face apply velocity-normal 0 range group "concrete" slot "block3"
; Save Block
model save                                     "Double Shear Clean"
; Step to Equilibrium
model largestrain                             on
zone mechanical damping combined
model solve

; Install Rock bolt
struct pile create by-line (0.1, 0.1, 0) (0.1, 0.1, 0.832) segments 70

struct node group 'Bottom' range position-z      0.0
struct node group 'Top'   range position-z      0.832
; Set Rock bolt Properties
struct pile property  rockbolt-flag              on    ...
                    young                        68.4e9  ...
                    poisson                      0.25   ...
                    cross-sectional-area          3.14e-4  ...
                    perimeter                    0.0628

; Set ultimate tensile strength
struct pile property  tensile-yield              15e3    ...
                    tensile-failure-strain        0.03    ...
                    plastic-moment                2.9e3    ...
                    moi-y                         3.3e-8    ...
                    moi-z                         3.3e-8    ...

```

```

        moi-polar          7.85e-9    ...
        coupling-cohesion-shear  5.15e7    ...
        coupling-stiffness-shear  6.12e7    ...
        coupling-cohesion-normal  9.95e7    ...
        coupling-friction-normal    45 ...
        coupling-stiffness-normal  5.5e8 ...
        coupling-friction-shear    45

; Set Shear test (Fix local nodal axes)
struct node fix system-local range group      "Bottom"
struct node fix system-local range group 'Top'

model solve

fish define force
    local sum = 0.0
    loop foreach local gp gp.list
        if gp.isgroup(gp,'concrete','block1') then
            sum = sum + gp.force.unbal.x(gp)
        endif
    global force = sum
    endloop
end

fish define disp
    gp = gp.near(0.1,0,0.416)
    disp = gp.disp.x(gp)
end

; Set Histories
history interval 500

```

fish history name 'force' @force

fish history name 'disp' @disp

struct node history name 'move' displacement-x position (0.1,0.1,0.416)

history export 'force' vs 'disp' file '40T 0kn 40MPa clean'

; Set Shear velocity

zone face apply velocity-x 1e-6 range group "West5"

model step 26000

Appendix E

Double shear with infilled shear interfaces numerical model: 20-tonne rock bolt with 20MPa host rock using FLAC3D

; Create Geometry/Zones Block 1

model new

; Create Geometry/Zones Washer 1

```
zone create brick point 0 (0, 0,0) point 1 (0.2, 0,0) ...
                point 2 (0, 0.2,0) point 3 (0, 0,0.016) ...
                size 2,5,2 ...
                group "washer" slot "washer1"
```

; Create Geometry/Zones Washer 2

```
zone create brick point 0 (0, 0,0.826) point 1 (0.2, 0,0.826) ...
                point 2 (0, 0.2,0.826) point 3 (0, 0,0.842) ...
                size 2,5,2 ...
                group "washer" slot "washer2"
```

; Create Geometry/Zones Block 1

```
zone create brick point 0 (0, 0,0.016) point 1 (0.2, 0,0.016) ...
                point 2 (0, 0.2,0.016) point 3 (0, 0,0.216) ...
                size 10,10,10 ...
                group "concrete" slot "block1"
```

; Create Geometry/Zones Infill Block 1

```
zone create brick point 0 (0, 0,0.216) point 1 (0.2, 0,0.216) ...
                point 2 (0, 0.2,0.216) point 3 (0, 0,0.221) ...
                size 2,5,2 ...
                group "infill" slot "I1"
```

; Create Geometry/Zones Block 2

```
zone create brick point 0 (0, 0,0.221) point 1 (0.2, 0,0.221) ...
                point 2 (0, 0.2,0.221) point 3 (0, 0,0.621) ...
                size 10,20,10 ...
```

```

group "concrete" slot "block2"

; Create Geometry/Zones Block 3
zone create brick point 0 (0, 0,0.621) point 1 (0.2, 0,0.621) ...
point 2 (0, 0.2,0.621) point 3 (0, 0,0.626) ...
size 2,5,2 ...
group "infill" slot "I2"

; Create Geometry/Zones Block 3
zone create brick point 0 (0, 0,0.626) point 1 (0.2, 0,0.626) ...
point 2 (0, 0.2,0.626) point 3 (0, 0,0.826) ...
size 10,10,10 ...
group "concrete" slot "block3"

; Create joints for washers and plates
zone interface "Washer" create by-face separate range position-z 0.016;
zone interface "Washer" create by-face separate range position-z 0.826;
zone interface "Shear1" create by-face separate range position-z 0.216;
zone interface "Shear2" create by-face separate range position-z 0.221;
zone interface "Shear1" create by-face separate range position-z 0.621;
zone interface "Shear2" create by-face separate range position-z 0.626;

zone interface "Washer" node property stiffness-normal 1e5 ...
stiffness-shear 1e5 ... ;shear modulus
friction 45 ...
cohesion 0

zone interface "Shear1" node property stiffness-normal 15000 ...
stiffness-shear 5000 ... ;shear modulus
friction 8.5 ...
cohesion 7.173e3

```

```

zone interface "Shear2" node property stiffness-normal      15000      ...
                                stiffness-shear          5000      ... ;shear modulus
                                friction                  8.5      ...
                                cohesion                   7.173e3

```

```

; Create Zone/Face groups

```

```

Zone face skin

```

```

; Assign Constitutive Model

```

```

zone mechanical damping combined

```

```

; Assign Constitutive Models for Washer

```

```

zone cmodel assign elastic range group "washer"

```

```

; Assign Constitutive Models for Concrete

```

```

zone cmodel assign strain-softening range group "concrete"

```

```

; Assign Constitutive Models for Infill

```

```

Zone cmodel assign mohr-coulomb range group "infill"

```

```

; Assign Properties for Concrete

```

```

zone property      density  7700      ...
                    bulk     210e9      ...
                    shear    34.05e9    ... ; Shear modulus
                    Range Group "washer"

```

```

zone property      density  2400 ...;
                    bulk     11e9      ... ;
                    shear    10e9      ... ; Shear modulus
                    friction  49.05      ...; derived numerically
                    cohesion  8.93e6     ...
                    tension   4.7e6      ...
                    dilation  12         ...; Taken from FLAC manual
                    Range Group "concrete"

```

```

Zone property      density  2000      ...
                    bulk     20e9      ...
                    shear    3.94e3     ...

```

```

friction 5.5 ...
cohesion 2.19e3 ...
Range Group "infill"

;Assign Boundary Conditions
zone face apply velocity-normal 0 range group "washer" slot "washer1"
zone face apply velocity-normal 0 range group "washer" slot "washer2"
; Block 1
zone face apply velocity-normal 0 range group "concrete" slot "block1"
; Block 2
zone gridpoint fix velocity-z 0 range group "concrete" slot "block2"
zone gridpoint fix velocity-y 0 range group "concrete" slot "block2"
; Block 3
zone face apply velocity-normal 0 range group "concrete" slot "block3"
; Infill
zone face apply velocity-normal 0 range group "infill" slot "I1"
zone face apply velocity-normal 0 range group "infill" slot "I2"
; Save Block
model save "Double Shear Clean"
; Step to Equilibrium
model largestrain on
zone mechanical damping combined

;model solve

; Install Rock bolt
struct pile create by-line (0.1, 0.1, 0) (0.1, 0.1, 0.84) ...
segments 100
struct node group "Start" range position-y 0.0
struct node group "End" range position-y 0.84
; Set Rock bolt Properties
; Set Rock bolt Properties

```

```

struct pile property  rockbolt-flag          on  ...

    young          69.4e9  ...
    poisson        0.25   ...
    cross-sectional-area    3.14e-4  ...
    perimeter      0.0628

; Set ultimate tensile strength
struct pile property  tensile-yield          6.75e3  ...
    tensile-failure-strain    0.02  ...
    plastic-moment           2.1e3  ...
    moi-y                    3.3e-8  ...
    moi-z                    3.3e-8  ...
    moi-polar                7.85e-9  ...
    coupling-cohesion-shear   5.15e6  ...
    coupling-stiffness-shear  9.5e7   ...
    coupling-cohesion-normal  5.95e6  ...
    coupling-friction-normal  45     ...
    coupling-stiffness-normal 3.75e8  ...
    coupling-friction-shear   45

; Set Shear test (Fix local nodal axes)
struct node fix system-local range group  "Start"
;struct node fix system-local range group  "End"

model solve

fish define force
    local sum = 0.0
    loop foreach local gp gp.list
    if gp.isgroup(gp,'concrete','block1') then
        sum = sum + gp.force.unbal.x(gp)
    endif

```

```
    global force = sum
  endloop
end
```

```
fish define disp
  gp = gp.near(0.1,0,0.421)
  disp = gp.disp.x(gp)
end
```

```
; Set Histories
history interval 500
```

```
fish history name 'force' @force
fish history name 'disp' @disp
```

```
struct node history name 'move' displacement-x position (0.1,0.1,0.421)
```

```
history export 'force' vs 'disp' file '40T 0kn 40MPa clean'
```

```
; Set Shear velocity
zone face apply velocity-x 1e-6 range group "West7"
```

```
model step 40000
```

Appendix F

Double shear numerical model sensitivity study: 30-tonne rock bolt with 40MPa host rock using FLAC3D

model new

; Create Geometry/Zones Washer 1

```
zone create brick point 0 (0, 0,0) point 1 (0.2, 0,0) ...  
point 2 (0, 0.2,0) point 3 (0, 0,0.016) ...  
size 2,5,2 ...  
group "washer" slot "washer1"
```

; Create Geometry/Zones Washer 2

```
zone create brick point 0 (0, 0,0.816) point 1 (0.2, 0,0.816) ...  
point 2 (0, 0.2,0.816) point 3 (0, 0,0.832) ...  
size 2,5,2 ...  
group "washer" slot "washer2"
```

; Create Geometry/Zones Block 1

```
zone create brick point 0 (0, 0,0.016) point 1 (0.2, 0,0.016) ...  
point 2 (0, 0.2,0.016) point 3 (0, 0,0.216) ...  
size 10,10,10 ...  
group "concrete" slot "block1"
```

; Create Geometry/Zones Block 2

```
zone create brick point 0 (0, 0,0.216) point 1 (0.2, 0,0.216) ...  
point 2 (0, 0.2,0.216) point 3 (0, 0,0.616) ...  
size 10,20,10 ...  
group "concrete" slot "block2"
```

; Create Geometry/Zones Block 3

```
zone create brick point 0 (0, 0,0.616) point 1 (0.2, 0,0.616) ...  
point 2 (0, 0.2,0.616) point 3 (0, 0,0.816) ...  
size 10,10,10 ...  
group "concrete" slot "block3"
```

; Create Zone/Face groups

Zone face skin

```

;; Create joints for washers and plates
zone interface "Washer" create by-face separate range position-z 0.016;
zone interface "Washer" create by-face separate range position-z 0.816;
zone interface "Shear" create by-face separate range position-z 0.216;range group
"Top2" group "Bottom3"
zone interface "Shear" create by-face separate range position-z 0.616;
;; Define washer and load plate interface properties
zone interface "Washer" node property stiffness-normal      1000      ...
                                stiffness-shear      1000      ... ; shear modulus
                                friction      45      ...
                                cohesion      0

zone interface "Shear" node property stiffness-normal      1000      ...
                                stiffness-shear      500      ... ; shear modulus
                                friction      8.5      ...
                                cohesion      7.173e3

; Assign Constitutive Model
zone mechanical damping combined
; Assign Constitutive Models for Washer
zone cmodel assign elastic range group "washer"
; Assign Constitutive Models for Concrete
zone cmodel assign strain-softening range group "concrete"
; Assign Properties for Concrete
zone property      density      7700      ...
                bulk      210e9      ...
                shear      34.05e9      ... ; Shear modulus
                Range Group "washer"
zone property      density      2400 ...;
                bulk      14.7e9      ... ;
                shear      13.4e9      ... ; Shear modulus
                friction      49.05      ...; derived numerically

```



```

        cohesion    8.93e6    ...
        tension     4.7e6     ...
        dilation    12       ...; Taken from FLAC manual
    Range Group "concrete"

; Assign Boundary Conditions
; Washers
zone face apply velocity-normal 0 range group "washer" slot "washer1"
zone face apply velocity-normal 0 range group "washer" slot "washer2"
; Block 1
zone face apply velocity-normal 0 range group "concrete" slot "block1"
; Block 2
zone gridpoint fix velocity-z 0 range group    "concrete" slot "block2"
zone gridpoint fix velocity-y 0 range group    "concrete" slot "block2"
; Block 3
zone face apply velocity-normal 0 range group "concrete" slot "block3"
; Save Block
model save                                "Double Shear Clean"
; Step to Equilibrium
model largestrain                        on
zone mechanical damping combined
;model solve

; Install Rock bolt
struct pile create by-line (0.2, 0.1, 0) (0, 0.1, 0.832) segments 70

struct node group 'Bottom' range position-z      0.0
struct node group 'Top'   range position-z      0.832
; Set Rock bolt Properties
struct pile property  rockbolt-flag            on    ...
                    young                      68.4e9    ...
                    poisson                    0.25    ...

```

```

cross-sectional-area    3.14e-4    ...
perimeter              0.0628

```

```
; Set ultimate tensile strength
```

```

struct pile property  tensile-yield      15e3    ...
                      tensile-failure-strain  0.03    ...
                      plastic-moment      2.9e3    ...
                      moi-y              3.3e-8    ...
                      moi-z              3.3e-8    ...
                      moi-polar          7.85e-9    ...
                      coupling-cohesion-shear  5.15e7    ...
                      coupling-stiffness-shear  6.12e7    ...
                      coupling-cohesion-normal  9.95e7    ...
                      coupling-friction-normal   45 ...
                      coupling-stiffness-normal  5.5e8 ...
                      coupling-friction-shear   45

```

```
; Set Shear test (Fix local nodal axes)
```

```

struct node fix system-local range group    "Bottom"
struct node fix system-local range group 'Top'

```

```
model solve
```

```
fish define force
```

```

local sum = 0.0
loop foreach local gp gp.list
if gp.isgroup(gp,'concrete','block1') then
    sum = sum + gp.force.unbal.x(gp)
endif
global force = sum
endloop

```

end

fish define disp

gp = gp.near(0.1,0,0.416)

disp = gp.disp.x(gp)

end

; Set Histories

history interval 500

fish history name 'force' @force

fish history name 'disp' @disp

struct node history name 'move' displacement-x position (0.1,0.1,0.416)

history export 'force' vs 'disp' file '40T 0kn 40MPa clean'

; Set Shear velocity

zone face apply velocity-x 1e-6 range group "West5"

model step 50000